Development of FRET-based glucose sensors for application in small scale cultivations

Inaugural-Dissertation

zur Erlangung des Doktorgrades
der Mathematisch-Naturwissenschaftlichen Fakultät
der Heinrich-Heine-Universität Düsseldorf

vorgelegt von

Julia Otten
aus Mönchengladbach

Jülich, Januar 2019

aus dem Institut für Bio- und Geowissenschaften (IBG-1: Biotechnologie)
der Forschungszentrum Jülich GmbH

Gedruckt mit der Genehmigung der
Mathematisch-Naturwissenschaftlichen Fakultät der
Heinrich-Heine-Universität Düsseldorf

Berichterstatter:

1. Prof Dr. Martina Pohl

2. Prof Dr. Michael Bott

Tag der mündlichen Prüfung: 07.04.2019

Ich versichere an Eides statt, dass die Dissertation von mir selbständig und ohne unzulässige fremde Hilfe unter Beachtung der „Grundsätze zur Sicherung guter wissenschaftlicher Praxis an der Heinrich-Heine-Universität Düsseldorf“ erstellt worden ist.

Bisher habe ich keine erfolgslosen Promotionsversuche unternommen und diese Dissertation nicht an einer anderen Fakultät vorgelegt.

Ort, Datum	Julia Otten

PUBLICATIONS IN THE COURSE OF THIS THESIS

PUBLICATIONS IN SCIENTIFIC JOURNALS:

Steffen V., Otten J., Engelmann S., et al., A Toolbox of Genetically Encoded FRET-Based Biosensors for Rapid L-Lysine Analysis, *Sensors* 16(10), 1604 (**2016**) [10.3390/s16101604]

Hoefig H., Otten J., Steffen V., et al. ,Genetically Encoded Förster Resonance Energy Transfer-Based Biosensors Studied on the Single-Molecule Level, *ACS Sensors* 3(8), 1462–1470 (**2018**) [10.1021/acssensors.8b00143].

Otten J., Tenhaef N., Jansen R., et al. A FRET-based biosensor for the quantification of glucose in culture supernatants of mL scale microbial cultivations. *Microb Cell Fact*.18(143) [10.1186/s12934-019-1193-y].

ORAL PRESENTATIONS (PRESENTING AUTHORS ARE UNDERLINED):

Otten J., Tenhaef N., Wiechert W., et al., Optimization and application of a FRET-based sensor for monitoring of glucose in small scale cultivations, *Biosensors 2018* , Miami, USA, **2018**

POSTER PRESENTATIONS (PRESENTING AUTHORS ARE UNDERLINED):

Steffen V., Otten J., Radek A., et al., FRET-based biosensors for online measurement of lysine production, *ProcessNet 2016,* , Germany, **2016**

Otten J., Steffen V., Wiechert W., et al. , Development of new FRET-based biosensors for extracellular metabolite analysis, *ProcessNet 2016*, Germany, **2016**

Steffen V., Otten J., Radek A., et al., A FRET-based lysine sensor toolbox with different affinity and sensitivity *Biosensors 2016*, Schweden, **2016**

Otten J., Steffen V., Wiechert W., et al., Development of a FRET-based biosensor for sugar detection *N2 Science Communication Conference*, Germany, **2017**

Otten J., Steffen V., Wiechert W., et al., Development of new FRET-based biosensors for extracellular metabolic analysis, *International Conference on Molecular Systems Engineering (ICMSE)*, Switzerland, **2017**

Table of content

I. Abstract

Within recent years biotechnology was established as an integral part of the economy. Especially in the context of bioeconomy microbial strain and process development are gaining momentum. Microbial producer strains, converting renewable feedstock into high value compounds, are able to compete with the petrol-based economy. To develop and monitor such strains, metabolite sensors are of great value to understand metabolite dynamics and screen for better producers. One type of such sensors are Förster-Resonance-Energy-Transfer (FRET)-based biosensors.

This type of genetically encoded sensors consist of a metabolite binding domain, sandwiched between two fluorescent proteins. Upon ligand binding the binding domain undergoes a conformational change which results in an altered FRET effect, due to changes in the distance/ orientation of the fluorescent proteins. In this work, a toolbox of FRET-based sensors for the detection and quantification of glucose was constructed and tested for the extracellular application in small scale cultivations. Besides, the molecular function of such sensors was analyzed in cooperation using single molecule fluorescence and small angle X-ray scattering (SAXS). All sensor variants are based on the periplasmic glucose-galactose binding protein from *E. coli* and carry the cyan fluorescent protein mTurquoise2 as FRET-donor and the yellow fluorescent protein Venus as FRET-acceptor. Important parameters like affinity, sensitivity and stability were optimized by the introduction of different linkers, mutation of the binding protein and by introduction of the HaloTag™ for simple covalent immobilization.

A glucose sensor variant with a linker between the binding protein and the FRET-donor resulted in the highest FRET-changes, as a result of large conformational changes between liganded and non-liganded states. This optimized soluble glucose sensor was applied for the at-line analysis of glucose in automated small scale microbial cultivations to demonstrate the potential of such sensors. The sensor performed competitive to established enzymatic and HPLC-based quantification methods for glucose. Further, the application of FRET-based glucose sensors was successfully demonstrated in microbial cultivations using a BioLector® devise.

Immobilization of the optimized sensor was shown to increase the stability and resulted in an immobilized glucose sensors, which could successfully be used online in a microtiter-based cultivation. After successful application in the milliliter-scale the immobilized sensor was also evaluated in a microfluidic, chip-based cultivation device at picoliter-scale. Using fluorescence microscopy the sensor, immobilized on beads, reliably indicated changes in glucose concentration thus demonstrating that FRET-based sensor beads are a promising tool also for an application in picoliter-scale bioreactors. This development paves the way for in chip-online-analysis of various metabolites in single cell studies, which is currently not possible.

II. Kurzfassung

In den letzten Jahren wurde die Biotechnologie zu einem festen Bestandteil der Wirtschaft. Insbesondere im Kontext der Bioökonomie gewinnen Stamm- und Prozessentwicklung immer weiter an Bedeutung. Mikrobielle Produzenten, die nachwachsende Rohstoffe zu hochwertigen Feinchemikalien umwandeln, können mit der ölbasierten Wirtschaft mithalten. Für die Entwicklung und Analyse solcher Stämme, sind Metabolitsensoren von großem Wert um Stoffwechselwege zu verstehen und nach besseren Produzenten zu suchen. Eine Klasse solcher Sensoren sind Förster-Resonanz-Energietransfer (FRET) -basierte Biosensoren. Diese genetisch codierten Sensoren setzen sich aus einer Metabolit-Bindedomäne, zwischen zwei fluoreszierenden Proteinen, zusammen. Eine durch Ligandenbindung induzierte Konformationsänderung, ruft Abstands- / Orientierungs-änderungen der fluoreszierenden Proteine hervor und führt so zu einem veränderten FRET-Effekt.

In dieser Arbeit wurde eine Toolbox von FRET-basierten Sensoren zur extrazellulären Quantifizierung von Glukose, in Kultivierungen im Mili- und Microliter Maßstab, entwickelt und getestet. Außerdem wurden, gemeinsam mit Kooperationspartnern, die molekularen Hintergründe solcher Sensoren mit Einzelmolekülfluoreszenzmessungen und Kleinwinkel-Röntgenstreuung (SAXS) analysiert. Alle Sensorvarianten basieren auf dem periplasmatischen Glucose-Galaktose-Bindeprotein aus *E. coli* und tragen das cyane Fluoreszenzprotein mTurquoise2 als FRET-Donor und das gelbe Fluoreszenzprotein Venus als FRET-Akzeptor. Wichtige Parameter wie Affinität, Empfindlichkeit und Stabilität wurden durch die Einführung verschiedener Linker, die Mutation des Bindeproteins und durch die Einführung des HaloTag™ zur einfachen kovalenten Immobilisierung optimiert.

Eine Sensorvariante mit einem Linker zwischen dem Bindeprotein und FRET-Donor zeigte die höchsten FRET-Änderungen, als Ergebnis großer Konformationsänderungen zwischen gebundenem und ungebundenem Zustand. Dieser optimierte, lösliche Glukosesensor wurde für die At-Line-Analyse von Glukose in automatisierten mikrobiellen Kultivierungen im kleinen Maßstab eingesetzt, um das Potenzial solcher Sensoren zu demonstrieren. Im Vergleich zu etablierten enzymatischen und HPLC-basierten Quantifizierungsmethoden für Glukose, konnte der Sensor überzeugen.

Es wurde gezeigt, dass die Immobilisierung des optimierten Sensors die Stabilität erhöht und zu immobilisierten Glukosesensoren führte, die online erfolgreich in einer Kultivierung in Mikrotiterplatten in einem BioLector® eingesetzt werden konnten. Nach erfolgreicher Anwendung im Milliliter Maßstab wurde der immobilisierte Sensor auch in einer Chip-basierten, mikrofluidischen Kultivierung im Pikolitermaßstab bewertet. In der Fluoreszenzmikroskopie

zeigte der immobilisierte Sensor zuverlässig Änderungen der Glukosekonzentration an und demonstriert damit, dass FRET-basierte Sensoren auch für eine Anwendung in Bioreaktoren im Pikolitermaßstab ein vielversprechendes Werkzeug sind. Diese Entwicklung ebnet den Weg für die Online-Analyse verschiedener Metaboliten in Einzelzellstudien, was derzeit nicht möglich ist.

III. Abbreviations

λ	wavelength
ΔR	FRET-ratio change
A	FRET-acceptor
ATP	adenosine triphosphate
BFP	blue fluorescent protein
BP	binding protein
CFP	cyan fluorescent protein
D	FRET-donor
eFP	enhanced fluorescent protein
em	emission / emission maxima
ex	absorption/ absorption maxima
FACS	fluorescence activated cell sorting
FLIM	fluorescence lifetime imaging microscopy
FP	fluorescence protein
FRET	Förster-resonance-energy transfer
fRFP	far red fluorescent protein
GFP	green fluorescent protein
GGBP	glucose- galactose binding protein
K_d	dissociation constant/ affinity
K_m	Michaelis-Menten constant
OFP	orange fluorescent protein
PBP	periplasmic binding protein
R	ratio / FRET-ratio
R_0	FRET-ratio without ligand
RFP	red fluorescent protein
R_{sat}	FRET-ratio at saturation with ligand
S	singlet state
SAXS	small angle x-ray scattering
smFRET	single molecule FRET
T	triplet state
TF	transcription factor
YFP	yellow fluorescent protein

Danksagung

Zu Beginn der Promotion stellt sich jedem sicherlich die Frage: Was bleibt am Ende? Sicherlich bleibt das gewonnene Wissen. Es bleibt der Stolz, etwas geschafft zu haben. Es bleibt der wissenschaftliche Fortschritt. Es bleiben wahrscheinlich auch die Publikationen, die dabei rauskommen. Was aber mindestens genauso wichtig ist, es bleibt die Dankbarkeit.

Daher möchte ich mich herzlich bei allen bedanken, die bei der Entstehung dieser Arbeit auf unterschiedlichste Weise geholfen haben. Zu allererste danke ich Frau Prof. Dr. Martina Pohl. Danke dafür, dass ich an diesem Thema arbeiten durfte und danke für die herausragende Betreuung und Unterstützung. Bei Herrn Prof. Wolfgang Wiechert möchte ich mich für die Möglichkeit bedanken, in Jülich arbeiten zu dürfen und für die Unterstützung der Arbeit. Ebenso danke ich Herrn Prof Dr. Michael Bott für die Übernahme des Koreferats.

Bei der gesamten Arbeitsgruppe Biokatalyse des IBG-1 unter Leitung von Frau Prof. Dr. Dörte Rother und Frau Prof. Dr. Martina Pohl möchte mich bedanken. Auch als zeitweise einziger Biosensor unter lauter Katalysatoren habe ich mich immer unterstützt gefühlt. In diesem Zuge möchte ich mich auch bei den technischen Mitarbeiterinnen der Gruppe bedanken. Vielen Dank Heike Offermann, Doris Hahn, Lilia Arnold, Ursula Mackfeld und Ilona Frindi-Wosch! Ohne euer geballtes Wissen und die unschätzbaren Erfahrungen hätte so manches sicherlich bedeutend länger gedauert, so es denn überhaupt geklappt hätte. Auch allen übrigen Mitgliedern der Gruppe sei gedankt, sowohl für die Hilfe im Labor oder Büro als auch für die fruchtbare und angenehme Arbeitsatmosphäre.

Mein spezieller Dank gilt Frau Dr. Victoria Steffen. Du hast es schon im Rahmen meiner Masterarbeit geschafft, mich für Biosensoren zu begeistern und die Unterstützung jedweder Natur nahm auch später nicht ab, nicht mal nach einem Wechsel in eine neue Stelle.

Neben der Wissenschaft und der Arbeit in Jülich gibt es auch weitere Aspekte im Forschungszentrum für die ich dankbar bin. Durch die Teilnahme an angewandter Biotechnologie im Rahmen von JuBräu sind auch gruppenübergreifend einige Kooperationen entstanden, ohne die diese Arbeit nicht so erfolgreich gewesen wäre. Daher auch ein herzliches Dankeschön an alle aktuellen und früheren Mitbrauer. Vielen Dank auch an Roman Jansen, Niklas Tenhaef und Christoph Westerwalbesloh. Die Kooperationen mit ihnen haben zu anderen Blickwinkeln, neuen Erkenntnissen und fruchtbaren Diskussionen geführt. Um Niklas Tenhaef zu zitieren, ihm danke ich dafür, „dass manche wissenschaftlichen Arbeiten zu mehr als Wissen führen“.

Was noch bleibt ist die unermessliche Dankbarkeit gegenüber meiner Familie, ohne meine Eltern Renate und Wolfgang Otten und meinen Bruder Phillip wäre es nie so weit gekommen. Sie haben mich in jedem Moment meines Lebens unterstützt, aufgefangen und motiviert.

1 General Introduction

1.1 Basic principle of fluorescence

In nature, multiple forms of light emission are known. The most common phenomena are grouped under the general principle of luminescence, encompassing phosphorescence and fluorescence. Sir Gabriel Stokes[1,2] was the first, who described these phenomena in 1853, while the molecular principles behind fluorescence emission were later elucidated by Aleksander Jablonski.[3] Until today the "Jablonski diagram"(Figure 1.1-1)[3] is used to describe the energetic processes and energy transfers. Fluorescent emission of light is also described as cold radiation, since the emission is not accompanied by a change in temperature.

If a fluorophore is hit by a photon, the electromagnetic radiation is absorbed by an electron within the molecule. This electron is then lifted from the singlet ground state (Figure 1.1-1, S_0) to an excited singlet state (S_1, S_2,...S_n). As the excited state is instable, the electron strives to return to the ground state, thereby losing the energetic surplus. The energy can be emitted in two ways: i) without light emission due to internal energy conversions, collisions or vibrations within the molecule or in contact with other molecules, and ii) by emission of a photon either in the form of fluorescence or phosphorescence.

In reality both mechanisms coexist, since prior to light emission, a distinct amount of energy is always lost via internal conversion, before reaching the lowest excited state (S_1), from which light emission through fluorescence or phosphorescence can occur to return to the ground state (S_0). As the emitted light is lower in energy compared to the excitation wavelength, the wavelength of the emitted light is red-shifted. This phenomenon is called "Stoke's shift".[1]

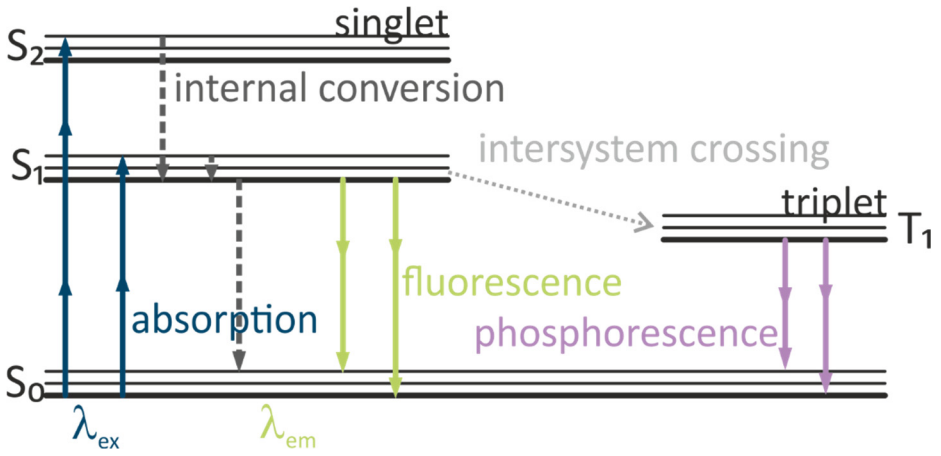

Figure 1.1-1: Jablonski Diagramm depicting the energetic conversions resulting in emission of light.[3] S_0, S_1, S_2 denote different singlet energy states of a photon. T_1 is the excited triplet state, resulting from a intersystem crossing before the occurrence of phosphorescene.

In contrast to fluorescence, which typically lasts for only nanoseconds[4], phosphorescence requires a forbidden spin transition from the singlet state to the triplet state called intersystem crossing. This very slow transition leads to emission of the absorbed energy in timescales between 1s to 1000 s.[5] The average duration of emission, also called fluorescence lifetime τ, is a characteristic parameter for each fluorophore and is used in imaging techniques, like fluorescence lifetime imaging microscopy (FLIM) to analyze e.g. cellular structures.[6]

1.1.1 Förster Resonance Energy Transfer (FRET)

The main fluorescence phenomenon used in this work is Förster Resonance Energy Transfer or FRET.[7] In contrast to other fluorescence-based techniques, like FLIM, at least two fluorescent molecules with different excitation and emission wavelengths are needed. If the emission wavelength of the so-called FRET donor overlaps with the excitation wavelength of the FRET acceptor (Figure 1.1-2a), both can show fluorescence, if only the donor is exited. Under optimal conditions the absorbed electromagnetic energy can be s transferred radiationless to the acceptor via dipole-dipole interactions.[7] The stronger the spectral overlap, the higher the potential for efficient FRET. This so-called FRET-efficiency describes the share of energy absorbed by the donor and transferred to the acceptor[8].

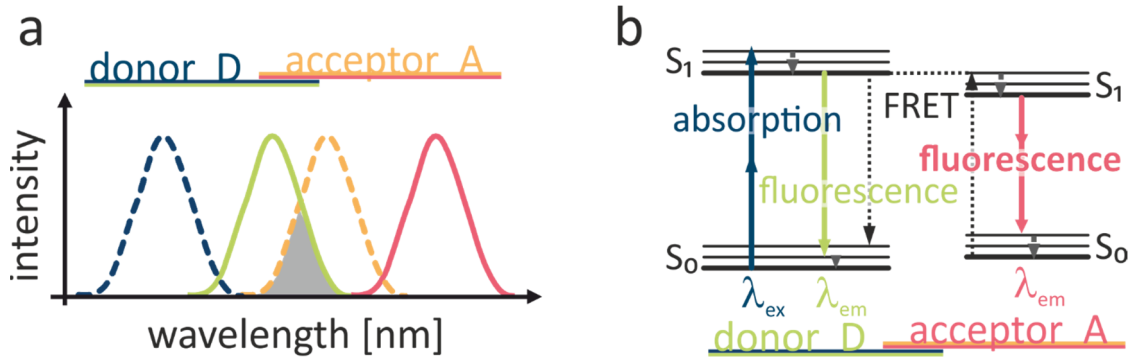

Figure 1.1-2 a: Spectral overlap between the emission and exitation spectra of donor and acceptor. The greater the overlap integral (grey) between emission spectrum of the donor and exitation spectrum of the acceptor, the more energy can be transferred via FRET. b: Extension of the Jablonski diagramm. Schematic presentation of the energy transfer via FRET between donor and acceptor.

With the spectral overlap as main prerequisite, the FRET-efficiency is additionally influenced by the distance between the FRET-partners, as well as their relative orientation. Typically, distances between 1 and 10 nm enable the necessary dipole-dipole interaction. The closer the dipoles approach, the stronger the energy transfer will be. The same holds true also for the orientation of the dipole moments: in a parallel orientation of both dipoles, the transfer efficiency is higher than in an antiparallel orientation. Due to the strong distance dependence, FRET is often

referred to as a molecular ruler. This “ruler function” can be used to quantify distances between organic molecules, especially using genetically encoded fluorophores. The distance at which energy transfer is 50% efficient (i.e., 50% of excited donors are deactivated by FRET) is defined by the Förster radius The magnitude of the Förster radius is dependent on the spectral properties of the donor and acceptor fluorophores.[9]

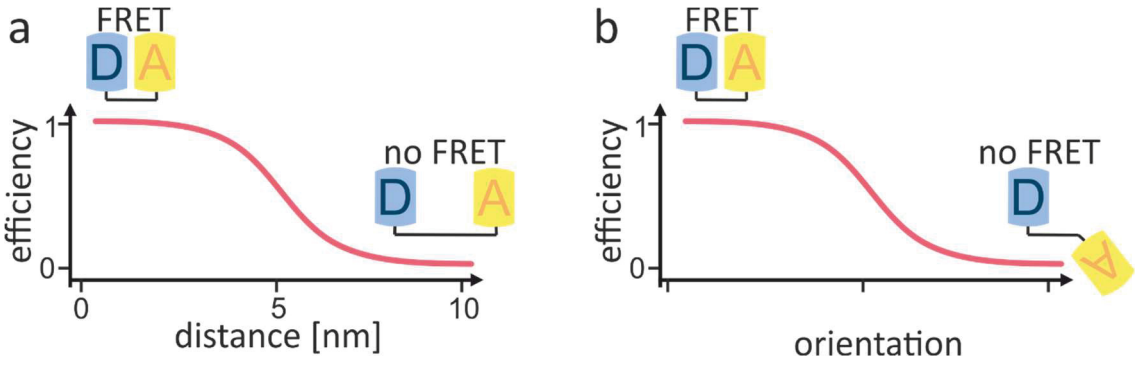

Figure 1.1-3: Prerequisites for high FRET efficiency. (a) FRET occures below 10 nm distance . The closer Donor (D) and Acceptor (A) are, the more energy can be transferred. (b) A parallel orientation of the dipole moments is also crucial for high energy transfer.

1.1.2 Green fluorescent protein

In nature many different fluorescent organic and inorganic compounds can be found. One example are proteins. In 1962 a famous form of fluorescent protein was first isolated and described: the Green Fluorescent Protein (GFP) originating from the jellyfish *Aequorea victoria*.[10] In its natural function, GFP interacts with Aequorin in the rim of the jellyfish. Aequorin is sensitive to Ca^{2+} ions and emits blue light with increasing Ca^{2+} concentration. Resonance energy transfer to the GFP results in an additional green emission (408 nm), shifting the overall emitted color of the jellyfish towards a greener appearance. After its discovery, it took almost another 30 years to produce a functional recombinant GFP version. Martin Chalfie was able to successfully introduce the coding gene of GFP into *Escherichia coli* and *Caenorhabditis elgans.*[11] From there on GFP became evermore important in almost any field of biology. Today further FP variants from different organisms are known and most colors of the visible and infrared spectrum of light can be covered with a specific GFP derivative.[12] The importance of GFP was highlighted with the Nobel prize in 2008, honoring the work of Osamu Shimomura, Martin Chalfie and Roger Y. Tsien.[10,11,13–16]

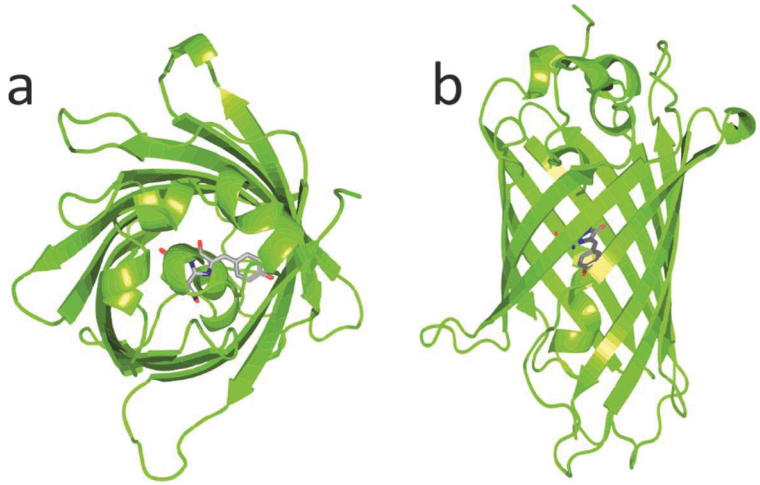

Figure 1.1-4: Structure of the Green Fluorescent Protein (GFP) from top (a) and sideview (b). The chromorphor is located inside a barrel formed by 11 β-sheets. (image created with PyMol using PDB code:2Y0G).

All fluorescent proteins of the GFP family show a very similar structure, independent of their original organism. The central chromophore, or more specific the fluorophore, is nested within a barrel formed by 11 antiparallel β-sheets protecting the fluorophore, as demonstrated in Figure 1.1-4. While the barrel is formed early during translation, the fluorophore needs time to maturate posttranslational. In wildtype (wt) GFP the amino acids S65, Y66 and G67 form the fluorophore. The autocatalytic formation starts with a cyclization, followed by a dehydrogenation and finally ends with an oxidation under consumption of atmospheric oxygen (see Figure 1.1-5).[17,18] The resulting β-hydroxybenzyliden-5-imidazolinon (β-HBI) contains a conjugated π-electron system (see Figure 1.1-5, green).Especially the last step is rate-limiting for the maturation of the GFP chromophore and can only occur under sufficient oxygen supply. Therefore, many approaches on optimizing GFP-like proteins aimed at reducing the maturation time.[19]

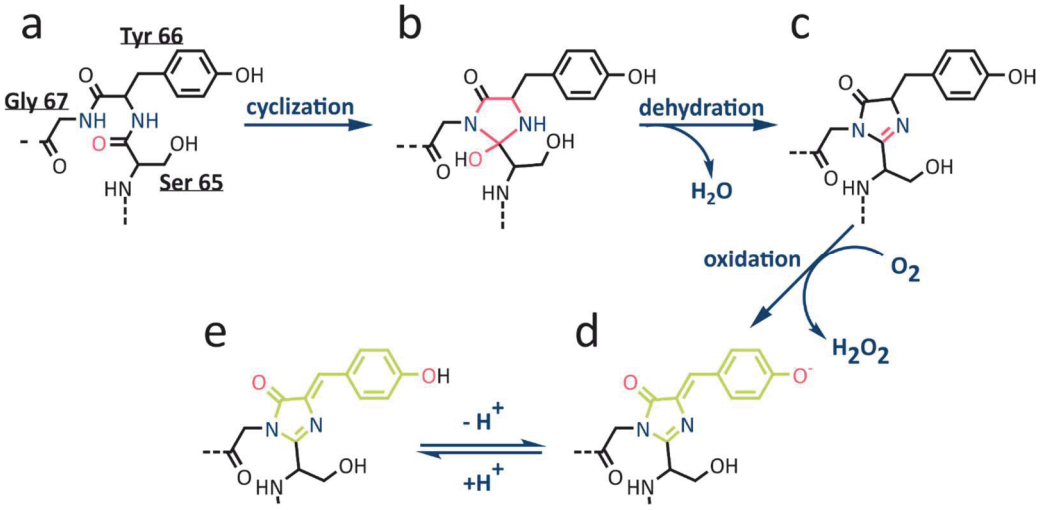

Figure 1.1-5: Mechanism of fluorophore maturation in GFP. (a) Ser65, Tyr66 and Gly67 form the fluorophore in GFP. Maturation starts with cyclization of the spine (b, red) followed by dehydration (c) which results in an imidazolinone. The final oxidation (d) forms conjugated bonds between the phenol and the imidazolinone (modified from Ref.[13,17,20]). Protonation (e) and deprotonation of the fluorophore result in two distinct emission maxima.

As mentioned above, there are many GFP-like color variants, either found in nature or created by protein engineering. Roger Tsien could demonstrate that the molecular environment and the fluorophore-forming amino acid residues are most important for the emission and absorption properties.[16] Based on their emission the multitude of variants can be grouped in seven clusters: blue (BFP, 440-470 nm), cyan (CFP, 471-500 nm), green (GFP, 501,520 nm), yellow (YFP, 521-550 nm), orange (OFP, 551-575 nm), red (RFP, 576-610 nm), and far red (fRFP, 611-660 nm).[21] Exchanges of the chromophore-forming amino acids resulted for example in BFP, where serine was exchanged by threonine and tyrosine was replaced by tryptophan (see Figure 1.1-5), resulting in a significant blue shift in emission. Additionally modifications of residues forming the barrel were performed, mainly to enhance certain properties. These “enhanced fluorescent proteins“ (eFP) show improved stability towards pH, temperature and ion concentrations, they feature higher quantum efficiencies, faster maturation or improved folding properties.[12,21,22]

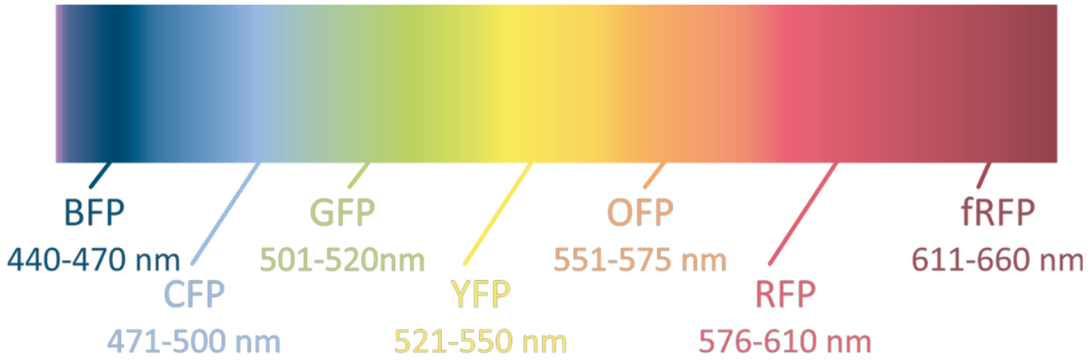

Figure 1.1-6: Spectral classes of fluorescent proteins (FP) sorted by increasing wavelength: blue (BFP), cyan (CFP), green (GFP), yellow (YFP), orange (OFP), red (RFP) and far red (fRFP).

Fluorescent proteins (FP) have been used in many different applications. For example they were used as markers to unravel the structure of mice brains on a cellular level.[23] Apart from being used as fluorescent markers, FPs can be utilized in biotechnological approaches. Fusion of an FP to transcription factors enables an accelerated screening of microbial strains by fluorescence activated cell sorting (FACS).[24] FPs can also be used to follow cell growth or production of target compounds like amino acids via quantification of the fluorescence.[24] These techniques usually employ only a single FP. With more than one FP also the principle of FRET is accessible. By choosing the right color combination, the spectral overlap can be maximized. Here, the combination of blue and yellow variants is especially useful. In this work, mainly two variants of GFP were used: mTurquoise2 (cyan) and Venus (yellow), which are described in more detail in the following.

The cyan mTurquoise2 was designed in an rational approach to maximize the quantum yield, based on evaluations of earlier described CFP variants.[25] Like all CFP variants, this FP carries the characteristic Y66W exchange (see Table 1.1-1). Substitution of the phenol side chain by an indole residue resulting in a blue shift of the absorption.[26,27]

Table 1.1-1: Modifications in the two fluorescent proteins used in this work. Exchanges are denoted in the one letter code and numbered relative to wt GFP. The amino acid exchanges affecting the change in color is highlighted in bold. The spectral color of the resulting FP is highlighted.

FP	Incorporated exchanges relative to wt GFP
mTurquoise2	F64L, **Y66W**, S72A, N146F, H148D, M153T, V163A, S175G, A206K, H231L
Venus	F46L, F64L, S65G, V68L, S72A, M153T, V163A, S175G, **T203Y**, H231L

In order to prevent dimerization the exchange A206K was introduced,[28] brightness was increased by the F64L and S72A exchanges.[28] Apart from H231L, which had no apparent effect,

all other substitutions were introduced to increase the photo stability, fluorescence life time (N146F) and to optimize folding properties.[29] With these improved properties mTurquoise2 is the ideal FRET partner for yellow color variants.[25] In this thesis Venus[30] was used, carrying the characteristic T203Y exchange to shift the emission from green to yellow (Table 1.1-1)[31]. Even though position 203 is not part of the fluorophore, introduction of a tyrosine at this position presumably results in π-π stacking with the phenol side chain of Y66 in the fluorophore.[32] This red-shifts both, emission and absorption, resulting in yellow fluorescence. The exchange F64L resulted in a faster maturation at 37°C,[30] while S65G increased the quantum yield.[13] Some of the most important properties of m Turquoise2 and Venus are collected in Table 1.1-2

Table 1.1-2: Characteristic properties of mTurquoise2 and Venus according to the original characterizations in literature (Ref. [25,30]).

	mTurquoise2[25]	**Venus**[30]
max absorption (λ_{ex})	434 nm	515 nm
max emission (λ_{em})	474 nm	528 nm
mol. extinction coeff. (ε)	30,000 $M^{-1}cm^{-1}$	92,200 $M^{-1}cm^{-1}$
quantum yield (ϕ)	0.93 ±0.02	0.57
pK_a	3.1	6.0

1.2 Genetically encoded biosensors

A biosensor is a system utilizing a biological sensing element connected to a transducer.[33] This definition holds true since 1987 and covers a very broad range of possible sensor constructs. The sensing unit can be derived, for example from enzymes, tissues, whole cells, membranes, antibodies, receptors or organelles.[33] A transfer of a detection event to the transducer generates a physiochemical signal that can be monitored. Because of this variety, biosensors are versatile tools for biotechnological applications. Apart from signaling via electrochemical processes, like in the most famous example, blood sugar detection for diabetes patients, optical biosensors are promising tools. In recent years such sensors have, for example, been used for intracellular metabolite analysis, oxygen quantification, and pH detection in microbial cultivations, and for phenotyping experiments in small- and microscales.[34–38] As proteins, FPs are genetically encoded, which enables their application also inside living cells.[39] Genetic fusion of a FP-encoding sequence to e.g. the gene encoding a receptor protein enables co-production of both, the receptor protein and the respective sensor.[24] When the expression of the receptor is triggered, so is the FPs, which can then be detected. Most genetically encoded sensors rely on coupling transcription factors (TF) to FPs.[24] This type of sensor indicates the activity of genetic elements and is produced when the respective gene is induced by, e.g. a target compound

produced by the cell. TF-based sensors are commonly used in single cell analysis, like fluorescence activated cell sorting (FACS)[38,40] or in picolitre scale bioreactors.[41] Nevertheless, they can only provide limited quantitative and temporal information. While the fluorescence intensity of GFP-like proteins is strongly influenced by their immediate environment, quenching metabolites can artificially decrease the signal and lead to false negative results. Additionally the posttranslational maturation of the FPs results in a temporal gap between expression of the TF - FP fusion and the detection of the fluorescent signal.[30] Even though, eFPs with faster maturation time are available, most commonly used variants still need maturation times in the range of at least 10 minutes at 37°C to reach 50 % maturation.[19] For example, when produced by *Escherichia coli*, the two FPs used in this work (mTurquoise2 and Venus) need 95.1 ± 9.3 minutes and 57.7 ± 5.2 minutes to reach 90 % maturation at 37°C, respectively.[19]

1.2.1 FRET-based biosensors

A special type of genetically encoded biosensors are FRET-based sensors. As describes above, FRET can occur between two FPs, with the transfer efficiency being depended on their distance and orientation (see 1.1.1). FRET-based sensors generate a ratiometric signal from the two fluorescence intensities emitted by donor and acceptor, which is independent of their concentration. The most simple model of such a FRET-based sensor consists of two GFP derivatives connected by a polypeptide, harboring an endonuclease cleavage site.[20] This type of sensor can be used to sense the presence of a specific endonuclease: upon cleavage of the polypeptide, the distance between the FPs changes and no more FRET occurs. In contrast, the use of specific recognition elements, for e.g. target metabolites, as a connecting part between two FPs enables concentration-dependent FRET-effects. An example for such a FRET-based sensor is based on the Ca^{2+} binding protein Calmodulin.[42,43] The binding of Ca^{2+} induces a conformational change in the Calmodulin, which presumably alters the orientation or distance of the FRET-pair, fused to either end. This changes also the transfer efficiency form the donor to the acceptor.

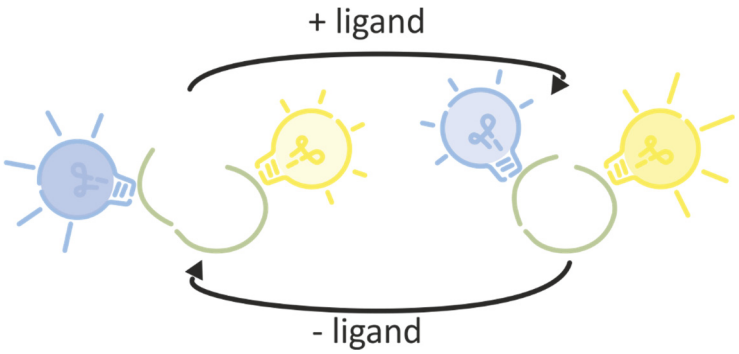

Figure 1.2-1: Schematic presentation of the functional principle of a FRET-based biosensor. Binding of a ligand induces a conformational change of the sensor, which alters the FRET-efficiency and results in changes in fluorescence intensities.

In many modern biosensors, periplasmic binding proteins (PBP) are used as sensing elements. PBPs constitute a large family of proteins found in the periplasm of gram-negative bacteria. They assist in transport and recognition of various metabolites via the cell membrane and are commonly part of receptor- or transporter complexes.[44] Due to their common functionality, PBP show a highly conserved tertiary structure consisting of two globular domains connected by a hinge region.[44,45] Binding of the ligand to the ligand binding site at the hinge region induces a conformational change, best described by comparison to a "Venus fly-trap"[44] Classically PBP can be clustered in three main classes, specifically based on the hinge region. While in class I the domains are connected via three strands, class II PBPs feature two connecting strands. The third class is characterized by only a single α-helix as connecting element.[46] PBP from all three classes can in principle be utilized in biosensors and many have already been used.[34,47,48] In these sensors, the conformational change of the PBP induces an altered FRET-efficiency (see Figure 1.2-1). This can be measured in form of a FRET-ratio (R). Alteration of the FRET-efficiency also alters the fluorescence intensity (I) of donor and acceptor, which can be expressed as ratio (*R*):

$$R = \frac{I_{acceptor}}{I_{donor}} \quad (1)$$

By expressing the signal as a ratio, the output of a sensor is less affected by variations in sensor concentration and is therefore more robust compared to the signal generated by a sensor with only one single fluorescence signal. Upon measuring the FRET-ratio for different ligand concentrations and plotting them as a function of the logarithmic ligand concentration [L], the binding isotherm of a specific sensor can be deduced (Figure 1.2-2a). These typically S-shaped plots allow the determination of several characteristic parameters: The difference between the maximum FRET ratio [R_{sat}], typically at saturation, and the ratio without ligand [R_0] describes the sensitivity of the sensor [ΔR] (Figure 1.2-2b), the inflection point of the curve reveals the affinity for the ligand [K_d]. The approximately linear region of the curve describes the dynamic range, in

which the correlation between FRET ratio and concentration is quasi-linear (on a logarithmic scale). Given a ligand excess, the affinity K_d can be calculated analogue to the Michaelis constant (K_M) of a Michaelis-Menten kinetic as demonstrated in Figure 1.2-2 c

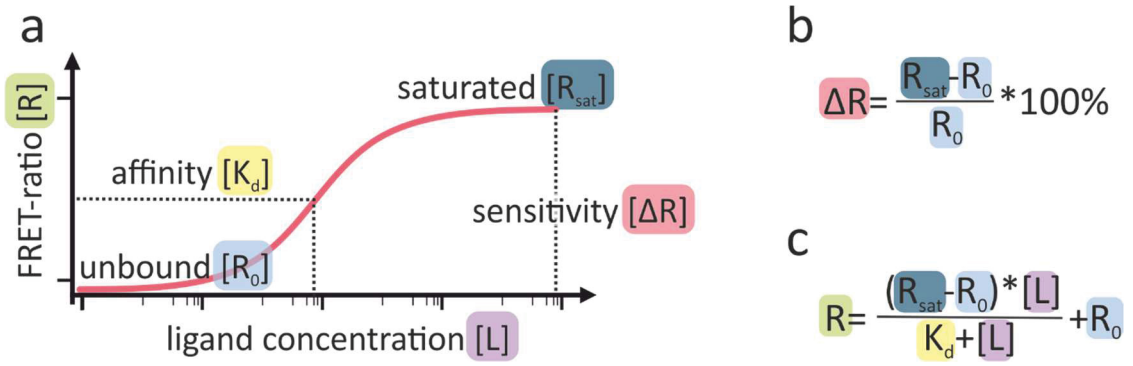

Figure 1.2-2a: Schematic presentation of a binding isotherm explaining the sensor parameters sensitivity [ΔR] and affinity [K_d] (at 50 % saturation). b: Formula used to calculate the sensitivity of a sensor. c: Formula used to calculate the affinity of a sensor. Characteristic variables were color-coded for visualization purposes.

1.3 FRET-based glucose detection

The periplasmic glucose-galactose-binding protein (GGBP) was used in the present work to develop a glucose sensor. Being part of the first specific chemo transporter identified in bacteria, GGBP originates from *E. coli,* encoded by the gene *mglB.*[49] The native binding protein binds D-glucose with a high affinity of ~290 nM through 13 hydrogen bonds, which are formed between the polar side chains in the glucose-binding site and the hydroxyl groups as well as oxygen residues of the sugar.[50] The resulting conformational change closes the binding protein by 31° in the opening cleft, as was deduced from respective crystal structure analyses.[51] Compared to other glucose binding proteins from other organism are known, e.g. from *Thermotoga* maritima[52] or *Salmonella typhimurium*[53], GGBP has been studied in great detail.[49–51,53,54] This large conformational change makes the GGBP ideal for the application in a FRET-based glucose sensor.

A first version of this glucose sensor was developed by Fehr *et al.* through fusing the GGBD between an enhanced cyan fluorescent protein (eCFP) and a yellow fluorescent protein (eYFP).[55] Introduction of mutations into *mglB* resulted in the sensors FLIPglu-170n and FLIPglu-600µ with affinities of 170 nM and 0.59 mM for glucose, respectively.[55] Based on these initial constructs multiple glucose sensors were produced, either by means of mutations in the binding protein or by alternating the construction scheme. One optimization attempt was to shift the cyan donor FP from the N-terminus closer to the GGBP binding site by integrating the FP between the 12th

and 13th residue of the GGBD. This resulted in the sensor FLII12Pglu-600µ, with a greatly increased ΔR, whilst retaining the affinity of K_d= 0.6 mM.[56] This sensor is used today in different intracellular applications and cell types [57–61] and the design principle is also used in this work. Nevertheless, as in recent years progress was made to engineer GFP derivatives that are less sensitive towards changes in their surrounding environment, donor and acceptor have been exchanges for the sophisticated FRET-pair mTurquoise2 and Venus[25,30,62].

1.3.1 Application of FRET-based biosensors

FRET-based biosensors founded on PBPs have been used in a range of different studies over the past years, mostly to detect concentration changes or quantify intracellular metabolites.[21,63] Despite their popularity, their application *in vivo* has distinct drawbacks. As was earlier demonstrated in our working group "Enzymes & Biosensors" at IBG-1, Forschungszentrum Jülich, the focus on characterizing two FRET-based sensor (glucose and maltose sensor) pointed out, that especially cellular metabolites like ATP and NAD, have a significant influence on this type of biosensor.[64,65] Additionally, the crowded intracellular milieu has an effect on the FPs as well as on the entire sensor. Especially YFPs have shown to be sensitive towards crowding.[66] Considering that the signal of a FRET-based biosensor is dependent on changes in distances of the FPs, it becomes evident that a crowded environment, as found inside cells, will likely compact the flexible sensor and therewith influence the FRET.

While FRET-based sensors offer great potential to elucidate dynamic cellular processes by measuring relative concentration changes, quantitative approaches require extensive calibration.[64] Besides intracellular applications, such FRET-based sensors were not characterized for *in vitro* applications, although the less complex environment, e.g. in cell supernatants, often enables calibration and thus quantification of target metabolites. Therefore we focused on the application of theses sensors as extracellular tools. This mode allows the use of defined media or buffers to characterize the sensor for a specific application, minimizing affection of the sensors. The functionality of this approach has already been successfully demonstrated with a FRET-based lysine sensor.[67] This sensor was used to quantify the product titers of a *Corynebacterium glutamicum* lysine producer.[67]

1.4 Measurement techniques

In the following, the different photometric techniques to detect and quantify fluorescence used in this work are briefly introduced. All four systems show a common principle: A light source is used to excite a sample, the resulting emitted light is than detected. Depending on the technique, the sample size varies from mL down to pL. The smaller the volume, the higher must be the resolution down to resolving single fluorescent molecules. Highly sensitive detectors are used in cultivation devices or microscopes to monitor growth and performance of microbial producers.

1.4.1 Plate-based spectroscopy

By far one of the most common devices in biotechnological labs are spectrophotometers. While classical photometers usually utilize cuvettes, modern plate-based spectrophotometers operate with micro titer plates, thereby drastically increasing the throughput. Additionally, most devices are multimode, enabling measurements of fluorescence as well as absorption and luminescence. Most devices use monochromator-based optics for a precise recording of spectral data. These qualities make a plate-based spectrometer ideal for characterization of FRET-based biosensors *ex vivo.* Due to the high throughput, a multitude of assays and combinations of sensors with e.g. media or possible ligands can be performed in relatively short time.

1.4.2 Confocal microscopy

Despite their superiority in throughput, plate-based photometers are limited to the detection of fluorescence resulting from ensembles of sensors. In order to investigate fluorescence and FRET on the level of a single sensor molecule, higher sensitivity is needed. Therefore, confocal microscopy is used. Precise excitation is granted by using pulsed lasers as light source and additional utilization of filters e.g. via dichroic mirrors. While in the classical light microscopy, a large area of a specimen is illuminated, in confocal microscopy the light is further focused through a pinhole. Therewith, only the area in the focal point is illuminated, which drastically increases the contrast. High contrast is highly desired in e.g. FLIM or FRET applications. The high sensitivity of this system can be used in single molecule (sm) spectroscopy. When using a minute sample size (fL to pL) and a highly diluted sample, one molecule at a time will diffuse through the focal point of the microscope and the emission of each photon can be detected. This technique is used to determine distances and FRET-efficiencies within molecules.[68]

1.4.3 Fluorescence in small scale cultivations

Combination of a cultivation device with spectroscopy resulted in microbioreactors like the BioLector®.[69] Here the miniaturized cultivation of up to 48 microbial cultures can be performed in parallel in micro titer plates. Apart from controlling temperature, humidity, and shaking frequency the devices allow optical readout, such as scattered light and fluorescence.[69] An optical system can reach each well of a micro titer plate. Usage of optical filters enables the detection of different fluorescence wavelengths at a time. While prototype cultivation devices equip each well of a 48 well plate with an optical fiber for constant, parallel measurements, commercially available systems measure one well and filter after another, limiting the temporal resolution.[70] Nevertheless, cultivation in small scale limits the process data gained due to volume restrictions. Established sensors for oxygen and pH was well as TF-based fluorescent sensors demonstrate the potential of combining fluorescence-based analytics with cultivation to facilitate strain and process development.[69,71,72] Volume is even more restricting in the microfluidic scale. Reducing the volume of a bioreactor to µL or pL renders sampling for offline analysis impractical. Yet, micro chips as bioreactors show great potential.[38,73,74] However, there is currently no method to analyze the metabolites in the environment of microbial cells in such chips. To develop a sensor applicable in such small volumes was one task of this thesis.

1.5 Aim of this thesis

Aim of this thesis was to enable the application of FRET-based biosensors as a tool for quantification of metabolites in small scale microbial cultures, using a FRET-based glucose sensor as an example.

A toolbox of FRET-based glucose sensors should be created to modulate the affinity and sensitivity by the introduction of linker sequences between the GGBP and the FPs. Thereby the FRET efficiency and ΔR should be maximized by modulating the distances and flexibility of the FPs. For the extracellular application sensors with altered affinities are needed, to measure in different concentration ranges. From this toolbox sensors with large ΔR would be used for further in-depth characterization.

Optimized glucose sensors will subsequently be applied in microbial cultivations of two platform organism: *Corynebacterium glutamicum* and *Escherichia coli* in the mL scale to broaden the analytic options of miniaturized bioreactors like the micro titer plate-based system BioLector®. Due to limitations in size and volumes, so far only a limited number of process parameters can be recorded in these systems. The FRET-based glucose sensor should be applied to quantify the consumption of glucose in such a system. In this regard, also the stability of the sensor is important. A previously characterized lysine sensor lacked long time stability.[67] Here immobilization of the FRET-based glucose sensor should be tested to solve this problem. Additionally, the application of the glucose sensor should also be extended to the µL scale. In bioreactors of only a few nano- or picolitre volume quantification of metabolites is hard by traditional approaches. As intracellular TF-based fluorescent biosensors have already been successfully used in this scale, the application of an extracellular FRET-based glucose sensor is promising.

2 Results

In the following section, the results are collected in the form of already published publications or in the form of manuscript. Each chapter is introduced with a brief summary stating the relevance of the data in context to this thesis and the contributions of all authors are given.

2.1 Sensor optimization and single-molecule studies.

The following results were published as:

Genetically Encoded Förster Resonance Energy Transfer-based biosensors Studied on the Single-Molecule level

Henning Höfig[1,2], Julia Otten[3], Victoria Steffen[3], Martina Pohl[3], Arnold J. Boersma[4], Jörg Fitter

ACS Senors 2018
Volume 3, Issue 8
Pages 1462-1470

The manuscript was adapted to the layout of this thesis, without any alterations of the content.

Context:

A toolbox of nine genetically encoded FRET-based glucose sensors was constructed and characterized. The toolbox was generated by introducing two different linker sequences between the GGBP and the FRET partners in different combinations. Apart from determination of affinity (K_d) and sensitivity (ΔR), the sensors were analyzed on the single molecule (sm) level. The smFRET measurements were applied to determine the energy transfer efficiencies of the different sensor variants. Differences between well performing sensors with large ΔR and less well performing sensors with small ΔR were identified. Additionally, the effect of molecular crowding on the sensor performance was evaluated. A sensor with a flexible linker between the donor FP and GGBP (sensor no. 2) displayed superior sensitivity (ΔR). In accordance to ensemble measurements, smFRET measurements demonstrated that this sensor displayed large differences in transfer efficiencies in the liganded and non-liganded state as a prerequisite for good performance.

Contributions:

Julia Otten and Victoria Steffen developed and constructed the biosensor toolbox and determined affinities and sensitivities. Henning Höfig, Jörg Fitter, Martina Pohl, and Arnold Börsma designed and planned the experiments. Henning Höfig performed the smFRET measurements, Henning Höfig and Jörg Fitter evaluated the smFRET data. Hennig Höfig and Jörg Fitter wrote the manuscript in consultation with all authors.

Genetically Encoded Förster Resonance Energy Transfer-based biosensors Studied on the Single-Molecule level

Henning Höfig[1,2], Julia Otten[3], Victoria Steffen[3], Martina Pohl[3], Arnold J. Boersma[4], Jörg Fitter [1,2,*]

[1] RWTH Aachen, I. Physikalisches Institut (IA), Aachen, Germany
[2] Forschungszentrum Jülich, ICS-5: Molecular Biophysics, Jülich, Germany
[3] Forschungszentrum Jülich, IBG-1: Biotechnology, Jülich, Germany
[4] Groningen Biomolecular Sciences and Biotechnology Institute, University of Groningen, Netherlands

* Correspondence should be addressed to fitter@physik.rwth-aachen.de Tel.: +49 241 80 27209 Fax: +49 241 80 22331

Keywords: glucose sensor, crowding sensor, single molecule FRET, conformational change, chromophore maturation

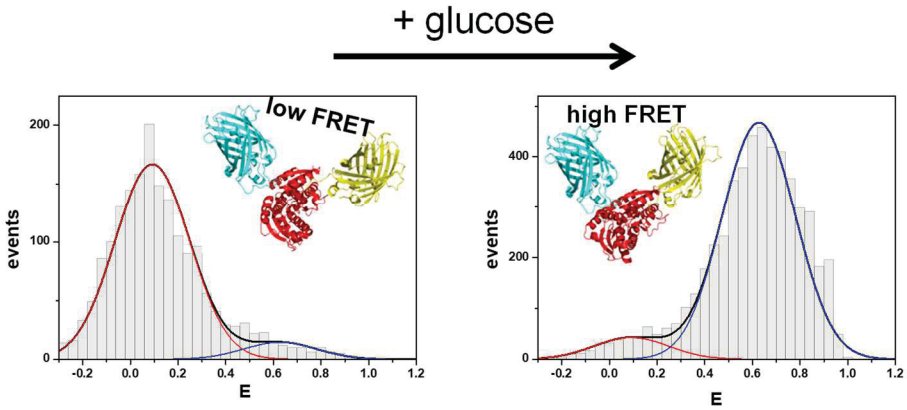

2.1.1 Abstract

Genetically encoded FRET-based biosensors for the quantification of ligand molecules change the magnitude of Förster Resonance Energy Transfer (FRET) between two fluorescent proteins upon binding a target metabolite. When designing highly sensitive sensors extensive sensor optimization is essential. However, it is often difficult to verify the ideas of modifications made to a sensor during sensor optimization process due to the limited information content of ensemble FRET measurements. In contrast, single-molecule detection provides detailed information and higher accuracy. Here, we investigated a set of glucose and crowding sensors on the single-molecule level. We report the first comprehensive single-molecule study of FRET-based biosensors with reasonable counting statistics and identify characteristics in the single-molecule FRET histograms that constitute fingerprints of sensor performance. Hence, our single-molecule approach extents the toolbox of methods aiming to understand and to optimize the design of FRET-based biosensors.

2.1.2 Introduction

Genetically encoded FRET-based biosensors are powerful analytical tools that can for example recognize the presence of specific small molecules or sense environmental conditions in vivo[1]. The sensors are fusion proteins that consist of a central sensing protein flanked by two fluorescent proteins. The optical read-out of the sensor is based on Förster Resonance Energy Transfer (FRET) between the fluorescent proteins that changes upon ligand binding to the sensing protein or due to other environmental impacts. There are various strategies how to optimize a sensor (i.e. increasing the change in FRET) concerning the central sensing protein, the fluorescent proteins (FPs), and linker sequences between them[1, 2]. However, a detailed molecular understanding of how a certain sensor modification affects FRET is lacking and is still an object of investigation[3-5]

A frequently employed application of FRET-based biosensors is the detection of intracellular metabolites. Prototypical examples of these sensors are those based on periplasmic binding proteins (PBPs) as the ligand binding protein and make use of the Venus-fly trap-principle[6-8]. According to Förster's theory, a substantial change of FRET is only accomplished if ligand binding alters the distance and/or the relative orientation between the chromophores of the FPs[9, 10]. This can be achieved by modification of the polypeptide linkers that connect the FPs to the ligand binding protein. However, one reason for difficulties in achieving sufficient sensor performance is the limited information content of ensemble FRET data which makes it hard to relate the impact of sensor modifications to the ideas that guide them.

Therefore, in this publication we present a new approach making use of single-molecule analysis to characterize different FRET-based sensors in more detail. Our approach benefits from the fact that single-molecule FRET (smFRET) can discriminate between coexisting conformational states in solution. Furthermore the use of confocal multi-parameter fluorescence detection delivers data of improved accuracy in determining the energy transfer efficiencies and in resolving contributions from distinct population as compared to usual ensemble measurements[11]. Thereby, we focus on sensors that use cyan and yellow FPs as a FRET pair. We demonstrate the potential of our approach by a comparative analysis of different variants of a glucose sensor which strongly vary with respect to their sensing performance. Furthermore, one glucose sensor variant and two recently developed specific crowding sensors[12] were investigated under crowding conditions. The related smFRET histograms exhibit a clearly different response to crowding as compared to glucose. In summary, each smFRET histogram displays a specific fingerprint of the respective sensor properties and elucidates the sensor's operating principles.

2.1.3 Materials and methods

a) Sensor constructs

Construction of nine investigated glucose sensor constructs with different linker properties was performed as described by Steffen et al.[13] The design of the sensor prototype (no. 1) is based on the composition of the sensor FLII12Pglu 600μ[9], with altered FP variants for improved fluorescent properties (see Fig. 1). Furthermore, additional amino acids flanking the central binding protein were inserted via restriction sites necessary for the cloning strategy (see SI Experimental Section for more details).

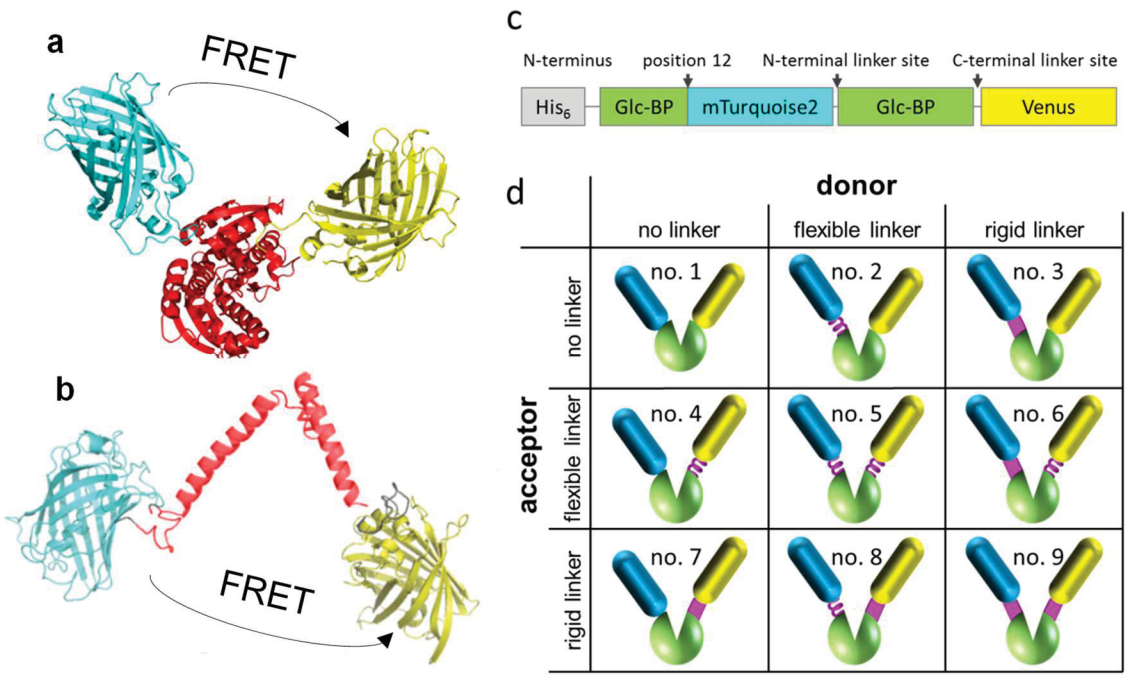

Figure 2.1-1: Graphical illustration of investigated biosensors. (a) Glucose sensor consisting of binding domain (red) equipped with donor (cyan) and acceptor (yellow) FPs. (b) Crowding sensor GE with linker domain (red) fused to donor (cyan) and acceptor (yellow) FPs. (c) Construction of the sensors composed of glucose-binding protein (Gl-BP), with inserted mTurquoise2 (donor) and Venus (acceptor). N-terminal and C-terminal linkers are taken from the linker toolbox (no linkers, flexible or rigid linkers). (d)Several applications of the toolbox approach are shown for combinations of flexible linkers, depicted as a purple helix, and stiff linkers, presented as a purple cylinder. All sensors carry additional amino acid sequences next to the central binding protein originating from restriction sites and an N-terminal His_6-tag (Tab. S1).

The studied crowding sensors consist of either an unstructured linker peptide with a length of 54 amino acid residues (G18) or α -helical peptide linker with a total length of 118 residues (GE), the latter shown in Fig. 1b. In both cases these linker elements were sandwiched between a

mCerulean3 donor and mCitrine acceptor. The sequences of the crowding sensor constructs G18 and GE can be found in ref.[14] Further details on sensor production and sample preparation are given in the SI Experimental Section.

b) Ensemble fluorescence measurements

Isothermal binding curves of the glucose sensors were determined in a microtiter plate spectrofluorimeter as described earlier[13]. Per well, 50 µl of sensor solution was mixed each with 50 µl of 24 different glucose solutions (20 mM MOPS, pH 7.3, final glucose concentrations 1 µM – 1.25 M). The ensemble characterization of a FRET-based biosensor (sensor concentration 1 µM) was performed by an intensity-based read-out. Upon donor excitation (at 420 nm) the typical double-peaked fluorescence emission spectrum was observed with emission maxima at 472 nm for the donor (I_D) and 524 nm for the acceptor (I_A), see Fig. S1a. The intensity ratio R = I_A/I_D was plotted as a function of the glucose concentration [G] and fitted with a sigmoidal curve

$$R = \left(R_{max} - R_{apo}\right)\frac{[G]}{K_D+[G]} + R_{apo} \quad (1)$$

where R_{apo} is the ratio without glucose, R_{max} is the ratio at saturated glucose concentrations, and K_D is the glucose concentration at which R increased to half of its maximal rise (Fig. S1b). A possible impact of donor-only fractions on R-values and related E-values was investigated in more detail as described in the SI Experimental Section (see Fig. S2, S1d). All graphs showing R-values as a function of glucose or crowder concentrations are based on three replicate measurements if not stated differently.

c) Single-molecule FRET measurements

Major limitations for successful smFRET studies are caused by (i) photo-physical drawbacks of the FPs, (ii) by a rather strong spectral overlap between donor and acceptor emission (Fig. S3) and (iii) by a non-negligible direct acceptor excitation (Fig. S4). At least two properties of our confocal microscope setup and the subsequent data analysis were crucial for the usability of the measured data: (i) concerning the excitation wavelength for the donor, the respective dichroic mirrors and emission filters were chosen such that the corresponding Raman scattering was excluded as far as possible from the fluorescence emission channel and (ii) the use of pulsed interleaved excitation (PIE) was mandatory to eliminate donor-only contributions from the measured data[15].

Measurements with diffusing sensor constructs were performed on a confocal microscope MicroTime 200 (PicoQuant, Berlin, Germany). Briefly, two pulsed diode lasers with emitting wavelengths of 437 nm (LDH-D-C-440, PicoQuant) and 509 nm (LDH-D-C-510, PicoQuant) were

operated at a frequency of 20 MHz with an average emission power of 17 µW and 5 µW, respectively. In sample solutions with highly diluted sensor molecules (a few picomolar) one can obtain energy transfer efficiencies for every single molecule by applying a burst analysis[16,17]. The measured time traces give access to photon bursts originating from single molecules appearing as dips in the inter-photon lag and could be selected by a suitable threshold value[18]. For each selected burst, donor and acceptor photon counts (F_D, F_A) after donor excitation were accumulated and corrected. For burst with $F_D + F_A > 20$ we calculated the energy transfer efficiency

$$E = \frac{F_A}{F_A + \gamma F_D} \tag{2}$$

for each burst. The determination of the correction factor □ was accomplished by plotting the invers stoichiometry (1/S) versus E (see Fig. S5)[19]. Due to the low molecular brightness of the involved FPs we used a total measuring time of 8-10 hours to obtain a few thousand up to a few ten thousand burst for each sample condition. The corrected E-values obtained for each burst were finally histogramed, depending on the number of available bursts we chose 30-80 bins for the whole range of E-values. By using the PIE excitation scheme we were able to compare histograms including donor-only contributions and those where donor-only bursts were sorted out (see Fig. S6).

The obtained FRET histograms of glucose and crowding sensor were fitted globally with one or two Gaussian distributions (Fig. S1c). All data analysis was performed with self-written MATLAB® (R2015b, 64-bit) scripts or using OriginPro (9.0.0G, 64bit). A more detailed description of all applied procedures is given in the SI Experimental Section.

2.1.4 Results and discussion

a) Ensemble versus single-molecule FRET data

A crucial parameter for FRET-based sensors is given by the change between the minimal (R_{apo}) and the maximal (R_{max}) ratio, i.e. $\Delta R = R_{max} - R_{apo}$ (see eq. 1 and Fig. S1b). Maximizing this change (ΔR) is of utmost importance when optimizing a FRET-based biosensor. Usually such measurements are performed with ensembles of sensor molecules, resulting in binding isotherms based on ensemble-averaged R-values[8, 9]. In contrast to ensemble data, single-molecule data can provide detailed information on coexisting sensor subpopulations, which in addition permits the discrimination of heterogeneities arising from experimental artifacts or impaired sample preparations[11]. In this respect also the degree of chromophore maturation of the individual fluorescent proteins (FPs) plays a critical role, because non-fluorescent donor or

acceptor FPs leads to inoperable sensor molecules. Due to the limited molecular brightness (i.e. number of emitted photons per fluorophore molecule in a given time interval) of FPs compared to commercially available organic fluorescent dyes, reports on single-molecule FRET studies of FP-equipped biosensors are rare in literature[20, 21]. In addition, FPs are prone to photo-bleaching which impedes single-molecule detection. However, as outlined in Section Materials and Methods, and in more detail in the SI Experimental Section, we managed to obtain reasonable single-molecule data from all sensor constructs.

As already mentioned, the ratio parameter R is typically utilized to quantify the performance of a specific sensor in ensemble studies. This parameter is well suited to compare the response to different ligand concentrations of one and the same sensor. In order to compare the performances of different FRET-based sensors among each other, a parameter on an absolute scale, like the transfer efficiency E is beneficial (see Eq. 2 in the Methods section for definition of E), since it can take values between zero and one. Compared to typical smFRET histograms measured with organic fluorescent dyes attached to the protein structure, we observed a pronounced broadening of the populations well beyond the shot noise limit (see example in Fig. S1c)[22]. In addition to triplet-state formation in the fluorophores or other fast blinking processes[23] this is most probably caused by the fact that the FPs show a remaining translational and rotational mobility relative to the sensing domain on a time scale longer than the experimental observation time (i.e. a few milliseconds). In such a scenario, the sensing domain remains either in the non-liganded or in the liganded state, while in both states the slightly mobile FPs either change their relative chromophore orientation or alter their spatial distance[21].

It is obvious that successful FRET measurements require two functional FPs. In practice, the degree of the chromophore maturation in the specific FP variant depends on several factors which can be different from one sensor construct to the other. Among others, the choice of the respective FP variant, the preparation in recombinant *E. coli*, as well as the layout of a sensor construct might influence the maturation efficiency of the chromophores[24]. In particular, if the acceptor FP in a sensor molecule is non-fluorescent the measured I_D-value is artificially increased and as a result the important ΔR-value cannot reach its potential maximal value (Fig. S1d). Therefore, knowing the value of the donor-only molecule fraction in a sensor population is crucial to evaluate the performance of a specific sensor construct. Single-molecule detection offers a unique possibility to quantify the donor-only fraction. An absorption measurement can obviously yield the total amount of fluorescent donors and acceptors in a sample. However, it cannot deliver a value for the donor-only fraction since the distribution of the FPs among the individual sensor molecules is not known. Hence, we exploited the dual-color excitation on the

confocal microscope to make use of two-color coincidence detection[25,26]. This single-molecule approach enables discrimination between sensor molecules carrying two functional FPs and those which fluoresce at only one color (Fig. S6). Of course, acceptor-only molecules also weaken the read-out signal, because they do not contribute to the signal at all. However, in a FRET experiment solely donor molecules are directly excited and, accordingly, varying acceptor-only fractions do not change the value of the FRET read-out itself, e.g. the FRET ratio R or transfer efficiency E.

b) Analysis of FRET-based glucose sensors with different linkers

In order to demonstrate the capability of utilizing transfer efficiency histograms to evaluate the performance of FRET-based biosensors, we analyzed various glucose sensors constructs with a systematic variation of different linker combinations between the glucose binding domain and the flanking FPs (see Fig. 1c,d). A similar linker toolbox approach was recently used to vary the sensor properties of a FRET-based L-lysine sensor[13]. All glucose sensor constructs were characterized by binding isotherms (cf. Fig. S1b) recorded with a microtiter plate fluorimeter. Some of the applied linker modifications gave highly improved signal changes compared to the prototype sensor (see also a similar behavior for the L-lysine sensor[13]). Deeper insight was obtained by measuring three different FRET efficiency histograms: (i) in the absence of glucose, (ii) at a millimolar concentration of glucose (approximately at the K_D), and (iii) at 125 mM glucose with fully saturated sensor molecules. The obtained FRET efficiency histograms show typically two populations representing two states. Consequently, they were fitted globally with two Gaussians that had the same mean position and width for all glucose concentrations, but individual statistical weights for each population (for details SI Experimental Section).

As a starting point, the sensor prototype (no. 1 in Fig 1d) was investigated. The prototype sensor showed only a modest signal change of $\Delta R = 0.40$ (Fig. 2a). The smFRET histogram shows two strongly overlapping populations in the absence of glucose (see Fig. 2c). Both populations are already centered at rather high mean transfer efficiencies ($E_1 = 0.57$ and $E_2 = 0.79$, see Tab. S2 for all fitting parameters). With increasing glucose concentration the population at $E_1 = 0.57$ is depopulated by approximately one third, while the other population at higher transfer efficiency increased its statistical weight accordingly. For this sensor construct we could not observe significant differences between the histograms measured at K_D of 7 mM glucose concentration (Fig. 2d) and at 125 mM (Fig. 2e). In principle we would expected that the histogram for 7 mM (Fig. 2d) show a relation of the statistical weights for both populations which is in between those found in Fig. 2c and Fig. 2e. However, a combination of effects originating from a rather small ΔR-values, form a strong overlap of the involved populations in the histogram, and from the

non-linearity between R- and E-values give rise to almost indistinguishable histograms for the K_D and the saturating concentration conditions in this case.

Next, we looked at sensor no. 2, which showed the largest glucose-induced signal change of all investigated sensors (ΔR = 0.98, see Fig. 2b). Here, the donor is connected via a flexible linker to the glucose binding protein. In the absence of glucose, we observed a dominant population (92 % statistical weight) centered at a rather low transfer efficiency of E_1 = 0.09 that is well separated from a much smaller population (8 %) at a high transfer efficiency of E_2 = 0.63 (Fig. 2f). With rising glucose concentration the statistical weight of the low FRET population decreased concomitant with an increase of the high FRET population (Fig. 2g). At saturating glucose concentration the high FRET population increased its statistical weight up to 91 %, while only a small low FRET population (9 %) was left (Fig. 2h and Tab. S2*)*. According to the development of smFRET histograms upon increasing glucose concentrations, the most reasonable model assumption for the underlying mechanism is to assign the non-liganded (open) state to the low FRET population and the fully liganded (closed) state to the high FRET population. Obviously, the large difference in the performance of sensors no. 1 and no. 2 measured in ensemble (cf. Fig. 2a,b) is reflected in a strong divergence between the corresponding smFRET histograms. We also measured smFRET histograms for some further sensor constructs.

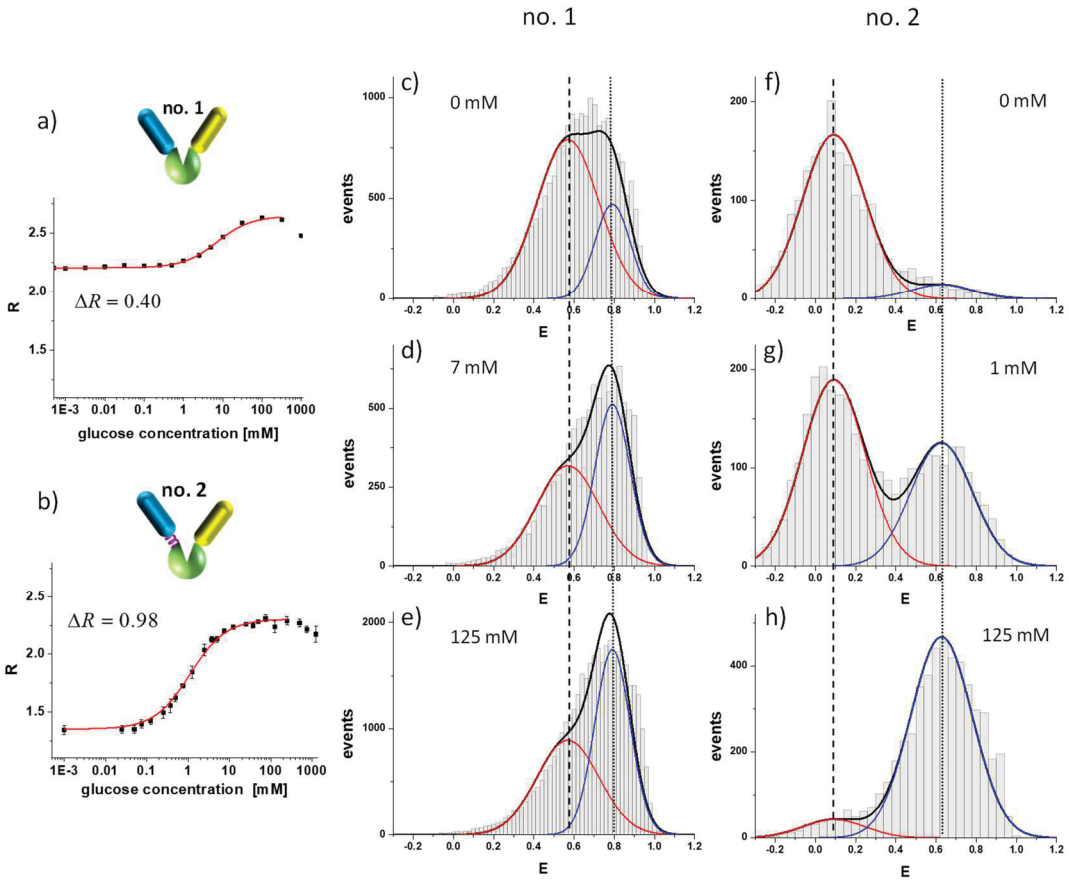

Figure 2.1-2: Ensemble characterization of construct no. 1 (a) and no. 2 (b) based on relative increase of FRET ratio parameter R supported by the corresponding glucose binding isotherm (red curve). FRET efficiency histograms (without donor-only contributions) at different glucose concentrations globally fitted with two Gaussians (same mean position and width for all glucose concentrations, but individual statistical weights for each population): without glucose (c,f), at K_D of binding isotherm (d,g), and at saturating glucose concentration of 125 mM (e,h). The difference in the mean position of both populations ($\Delta E_{pop} = E_2 - E_1$) shown by dashed ($E_1$) and dotted ($E_2$) vertical lines. For more details see Supporting Information.

In fact, the two sensors shown in Fig. 2 display two extreme scenarios of possible sensor behavior. Other constructs obtained from the toolbox exhibited performances that are in between the above described extreme scenarios (see Fig. S7). Based on the smFRET histograms of all investigated sensor constructs, mainly two conclusions seem to be essential to achieve the intended large signal change ΔR; (i) The non-liganded state should be accumulated in a population at low transfer efficiency in order to allow for a large ΔE with respect to the population of the liganded state at higher transfer efficiencies. (ii) Under ideal conditions, a preferably complete transfer of molecules from the low FRET population towards the high FRET population should take place with increasing ligand concentration. Both conditions are fulfilled to a large extend for the sensor construct no. 2. In contrast to this, the performance of the sensor prototype no. 1 is impaired: first, by a much smaller ΔE_{pop} between the low FRET and high FRET

population and second, by an incomplete transfer of molecules from the low FRET state towards the high FRET state.

The major goal in designing highly sensitive sensors is to establish a robust conversion of a relative small ligand-induced conformational change within the glucose-binding protein into a measurable rearrangement of the FPs resulting in the highest possible ΔE. Here, single-molecule data provide valuable information on the extent to which this requirement is fulfilled. We can distinguish between scenarios with an insufficient translation mechanism (i.e. a small ΔE_{pop} between non-liganded and liganded states, Fig. 2) and those, where in principle a reasonable conversion mechanism is established, but only a limited fraction of all sensor molecules makes use of it. In fact, often a combination of both problems was observed. From investigations of the sensor constructs investigated in this study, we learned that the linker between the N-terminal donor and the glucose binding protein is most important with the introduction of either a flexible or a rigid linker resulting in functional sensor constructs having the desired features (sensors no. 2 and no. 3) (Fig. 2, Fig. S7). By contrast, the additional introduction of a linker between the acceptor and the glucose binding protein (sensors no. 5 and no. 8) lowered the sensor performance, since a significant fraction of sensor molecules is already converted into the high FRET state in the absence of glucose (Fig. S7). The absence of linkers (sensor no. 1) or only a linker at the acceptor FP site (sensor no. 4) gave even weaker sensor performances. Since the remaining sensors produced with the linker-tool box approach (no. 6, no. 7, no. 9) showed rather poor performance, we do not expect further insights from smFRET histograms and omitted therefore single-molecule studies for these constructs. For all six sensor constructs which we analyzed on single-molecule level we also calculated averaged R-values and compared them to the related values from the ensemble measurements. Within the limits of errors, this comparison revealed a reasonable consistency between ensemble and single-molecules measurements (see Fig. S8).

Table 2.1-1: Parameters characterizing the sensor performance

sensor construct no.	ΔR^a	$\Delta E_{avg,D0}{}^b$	ΔE_{avg}	$\Delta E_{pop}{}^c$	$\Delta E_{avg,D0}/\Delta E_{pop}{}^d$	$\Delta E_{avg}/\Delta E_{pop}$
1	0.40	0.040	0.066	0.221	18%	30%
2	0.98	0.302	0.467	0.536	56%	87%
3	0.92	0.268	0.390	0.468	57%	83%
4	0.22	0.135	0.183	0.305	44%	60%
5	0.49	0.224	0.313	0.394	57%	79%
8	0.52	0.088	0.133	0.293	30%	45%

[a] ΔR-values characterize the sensor sensitivity at ensemble level; [b] $\Delta E_{avg,D0}$ represents the difference of the average FRET efficiency E between 0 mM and 125 mM glucose including the donor-only contribution with $\Delta E_{avg,D0}=(1-x_{D0})\ \Delta E_{avg}$, where x_{D0} is the donor-only fraction (see Fig. S9) and ΔE_{avg} is the difference between the average single-molecule E measured at 0 mM and 125 mM glucose without donor-only contributions ($\langle E \rangle_{sm}$ in Tab. S2); [c] ΔE_{pop} values give the difference between low FRET (E_1) to the high FRET (E_2) state; [d] The difference between $\Delta E_{avg,D0}/\Delta E_{pop}$ and $\Delta E_{avg}/\Delta E_{pop}$ enumerates the reduction in the sensor performance solely caused by donor-only fractions.

The comparison of three different ΔE values in Tab. 1, calculated from the obtained smFRET histograms, allowed a stepwise identification and quantification of properties that reduced the sensor performance. First, the difference of the average transfer efficiency between 0 mM and 125 mM glucose is calculated, in one case by including the donor-only molecules ($\Delta E_{avg,D0}$) and in another case after sorting them out (ΔE_{avg}). Second, we quantify the difference between the mean positions of the low FRET and high FRET population (ΔE_{pop}). Finally, we give $\Delta E_{avg,D0}$ and ΔE_{avg} in relation to $\Delta E_{pop,}$ because ΔE_{pop} defines the ultimate limit for the specific sensor performance, i.e. all sensor molecules shift completely from the low FRET to the high FRET state. The higher the value of ΔE_{pop} the better is the conversion of the glucose-induced conformational change into a change in FRET efficiency. How efficient the sensor construct makes use of this conversion, i.e. which fraction of the sensor molecules changes from the low FRET to the high FRET state, is given by $\Delta E_{avg}/\Delta E_{pop}$. Here, the sensor constructs no. 2 and no. 3 show the highest ΔE_{pop} and also a large fraction of the molecules makes use of the transition (87 % and 83 %, respectively). Sensors no 4, 5 and 8 show intermediate ΔE_{pop}-values and additionally a lower fraction of molecules take part in the transition (between 45 % and 79 %). At last, we estimated how large the change in FRET efficiency would be, if donor-only molecules could not be excluded (like in ensemble measurements), based on the donor-only fraction given in Fig. S9. Since the glucose sensor constructs have a donor-only fraction in the order of 30-40%, we likewise

observed a corresponding reduction of their potential FRET change. As mentioned already, R- and E-values are in general not proportional to each other and a comparison between both is not straight forward. This is also visible by the fact that the absolute value of E is crucial for the ensemble read-out in terms of R-values. On the one hand, the impact of errors on R due to varying donor-only fractions is much weaker, if the absolute values of E is small (see SI Experimental Section). On the other hand, the sensitivity (given Table 1 as ΔR) is much higher for larger absolute E values, due to the non-linear relationship between R-values and transfer efficiencies E (Fig. S2b). This is demonstrated by comparison of sensors no. 1 and no. 4. The $\Delta E_{avg,D0}$ of construct no. 4 is approximately 3-fold higher as compared to that of construct no.1. However, the ΔR value of construct no. 4 is by a factor of two smaller as compared to that of construct no. 1, because the latter works on higher absolute values of E (cf. Tab. S2).

In summary, an ideal sensor would display (i) a low donor-only fraction (efficient acceptor maturation), (ii) a large difference in FRET efficiency between population means of non-liganded and liganded state, and finally (iii) a complete transfer from the low FRET population (non-liganded) to the high FRET population (liganded). At the time we do not really understand the molecular mechanisms which lead to the fact that a certain fraction of sensors shows already (closed) high FRET states in the absence of glucose and why not all sensor molecules adopt the high FRET state at saturating glucose concentrations. Although some of the investigated sensor constructs show already a quite reasonable performance (sensor no. 2 and no. 3), there is additional potential to improve the sensors further, for example by employing circularly permuted FPs[4,27].

c) Impact of crowding effects on FRET-based sensors

Since genetically encoded FRET-based biosensors are often employed in the crowded environment of the cytosol, we make use of the single-molecule approach to elucidate how molecular crowding affects such sensors. As known from previous studies, high concentrations of crowding agents have the potential to compact biological macromolecules[28,29]. This behavior was also observed for FRET-based biosensors, for example promoted by synthetic macromolecular crowding agents producing more compact conformations of the sensor caused by excluded volume effects[30]. However, this effect is typically undesired for metabolite sensors, because it impedes the usability of an *in vitro* calibration for data measured *in vivo*. In contrast, FRET-based biosensors were recently developed that specifically sense macromolecular crowding[12,31]. These sensors can potentially map how much crowded certain compartments of the cell are and, therefore, gain insight how crowding influences cellular processes. Here we

investigated the effect of artificial crowding caused by polyethylene glycol (PEG) on glucose sensor no. 2 and on two crowding sensors.

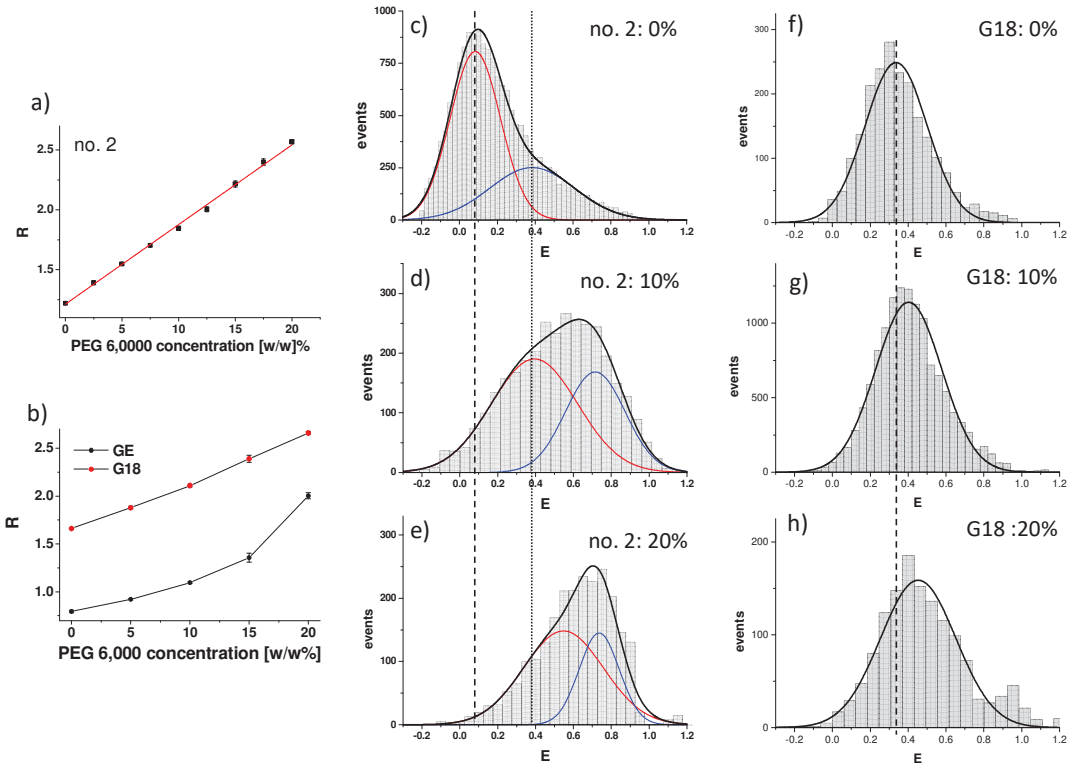

Figure 2.1-3: Ensemble fluorescence intensity ratio R for glucose sensor no. 2 (a) and for crowding sensors G18, GE (b) for different PEG 6,000 concentrations. smFRET efficiency histograms of sensor no. 2 for increasing PEG 6,000 concentrations fitted individually with two populations (c-e). A clear shift of the population means with increasing crowder concentration is observed, which is visualized by vertical reference lines positioned at the low FRET peak (dashed) and at the high FRET peak (dotted) as referenced for non-crowding conditions (i.e. 0%). smFRET efficiency histograms obtained for G18 sensor were fitted with a single Gaussian (f-h). All parameters obtained from the histogram fitting are given in Tab S2,3. Note that experimental data in Fig. 2f and in 3c (both sensor no. 2) which were measured under the same environmental conditions show a certain diversity. This is caused by varying sample properties/ qualities of sensors from different batches and not due to measuring process itself. Different samples from one and the same batch exhibit a rather high reproducibility as shown in Fig. S10.

The studied crowding sensors consist of either an unstructured linker peptide with a length of 54 amino acid residues (G18) or a α-helical peptide linker with a total length of 118 residues (GE), see Fig. 1b. All sensors were titrated with the PEG 6,000 (molecular mass of 6 kDa) up to concentrations of 20% (w/w). The resulting response to PEG 6,000 for both, the glucose and the crowding sensors, in terms of I_A/I_D is shown in Fig. 3a,b. Earlier studies on crowding sensors gave similar results[12,31]. The smFRET efficiency histograms of glucose sensor no. 2 in presence of increasing PEG 6,000 concentrations are displayed in Figure 3c-e. The measured distribution of

FRET efficiencies were fitted again with two populations, as in the case of glucose titrations (cf. Fig. 2).

Also upon increasing crowder concentration the FRET efficiency histograms are best fitted using a two-state model since the histograms exhibit a rather broad single peaked, but asymmetric distribution which can only be fitted reasonable well with two components. Essentially the two populations show an increasing overlap and a pronounced shift to larger E-values in contrast to glucose titrations, where the histogram were best described by fixed population positions (see Figure S11 for comparison of different fitting approaches). This is a clear difference to the behavior of above described effects due to glucose binding where the population peak positions do not alter but the relative occupancies of the respective populations. However, both additives (glucose and PEG) cause a structural compaction of the sensor constructs, but obviously driven by different molecular mechanisms. According to this observation glucose binding is related to a conformational selection model where equilibrium of at least two states preexists of which at least one state is able to bind glucose. Interestingly, rather high crowder concentrations led to even higher transfer efficiency values (E) compared to saturating glucose concentrations (cf. Fig. 2h and Fig. 3e). But even under conditions of relative strong crowding, further adding of glucose leads to an increase of FRET (see Fig. S12).

In contrast to the glucose sensors, the smFRET histograms of both crowding sensors show clearly a single population in aqueous buffer solutions (Fig. 3f-h and Fig. S13b-d). Crowding sensors with increased crowder concentration resulted in FRET efficiency histograms with pronounced shifts of the population mean, but still no appearance of a second population. Altogether, these observations lead to the conclusion that the crowding sensors do not show distinct long-lived states, but most probably display an ensemble of different conformations. Increased crowder concentrations generate sensors with more compact conformations which led to a continuous shift of the population to higher transfer efficiencies. However, they seem not to reach a defined saturating state at high crowder concentrations[14]. A similar crowder-induced peak shift was already observed earlier in smFRET studies on several dye-labelled intrinsically disordered proteins[29]. In summary, our single-molecule data reveals that the response mechanisms to crowding are rather similar for both types of sensors. Compared to the G18 and GE crowding sensors, the glucose sensor no. 2 seems to be even more sensitive in the regime of low crowder concentrations (i.e. below 10 % (w/w) PEG 6,000, see Fig. S13a). Unfortunately, a direct application of the glucose sensor as a crowding sensor in the cytosol is not straightforward, since metabolites in the cytosol like glucose would bias the read-out of crowding[30]. On the other hand, an *in vivo* application of the glucose sensors, which is typically performed in a crowded environment of the cytosol, would need a crowding adapted calibration of sensors in order to

deliver reliable ligand concentration from the sensor read-out. However, further improved crowding sensors may for example exhibit multiple states which populate or depopulate as a function of crowding. Here our single molecule approach can contribute to identify or validate the targeted properties.

2.1.5 Conclusion

The aim of this study was to elucidate properties and functionalities of genetically encoded FRET-based biosensors in more detail by employing single-molecule spectroscopy. So far, smFRET studies on these sensors have not been performed on a quantitative level, mainly due to photo-physical drawbacks of fluorescent proteins. Another difficulty with CFP and YFP (and derivatives thereof) utilized as FRET pairs is given by a strong spectral cross-talk and non-negligible direct YFP excitation. However, by employing state-of-the-art data acquisition and analysis, as well as long measuring times we obtained meaningful FRET efficiency histograms, even in the presence of high concentrations of macromolecular crowding agents. We obtained a reasonable number of useful burst which is still about tenfold lower as compared to conventional smFRET studies with organic fluorescent dyes for the same data acquisition time.

Our single-molecule approach allows for identifying limiting factors that inhibit a good (glucose) sensor performance. It thereby offers possible starting points to improve the performance or may reveal that the sensor has almost reached its full performance. Although our data cannot provide a detailed protocol how the linkers should be modified to improve the sensor, it nevertheless provides valuable indications. For example, a FRET efficiency histogram of a glucose sensor that shows a large distance between its populations, but only a small fraction of the molecules transfer between the populations might indicate that the conformational change is partly hindered. A minor linker modification, e.g. an extension, might in this case improve the sensor performance. In contrast, a sensor with a weak signal change but making use of the full population transfer might need a complete revision of the sensor design, e.g. by changing the insertion positions of the fluorescent proteins. Furthermore, single-molecule detection allows for excluding the donor-only bias from the data and even for quantifying the donor-only fractions. We observed significant differences between the donor-only fractions among the tested glucose sensors, but also between the glucose sensors and the crowding sensors. This information can also be used to guide sensor design. Of course, chromophore maturation is a complex interplay of environmental parameters that the fluorescent proteins encounter. However, in particular improved YFP variants might increase the maturation efficiency and reduce the donor-only fraction. Although single-molecule FRET data is much less biased by experimental artifacts compared to ensemble data, a detailed discrimination between rotational

movements and relative translational distance changes between the fluorescent proteins is still not straightforward. This knowledge would indeed give an important additional impact on a more targeted sensor design. Thus, we propose a combination of smFRET, small angle x-ray scattering (SAXS)[32], and computational modelling[33,34] as the most promising approach to achieve further progress.

Finally, we would like to state that the strength of our approach is given by the ability to characterize the performance of FRET sensors by employing smFRET. As a prerequisite, highly diluted samples in pure buffers (or with pure ingredients like PEG crowders) and rather long measuring times are required. Therefore, routine measurements to apply these sensors in physiological environments, like in cell culture supernatants or directly in cells, typically performed with microtiter plate readers or by FLIM (fluorescence life-time imaging) measurements, is so far not a targeted application of our approach.

2.1.6 Associated content

Supporting Information

Supporting Experimental Section referring to DNA and protein sequences of glucose and crowding sensor constructs, protein production and purification, sample preparation and storing; Supporting methodical details about Ensemble fluorescence measurements, Production of sensors with different donor-only fraction, Donor-only implications for ensemble data, Confocal microscopy, smFRET measurements and data analysis, smFRET histogram analysis, and Two color coincidence detection, Comparison of single molecule versus ensemble data; Figures S1-S13 showing Schematic comparison of ensemble and single molecule data, Effect of different donor-only contributions emulated by photo-bleaching series, Illustration of spectral overlap between donor and acceptor emission, Determination of donor leakage and direct acceptor excitation, Determination of correction factor $\boldsymbol{\gamma}$, Impact of donor-only contribution to FRET histograms, Ensemble and smFRET data for glucose sensor construct no. 3,4,5,8, Comparison of single molecule versus ensemble data, Donor-only fraction of all investigated sensor constructs, Reproducibility of smFRET sensor measurements, Individual versus global FRET histogram fitting of crowded glucose sensors, Impact of crowding on glucose sensing, FRET efficiencies of crowding sensors and crowded glucose sensors; Tables S1-S3 presenting Overview on the composition of the employed glucose sensor variants, Overview on parameters obtained from histogram fittings of glucose sensors, Overview on parameters obtained from histogram fittings of crowding sensors.

Author information
Corresponding Author: * fitter@physik.rwth-aachen.de Tel.: +49 241 8027209

ORCID

Jörg Fitter: 0000-0002-4503-2079

Arnold J. Boersma: 0000-0002-3714-5938

Henning Höfig: 0000-0003-0506-783X

Julia Otten: 0000-0002-2015-1215

Martina Pohl: 0000-0001-9935-5183

Victoria Steffen: 0000-0001-8927-0784

Author Contributions
J.F., H.H. M.P. and A.B. designed the research; H.H., J.O., and V.S. performed the research; M.P., V.S., J.O., and A.B. developed sensor constructs; H.H. analyzed the data and H.H. and J.F. wrote the manuscript in consultations with all authors.

Notes
The authors declare no competing financial interest.

Acknowledgements

The authors would like to thank Drs. M. Gabba and M. Cerminara for initial support with the installation of the lasers, as well as Dr. J. Walter for preparing illustrations for Fig. 1. H.H. acknowledges the International Helmholtz Research School on Biophysics and Soft Matter (BioSoft) for financial support.

2.1.7 References

1. Sanford, L.; Palmer, A. Recent Advances in Development of Genetically Encoded Fluorescent Sensors. *Methods Enzymol*. 2017, **589**, 1−49.
2. Okumoto, S.; Jones, A.; Frommer, W. B. Quantitative Imaging with Fluorescent Biosensors. *Annu. Rev. Plant Biol*. 2012, **63**, 663− 706.
3. Komatsu, N.; Aoki, K.; Yamada, M.; Yukinaga, H.; Fujita, Y.; Kamioka, Y.; Matsuda, M. Development of an optimized backbone of FRET biosensors for kinases and GTPases. *Mol. Biol. Cell* 2011, **22**, 4647−56.
4. Ohta, Y.; Kamagata, T.; Mukai, A.; Takada, S.; Nagai, T.; Horikawa, K. Nontrivial Effect of the Color-Exchange of a Donor/ Acceptor Pair in the Engineering of Förster Resonance Energy Transfer (FRET)-Based Indicators. *ACS Chem. Biol*. 2016, **11**, 1816−22.
5. Ast, C.; Foret, J.; Oltrogge, L. M.; De Michele, R.; Kleist, T. J.; Ho, C. H.; Frommer, W. B. Ratiometric Matryoshka biosensors from a nested cassette of green- and orange-emitting fluorescent proteins. *Nat. Commun*. 2017, **8**, 431.

6. de Lorimier, R. M.; Smith, J. J.; Dwyer, M. A.; Looger, L. L.; Sali, K. M.; Paavola, C. D.; Rizk, S. S.; Sadigov, S.; Conrad, D. W.; Loew, L.; Hellinga, H. W. Construction of a fluorescent biosensor family. *Protein Sci*. 2002, **11**, 2655−75.

7. Dwyer, M. A.; Hellinga, H. W. Periplasmic binding proteins: a versatile superfamily for protein engineering. *Curr. Opin. Struct. Biol*. 2004, **14**, 495−504.

8. Moussa, R.; Baierl, A.; Steffen, V.; Kubitzki, T.; Wiechert, W.; Pohl, M. An evaluation of genetically encoded FRET-based biosensors for quantitative metabolite analyses in vivo. *J. Biotechnol*. 2014, **191**, 250−259.

9. Deuschle, K.; Okumoto, S.; Fehr, M.; Looger, L. L.; Kozhukh, L.; Frommer, W. B. Construction and optimization of a family of genetically encoded metabolite sensors by semirational protein engineering. *Protein Sci*. 2005, **14**, 2304−2314.

10. Campbell, R. E. Fluorescent-protein-based biosensors: modulation of energy transfer as a design principle. *Anal. Chem*. 2009, **81**, 5972−9.

11. Sisamakis, E.; Valeri, A.; Kalinin, S.; Rothwell, P. J.; Seidel, C. A. Accurate single-molecule FRET studies using multiparameter fluorescence detection. *Methods Enzymol*. 2010, **475**, 455−514.

12. Boersma, A. J.; Zuhorn, I. S.; Poolman, B. A sensor for quantification of macromolecular crowding in living cells. *Nat. Methods* 2015, **12**, 227.

13. Steffen, V.; Otten, J.; Engelmann, S.; Radek, A.; Limberg, M.; Koenig, B. W.; Noack, S.; Wiechert, W.; Pohl, M. A Toolbox of Genetically Encoded FRET-Based Biosensors for Rapid L-Lysine Analysis. *Sensors* 2016, **16**, 1604.

14. Liu, B. Q.; Aberg, C.; van Eerden, F. J.; Marrink, S. J.; Poolman, B.; Boersma, A. J. Design and Properties of Genetically Encoded Probes for Sensing Macromolecular Crowding. *Biophys. J*. 2017, **112**, 1929−1939.

15. Muller, B. K.; Zaychikov, E.; Brauchle, C.; Lamb, D. C. Pulsed interleaved excitation. *Biophys. J*. 2005, **89**, 3508−3522.

16. Eggeling, C.; Berger, S.; Brand, L.; Fries, J. R.; Schaffer, J.; Volkmer, A.; Seidel, C. A. M. Data registration and selective single- molecule analysis using multi-parameter fluorescence detection. *J. Biotechnol*. 2001, **86**, 163−180.

17. Deniz, A. A.; Laurence, T. A.; Dahan, M.; Chemla, D. S.; Schultz, P. G.; Weiss, S. Ratiometric single-molecule studies of freely diffusing biomolecules. *Annu. Rev. Phys*. Chem. 2001, **52**, 233−253.

18. Fries, J. R.; Brand, L.; Eggeling, C.; Kollner, M.; Seidel, C. A. M. Quantitative identification of different single molecules by selective time-resolved confocal fluorescence spectroscopy. *J. Phys. Chem*. *A* 1998, **102**, 6601−6613.

19. Kudryavtsev, V.; Sikor, M.; Kalinin, S.; Mokranjac, D.; Seidel, C. A. M.; Lamb, D. C. Combining MFD and PIE for Accurate Single- Pair Forster Resonance Energy Transfer Measurements. *ChemPhy- sChem* 2012, **13**, 1060−1078.

20. Brasselet, S.; Peterman, E. J. G.; Miyawaki, A.; Moerner, W. E. Single-molecule fluorescence resonant energy transfer in calcium concentration dependent cameleon. *J. Phys. Chem. B* 2000, **104**, 3676−3682.

21. Kyrychenko, A.; Rodnin, M. V.; Ghatak, C.; Ladokhin, A. S. Joint refinement of FRET measurements using spectroscopic and computational tools. *Anal. Biochem*. 2017, **522**, 1−9.

22. Nir, E.; Michalet, X.; Hamadani, K. M.; Laurence, T. A.; Neuhauser, D.; Kovchegov, Y.; Weiss, S. Shot-noise limited single- molecule FRET histograms: comparison between theory and experiments. *J. Phys. Chem. B* 2006, **110**, 22103−22124.

23. Kalinin, S.; Sisamakis, E.; Magennis, S. W.; Felekyan, S.; Seidel,C. A. On the origin of broadening of single-molecule FRET efficiency distributions beyond shot noise limits. *J. Phys. Chem. B* 2010, **114**, 6197−6206.

24. Newman, R. H.; Fosbrink, M. D.; Zhang, J. Genetically Encodable Fluorescent Biosensors for Tracking Signaling Dynamics in Living Cells. *Chem. Rev*. 2011, **111**, 3614−3666.

25. Li, H. T.; Ying, L. M.; Green, J. J.; Balasubramanian, S.; Klenerman, D. Ultrasensitive coincidence fluorescence detection of single DNA molecules. *Anal. Chem.* 2003, **75**, 1664−1670.

26. Kempf, N.; Remes, C.; Ledesch, R.; Zuchner, T.; Hofig, H.; Ritter, I.; Katranidis, A.; Fitter, J. A Novel Method to Evaluate Ribosomal Performance in Cell-Free Protein Synthesis Systems. *Sci. Rep.* 2017, **7**, 467535.

27. Baird, G. S.; Zacharias, D. A.; Tsien, R. Y. Circular permutation and receptor insertion within green fluorescent proteins. *Proc. Natl. Acad. Sci. U. S. A*. 1999, **96**, 11241−6.

28. Dhar, A.; Samiotakis, A.; Ebbinghaus, S.; Nienhaus, L.; Homouz, D.; Gruebele, M.; Cheung, M. S. Structure, function, and folding of phosphoglycerate kinase are strongly perturbed by macromolecular crowding. *Proc. Natl. Acad. Sci. U. S. A.* 2010, **107**, 17586−91.

29. Soranno, A.; Koenig, I.; Borgia, M. B.; Hofmann, H.; Zosel, F.; Nettels, D.; Schuler, B. Single-molecule spectroscopy reveals polymer effects of disordered proteins in crowded environments. *Proc. Natl. Acad. Sci. U. S. A*. 2014, **111**, 4874−4879.

30. Groen, J.; Foschepoth, D.; te Brinke, E.; Boersma, A. J.; Imamura, H.; Rivas, G.; Heus, H. A.; Huck, W. T. S. Associative Interactions in Crowded Solutions of Biopolymers Counteract Depletion Effects. *J. Am. Chem. Soc*. 2015, **137**, 13041−13048.

31. Gnutt, D.; Gao, M.; Brylski, O.; Heyden, M.; Ebbinghaus, S. Excluded-Volume Effects in Living Cells. *Angew. Chem., Int. Ed.* 2015, **54**, 2548−2551.

32. Mertens, H. D. T.; Piljic, A.; Schultz, C.; Svergun, D. I. Conformational analysis of a genetically encoded FRET biosensor by SAXS. *Biophys. J*. 2012, **102**, 2866−75.

33. Pham, E.; Chiang, J.; Li, I.; Shum, W.; Truong, K. A. computational tool for designing FRET protein biosensors by rigid- body sampling of their conformational space. *Structure* 2007, **15**, 515−23.

34. Reinartz, I.; Sinner, C.; Nettels, D.; Stucki-Buchli, B.; Stockmar, F.; Panek, P. T.; Jacob, C. R.; Nienhaus, G. U.; Schuler, B.; Schug, A. Simulation of FRET dyes allows quantitative comparison against experimental data. *J. Chem. Phys*. 2018, **148**, 123321.

2.2 Application of FRET-based glucose sensors in small scale cultivations

The following results were published as:

A FRET-based biosensor for the quantification of glucose in culture supernatants of mL scale microbial cultivations

Julia Otten, Niklas Tenhaef, Roman P. Jansen, Johannes Döbber, Lisa Jungbluth, Stephan Noack, Marco Oldiges, Wolfgang Wiechert, Martina Pohl

Microbial Cell Factories 2019
Volume 18, Issue 1

The manuscript was adapted to the layout of this thesis, without any alterations of the content.

Context:

The best performing sensor type from the previous chapter (sensor no. 2, in this manuscript denoted as $Glu^{[-]}$) was evaluated for the application in small scale cultivations. The characterization of performance and stability in typical cultivation media CGXII and M9 for *C. glutamicum* and *E. coli*, respectively, demonstrated a quenching effect by this media, which was more pronounced in CGXII. Quenching effects of CGXII medium could be circumvented by dilution of at least a factor of 10. Dilution was additionally useful as it enables the quantification of D-glucose also in supernatants with concentrations blow the sensor K_d of ~1mM. Therewith, the sensor was successfully applied in an at-line process for D-glucose determination of a *C. glutamicum* cultivation in the range of 400 mM to 0.4 mM. Additionally, the sensor was equipped with a HaloTag™ to facilitate covalent immobilization, which had a stabilizing effect. In contrast to the soluble $Glu^{[-]}$ sensor, the immobilized sensor (denoted as $Glu^{[+Halo]}$) is not degraded by shaking and withstands storage at temperatures above 25°C for up to three days. The immobilized sensor was successfully applied as an online tool in a microbioreactor (BioLector®) for the quantification of D-glucose in an *E. coli* cultivation using M9 medium.

Both applications, at-line and online, demonstrate the potential of FRET-based sensors in milliliter scale cultivations, especially as there are currently no online sensors available for cultivation devices in this scale. Such sensors have a great potential to speed up parallelized strain optimization.

Contributions:

Julia Otten and Martina Pohl, Stephan Noack, and Marco Oldiges planned the research. Julia Otten constructed and characterized the FRET-based sensors. Niklas Tenhaef and Julia Otten performed the at-line experiments, Roman Jansen and Julia Otten performed the online experiments. Julia Otten and Martina Pohl wrote the manuscript in consultation of all coauthors. Niklas Tenhaef contributed parts of the manuscript.

A FRET-based biosensor for the quantification of glucose in culture supernatants of mL scale microbial cultivations

Julia Otten[1], Niklas Tenhaef[1], Roman P. Jansen[1], Johannes Döbber[1], Lisa Jungbluth[1], Stephan Noack[1], Marco Oldiges[1], Wolfgang Wiechert[1], Martina Pohl[1]*

[1]Forschungszentrum Jülich GmbH, IBG-1 Biotechnology, D-52415 Jülich, Germany

Corresponding author: Prof. Dr. Martina Pohl, ma.pohl@fz-juelich.de

2.2.1 Abstract

Background:

In most microbial cultivations D-glucose is the main carbon and energy source. However, quantification of D-glucose especially in small scale is still challenging. Therefore, we developed a FRET-based glucose biosensor, which can be applied in microbioreactor-based cultivations. This sensor consists of a glucose binding protein sandwiched between two fluorescent proteins, constituting a FRET pair. Upon D-glucose binding the sensor undergoes a conformational change which is translated into a FRET-ratio change.

Results:

The selected sensor shows an apparent K_d below 1.5 mM D-glucose and a very high sensitivity of up to 70 % FRET-ratio change between the unbound and the glucose-saturated state. The soluble sensor was successfully applied online to monitor the glucose concentration in an *Escherichia coli* culture. Additionally, this sensor was utilized in an at-line process for a *Corynebacterium glutamicum* culture as an example for a process with cell-specific background (e.g. autofluorescence) and medium-induced quenching. Immobilization of the sensor via HaloTag® enabled purification and covalent immobilization in one step and increased the stability during application, significantly.

Conclusion:

A FRET-based glucose sensor was used the quantify D-glucose consumption in microtiter plate based cultivations. To the best of our knowledge, this is the first method reported for online quantification of D-glucose in microtiter plate based cultivations. In comparison to D-glucose analysis via an enzymatic assay and HPLC, the sensor performed equally well, but enabled much faster measurements, which allowed to speed up microbial strain development significantly.

Keywords:

Sensor beads; online glucose measurement; micro cultivation; glucose binding protein; mTurquoise2; Venus; Biolector

2.2.2 Introduction

Although a broad variety of chemical compounds is already produced via microbial cultivation, the development of new processes and strains for the production of, e.g., non-natural high value products using synthetic biology approaches and microbial communities is gathering momentum. In this respect, bioprocess development at small scales is becoming ever more important. Microbioreactors enable the acceleration of process development by increasing the throughput, since cultivation and characterization of multiple strains can be parallelized [1]. However, available microbioreactor approaches still cover a limited number of sensors for online measurements, e.g., dissolved oxygen, biomass, pH, and fluorescence. Additional online signals, for example to measure consumption of the C-source, are highly desirable to estimate substrate uptake rates which are often correlated to productivity.

Even though enzymatic assays are routinely used to quantify D-glucose in samples from microbial cultivations [2,3], application in small scale is still limited to at-line processes. Therefore, samples from respective cultivations require a multi-step workup procedure to be processed with enzymatic assays. In contrast genetically encoded fluorescence-based sensors could in principle be used online, as cells could co-produce such sensors, eliminating time-consuming sample workup operations. To enable high throughput screening using fluorescence-associated cell sorting (FACS) various fluorescence-based sensor techniques have been developed [4]. One option are Förster resonance energy transfer (FRET)-based biosensors [5,6], which are available for a broad range of small molecules and are almost exclusively used intracellularly [4,7]. In general FRET-based biosensors consist of two fluorescent probes (donor and acceptor) fused to a central metabolite binding protein (BP). Under optimal conditions FRET occurs between the two probes upon excitation of the donor, which transfers energy also to the acceptor. As a result, both fluorescent probes show different fluorescence intensities depending on the FRET effect. This effect is in a certain range dependent on the concentration of the metabolite recognized by the central binding protein. Due to the conformational changes of the binding protein, the FRET efficiency is either increased or decreased. Biosensors located in the cytoplasm of cells are limited to transmit qualitative information on concentration changes of the target metabolite inside the cell, since such systems cannot be properly calibrated [8]. In contrast, extracellular applications of such sensors in the fermentation broth of producer cells enables quantitative detection of the target metabolite due to an easier calibration of such systems, as we have recently demonstrated for L-lysine [9].

In the present study, we have developed and successfully applied a FRET-based biosensor to monitor D-glucose as a C-source in milliliter scale microbial cultivation experiments. The

biosensors were constructed by fusing a cyan (donor; mTurquoise2) and a yellow (acceptor; Venus) variant of the green fluorescent protein (GFP) to either end of a periplasmic glucose/galactose-binding protein (MglB) from *E. coli.* MglB is highly specific for glucose and galactose [10]. Binding of these sugars results in a conformational change [11], which is translated to changes in distance, orientation, and thus energy transfer between the fluorescent proteins. Our sensor construct is based on a previously described glucose sensor (FLII^{12}P-glu600µ) [12,13], but we used mTurquoise2 and Venus as a FRET pair to reduce the environmental influence on the sensor signal. Especially the fluorescence intensity of mTurquoise2 is reportedly more stable and bright even at changing pH and ion concentrations [14–16]. Venus also exhibits a reduced sensitivity towards such changes compared to other yellow variants of GFP (YFP, Citrine) [17–19]. Besides the signal intensity, the sensor affinity (K_d) must be adopted to the concentration range of the screening system and its sensitivity, the FRET-ratio change between the unbound state and fully metabolite-saturated state, must be high enough to detect the signal behind the background of the cellular supernatant.

Both aspects were recently addressed by the creation of a glucose sensor toolbox using different linker sequences [20]. From this toolbox a sensor with a flexible $(GGS)_4$ linker sequence between mTurquoise2 and the MglB was selected, which increased the transfer efficiency and results in a sensor with an affinity in the low millimolar range (< 1.5 mM; Supplementary material Fig. S1) and a very high sensitivity (~70 % FRET-ratio change). The sensor constructs used in this work are based on the glucose sensor no. 2 developed previously [20] (for details see Methods and Supplementary material).

A soluble Glu$^{[-]}$ and the Halo-tagged version of the glucose sensor Glu$^{[+Halo]}$ were tested in different formulations to demonstrate the potential for at-line as well as online quantification in two common platform organisms: *Corynebacterium glutamicum* and *Escherichia coli,* in the typical cultivation media CGXII and M9, respectively. The soluble Glu$^{[-]}$ sensor can be reliably applied for at-line measurements, demonstrating the potential of FRET-based sensors for process development. In addition, we developed a simple strategy to enable purification, immobilization, and, most significantly, also stabilization of the sensor via the HaloTag® system [21,22], which allowed for the application of the immobilized sensor Glu$^{[+Halo]}$ online under cultivation conditions. To the best of our knowledge this is the first time, a FRET-based biosensor was used for the online detection of glucose in milliliter scale cultivation.

2.2.3 Methods

a) Protein design

The biosensor without HaloTag® ($Glu^{[-]}$) used in this study is based on sensor no. 2 in a recent publication [20] with a modification of the hexahistidine tag (His-tag). In contrast to sensor no.2 the His-tag was translocated to the C-terminus of the protein via overlap extension PCR [23]. Additionally, the central MglB carries a L238M exchange to reduce the affinity for glucose [24]. The His-tag of the biosensor with HaloTag® ($Glu^{[+Halo]}$) remained at the N-terminus while the sequence for the HaloTag® was fused to the C-terminus via Gibson assembly using NEB Gibson assembly kit [22,25]. For DNA sequences, protein sequences, and primers see Supplementary material.

b) Sensor production & purification

For production of both sensor variants ($Glu^{[-]}$ and $Glu^{[+Halo]}$) chemically competent *E. coli* BL21(DE3) cells were transformed with the plasmids encoding the respective sensor variant [26]. Transformed cells were grown over night on LB-agar plates containing 100 mg/mL ampicillin. A single colony was used to inoculate 20 mL LB media and grown over night at 37°C. To inoculate the main culture (1 L) in auto induction medium, 1 mL of this pre-culture was used [27]. Cells were grown for two hours at 37°C and additional 70 hours at 20°C at 150 rpm in baffled 2 L flasks (400 mL). Cells were harvested by centrifugation and stored at -20°C until further use. For sensor purification 10 % (w/v) cells were suspended in buffer (20 mM MOPS, 150 mM NaCl, 20 mM imidazole, pH 7.3) and disrupted via high-pressure homogenization in three passages using an Avestin Emulsiflex–C5 (Avestin Europe GmbH, Mannheim, Germany). Purification was performed via the His-tag using affinity chromatography on Ni-NTA agarose (Qiagen, Hilden, Germany), followed by size exclusion chromatography as previously described [9]. Finally, the sensor was concentrated to 20 µM through ultrafiltration (Amicon Ultra Centrifugal filter, 30 kDa cut-off) (Merck Millipore, Darmstadt, Germany) and stored in 20 mM MOPS buffer, pH 7.3 at -20°C.

c) Protein determination

Protein concentration of the soluble sensor was measured photometrically using the molar extinction coefficient of Venus ($\varepsilon_{515\ nm}$= 92,200 mol^{-1} cm^{-1}) [18].

d) Calibration/ binding isotherms

Binding isotherms and the calibration for the at-line process were recorded in a microtiter plate using 50 µL soluble sensor (2 µM), which was mixed with 50 µL MOPS buffer (20 mM, pH 7.3) containing D-glucose in the range from 0 mM to 1000 mM. The measurements were performed in a microtiterplate spectrofluorimeter (M-200 or M-1000, Tecan, Männedorf, Switzerland) at room temperature. Binding isotherms with varying medium content of either CGXII- or M9-medium were recorded with medium concentrations ranging from 2.5 to 90 % (v/v) by replacing the respective volume of MOPS buffer. For each measurement the arithmetic average of 10 measurement cycles was calculated [8]. mTurquoise2 was excited at 428 ± 20 nm, the corresponding emission of both FRET partners were recorded at 485 ± 20 nm for mTurquoise2 [14] and 528 ± 20 nm for Venus [18]. The FRET-ratio *R* was calculated as fluorescence intensity of the acceptor divided by the intensity of the donor according to equation (1).

$$R = \frac{I_{acceptor}}{I_{donor}} \quad (1)$$

Parameters from the binding isotherms were deduced from fitting the data using the following equation (2) [28]:

$$R = \frac{(\Delta R)*[S]}{K_d+[S]} + R_0 \quad (2)$$

were R_0 describes the FRET-ratio in absence of D-glucose, ΔR (R_{sat} – R_0) referring to sensor sensitivity, is the maximum change in FRET-ratio at saturation of the sensor with glucose (R_{sat}), and the dissociation constant K_d, which describes the apparent affinity of the sensor, is deduced at half-maximal saturation from the inflection point of the binding isotherm. The normalized ΔR was determined as $\Delta R/R_0$*100%. Additionally, the dynamic range of a sensor can be derived from the quasi-linear region in the semi-logarithmic representation of the binding isotherm (see Supplementary material, Fig. S1). The binding isotherms were recorded on devices differing in resolution and sensitivity, such as plate readers (Tecan M-1000, Tecan M-200), and the microbioreactor BioLector® (m2p labs, Baesweiler, Germany). As a result the deduced apparent affinity of the sensor varied in the range of 0.4 to 1.5 mM, depending on the utilized device. Therefore, calibrations used for further calculation of the D-glucose concentration in the culture broth were always performed in the same device, under the same conditions as the corresponding experiments.

e) Stability measurements

Thermal stability measurements were performed by incubating the sensors $Glu^{[-]}$ (2 µM) and $Glu^{[+Halo]}$(immobilized) in MOPS-buffer (20 mM, pH 7.3) at different temperatures (25°C, 4°C,

and -20°C). Measurements were performed in a Tecan M-200 spectrophotometer. After excitation of the donor mTurquoise2 at λ_{ex} 420 ± 9 nm, emission spectra from λ_{em} 460 nm to 650 nm were recorded regularly to follow a possible decrease of the fluorescence intensity. From these spectra the FRET-ratio at maximum emission of mTurquoise2 and Venus was calculated according to equation (1). Additionally, SDS-PAGE was performed using 19.5 µL of the respective sensor sample, 7.5 µL NuPAGE® sample reducing agent (10x) and 3 µL NuPage® SDS sample buffer (4x) (ThermoFischer Nunc, Waltham, MA, USA). We used NuPage® 4-12 % Bis-TRIS gels of 1 mm thickness (ThermoFischer Nunc, Waltham, MA, USA) and the PageRuler Plus Prestained Protein Ladder (ThermoFischer Nunc, Waltham, MA, USA) as marker. Gels were run at 200 V for 45 minutes [29].

Measurements to determine the stability against shaking were performed in a flower plate in the BioLector® (m2p labs, Baesweiler, Germany). Here 50 µL of the sensors $Glu^{[-]}$ (2 µM) and $Glu^{[+Halo]}$(immobilized) were mixed with 750 µL of MOPS buffer (20 mM, pH 7.3) or M9 medium, respectively. Fluorescence emission of mTurquoise2 (λ_{em}=486 ± 5 nm) and Venus (λ_{em}=532 ± 5 nm) were measured after excitation at λ_{ex}= 430 ± 5 nm.

f) At-line analysis

Calibration of the soluble sensor versions ($Glu^{[-]}$) for the at-line analysis was performed as described above. To mimic process conditions *C. glutamicum* ATCC 13032 was grown over night in CGXII medium at 30 °C [30,31] containing fructose (20 g/L, 112 mM) as the main C-source. A sample of the cell suspension (15 µL) was diluted with 285 µL MOPS buffer (20 mM, pH 7.3) containing glucose in the concentration range from 0 g/L to 45 g/L (250 mM). From these diluted samples 50 µL were mixed with the $Glu^{[-]}$ solution (50 µL, 2 µM) in clear 300 µL micro titer plates (ThermoFischer Nunc, Waltham, MA, USA). Calibration was performed in quadruplet.

The at-line process and analysis were carried out on a customized Tecan Freedom EVO200 robotic (Tecan, Männedorf, Switzerland) pipetting platform with integrated BioLector®, centrifuge (Sigma Laborzentrifugen GmbH, Osterode am Harz, Germany), and spectrofluorimeter (Tecan M-200) [3]. For cultivation *C. glutamicum* ATCC 13032 was incubated in 1000 µL CGXII medium containing D-glucose (20 g/L) in 48-well flower plates (m2p-labs GmbH, Baesweiler, Germany) at 1400 rpm and 30 °C. Every hour three wells were sampled and a technical duplicate of 15 µL was used for the at-line D-glucose analysis, respectively. The remaining material was centrifuged to remove cells and the supernatant was stored at 4 °C for comparative offline analysis via HPLC and enzymatic D-glucose analysis as earlier described [2].

During cultivation pH, pO_2, and biomass formation (measured as scattered light of 620 nm, referred to as "backscatter") were recorded online by the BioLector®.

g) Sensor immobilization

Immobilization of the $Glu^{[+Halo]}$ sensor was performed at room temperature. Before use, the Halo-Link® resin (particle size= 45-165 µm, Promega, Mannheim, Germany) was washed twice with MOPS buffer (20 mM, pH 7.3). A suspension of the resin (100 µL) was incubated with 1 mL $Glu^{[+Halo]}$ solution (20 µM) for one hour in a 1.5 mL Eppendorf tube under constant slow inversion. After centrifugation in a tabletop centrifuge (10 s, 2000 x *g*, Sprout Minicentrifuge, Biozym, Hessisch Oldendorf, Germany) the supernatant was removed. Afterwards the resin was washed twice with 20 mM MOPS buffer. The immobilized $Glu^{[+Halo]}$ sensor was stored at 4 °C suspended in MOPS buffer (20% v/v) in the dark. Loading of the beads with the sensor was estimated by comparing the absorption of Venus (λ_{ex}= 515 nm, ε = 92,200 $M^{-1}cm^{-1}$) of the sensor solution before and after immobilization.

h) Online analysis

Online analysis of the glucose concentration was performed with the immobilized $Glu^{[+Halo]}$ sensor in a BioLector®. *E. coli* K12 MG1655 was cultivated in 750 µL M9 medium (modified from [32]) containing 5 g/L (28 mM) D-glucose, at 900 rpm and 30°C. Immobilized biosensor (50 µL of the suspension (20 % v/v) in MOPS buffer (20 mM, pH 7.3) was added to one row of wells in a 48-well flower plate (m2p labs, Baesweiler, Germany). Apart from biomass concentration (measured as scattered light of 620 nm, referred to as "backscatter") also two fluorescent signals (λ_{ex}= 430 ± 5 nm, λ_{em} = 486 ± 5 nm and λ_{ex}= 430 ± 5 nm, λ_{em} = 532 ± 5 nm) were recorded in the BioLector®. D-Glucose concentration standards for the online calibration were prepared by mixing M9 medium (750 µL) with 20 concentrations ranging from 0 mM to 100 mM (0 g/L to 18 g/L) D-glucose with 50 µL bead suspension on the same plate. The calibration curve is described by a saturation kinetic equation whose parameters are fitted to the measured calibration data by minimizing the sum of squares (Supplementary material Fig. S9).

Prior to the online D-glucose analysis, we monitored the growth of *E. coli* MG1655 under the described process conditions also in the presence of immobilized $Glu^{[+Halo]}$ in more detail to exclude growth limitations. Therefore additionally to the backscatter and the two fluorescent signals, pH and pO_2 were recoded online by the BioLector®. The resulting data is shown in the Supplementary material (Fig. S10).

2.2.4 Results & discussion

a) Sensor characterization

The D-glucose concentration in microbial cultivations typically ranges from 0 to 200 mM, which requires a comparably low affinity of the D-glucose sensor in the lower millimolar range to sense D-glucose depletion. The first sensor variant, $Glu^{[-]}$, studied in this work, shows K_d-values of 0.4 ± 0.1 mM for D-glucose and a very good sensitivity in buffer, as can be deduced from a FRET ratio change (ΔR) of 75 % between the unbound and the bound state (Supplementary material, Fig. S1). Thus, the detection range in MOPS buffer is between 0.01 mM to 10 mM (0.0018 g/L to 1.8 g/L) D-glucose.

Besides high signal intensity the sensor must also be stable under the conditions applied in a microbioreactor, where the biosensor is challenged by temperature and mechanical stress through shaking. First, the thermal stability of the soluble $Glu^{[-]}$ sensor was tested regarding its stability at different temperatures. Whilst the FRET-ratio in the presence and absence of D-glucose remained stable for 21 days of incubation at 4°C and -20°C, respectively, the FRET-ratios were already clearly altered after 3 days at 25°C (Fig. 1a), which clearly limits the applicability of this sensor at room temperature. Thus, the senor is suitable for lab scale application with cultivation times in the range of 24 to 48 hours. SDS-PAGE analysis revealed that the observed instability is caused mainly by an increasing degradation of the fusion protein (Fig. 1b). The biosensor protein degrades into fragments of about 30 kDa (Fig. 1b, red box), which matches the sizes of both FPs as well as the central MglB, respectively. Similar results were also obtained earlier during crystallization attempts of different similar sensors (data not shown). However, the underlying mechanism is still to be elucidated.

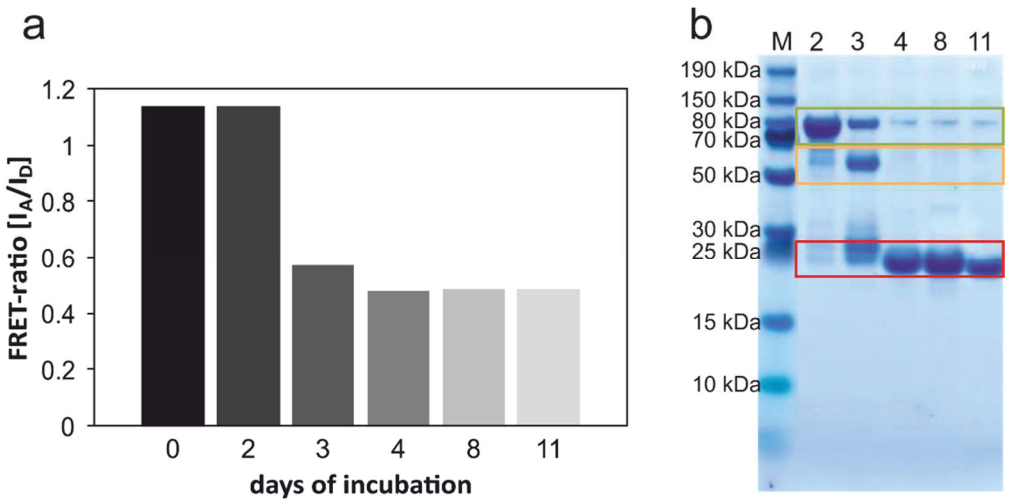

Figure 2.2-1: Stability of the Glu[-] sensor (20 µM) in MOPS buffer (20 mM, pH 7.3) at 25°C. (a) FRET-ratio of the Glu[-] sensor showing clear evidence of degradation after incubation for 3 days. (b) SDS-PAGE analysis of the Glu[-] sensor. Labels above the lanes mark the number of days of incubation. The size of the full-length protein is ~90 kDa (green box). After two days at 25°C the sensor starts to degrade into smaller fragments of ~60 kDa (orange box, lane 3) and ~25-30 kDa (red box). After 4 days (lanes 4-11) the sensor is fully degraded into fragment of ~25- 30 kDa (for details see text).

Apart from temperature, the sensor must be stable also towards different cultivation media. In order to thoroughly test the application of the novel D-glucose sensor for application with *Corynebacterium glutamicum*, CGXII medium was tested as a typical cultivation medium [30] concerning the influence on the sensor properties. The respective binding isotherm of the Glu[-] sensor recorded in the presence of the culture medium demonstrates a strong influence of CGXII medium on the sensor sensitivity relative to buffer (see Supplementary material, Fig. S2). On account of the strong background and quenching of CGXII medium, measurements are only reasonable with CGXII medium diluted with at least 95% buffer (v/v). Additionally, this dilution enables measurements in the presence of *C. glutamicum* cells. Thus, cell separation before at-line measurement of D-glucose is not necessary. Fortunately, the medium did not affect the apparent K_d of the sensor variant, indicating that the quenching effect of the medium influences the fluorescent proteins and not the MglB (Supplementary material, Fig. S2). The detection limits of 0.01 mM to 10 mM (0.0018 g/L to 1.8 g/L) D-glucose can, however, be shifted by dilution of the cultivation samples. Dilution by a factor of 40 would enable D-glucose quantification from 0.4 mM to 400 mM (0.072 to 72 g/L), which covers the concentration range of most microbial cultivations.

A further prerequisite for the application of such sensors is the reproducibility of calibrations during a typical cultivation experiment, indicating its stability under process conditions. Repeated, comparative calibrations in MOPS buffer in the presence and absence of CGXII

medium (2.5 % v/v, a dilution of 1:40) showed no significant effect on the apparent affinity (K_d) and the signal intensity of the Glu[-] sensor. As demonstrated in Fig. 2 the binding isotherms remained stable over the entire experiment, demonstrating that this sensor can be used for repeated measurements.

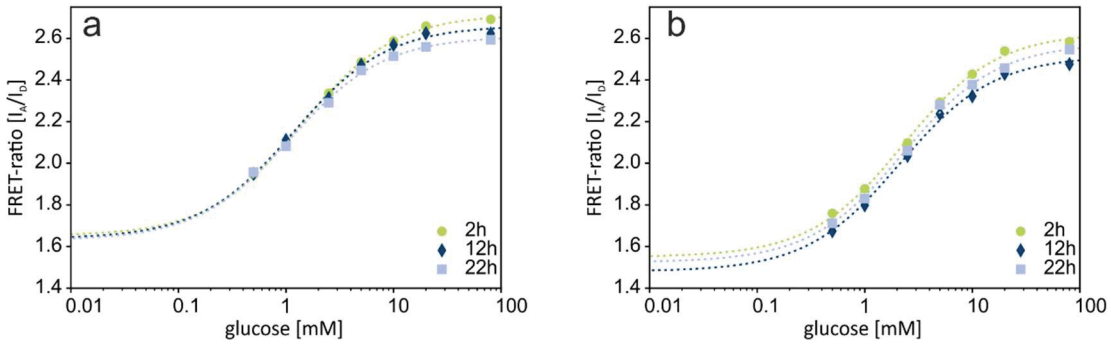

Figure 2.2-2: Binding isotherm of the Glu[-] biosensor in either MOPS (20 mM, pH 7.3) (a) with CGXII medium (2.5 % v/v) and (b) without addition of medium without shaking. The FRET-ratio (I_A/I_D) was calculated from the emissions of the donor mTurquoise2 at 485 nm (± 20 nm) and acceptor Venus at 528 nm (± 20 nm) after exitation of the donor at 428 nm (± 9 nm) according to equation (1). Between measurements the sensor was stored protected from light at 4 °C. The curves (dotted) were fitted to the data according to equation (2).

Besides thermal degradation and media effects, also shaking of the Glu[-] sensor in the Flowerplates® of the BioLector® device turned out to be deleterious, because the emission of both FRET-partners decreased significantly (see Supplementary material, Fig. S5). A decrease in both emission intensities indicates a degradation of at least the donor and most likely also the acceptor. Additionally, shaking frequencies > 800 rpm resulted in aggregation of the Glu[-] sensor (data not shown). The aggregated sensor did no longer respond to changes in D-glucose concentration, making the Glu[-] sensor not suitable for an online application in shaken cultures. However, the soluble Glu[-] sensor can be applied in an automated process to measure D-glucose at-line. In such a setting the biosensor stock can easily be stored at 4°C between measurements, which drastically increases its lifetime. Furthermore, the Glu[-] sensor will not be exposed to shaking, which is beneficial for the sensor stability.

b) At-line application of the soluble sensor

With a sufficiently stabile sensor and reproducible calibration at hand, an at-line D-glucose quantification protocol for the widely used production strain *Corynebacterium glutamicum* was established (see Supplementary material, Fig. S7). During cultivation of *C. glutamicum* ATCC 13032 in the BioLector®, biomass growth, oxygen consumption, and pH changes were monitored online. As described in Methods, three samples were taken every hour by a liquid

handling system, diluted, and the D-glucose concentration was measured using the Glu[-] biosensor (see Supplementary material, Fig. S8 for calibration). The supernatant of the remaining samples were stored at 4°C for comparative offline analytics using HPLC and an enzymatic D-glucose assay [2].

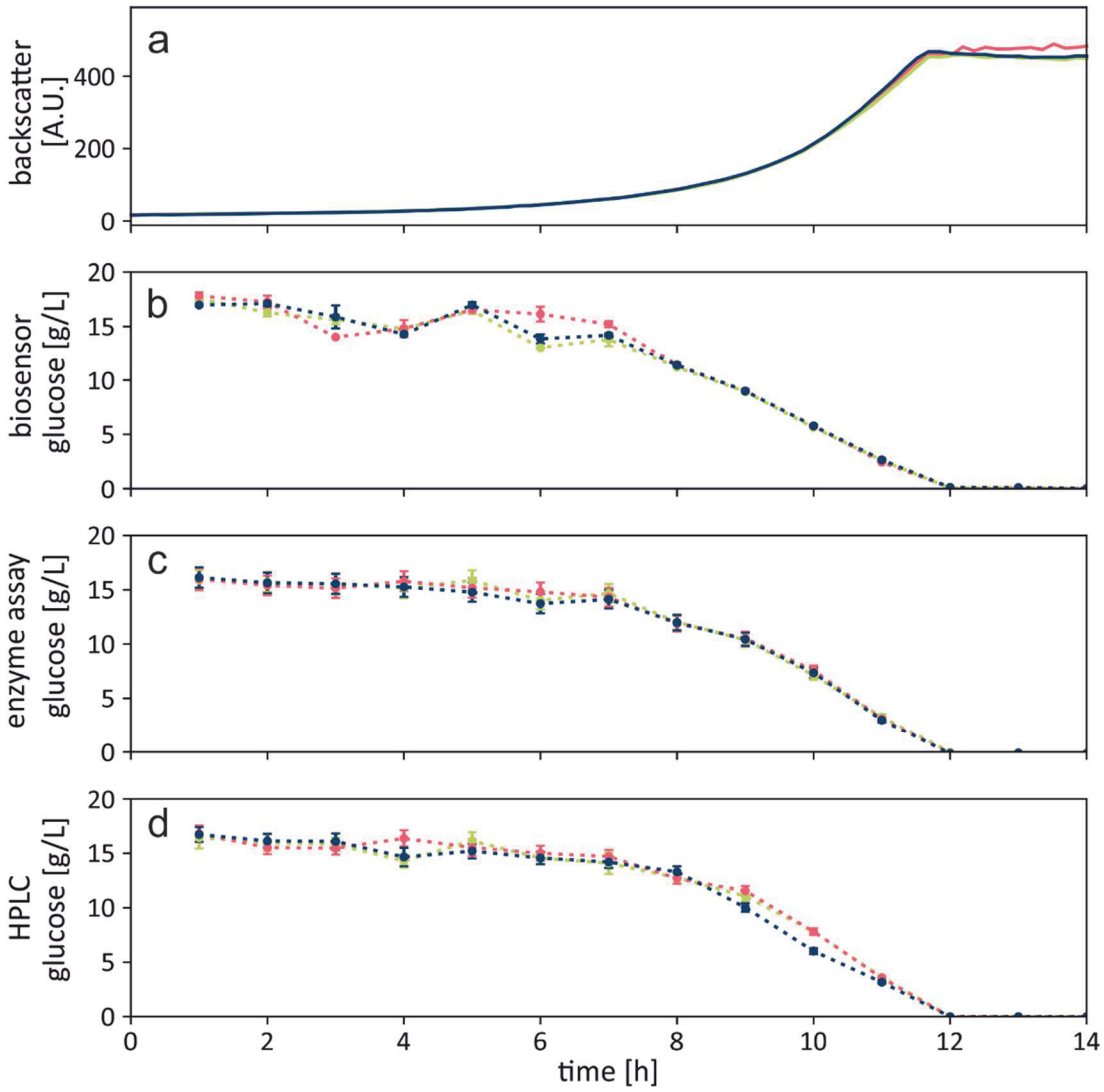

Figure 2.2-3: Biomass growth (a) and D-glucose consumption of *C. glutamicum* ATCC 13032 in CGXII medium followed via (b) the Glu[-] sensor, (c) enzymatic D-glucose assay, and (d) HPLC analysis. While the sensor assay could be performed at-line, enzymatic and HPLC assays were carried out offline after the cultivation was ended. Each curve resembles a biological replicate. The error bars represent the standard deviation (SD) within three technical replicates.

As demonstrated in Fig. 3 the Glu[-] sensor assay performed very well and represented the consumption of D-glucose in accordance to HPLC and enzymatic assay analyses. Notably, the measurement was performed in the presence of bacterial cells, using a low amount of sample (15 µL) and a very short incubation time (< 1 min). These properties facilitate a fast measurement process and thus, our workflow allows for quantification of D-glucose in a high number of samples during the runtime of the cultivation process.

Enzymatic assays are routinely used to quantify D-glucose in samples from microbial cultivations [2,3] and can also be used in an automated at-line setup [33]. However, there are pronounced drawbacks: Firstly, they require previous separation of the bacterial cells, often by means of centrifugation or filtration. This adds complexity to the workflow, is more time-consuming, and requires a complex liquid handling platform. In contrast, the D-glucose sensor assay only needs dilution steps, which can be performed quickly with standard liquid handling operations. Secondly, enzymatic assays involve incubation steps between 10 minutes [34] and 30 minutes [2]. While this time-consuming step is unproblematic when large numbers of samples are processed in parallel, it limits the interval of at-line measurements. For example, a previous study demonstrated at-line D-glucose measurements via an enzymatic assay in 80 min intervals [33]. The Glu[-] biosensor, on the other hand, responds immediately to D-glucose in its environment also in the presence of cells, which paves the way to very short measurement cycles and thus increases the density of data.

To the best of our knowledge there is currently no at-line HPLC method established for microbioreactors due to long retention times and sometimes elaborate sample preparations [35]. Whilst sample preparation by filtration could be readily automated, the drawback of measuring only one sample at a time severely hinders the application of at-line HPLC methods in microbioreactor cultivations, which often include multiple parallel cultivations. However, chromatographic methods have the advantage of measuring multiple analytes in one run.

c) Immobilization

After having successfully set up an at-line measuring protocol in CGXII medium, we next aimed at the application for online measurements. As demonstrated above, the soluble Glu[-] sensor lacks long term stability at temperatures > 25°C and is prone to mechanical stress. Mechanical stress cannot be avoided, since agitation is essential for any microbial cultivation to ensure sufficient mixing and, in case of aerobic cultivation, oxygen transfer. Thus, the sensor stability should be improved. Initial immobilization studies via the His-tag failed, because the Co^{2+}-chelate bond to the nitrilotriacetic acid-functionalized silica beads (Dynabeads,

ThermoScientific) was not stable under process conditions (data not shown). An alternative approach is the immobilization via the HaloTag® [21], which provides covalent immobilization and purification in one step starting also directly from crude cell extracts, as was recently successfully demonstrated for the immobilization of different enzymes [22,36,37].

Fusion of the HaloTag® to the C-terminus of the D-glucose sensor resulted in the sensor Glu$^{[+Halo]}$. This fusion decreased the overall FRET-ratio as well as the ΔR in solution from 75 % to almost 40 % when compared to the Glu$^{[-]}$ sensor. However, upon immobilization the Glu$^{[+Halo]}$ sensor regains the functionality and high signal intensity (ΔR 74 %) of the Glu$^{[-]}$ sensor (for details see Supplementary material, Fig. S1). This surprising result can be explained as follows: As we have shown earlier, the FRET efficiency (signal intensity) is strongly influenced by the distance and flexibility of the donor FP mTurquoise2 relative to the central glucose binding protein (MglB) [20]. Due to a similar size of FP and HaloTag® (about 30 kDa), negative steric effects of the C-terminal HaloTag® in a soluble sensor formulation cannot be excluded, which would explain the decrease of the overall transfer efficiency, as shown in the emission spectra (Fig. 4). Here the reduced transfer efficiency is reflected in a decreased emission of the acceptor Venus after excitation of the donor mTurquoise2 (λ_{ex}= 425 ±9 nm). As the HaloTag® is located at the C-terminus of the sensor, the protein is probably distorted, thereby altering the distance and/or orientation between donor and acceptor. Immobilization on the surface of the Sepharose® beads presumably reduces the interaction of the HaloTag® with the FRET partners resulting in re-established functionality. Remarkably, the affinity (K_d) of the sensor was not influenced by the addition of the tag or the immobilization. In the soluble formulation, as well as in the immobilized form, the affinity remained in the same range (0.8 mM ±0.2 mM), indicating that the HaloTag® does not influence the D-glucose binding site (Supplementary material, Fig. S1).

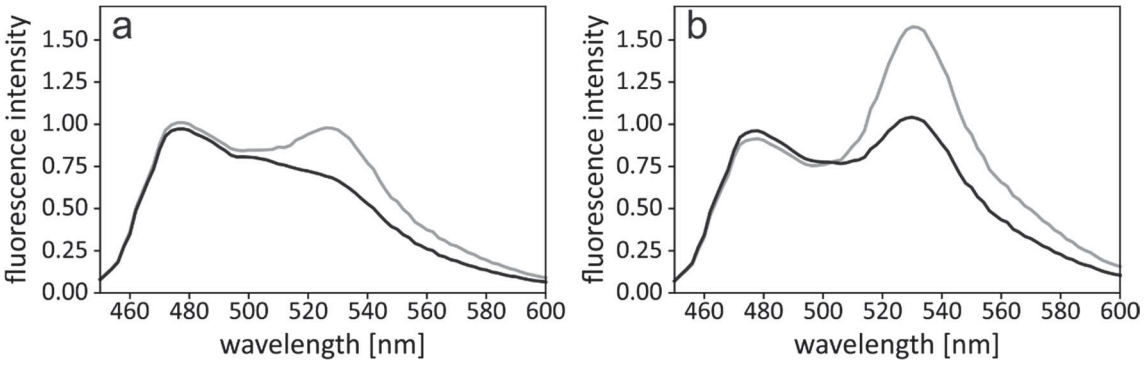

Figure 2.2-4: Emission spectra of the Glu$^{[+Halo]}$ sensor (a) not immobilized and (b) immobilized on HaloLink® resin. Spectra were obtained after excitation of the FRET-donor mTurquoise2 at λ_{ex}= 425 nm (±9 nm) in the presence (black curve) and absence (grey curve) of 1 M D-glucose. Intensities are normalized to the emission at 485 nm (λ_{em} mTurquoise2).

Compared to other immobilization techniques for such sensors, such as encapsulation, the site-oriented immobilization via the HaloTag® is superior, as neither the flexibility nor the accessibility of the immobilized sensor is negatively influenced. In a previous study a similar FRET-based D-glucose sensor was encapsulated in silica particles, which significantly reduced the FRET intensity [38]. Furthermore, the biosensor can be directly immobilized from crude cell extract, thereby avoiding laborious and expensive chromatographic protein purification [39].

d) Online application of the immobilized glucose sensor

With the $Glu^{[+Halo]}$ sensor covalently immobilized on the surface of Sepharose® beads, the stability of the sensor towards mechanical stress was greatly increased, which was a prerequisite to apply these beads directly in a microbial cultivation (Supplementary material, Fig. S6). While the immobilization solves the stability issues, the quenching of CGXII medium remained. Additionally, an increasing concentration of *C. glutamicum* also leads to an increased background due to autofluorescence [40]. To overcome this, the immobilized $Glu^{[+Halo]}$ sensor was tested in M9 medium, a typical cultivation medium for *Escherichia coli* [32]. Despite a reduction of ΔR to 35 %, the change in FRET-ratio is distinguishable (see Supplementary material, Fig. S3). As a consequence, measurements in M9 medium could be performed with sensor directly in the cultivation, which facilitates an online application.

The results from online application of the immobilized $Glu^{[+Halo]}$ sensor during a cultivation of *E. coli* K12 MG1655 in M9 medium are shown in Fig. 5. Throughout the cultivation both fluorescent signals of the sensor were monitored by the BioLector® and the FRET-ratio (I_A/I_D) was calculated. The extracellular D-glucose concentration was then calculated based on the FRET-ratio and a calibration of the immobilized $Glu^{[+Halo]}$ sensor in the same medium within the same flower plate (see Supplementary material, Fig. S9 for the calibration). The consumption of D-glucose could be followed over the entire cultivation experiment (20 hours). Here the $Glu^{[+Halo]}$ sensor had a detection range between 0.02 and 2 mM (0.0036 and 0.36 g/L). Consistent with this range, upon depletion of D-glucose (after 18 hours), no further change of the FRET-signal could be detected. Even though no D-glucose was left in the medium, the biomass increased further, presumably as a result of an overflow metabolism [41].

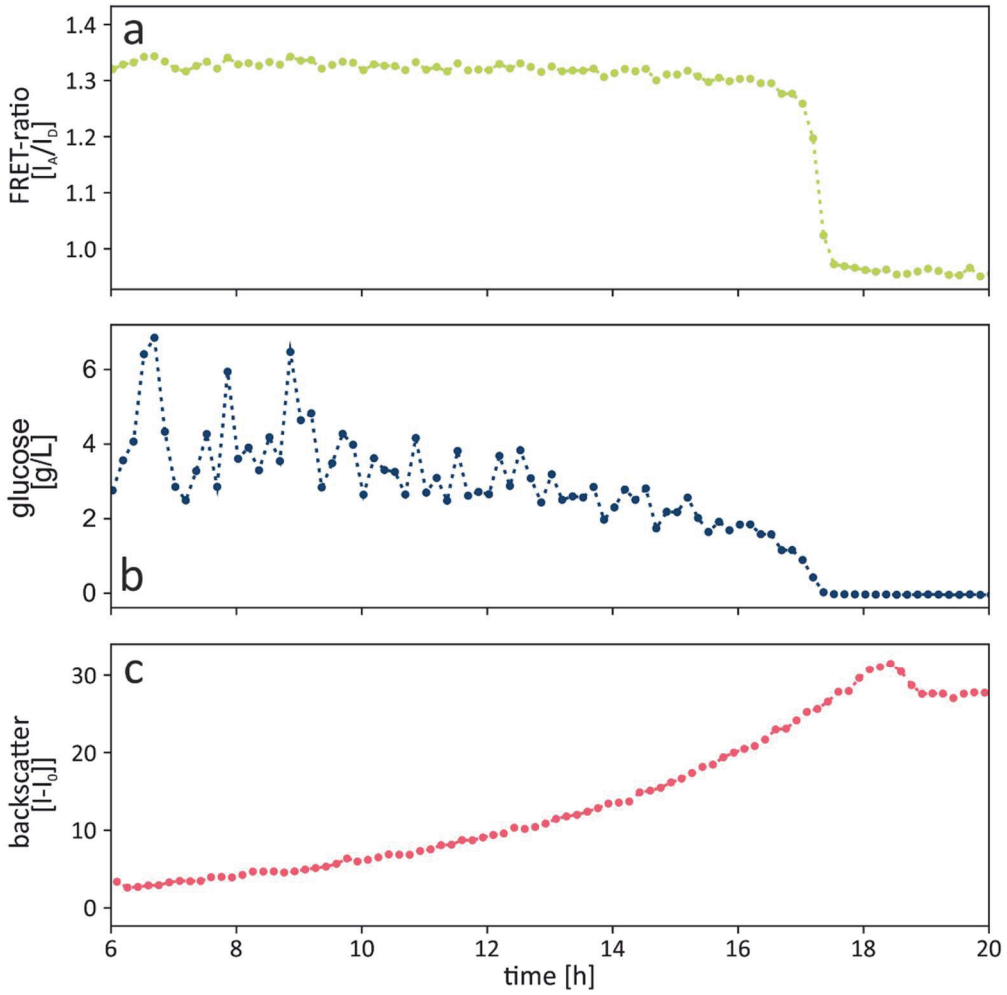

Figure 2.2-5 FRET-ratio (a), glucose depletion (b) and biomass growth (c) in an *E. coli* cultivation measured with the FRET-based biosensor immobilized on HaloLink® resin. The FRET-ratio was used to calculate the current D-glucose concentration based on a calibration of the immobilized sensor (see Supplementary material, Fig. S9).

The advantage of the online measurement goes in line with the drawback of being limited to a certain measuring window defined by the dynamic range of the sensor. Unlike at-line measurements, where the final D-glucose concentration in the samples can be adopted to the sensor affinity, online measurements require either sensors with a broader dynamic range or different sensors with respective affinities to cover a broader concentration range of the target metabolite. The affinity of a D-glucose sensor can be adjusted either by respective amino acid substitution in the glucose binding proteins [24,42,43], by choosing alternative glucose binding proteins with lower affinity [44,45], or by insertion of linker sequences [9,20]. As so far no FRET-based sensor with a very broad detection range is known [7], the combination of multiple D-glucose sensors with different affinities and FRET-pairs immobilized on a single carrier could be considered to broaden the detection range.

2.2.5 Conclusion

We have successfully used a soluble and an immobilized FRET-based D-glucose biosensor to monitor the consumption of D-glucose in small scale microbial cultivations on the example of two common producer strains: *C. glutamicum* and *E. coli*.

We proposed an at-line process using the soluble Glu$^{[-]}$ biosensor. This setup performed well compared to established offline methods like HPLC and enzymatic D-glucose quantification. By using an automated process for sampling and dilution steps, the dynamic range of the Glu$^{[-]}$ sensor was increased by a factor of 40 to 0.4 - 400 mM (0.072 to 72 g/L) and quenching effects of media components were reduced. The presented sensor retained a very high sensitivity with a FRET-ratio change ~60 %.

The immobilization of the sensor variant with HaloTag®, Glu$^{[+Halo]}$, covalently on Sepharose® beads increased the stability towards mechanical stress while retaining the apparent affinity (~0.8 mM) and sensitivity of the Glu$^{[-]}$. The immobilized sensor was then successfully utilized in a microbioreactor to detect the consumption of D-glucose online. So far, no other direct quantification of D-glucose in small scale cultivation devices is possible. Despite the low detection range of the sensor, the immobilized Glu$^{[+Halo]}$ could be used for the online detection and D-glucose control of typically carbon limited fed-batch experiments in milliliter scale.

To further explore the applicability of the immobilized D-glucose sensor, it can also be used in the proposed at-line process. This would broaden the detectable concentration range and enables its application also in media with a strong background, because the culture supernatant can be diluted. For recycling of the immobilized sensor, magnetic particles would be the best option as those are already available with surface modification for the HaloTag® system. Here, the magnetic retention of beads enables washing and sensor recovery.

In conclusion, FRET-based biosensors are now ready to use for metabolite quantification in culture supernatants. Considering the huge variety of periplasmic binding proteins [7,42,46], the range of available FRET pairs [47] and the already available linker toolboxes [9,20] such biosensors can be tailored for the respective application to promote strain and process development in synthetic biology.

Declarations

Ethics approval and consent to participate
Not applicable
Consent for publication
Not applicable

Availability of data and material

The datasets used and/or analyzed during the current study are available from the corresponding author on reasonable request.

Competing interests

The authors declare no conflict of interest.

Funding

This project was partly funded by the German Federal Ministry of Education and Research (BMBF) within the project Optosys, FKZ 031A167B (J.O.) and Molecular Interaction Engineering, FKZ 031A095 (J.D.). Additionally this work was partly funded by the Bioeconomy Science Center (BioSC, Grant. No. 325-40000213) as part of the Focus FUND project "HyImPAct – Hybrid processes for important precursor and active pharmaceutical ingredients." (N.T). Further funding was received from the Enabling Spaces Program "Helmholtz Innovation Labs" of the German Helmholtz Association to support the "Microbial Bioprocess Lab" (R.J). The founding sponsors had no role in the design of the study, in the collection, analyses, or interpretation of data; in the writing of the manuscript, and in the decision to publish the results.

Authors' contributions

J.O, M.P., S.N. and M.O. planned the research. J.O. constructed and characterized the FRET-based sensors. N.T and J.O performed the at-line experiments, R.J. and J.O. performed the online experiments. J.O. and M.P. wrote the manuscript in consent with all authors.

Acknowledgements

We thank Eric von Lieres for his support in data evaluation.

2.2.6 References

1. Hemmerich, J., Noack, S., Wiechert, W. & Oldiges, M. Microbioreactor Systems for Accelerated Bioprocess Development. *Biotechnol. J.* **13,** 1700141 (2018).
2. Unthan, S., Radek, A., Wiechert, W., Oldiges, M. & Noack, S. Bioprocess automation on a Mini Pilot Plant enables fast quantitative microbial phenotyping. *Microb. Cell Fact.* **14,** 32 (2015).
3. Hemmerich, J. *et al.* Less Sacrifice, More Insight: Repeated Low-Volume Sampling of Microbioreactor Cultivations Enables Accelerated Deep Phenotyping of Microbial Strain Libraries. *Biotechnol. J.* 1800428 (2018).
4. Zhang, J., Jensen, M. K. & Keasling, J. D. Development of biosensors and their application in metabolic engineering. *Curr. Opin. Chem. Biol.* **28,** 1–8 (2015).
5. Carlson, H. J. & Campbell, R. E. Genetically encoded FRET-based biosensors for multiparameter fluorescence imaging. *Curr. Opin. Biotechnol.* **20,** 19–27 (2009).
6. Mohsin, M., Ahmad, A. & Iqbal, M. FRET-based genetically-encoded sensors for quantitative monitoring of metabolites. *Biotechnol. Lett.* **37,** 1919–1928 (2015).
7. Sanford, L. & Palmer, A. Recent Advances in Development of Genetically Encoded Fluorescent Sensors. in *Methods in Enzymology* **589,** 1–49 (2017).

8. Moussa, R. *et al.* An evaluation of genetically encoded FRET-based biosensors for quantitative metabolite analyses in vivo. *J. Biotechnol.* **191,** 250–259 (2014).

9. Steffen, V. *et al.* A Toolbox of Genetically Encoded FRET-Based Biosensors for Rapid l-Lysine Analysis. *Sensors* **16,** 1604 (2016).

10. Vyas, N., Vyas, M. & Quiocho, F. Sugar and signal-transducer binding sites of the *Escherichia coli* galactose chemoreceptor protein. *Science* **242,** 1290–1295 (1988).

11. Borrok, M. J., Kiessling, L. L. & Forest, K. T. Conformational changes of glucose/galactose-binding protein illuminated by open, unliganded, and ultra-high-resolution ligand-bound structures. *Protein Sci.* **16,** 1032–1041 (2007).

12. Deuschle, K. *et al.* Construction and optimization of a family of genetically encoded metabolite sensors by semirational protein engineering. *Protein Sci.* **14,** 2304–2314 (2005).

13. Fehr, M. *et al.* Development and use of fluorescent nanosensors for metabolite imaging in living cells. *Biochem. Soc. Trans.* **33,** 287–290 (2005).

14. Goedhart, J. *et al.* Structure-guided evolution of cyan fluorescent proteins towards a quantum yield of 93%. *Nat. Commun.* **3,** 751 (2012).

15. Bajar, B., Wang, E., Zhang, S., Lin, M. & Chu, J. A Guide to Fluorescent Protein FRET Pairs. *Sensors* **16,** 1488 (2016).

16. Markwardt, M. L. *et al.* An Improved Cerulean Fluorescent Protein with Enhanced Brightness and Reduced Reversible Photoswitching. *PLoS One* **6,** e17896 (2011).

17. Rekas, A., Alattia, J.-R., Nagai, T., Miyawaki, A. & Ikura, M. Crystal Structure of Venus, a Yellow Fluorescent Protein with Improved Maturation and Reduced Environmental Sensitivity. *J. Biol. Chem.* **277,** 50573–50578 (2002).

18. Nagai, T. *et al.* A variant of yellow fluorescent protein with fast and efficient maturation for cell-biological applications. *Nat. Biotechnol.* **20,** 87–90 (2002).

19. Rizzo, M. a, Springer, G., Segawa, K., Zipfel, W. R. & Piston, D. W. Optimization of Pairings and Detection Conditions for Measurement of FRET between Cyan and Yellow Fluorescent Proteins. *Microsc. Microanal.* **12,** 238–254 (2006).

20. Höfig, H. *et al.* Genetically Encoded Förster Resonance Energy Transfer-Based Biosensors Studied on the Single-Molecule Level. *ACS Sensors* **3,** 1462–1470 (2018).

21. Los, G. V. *et al.* HaloTag: A Novel Protein Labeling Technology for Cell Imaging and Protein Analysis. *ACS Chem. Biol.* **3,** 373–382 (2008).

22. Döbber, J. & Pohl, M. HaloTag^{TM}: Evaluation of a covalent one-step immobilization for biocatalysis. *J. Biotechnol.* **241,** 170–174 (2017).

23. Heckman, K. L. & Pease, L. R. Gene splicing and mutagenesis by PCR-driven overlap extension. *Nat. Protoc.* **2,** 924–932 (2007).

24. Peroza, E. A., Boumezbeur, A.-H. & Zamboni, N. Rapid, randomized development of genetically encoded FRET sensors for small molecules. *Analyst* **140,** 4540–8 (2015).

25. Gibson, D. G. *et al.* Enzymatic assembly of DNA molecules up to several hundred kilobases. *Nat. Methods* **6,** 343–345 (2009).

26. Hanahan, D. Studies on transformation of *Escherichia coli* with plasmids. *J. Mol. Biol.* **166,** 557–580 (1983).

27. Studier, F. W. Protein production by auto-induction in high-density shaking cultures. *Protein Expr. Purif.* **41,** 207–234 (2005).

28. Lakowicz, J. R. *Principles of fluorescence spectroscopy*. (Springer, 2006).

29. Laemmli, U. K. Cleavage of Structural Proteins during the Assembly of the Head of Bacteriophage T4. *Nature* **227,** 680–685 (1970).

30. Keilhauer, C., Eggeling, L. & Sahm, H. Isoleucine synthesis in *Corynebacterium glutamicum*: molecular analysis of the ilvB-ilvN-ilvC operon. *J. Bacteriol.* **175,** 5595–5603 (1993).

31. Unthan, S. *et al.* Beyond growth rate 0.6: What drives *Corynebacterium glutamicum* to higher growth rates in defined medium. *Biotechnol. Bioeng.* **111,** 359–371 (2014).

32. Sambrook, J., Fritsch, E. F. & Maniatis, T. *Molecular cloning: a laboratory manual. Molecular cloning: a laboratory manual.* (Cold Spring Harbor Laboratory Press, 1989).

33. Nickel, D. B., Cruz-Bournazou, M. N., Wilms, T., Neubauer, P. & Knepper, A. Online bioprocess data generation, analysis, and optimization for parallel fed-batch fermentations in milliliter scale. *Eng. Life Sci.* **17,** 1195–1201 (2017).

34. Knepper, A., Heiser, M., Glauche, F. & Neubauer, P. Robotic Platform for Parallelized Cultivation and Monitoring of Microbial Growth Parameters in Microwell Plates. *J. Lab. Autom.* **19,** 593–601 (2014).

35. Tohmola, N. *et al.* On-line high performance liquid chromatography measurements of extracellular metabolites in an aerobic batch yeast (*Saccharomyces cerevisiae*) culture. *Biotechnol. Bioprocess Eng.* **16,** 264–272 (2011).

36. Döbber, J., Pohl, M., Ley, S. V. & Musio, B. Rapid, selective and stable HaloTag- *Lb* ADH immobilization directly from crude cell extract for the continuous biocatalytic production of chiral alcohols and epoxides. *React. Chem. Eng.* **3,** 8–12 (2018).

37. Döbber, J., Gerlach, T., Offermann, H., Rother, D. & Pohl, M. Closing the gap for efficient immobilization of biocatalysts in continuous processes: HaloTag^{TM} fusion enzymes for a continuous enzymatic cascade towards a vicinal chiral diol. *Green Chem.* **20,** 544–552 (2018).

38. Faccio, G. *et al.* Encapsulation of FRET-based glucose and maltose biosensors to develop functionalized silica nanoparticles. *Analyst* **141,** 3982–3984 (2016).

39. Tufvesson, P., Lima-Ramos, J., Nordblad, M. & Woodley, J. M. Guidelines and Cost Analysis for Catalyst Production in Biocatalytic Processes. *Org. Process Res. Dev.* **15,** 266–274 (2011).

40. Binder, S. *et al.* A high-throughput approach to identify genomic variants of bacterial metabolite producers at the single-cell level. *Genome Biol.* **13,** R40 (2012).

41. Vemuri, G. N., Altman, E., Sangurdekar, D. P., Khodursky, A. B. & Eiteman, M. A. Overflow Metabolism in *Escherichia coli* during Steady-State Growth: Transcriptional Regulation and Effect of the Redox Ratio. *Appl. Environ. Microbiol.* **72,** 3653–3661 (2006).

42. Dwyer, M. a. & Hellinga, H. W. Periplasmic binding proteins: a versatile superfamily for protein engineering. *Curr. Opin. Struct. Biol.* **14,** 495–504 (2004).

43. Hsieh, H. V., Pfeiffer, Z. A., Amiss, T. J., Sherman, D. B. & Pitner, J. B. Direct detection of glucose by surface plasmon resonance with bacterial glucose/galactose-binding protein.

Biosens. Bioelectron. **19,** 653–660 (2004).

44. Tian, Y. *et al.* Structure-based design of robust glucose biosensors using a *Thermotoga maritima* periplasmic glucose-binding protein. *Protein Sci.* **16,** 2240–2250 (2007).

45. Jeffery, C. J. Engineering periplasmic ligand binding proteins as glucose nanosensors. *Nano Rev.* **2,** 5743 (2011).

46. Liu, Y., Liu, Y. & Wang, M. Design, Optimization and Application of Small Molecule Biosensor in Metabolic Engineering. *Front. Microbiol.* **8,** 2012 (2017).

47. Rodriguez, E. A. *et al.* The Growing and Glowing Toolbox of Fluorescent and Photoactive Proteins. *Trends Biochem. Sci.* **42,** 111–129 (2017).

2.3 Application of immobilized FRET-based biosensors in µL scale cultivations

The following results are not yet submitted for publication, because a final experiment is still missing.

A novel platform solution for quantitative microfluidic single-bead D-glucose measurement with high spatio-temporal resolution

Julia Otten, Christoph Westerwalbesloh, Daniel-Timon Spanka, Dietrich Kohlheyer, Wolfgang Wiechert, Martina Pohl

Context:

Additionally to the application in the milliliter range, demonstrated in the previous chapter 2.2, the immobilized FRET-based biosensor Glu$^{[+Halo]}$, was evaluated for the application in microfluidic environments. The general potential of the immobilized Glu$^{[+Halo]}$ sensor for microfluidics was successfully demonstrated by monitoring sensor beads and their response to D-glucose in a PDMS-chip for at least for 24 h. Furthermore, the immobilized Glu$^{[+Halo]}$ sensor was not significantly affected by the presence of *E. coli* cells as a typical platform organism. As the sensor beads displayed no mayor bleaching effects and responded quickly to glucose concentration changes, they can be regarded as suitable for an application in chip-based pico-bioreactors.

Nevertheless, final experiments to demonstrate the feasibility of immobilized FRET-based biosensors as tools for strain development and characterization in microfluidic chips are still missing, due to size limitations of the commercially available sensor beads. In such an experiment, sensor beads of approximately the same size like microbial cells should be entrapped together with *E. coli* cells in a batch cultivation to quantify the consumption of D-glucose in the direct cellular environment.

The glucose sensor Glu$^{[+Halo]}$ clearly demonstrates the power of immobilized FRET-based sensors as tools in microfluidic cultivations. Currently no other system is available capable of online metabolite quantification on a single cell level

Contribution:

Julia Otten, Christoph Westerwalbesloh, Martina Pohl and Dietrich Kohlheyer designed and planned the experiments. Julia Otten designed and optimized the sensor. Julia Otten, Christoph Westerwalbesloh, and Daniel-Timon Spanka performed the experiments. Julia Otten evaluated the data. Julia Otten and Martina Pohl wrote the manuscript in consultation with all authors. Christoph Westerwalbesloh contributed parts of the manuscript.

A Novel Platform Solution For Quantitative Microfluidic Single-Bead D-Glucose Measurement With High Spatio-Temporal Resolution

Julia Otten[1], Christoph Westerwalbesloh[1], Daniel-Timon Spanka[1], Dietrich Kohlheyer[1,2], Wolfgang Wiechert[1], Martina Pohl[1*]

[1] Forschungszentrum Jülich GmbH, IBG-1: Biotechnology, Germany

[2] RWTH Aachen University, Aachener Verfahrenstechnik (AVT.MSB), Aachen, Germany

2.3.1 Abstract

Microfluidics offers great potential in microbiology. Miniaturization of cultivation vessels and automated monitoring of single cells under a microscope allow for higher throughput and detailed phenotyping. Nevertheless, the cultivation of cells in µL-scale bioreactors currently lacks sensors to quantify extracellular metabolites that are either consumed or produced by the cells. FRET-based sensors have already been proven to be reliable tools for the quantification of extracellular metabolites. Here we present a genetically encoded, immobilized FRET-based biosensor, which enables the detection of glucose in µL-scale bioreactors. The sensor consists of a glucose binding protein sandwiched between mTurquoise2 and Venus as FRET-pair. Upon ligand binding the binding protein undergoes a conformational change, which is transferred to the FRET-pair and results in a FRET-ratio change. The ratiometric signal is therewith independent of background and sensor concentration. The sensor was immobilized via the HaloTag™ on the surface of beads. These beads gave a stable clearly detectable signal in a time-lapse microscopy setting. The sensor beads were applied to monitor changes in glucose concentration in a PDMS chip in pure Wilms-MOPS medium as well as in the presence of *E. coli* MG 1655. The sensor beads responded fast and reproducibly during the 16 hours lasting experiment, indicating the great potential of FRET-based sensors in µL-scale cultivation as a non-invasive online measuring tool next to single cells.

2.3.2 Introduction

Cultivation of microbial cells in µL scale enables valuable insights on the single cell level.[1] For example, co-cultivations can help to understand interactions between symbiotically living strains,[2] heterogeneity studies can be performed[3] and cell division can be analyzed.[4] In recent years, time-lapse fluorescence microscopy has become increasingly popular and powerful to monitor micro-, nano- and even picoliter scale bioreactors.[5,6] Due to the small volumes, such bioreactors enable the parallelized analysis of a large number of samples using only very limited volumes of cultivation medium and microbial cells. In this small scale, fluorescence, as a very

sensitive non-invasive method, is essential to monitor effects. Time-lapse fluorescence microscopy easily allows for single cell analysis by following microbial growth or gene expression inside microbial cells using respective fluorescent markers and reporters,[7] whereas the determination of non-fluorescent metabolites in the cell environment is extremely challenging. Advanced mass spectrometry methods allow the reduction of sample volumes to 50 nL.[8] Additionally increased sensitivities detect concentrations in the sub-milimolar range mimicking concentrations in 1 pL volumes.[9] Nevertheless, they still require laborious instrumental setup and enable only offline measurements. Further, currently no coupling to micro-chip based cultivations is available.[9]

Knowledge of the concentration change of key components in the media composition around growing cells, either provided by the medium or secreted by the cells, would yield valuable information concerning the optimization of growth parameters and the identification of producer strains. Here fluorescent, FRET-based biosensors have been proven advantageous. FRET-based biosensors, employing two derivatives of the green fluorescent protein (GFP) fused to either end of a central metabolite binding protein, enable detection of metabolites inside cells.[10] As we have shown previously, it is impossible to calibrate these FRET-based biosensors for intracellular quantification of metabolites.[11] However, such sensors can be reliably applied outside living cells to quantify metabolites in the cell supernatant, as we have demonstrated recently for L-lysine[12] and D-glucose[13] in a micro cultivation device. Both sensors were applied in soluble form, but lacked stability. Here covalent immobilization via the HaloTag™[14] was specifically useful.[13] This technique has proven to increase stability of several enzymes[15–17] and did also significantly increase the stability of the $Glu^{[+Halo]}$ sensor, as was recently demonstrated.[13] Immobilization on Sepharose beads did not influence the sensor parameters. The sensor shows an apparent affinity in the range of 0.7 mM and a high sensitivity of up to 70 % FRET-ratio change.

In this study, this immobilized D-glucose sensor $Glu^{[+Halo]}$ was evaluated for application in microfluidic chips. The sensor consists of a fusions of the fluorescence proteins mTurquoise2 (cyan, donor) and Venus (yellow, acceptor) to either end of a periplasmic glucose-galactose binding protein (GGBP) from E. coli.[18] The conformational change induced by the ligands D-glucose or D-galactose,[19] results in altered orientation and/or distance of the FRET-partners. These structural changes affect the energy transfer between the fluorescent proteins and therewith the FRET-ratio.[20] Besides using a senor with bright and stable FRET-partners, the sensitivity (ΔR, FRET ratio change of the non-liganded state and fully liganded state) must be highest within the range of D-glucose used in the respective cultivation. This was recently achieved by introducing a flexible $(GGS)_4$ linker between the donor and the binding protein.[18]

Although there are several glucose sensors available, continuous monitoring of glucose using optical sensors is still limited and is also in large scale usually performed at-line.[21] However, for the microscale so far optical methods to monitor extracellular metabolites are scarce.[21]

We demonstrate that our designed immobilized glucose sensor can be used for online glucose quantification in different microscale bioreactors. To the best of our knowledge this is the first time that this type of an optical glucose sensor has been described for such scale.

2.3.3 Results

We recently pointed out advantages of an immobilized Glu$^{[+Halo]}$ biosensor as analytical tool for microbial cultivations.[13] To facilitate strain development and biotechnological applications with minimal resources and high resolution, the applications of this sensor in µscale bioreactors was studied.

a) General functionality

Preliminary experiments to estimate the suitability of the immobilized Glu$^{[+Halo]}$ biosensor for applications in microfluidic chips were performed on a glass slide to examine the change in signal intensity under a fluorescence microscope. The sensor was covalently immobilized on the surface of HaloLink™ Sepharose beads. Both fluorescent signals of the donor and the acceptor could be successfully recorded (Figure 2.3-1). The addition of D-glucose (100 mM in 20 mM MOPS buffer) resulted in an altered FRET ratio (ΔR 32%) indicating the functionality of the Glu$^{[+Halo]}$ sensor. Based on these studies further investigation using time-lapse fluorescence microscopy in microfluidic chips were performed.

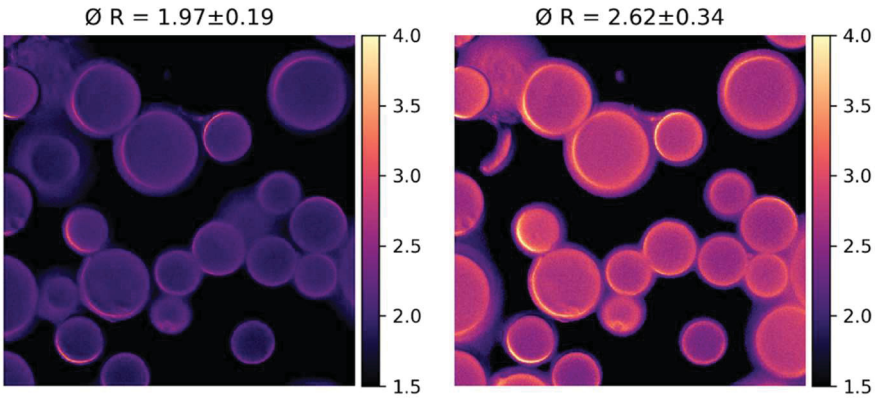

Figure 2.3-1: FRET ratio of immobilized Glu$^{[+Halo]}$ on HaloLink™ Sepharose beads positioned on a glass slide prior (left) and after (right) addition of 10 µl D-glucose (100 mM in 20 mM MOPS buffer).The overall mean FRET-ratio was altered by 32 %. λ_{ex}:436 ± 12 nm, λ_{em} donor (mTurquoise2): 470 ± 12 nm, λ_{em} acceptor (Venus): 535 ± 15 nm

b) Sensor bead performance in customized chip

As shown previously for similar sensors detecting D-glucose sensor and a maltose,[11] as well as L-lysine,[12] the signal intensity of FRET-based biosensors strongly depends on the surrounding medium. We therefore tested the Glu$^{[+Halo]}$ sensor with Wilms-MOPS medium, a frequently used minimal medium in microscale cultivations of the platform organism E. coli.[22] This medium is well defined and therefore facilitates reproducibility, in contrast to complex media.

Most chip reactors in microliter scale consist of poly dimethyl siloxane (PDMS) and are designed to trap and monitor single microbial cells in channels or chambers in the range of a few nm height.[6,22] However, previously used HaloLink™ Sepharose beads (45 – 165 µm) are far too large for such chips. Additionally, the broad size distribution is problematic for an automated image analysis. Even though also available magneHaloLink™ beads (diameter ~60 µm) are still too large, their size is much more uniform. Additionally, the magnetic functionality enables easy recycling of Glu$^{[+Halo]}$ biosensor (data not shown). Further experiments were therefore conducted with these magnetic beads.

To enable the usage of the magnetic beads, the dimensions of the PDMS chip was adopted to harbor the magneHaloLink™ beads loaded with the Glu$^{[+Halo]}$ sensor. The chip consisted of straight channels with three stair-like structures per channel, which gradually decrease the height in order to trap the magnetic particles as demonstrated in Figure 2.3-2 and in more detail in the supplementary information (Appendix page 143). After immobilization of the Glu$^{[+Halo]}$ sensor the magnetic beads were flushed into the channel using MOPS buffer (20 mM, pH 7.3) where they were trapped in the stair structures. Afterwards the Glu$^{[+Halo]}$ sensor beads were located and at least 10 positions were selected to be followed with time-lapse fluorescence spectroscopy over time.

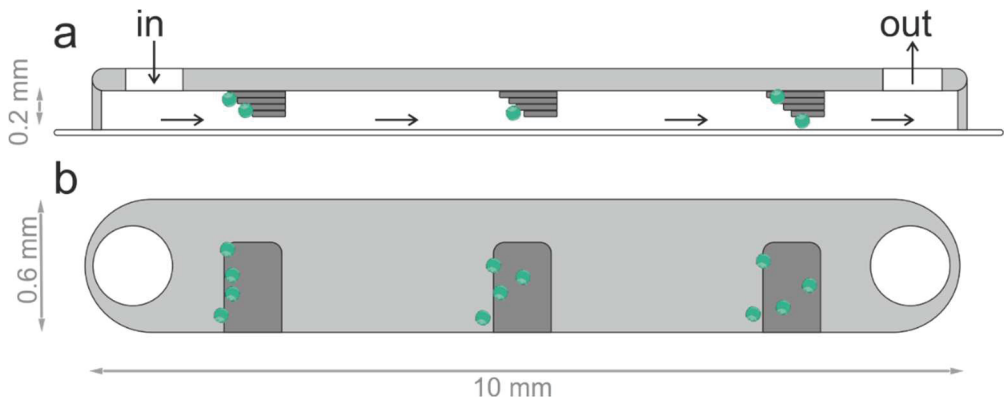

Figure 2.3-2: Side view (a) and top view (b) of a schematic presentation of the PDMS chip mounted onto a glass slide.PDMS material is indicated in shades of gray. The stair-like structures (darker grey) gradually decrease the height of channel by 0.02 mm per step. By flushing in the immobilized Glu$^{[+Halo]}$ sensor on magneHaloLink™ beads (indicated in green), the beads are trapped at the stair-like structures. For a more detailed presentation please refer to the supplementary information (Appendix page 143).

In previous studies with this sensor, the immobilized sensor showed a detection range between 0.01 and 10 mM D-glucose.[13] It can be assumed that the sensor would perform similar under µL-scale conditions. In order to test the functionality of the sensor beads inside the PDMS chip, the beads were first trapped in the stair-like structures (see Figure 2.3-2). Afterwards an alternating flow between Wilms-MOPS medium with or without D-glucose (10 mM) was applied. As demonstrated in Figure 2.3-3, the sensor beads are well visible in the PDMS chip and the changes in D-glucose concentration are detectable by respective FRET changes. By calculating the FRET-ratio and applying a heat map representation, a clear change in FRET-ratio between states with and without D-glucose could be shown in the monitored positions. Between 10 mM and 0 mM the FRET-ratio changes gradually with a maximum ΔR of 31 ± 1%. The ΔR is similar to earlier observations in minimal *E. coli* cultivation media. Calibration of the immobilized Glu$^{[+Halo]}$ sensor in M9 medium showed a ΔR of 35%[13] with no influence on the affinity of the senor. The signal started decreasing as soon as the D-glucose concentration decreases (green arrow) and increased again with increasing concentration (blue arrow) restoring the initial FRET-ratio. It can be therefore concluded that the sensor beads were stable during the whole experiment (2h) and thus are well suited for metabolite analysis at µL-scale.

Nevertheless, it should be noted that the sensor responses significantly faster towards an increasing concentration of D-glucose. Between two data points (20 minutes), D-glucose addition results in a stable high signal. In contrast the decreasing of the signal due to removal of D-glucose through washout lasted for 5 data points (2 hours), significantly longer than the time of roughly 70 s - 80 s needed to completely exchange the volume of the chip. To this point we cannot explain this behavior.

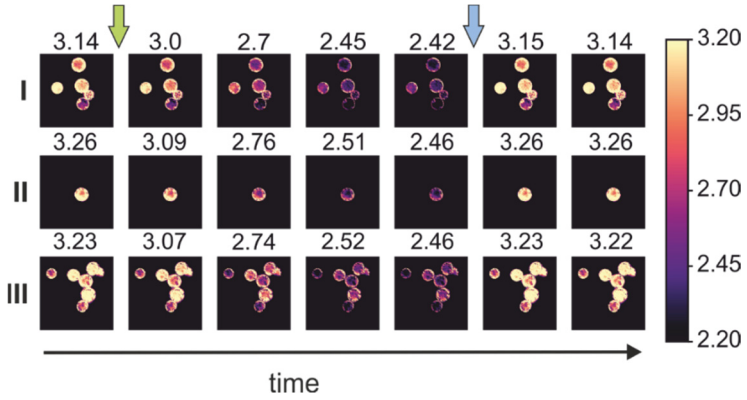

Figure 2.3-3: False colored image of the FRET ratio of the immobilized Glu$^{[+Halo]}$ sensor on magnetic resin. Exemplarily three positions of sensor beads (I, II, III) are depicted. The FRET-ratio (given above each image) was calculated as the mean per image. At the points in time marked by arrows either Wilms-MOPS medium (green) or Wilms-Mops medium with 10 mM D-glucose were supplied (blue). Interval between images = 20 minutes.

c) Pulsing studies with and without *E. coli*

As microbial cultivations typically last several hours, the immobilized Glu$^{[+Halo]}$ sensor must be stable for about 20 h. Additionally, the sensor should detect changes in D-glucose concentration, resulting for example from pulsed feeding, with only little delay. To demonstrate the reversibility and stability of the D-glucose detection, the immobilized Glu$^{[+Halo]}$ sensor was tested in a continuous pulsing setup monitored via time-lapse microscopy. As demonstrated in Figure 2.3-4,the sensor was repeatedly exposed to an environment with and without D-glucose by applying an altering flow of Wilms-MOPS medium containing no D-glucose (S1) or 10 mM D-glucose (S2), 500 nL/min) additional to a constant flow of medium without D-glucose (S3, 500 nL/min).

The experiment showed that a total flow rate of 1000 nL/min does not strip the sensor from the beads. Neither were the particles moved, although no magnetic force was applied. Thus, beads could be monitored for the entire experimental setup (24 h). As demonstrated in Figure 2.3-4, a FRET-ratio change (ΔR) of ~32 % was consistent over the entire experiment. The change of roughly 32 % in Wilms-MOPS medium is similar to the change in MOPS buffer shown in Figure 2.3-4, indicating no quenching effect of the media or the PDMS environment. In accordance to previous results, the sensor responded towards concentration changes and we could demonstrate the reversibility of the D-glucose binding. Every glucose pulse (flow 1 µl/min) lasted 2 hours. As soon as the 10 mM D-glucose supply ended the FRET-ratio decreased, reaching the minimum just prior to a new pulse (after 2 hours).

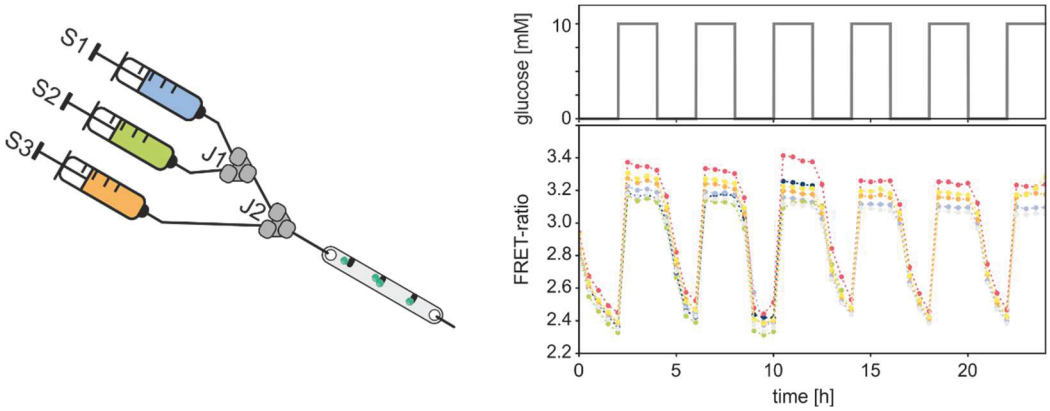

Figure 2.3-4 left: Flow diagram depicting the syringes (S1-3) and joints (J1&2) connected to a channel on a PDMS chip used for the pulsing experiment.50 % of the overall flow was generated by altering the flow of 500 nL/min between S1 (10 mM D-glucose in Wilms-MOPS media) and S2 (Wilms-MOPS w/o D-glucose). Remaining 50 % of the flow results from 500 nL/min S3 (Wilms-MOPS w/o D-glucose). right: FRET-ratio of the immobilized Glu$^{[+Halo]}$ sensor in Wilms-MOPS medium with D-glucose pulsing above (grey). Each color resembles a defined position in the PDMS chip. The FRET-ratio was calculated as the mean over all beads in a single image. For details see Methods.

With this experiment we could demonstrate the functionality of the sensor in a well-defined cultivation medium for 24 hours. Even though the FRET-ratio differed slightly (R_{sat} ± 2 %, R_0 ± 3%) between each position in the chip, the mean FRET-ratio change (ΔR) was consistent over all positions with the same error (ΔR ± 2%). A slight decrease of the ratio under glucose saturation over time of 3 percent is presumably a result of bleaching effects of the fluorescent proteins. Still the functionality remained, and the sensor beads responded with a constant ΔR of 32 %.

After the reliability of the Glu$^{[+Halo]}$ sensor beads was demonstrated, in the following experiment *Escherichia coli* MG1655 cells, grown in Wilms-MOPS medium, were added via syringe S3* (Figure 2.3-5). Similar to the first experiments, the sensor responded quickly and reproducible to each D-glucose pulse (see Figure 2.3-5). Compared to the FRET-ratio change in the absence of *E. coli* cells (32 % ΔR) the addition of D-glucose resulted in a slightly lower signal intensity change of ~25 % ΔR. The decreased ΔR likely resulted from a change in pH introduced by S3*, as the Wilms-MOPS medium in this syringe had already been metabolized by *E. coli* and therewith had a lower pH.[23] Nevertheless, the response of the beads could be monitored over the entire experiment (16 hours) indicating no significant influence of the cells.

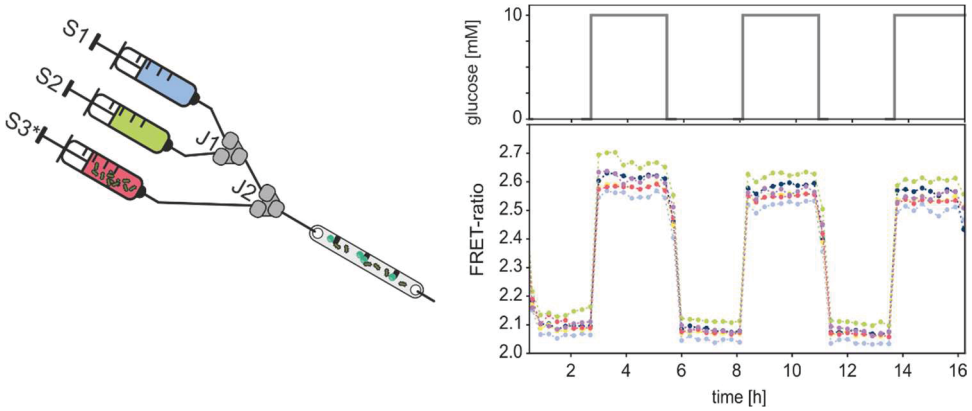

Figure 2.3-5 left: Flow diagram depicting the syringes (S1-3*) and joints (J1&2) connected to a channel on a PDMS chip used for the pulsing experiment.50 % of the overall flow was generated by altering the flow of 500 nL/min between S1 (10 mM D-glucose in Wilms-MOPS media) and S2 (Wilms-MOPS w/o D-glucose). Remaining 50 % of the flow results in 500 nL/min from S3* (*E. coli* MG1655 in metabolized Wilms-MOPS w/o D-glucose). right: FRET-ratio of the immobilized Glu$^{[+Halo]}$ sensor in Wilms-MOPS medium with D-glucose pulsing above (grey) in the presence of cells. Each color resembles a defined position in the PDMS chip. The FRET-ratio was calculated as the mean over all beads in a single image. For details see Methods.

As the sensor beads are easily distinguishable form the background, computational analysis of the data is possible without the necessity of elaborate image processing filters. We could demonstrate the functionality of the magnetic Glu$^{[+Halo]}$ sensor beads for the detection of concentration changes in a microfluidic chip, in the presence and absence of bacterial cells. The next step will be to monitor D-glucose depletion next to *E. coli* cells in a respective cultivation experiment.

Unfortunately, due to the size of the magnetic beads, currently no chip design is available were the beads could be used for a cultivation on the single cell level. Therefore, sensor beads and microbial cells cannot be used in the same experiment and smaller sensor beads with diameters in the range of a bacterial cell (1 to 10 µm) are necessary. With the current chip/sensor bead system the resolution of bacterial cells is not possible, since the sensor beads are by a factor of 10 larger than a single cell and channel height in the specifically designed chip is much too large for a bacterial monolayer (Figure 2.3-2).

Additionally, the channel volumes (about 1.2 µL) necessary for the current sensor beads cause a higher flowrate than smaller channel and tubing geometries. Slower flow would result in blurred transitions between the glucose pulses due to increased mixing in channel and tubing. Additionally, the flow rate of 1 µL/min counteracted the evaporation of the medium, enhanced by relatively large surface area (6 mm^2) of the channel. Due to this high flow rate, glucose consumption of the cells on their passage through the chip cannot be resolved. During their

residence time of about 70 seconds, even under ideal conditions, we estimated that *E. coli* would consume less than 2 mM of D-glucose prior to leaving the chip. Even though the applied $Glu^{[+Halo]}$ sensor has a dynamic range between 0.01 and 10 mM (see Supplementary information, Appendix page 143) changes in concentration close to the boundaries of the dynamic range cannot be resolved ideally.[13] Therefore, a change from 10 to 8 mM D-glucose caused by the *E. coli* cells would currently lie within the error range.

Further proper calibration of the $Glu^{[+Halo]}$ sensor in a PDMS chip has yet to be established. The binding isotherm for the FRET-based sensor in microtiter plate reader cannot be transferred to µscale experiments monitored by time-lapse microscopy, as the detection limits and measurement capacity of a micro-titer plate reader and a fluorescence microscope cannot be compared. The preparation of respective sensor beads with smaller diameters is currently ongoing as well as the development of an appropriate calibration scheme.

2.3.4 Conclusion

We propose the application of FRET-based D-glucose sensor, immobilized on beads, as a tool to monitor the changes in D-glucose concentration in picoliter scale bioreactors. While research on calibration and quantification is still ongoing, the immobilized $Glu^{[+Halo]}$ sensor was already successfully used in a microscopic time-lapse setting to detect D-glucose pulses in a feed medium. Here an overall FRET-ratio change of about 30 % and 25 % in the absence and in the presence of *E. coli* was shown, respectively. This sensitivity is high enough to be computationally distinguished from the background, additionally to the distinct shape of the sensor beads.

For the utilization of the sensor with platform organism like *E. coli* or *Corynebacterium glutamicum,* smaller beads for immobilization of the $Glu^{[+Halo]}$ would be needed. The preparation of such beads would open the door for the application in picobioreactor. As the FRET-based sensors can easily be modified by exchanging the binding protein to recognize other metabolites,[24] we are confident that the positive results with this FRET-based biosensor can be transferred to construct and apply similar FRET-based sensors for other metabolites like lysine.[12] As there are currently no other methods for online analysis in single cell cultivation[9] this would be of great value and potential for single cell analysis.

2.3.5 Methods

a) Protein preparation

The used sensor Glu[+Halo] was produced in *E. coli* Bl21(DE3) and purified as previously described.[13]

b) Immobilization

For the immobilization of the Glu[+Halo] sensor either HaloLink™ Sepharose or magnetic magneHaloLink™ beads (Promega, Mannheim, Germany) were used. Prior to contact with the purified Glu[+Halo] sensor protein, 100 µL bead suspension (20 % v/v) were washed twice with MOPS buffer (20 mM, pH 7.3). The magnetic beads were retained with a magnet and the supernatant was removed before the sensor solution (200 µL) was added. The Sepharose beads were separated via centrifugation from the liquid phase. After addition of the Glu[+Halo] sensor (2.6 mg/mL) both types of sensor beads were incubated for up to one hour under constant slow inversion in a 1.5 mL Eppendorf tube at room temperature. After immobilization, the supernatant was removed, and the beads were washed twice with MOPS buffer (20 mM, pH 7.3). The immobilized Glu[+Halo] sensor was stored as 20 % suspension in MOPS buffer (20 mM, pH7.3, 20 %) at 4°C.

c) Micro scale chip design and manufacturing

The PDMS chips for the pulsing experiment study were fabricated using a custom-made 3D printed mold. The mold was stereolithographically printed using a Form2 printer (Formlabs GmbH, Berlin, Germany) using black photo reactive resin RS-F2-GPBK-04 (Formlabs GmbH, Berlin, Germany) and a layer height of 25 µm. After printing, residual resin was removed using 2-propanol. The 3D model required for the 3D print was created using Solidworks (Dassault Systemes Deutschland GmbH, Stuttgart, Germany). The mold for the PDMS chips incorporated 4 copies of the chips to fabricate multiple chips in parallel.

For production of the PDMS chips, 35 g of a 10:1 mixture of the polymer base and cross linker (Silicone Elastomer Kit \#184, Dow Corning, Midland) were mixed and then degassed in a desiccator (Duran, Germany) at 200 mbar for 30 minutes. The transparent bubble free mixture was poured into the mold and crosslinked at 45° C for 3 hours inside an oven (UN 200, Memmert, Germany). The height of the hardened PDMS layer was roughly 2 mm. Afterwards the PDMS was removed from the mold, cut into single chips and inlets and outlets were punched using a punching tool (Ø 0.75 mm, Fisher Scientific, Germany).

All working steps were performed under a crossflow clean bench to reduce contamination with particles. The chips were also rinsed with 2-propanol and dried under nitrogen gas flow. Remaining particles were removed using duct tape. The chip and a glass slide of 170 µm thickness serving as the glass bottom were subsequently placed in a plasma generator and both parts were oxygen plasma treated for 25 seconds (Femto Plasma Cleaner, Diener Electronics, Germany) at 0.8 mbar with a gas flow of 15 sccm. Immediately afterwards the PDMS chip was placed on the glass slide to initiate bonding. Bonded PDMS chips were stored at ambient temperature for up to three months.

d) Microscope FRET-set up

The PDMS chip was placed on an inverted fluorescence microscope (Nikon Ti Eclipse, Nikon Corporation, Japan). The system was equipped with an incubator (PeCon GmbH, Germany), an objective with 20× magnification (Plan Apo DIC M N2; Nikon, Japan) and a perfect focus system (PFS) (Nikon Corporation, Japan) for focus drift compensation. A dual filter setup was used to detect FRET with two Andor Luca-R DL-880 cameras (Andor Technology Ltd, Northern Ireland). A Lambda DG-4 wavelength switcher was used to filter for excitation at 436 nm ± 10 nm for 200 ms with 33% intensity to reduce bleaching. Two filter cubes were mounted, the first bearing only a dichroic mirror to exclude excitation wavelength, and the second filter cube had two filters for dual emission at 470 ± 12 nm (cyan emission) and 535 ± 15 nm (yellow emission), separated by a beam splitter (491 nm). For a schematic presentation of the microscopic set up, as well as for further filter details please refer to the supplementary information (Appendix, page 142).

e) Pulsing experiments

Tubing connection: Wilms-MOPS medium was prepared according to the literature.[22] For each pulsing experiment, one channel with three sets of stair-like structures on a PDMS chips was used (see supplementary information for chip design; Appendix page 143). The channel was connected by tubing (Saint-Gobain, Paris) with proper junctions (Precision tips, Nordson, Erkrath) to the medium supply syringes (ILS, Fürstenfeldbruck). The flow into the chip was provided by low-pressure syringe pumps (Cetoni, Korbussen) using three syringes. Those were loaded with different content as follows: syringes one (S1) and three (S3) contained Wilms-MOPS medium without D-glucose, syringe two (S2) contained the same medium with 10 mM D-glucose. The outlets of S1 and S2 were connected via tubing (Saint-Gobain, Paris) to a y-shaped junction (J1). The outlet of J2 and the outlet of S3 were connected again to a y-shaped junction (J2) as final outlet prior to the chip (please refer to Figure 2.3-3 for a schematic presentation).

Chip loading and connection: After immobilization of the sensor Glu$^{[+Halo]}$ on magneHaloLink™ beads (according to b), the respective suspension was injected into the channel via a syringe (1 mL, ILS, Gurstenfeldrück, Germany) followed by an air bubble to trap the sensor beads in the stair-like structures as earlier described.[25] After loading a channel with beads and placing the chip on the microscope, the outlet of J2 was connected and a flow of 500 nL/min was applied to S3 and S2 each, while S1 remained at 0 nL/min, resulting in a combined flow rate of 1 µL/min with 10 mM D-glucose present in the channel as starting condition. The experiment was started by switching the flow to S1 and every two hours the flow (500 nL/min) was altered between S1 and S2 to either remove D-glucose from the channel or introduce new D-glucose. This flow rate resulted in a residence time of ~72 s based on a channel volume of ~1.2 µl.

Pulsing experiment containing cells: *Escherichia coli* MG1655 was grown in a three step cultivation to saturation according to Ref.[22], first in LB- media followed by two overnight cultivations in 20 mL Wilms-MOPS media. For experiments in the presence of *Escherichia coli* MG1655, the supply of cells into the channel was established via S3*. In this set up S3* contained instead of medium, *E. coli* MG1655 cells in the Wilms-MOPS medium they were previously cultivated in.

Imaging: Images were recoded for up to 24 hours at a 20 minute interval in the microscopic set up according to d). Experiments were performed at room temperature under exclusion of light.

f) Image processing

Image processing was performed using python code (version 3.6, Python Software Foundation, python.org) with the packages pandas version 0.20 (McKinney, 2010), numpy version 1.13[27], matplotlib version 2.1[28] and nd2reader (version 3.0). After transforming the generated images into a 2D data matrix and setting an intensity threshold (<2000) to filter for background and noise, the FRET ratio was calculated. Therefore, the intensity of the acceptor Venus was divided by the intensity of the donor mTurquoise2. For the plots in Figure 2.3-4 and Figure 2.3-5, a mean over the entire matrix was calculated and plotted as a function of time. Given errors result from the standard deviation over the analyzed positions in a channel if not stated otherwise.

2.3.6 References

1. Rosenthal, K., Oehling, V., Dusny, C. & Schmid, A. Beyond the bulk: disclosing the life of single microbial cells. *FEMS Microbiol. Rev.* **41,** 751–780 (2017).
2. Burmeister, A. *et al.* A microfluidic co-cultivation platform to investigate microbial interactions at defined microenvironments. *Lab Chip* **19**, 98-110 (2019).
3. Binder, D. *et al.* Homogenizing bacterial cell factories: Analysis and engineering of phenotypic heterogeneity. *Metab. Eng.* **42,** 145–156 (2017).
4. Grünberger, A. *et al.* A disposable picolitre bioreactor for cultivation and investigation of industrially relevant bacteria on the single cell level. *Lab Chip* **12,** 2060 (2012).
5. Muzzey, D. & van Oudenaarden, A. Quantitative Time-Lapse Fluorescence Microscopy in Single Cells. *Annu. Rev. Cell Dev. Biol.* **25,** 301–327 (2009).
6. Gruenberger, A. *et al.* Microfluidic Picoliter Bioreactor for Microbial Single-cell Analysis: Fabrication, System Setup, and Operation. *J. Vis. Exp.* **82**, 50560 (2013).
7. Binder, S. *et al.* A high-throughput approach to identify genomic variants of bacterial metabolite producers at the single-cell level. *Genome Biol.* **13,** R40 (2012).
8. Diefenbach, X. W. *et al.* Enabling Biocatalysis by High-Throughput Protein Engineering Using Droplet Microfluidics Coupled to Mass Spectrometry. *ACS Omega* **3,** 1498–1508 (2018).
9. Demling, P., Westerwalbesloh, C., Noack, S., Wiechert, W. & Kohlheyer, D. Quantitative measurements in single-cell analysis: towards scalability in microbial bioprocess development. *Curr. Opin. Biotechnol.* **54,** 121–127 (2018).
10. Sanford, L. & Palmer, A. Recent Advances in Development of Genetically Encoded Fluorescent Sensors. in *Methods in Enzymology* **589,** 1–49 (Elsevier Inc., 2017).
11. Moussa, R. *et al.* An evaluation of genetically encoded FRET-based biosensors for quantitative metabolite analyses in vivo. *J. Biotechnol.* **191,** 250–259 (2014).
12. Steffen, V. *et al.* A Toolbox of Genetically Encoded FRET-Based Biosensors for Rapid l-Lysine Analysis. *Sensors* **16,** 1604 (2016).
13. Otten, J. *et al.* A FRET-based biosensor for the quantification of glucose in culture supernatants of mL scale microbial cultivations. *Microb. Cell Fact.* **18,** 143 (2019).
14. Los, G. V. *et al.* HaloTag: A Novel Protein Labeling Technology for Cell Imaging and Protein Analysis. *ACS Chem. Biol.* **3,** 373–382 (2008).
15. Döbber, J. & Pohl, M. HaloTag™: Evaluation of a covalent one-step immobilization for biocatalysis. *J. Biotechnol.* **241,** 170–174 (2017).
16. Döbber, J., Gerlach, T., Offermann, H., Rother, D. & Pohl, M. Closing the gap for efficient immobilization of biocatalysts in continuous processes: HaloTag™ fusion enzymes for a continuous enzymatic cascade towards a vicinal chiral diol. *Green Chem.* **20,** 544–552 (2018).
17. Döbber, J., Pohl, M., Ley, S. V. & Musio, B. Rapid, selective and stable HaloTag- Lb ADH immobilization directly from crude cell extract for the continuous biocatalytic production of chiral alcohols and epoxides. *React. Chem. Eng.* **3,** 8–12 (2018).
18. Höfig, H. *et al.* Genetically Encoded Förster Resonance Energy Transfer-Based Biosensors Studied on the Single-Molecule Level. *ACS Sensors* **3,** 1462–1470 (2018).

19. Borrok, M. J., Kiessling, L. L. & Forest, K. T. Conformational changes of glucose/galactose-binding protein illuminated by open, unliganded, and ultra-high-resolution ligand-bound structures. *Protein Sci.* **16,** 1032–1041 (2007).

20. Lakowicz, J. R. *Principles of fluorescence spectroscopy*. (Springer, 2006).

21. Gruber, P., Marques, M. P. C., Szita, N. & Mayr, T. Integration and application of optical chemical sensors in microbioreactors. *Lab Chip* **17,** 2693–2712 (2017).

22. Kaganovitch, E. *et al.* Microbial single-cell analysis in picoliter-sized batch cultivation chambers. *N. Biotechnol.* **47,** 50–59 (2018).

23. Scheidle, M. *et al.* Controlling pH in shake flasks using polymer-based controlled-release discs with pre-determined release kinetics. *BMC Biotechnol.* **11,** 25 (2011).

24. Hou, B.-H. *et al.* Optical sensors for monitoring dynamic changes of intracellular metabolite levels in mammalian cells. *Nat. Protoc.* **6,** 1818–1833 (2011).

25. Probst, C. *et al.* Rapid inoculation of single bacteria into parallel picoliter fermentation chambers. *Anal. Methods* **7,** 91–98 (2015).

26. McKinney, W. Data structures for statistical computing in python. in *Proceedings of the 9th Python in Science Conference* **445,** 51–56 (2010).

27. Oliphant, T. E. *A guide to NumPy*. **1,** (2006).

28. Hunter, J. D. Matplotlib: A 2D Graphics Environment. *Comput. Sci. Eng.* **9,** 90–95 (2007).

3 Overall discussion

The following chapters will give a general overview over the topic of this thesis and put data presented in chapters 2.1, 2.2 and 2.3 as well as currently unpublished results concerning the structural investigation into perspective. Starting from a single FRET-based glucose sensor a whole toolbox of sensor variants was constructed and the best sensor variant was finally tested as a novel measuring tool in small scale microbial cultivations.

Figure 3.1 Design of the glucose sensor prototype used by Roland Moussa[64] (a) compared to the design of the sensors used in this work, on the example of sensor no. 1 (b).

Starting from a prototype sensor (see Figure 3.1), the sensor was evolved towards two applicable sensor formulation. The first optimization introduced new fluorescent proteins (see Figure 3.1), in the second step linkers were integrated (see Figure 3.2). For a third optimization the His-tag was translocated. A fourth optimization incorporated a mutation of the binding protein and the final and fifth step was the immobilization of the sensor.

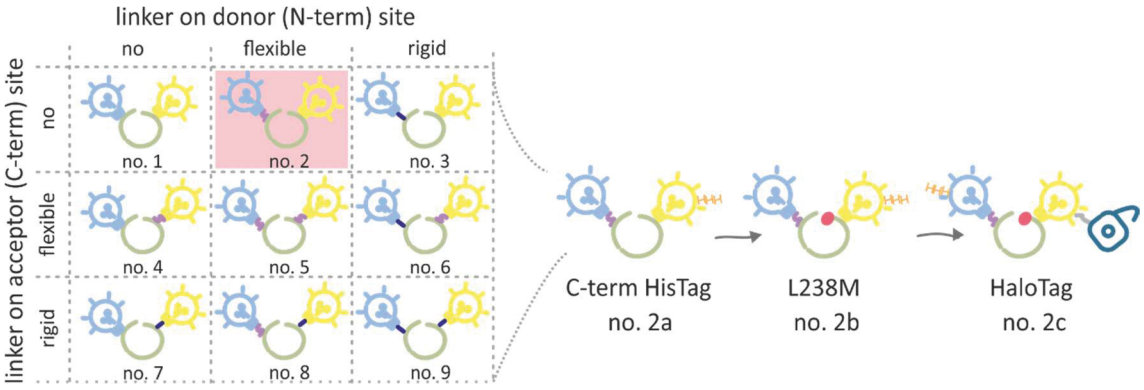

Figure 3.2: Linker-toolbox of the nine glucose sensors generated by introduction and combination of flexible and rigid linkers and the consecutive optimization steps of sensor no. 2 towards the applicable sensor variants no. 2b ($Glu^{[-]}$) and no. 2c ($Glu^{[+Halo]}$). Each icon represents a sensor of the respective optimization step. Linkers are indicated in pink (flexible s-shaped) and purple (rigid I-shaped), the His-tag in orange, an L238M exchange in the GGBP is indicated in red and the HaloTag in dark blue.

The discussion is structured, according to the different steps of sensor optimization. The chapters focus on the effect different alternations had on the sensor properties and aims at identifying a general principle for the construction of an optimal sensor. In the following

chapters these steps are described and discussed in detail and resulting effects on the sensors are evaluated.

3.1 Optimization step 1: Fluorescence proteins

As mentioned in the introduction a large variety of GFP-like fluorescent proteins are currently available and further optimization of these important proteins is ongoing.[12] The sensor chassis used to start of this project has earlier been developed in 2005 in the Frommer group [56] and only minor alternation were performed by Roland Moussa, who started the work on FRET-based biosensors in our working group.[64,65] Nevertheless, the sensor still lacked environmentally stable fluorescent proteins (FP). Therefore, the first optimization step concerned the selection of a pair of FPs with improved stability against environmental influences as well as with improved brightness. Of special interest was hereby to minimize the influence of changing pH-values. An altered brightness of one or both FRET-partners due to the pH changes, would influence the FRET ratio independently of a glucose binding event and thus would falsify the results. Additionally the chosen FPs must fulfil the requirements for FRET, by displaying a large spectral overlap between donor and acceptor (see chapter 1.1.1 in the introduction).[12] Twelve different FPs, from five spectral classes were tested: blue (BFP)[76], cyan (mTurquoise2, Cerulean, eCFP)[25], green (Clover, EGFP) [77,78], yellow (Venus, cpVenus, Citrine, Ypet) [21,30,79,80] and red (mRuby2, mCherry)[81,82]. Based on their spectral characteristics, possible combinations for FRET would be: blue donor with cyan acceptor, cyan donor with either green or yellow acceptor, green donor with red acceptor. Green-yellow as well as cyan-blue FRET pairs however, would not be ideal, because the emission maxima are rather close. This can cause bleed-through, also known as crosstalk. For the detection of two different fluorophores, two photomultipliers or optical filter sets are used. If bleed-through occurs, emission of one FP can be detected by both photomultipliers/filter sets, thus overestimating the intensity readout of the second FP.[83]

A test of the purified FPs [l]withat different pH values revealed that especially green variants suffer from a strong influence of pH on the fluorescence intensity (Figure 3.3). A quenching of up to 50 % by a change of one pH unit would overlay any FRET change caused by glucose binding. Even though, RFPs are insensitive towards pH changes between pH 6 and pH 8, a red-green FRET-pair is not feasible, as a result of the strong sensitivity towards pH of the GFPs. Combining a yellow with a cyan FP is very popular and a lot of work was done on optimizing this FRET pair,[25,84–87] even though the YFPs still suffer from a mediocre pH sensitivity.

[l] purification analog to the method described in chapter 2.2.

In the present case, the combination of mTurquoise2 with either YPet or Venus would have been appropriate, especially as a resulting sensor, intended for an extracellular use, is likely not to experience pH–values below pH 6.5. Based on the prototype, a sensor with mTuquoise2 as FRET-donor and Venus as FRET-acceptor was constructed (see Figure 3.1), whereas the introduction of YPet as an acceptor resulted in a nonfunctional sensor.

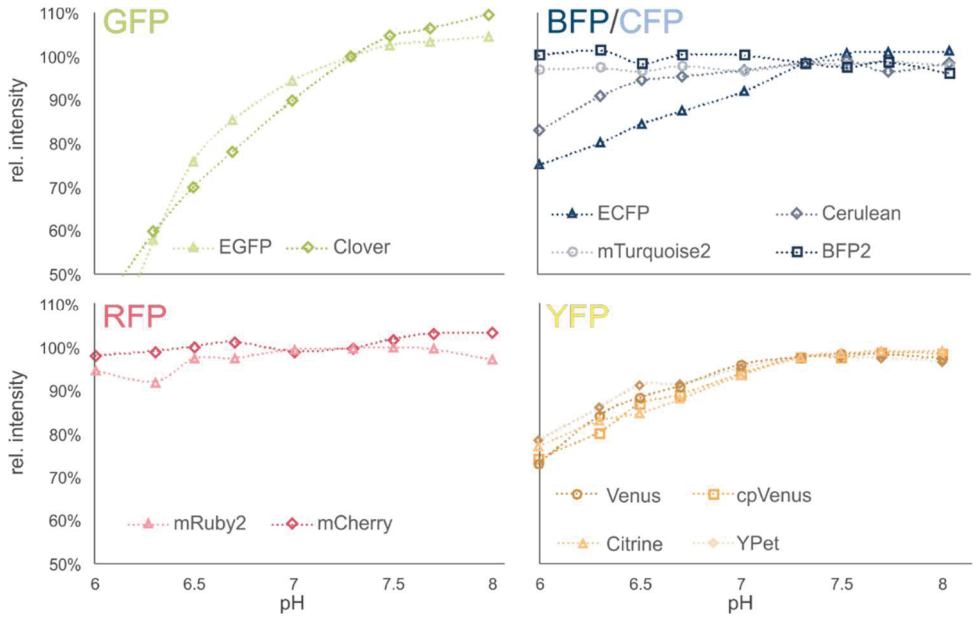

Figure 3.3: Emission intensity of different FPs towards different pH values. Purified protein (2 µM) was mixed with 20 mM MOPS buffer of different pH-values and the emission intensity after excitation at their specific absorption maxima was determined (EGFP: λ_{ex}=490 nm, λ_{em}=510 nm, Clover: λ_{ex}=480 nm, λ_{em}=522 nm, BFP: λ_{ex}=400 nm, λ_{em}=458 nm, mTurquoise2: λ_{ex}=430 nm, λ_{em}=479 nm , Cerulean: λ_{ex}=430 nm, λ_{em}=482 nm, ECFP: λ_{ex}=430 nm, λ_{em}=484 nm, mRuby2: λ_{ex}=540 nm, λ_{em}=601 nm, mCHerry: λ_{ex}=560 nm, λ_{em}=616 nm, YPet: λ_{ex}=490 nm, λ_{em}=534 nm, Citrine: λ_{ex}=490 nm, λ_{em}=535 nm, Venus: λ_{ex}=490 nm, λ_{em}=534 nm, cpVenus: λ_{ex}=490 nm, λ_{em}=535 nm. Intensities were normalized, to emission at pH 7.3.

The new sensor with mTurquoise2 and Venus was the basis for all sensors used in this work and was dedicated as sensor no.1. Compared to the first sensor used by Roland Moussa, which carried ECFP and Citrine as FRET pair, sensor no.1 performed similar.[64,65]. Nevertheless the affinity was reduced, supposedly as a result of the introduction of restriction sites between the different the three sensor building blocks (see Figure 3.1).

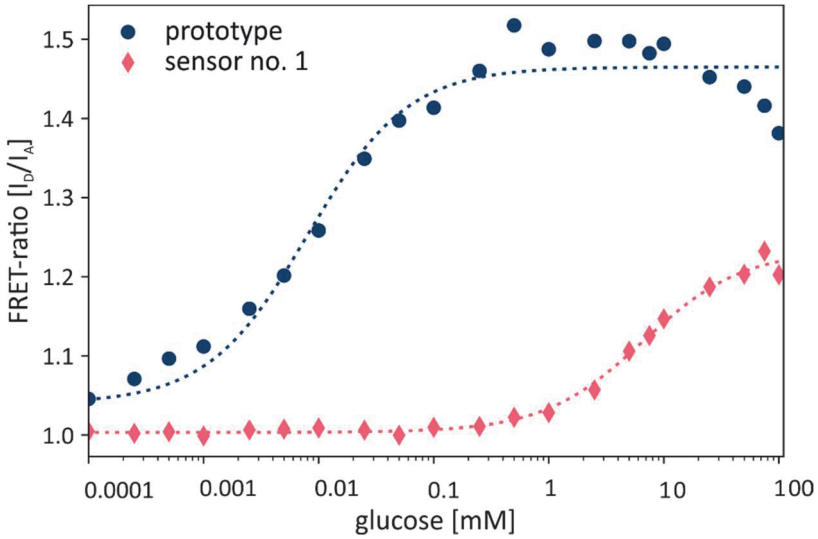

Figure 3.4: Binding isotherm of the sensor prototype with eCFP and Citrine as FRET-pair compared to the isotherm of sensor no. 1 with mTurquoise2 and Venus as FRET-pair. n=1, the displayed FRET-ratio was normalized to R_0.

As can be deducted from Figure 3.4, the change in FRET-ratio (sensitivity, ΔR) between the non-liganded (R_0) and liganded state (R_{sat}) is relatively small with only 22%. As one aim of this thesis was to apply a FRET-based sensor in microbial cultivations, further optimization was needed to significantly increase the FRET-ratio change. This was achieved by the introduction of linkers as described in the following chapter.

3.2 Optimization step 2: Influence of linker sequences

After optimization of the basic fluorescence properties the available scope of glucose sensors was broadened by introduction of linker sequences between the binding protein and the FPs. In a previous work, this approach has already resulted in significantly altered properties for a L-lysine sensor.[67,88] But why would the introduction of linkers between the glucose binding protein and the flanking FPs influence these properties at all? FRET-based biosensors of the Venus-fly-trap type function due to conformational changes,[89] which in some way alters the distance and/or orientation of the FPs towards each other. The use of linkers can influence this in three ways: i) they can work like a lever and enhance the degree of movement of the binding protein, induced by the conformational change upon binding; ii) a higher rotational freedom of one or both FPs would increase the statistical occurrence of ideal positioning of the FRET-partners, resulting in a higher FRET-efficiency; iii) the FPs are not yet close enough or positioned parallel for a high FRET-efficiency, connecting them to linkers would alter their position towards each other.

Within the bachelor project of Larissa Kever the effect of integration of flexible (GGS_4)[90] or rigid linkers (KLYPYDVPDA)[91] on the general performance of the glucose sensor was investigated, resulting in a toolbox of nine different sensors including sensor described in the previous chapter (sensors no. 1 – no. 9, see Figure 3.2).[92] Compared to the already mentioned toolbox of L-lysine sensors,[88] most linker combination influenced the lysine sensor as well as in the glucose sensor similarly. In general, the introduction of a linker between the donor FP and the binding protein had a strong positive effect on the sensitivity (ΔR) of a sensor (Figure 3.5), with one exception: For the lysine sensor, a rigid linker between the blue FP and the binding protein had a deleterious effect. This construct did not respond to changes of the L-lysine concentration at all.[67,88] In contrast, the same linker was beneficial for the glucose sensor, as it drastically increased the sensitivity almost threefold to more than 80 % (ΔR). The rather rigid structure of this linker has been described to form a turn in the secondary structure[91] which could create distance between the glucose binding protein and the FPs. Besides, an integration of only a linker between binding protein and yellow FP (Venus) in the glucose sensor decreased the sensitivity, indicating that the acceptor is already in a good position for efficient FRET without the linker. Interestingly, an additional linker between mTurquoise2 and the glucose binding protein could restore or even increase the ΔR, possibly by readjusting the orientation or distance of the FRET-partners.

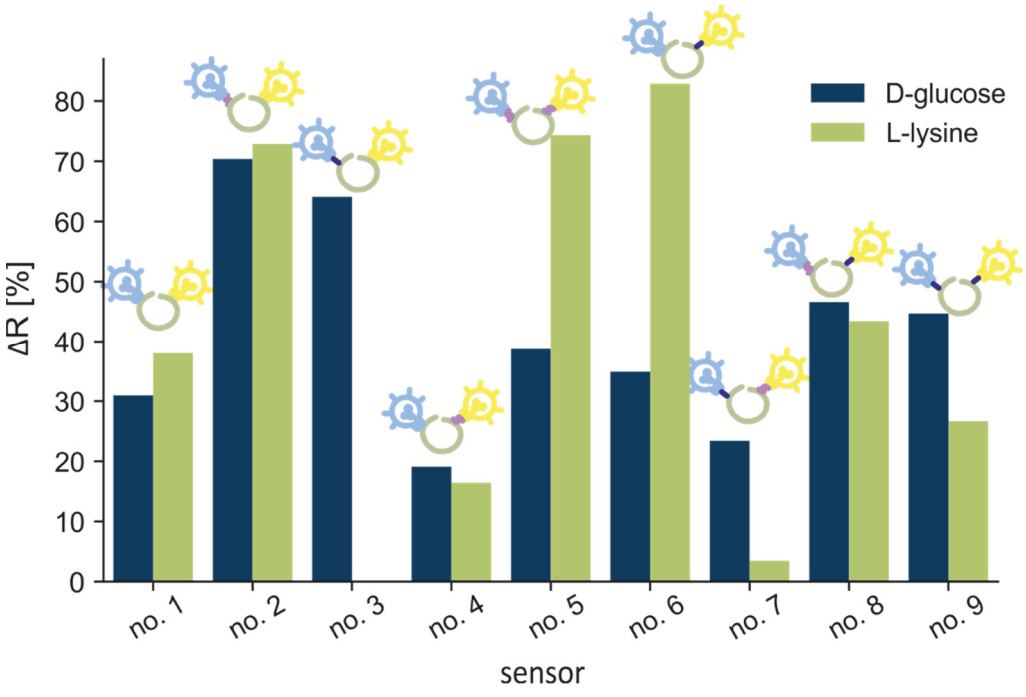

Figure 3.5: Comparison of the FRET-ratio changes (ΔR) of the sensor linker-toolboxes for L-lysine[88] and D-glucose[92]. For further details see legend Fig. 3.2.

In chapter 2.1 the sensors with different linker combinations were investigated on a single molecule level. It was also aimed at evaluating the FRET-efficiency of sensors with a high ΔR compared to low ΔR. Single molecule FRET (smFRET) analysis underlined the effect of linker introduction. For both sensors with a linker between binding protein and mTurquoise2 the energy transfer was significantly increased, while the construct with the flexible linker performed even better than the rigid linker (Figure 2.1-3 for sensor no. 2 with flexible linker and Figure S 1.1-7 (Appendix page 122) for the sensor no. 3 with rigid linker). Introduction of a second linker between GGBP and Venus did not result in further improvement. This indicated that the major contribution in altering the FRET-efficiency is associated to the N-terminal domain of the GGBP.

Additionally, the energy transfer data gained from smFRET measurements clearly demonstrated that the studied FRET-based sensors do not show a simple two-state model, where one state corresponds to low transfer efficiency in the non-liganded state and the other one to high transfer efficiency in the liganded state. Already in the non-liganded state the ensemble of sensor molecules displays populations with low as well as high transfer efficiencies in different proportions (see Figure 2.1-2 and chapter 2.1.4a). This indicated that the glucose sensor undergoes a constant change in conformation, resulting in a multitude of possible transfer efficiencies. Without ligand, the majority of molecules display lower transfer efficiencies. At higher ligand concentrations the higher transfer efficiencies, resembling a closed conformation, occurs statistically more often, as the closed conformation of the GGBP is more stable than the open state.[93] For the construction of a sensor, understanding this behavior is important. For well performing sensors, populations in the low energy transfers and the high transfer efficiency need to be well separated, corresponding to large conformational changes. Additionally, the addition of ligand should result in a strongly pronounces shift of populations towards the higher transfer efficiencies. This behavior was displayed by the sensor no.2 (see Figure 2.1-2).

Nevertheless, structural evidence of the change in FRET-efficiency as a result of changes in orientation, distance or flexibility is still missing. Up to now, no crystal structure of the FRET-based glucose sensor could be obtained, despite major efforts[II]. Independent of buffers, additives and conditions used for crystallization, the sensor degraded. In agreement with the results from stability measurements with the sensor Glu[-] (see 2.2, Figure 2.2-1 for a respective SDS-PAGE) the fusion protein fragments into the three components – the GGBP and the FPs.

[II] Cristallization trials were performed in cooperation with PD Dr. Renu Batra.Safferling and Joachim Granzin, ICS-6 Forschungszentrum Jülich

Therefore, the only crystals obtained contained single FPs, either Venus or mTurquoise2 (unpublished results).

Not all of the nine constructs of the linker-toolbox were ideal for further studies and especially not for application purposes. While introduction of an N-terminal linker of any kind between mTurquoise2 and the GGBP led to a high sensitivity, the affinity was mostly not affected. Besides, a C-terminal flexible linker between the GGBP and Venus resulted in a strong increase in affinity from 7.5 mM (no. 1) to 38 mM (sensor no. 4). Finally three sensor variants were chosen for further studies: a sensor no linkers (sensor no.1) and both sensors with only one flexible GGS_4 linker as they presented extremes within the linker-toolbox (sensors no. 2. and no.4, see Figure 3.6).

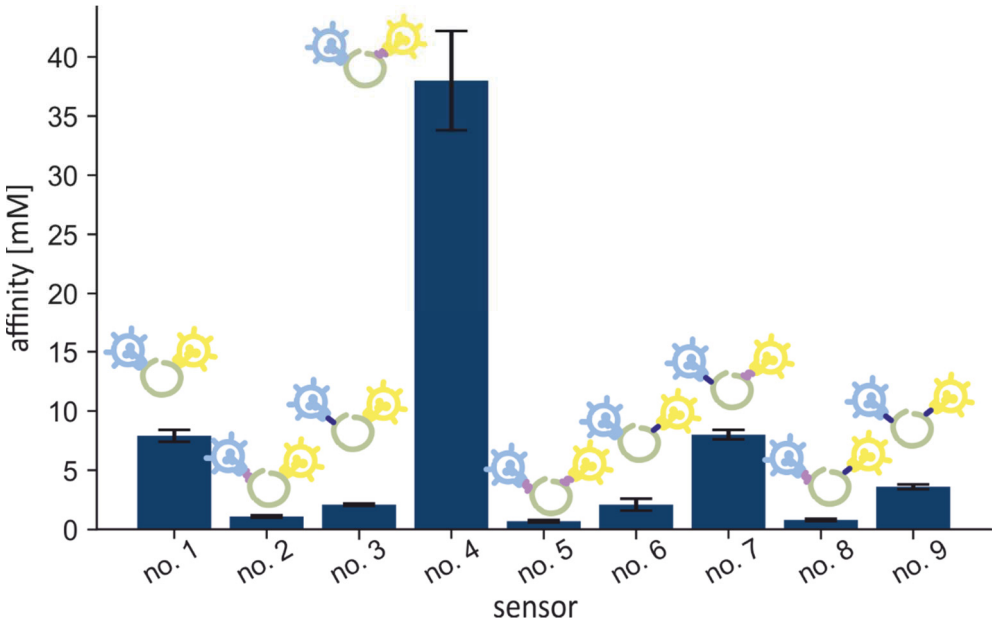

Figure 3.6: Affinity (K_d) of the sensor variants for D-glucose of the linker-toolbox (modified from the bachelor thesis of Larissa Kever [92]); n=3.

3.3 Optimization step 3: Increasing the active sensor fraction

As already mentioned in the previous chapter, the single molecule measurements (chapter 2.1) indicated that the different sensor preparations contained significant donor-only fractions, respectively (2.1.4b). The donor-only fraction contains sensor-molecules where the acceptor FP (Venus) is either not present or not functional. This sensor fraction, exhibiting only donor fluorescence, “dilutes” the signal of the fully functional sensor molecules, which falsifies the calculation of the FRET-ratio, as the intensity of mTurquoise2 is not decreased via FRET to Venus as demonstrated in Figure S 1.1-1d (Appendix page no117).

Insufficient maturation time for the FPs could be excluded, as the time used for cultivation (72 hours) and consecutive purification of the sensor protein was long enough for a full maturation of donor and acceptor, and both FPs display maturations times below 2 hours according to literature.[19] Thus, a truncated fraction, lacking the Venus protein, was assumed. As the His-tag of the sensors was initially positioned at the N-terminus of the sensor protein, it is expressed first. If the protein production is terminated prematurely, truncated sensor proteins still harbor the His-tag and will be co-purified with full-length sensor proteins. To circumvent purification of truncated constructs, the His-tag was translocated to the C-terminus, resulting sensors carry the index "a" in der nomenclature (compare Figure 3.2). Surprisingly, smFRET measurements of only full-length constructs showed no positive effect on the sensor fraction with active donor and acceptor (data not shown). The donor-only fraction appeared to be within the same range (ca. 30%) as indicated by respective smFRET measurements, independent of the position of the His-tag (Figure S 1.1-9).

Independent of the fluorescent activity, the shift of the His-tag to the C-terminus reduced the heterogeneity of purified proteins, ensuring only full-length proteins were purified. This, now homogenous protein could be concentrated to ~100 mg/mL without precipitation (data not shown), facilitating further structural analysis, as pointed out in the following.

As it was not possible to crystallize the sensor[III], small angle X-ray scattering (SAXS) experiments were performed[IV]. The experiments aimed at determining and comparing the excluded volume of the sensor in the presence and absence of added D-glucose in order elucidate the structural changes behind the observed FRET effect. Specifically, the three sensors identified in chapters 2.1 and 3.2, sensor no. 1a ("prototype", no linkers), no. 2a (N-terminal flexible linker), and no. 3a (C-terminal flexible linker) were studied, as they display clearly distinguishable differences in FRET-efficiency, sensitivity, and affinity based on the linker position. The SAXS-measurements revealed that especially the sensor no. 2a with a flexible linker between mTurquoise2 and the GGBP displayed a significantly more compact structure in the presence of glucose which could not be demonstrated with sensors no. 1a and no. 3a (Figure 3.7).

[III] Sensor no. 1, 2 and 2c were used for crystallization trials.
[IV] SAXS measurements were performed in cooperation with Dr. Andreas Stadler and Mona Sarter, JCNS-1 Forschungszentrum Jülich

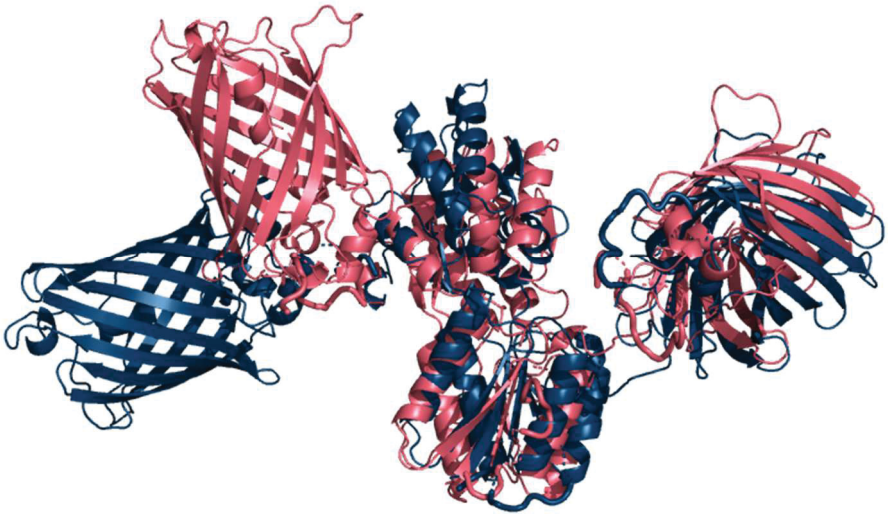

Figure 3.7: Comparative structural models of the non-liganded (blue) and liganded (red) conformation of the glucose sensor no. 2a. The models were obtained from rigid-body modelling with the CORAL program[94] using experimental SAXS data as input. The more compact structure of the liganded conformation is in accordance with the reduced Guinier radius found in the SAXS experiment.

Together with the results from chapter 2.1 it can be stated that a high sensor sensitivity (high ΔR) is correlated with a large conformational change upon glucose binding. As indicated by the SAXS results, the structural changes shown for sensor no. 2a (Figure 3.7) occur predominantly in the N-terminal domain of the GGBP, which is then transferred to N-terminal mTurquoise2. Thereby the flexible linker is likely to function as a lever, increasing the distance change between mTurquoise2 and Venus induced by the structural alteration of the central GGBP upon glucose binding. Even though this is a hint for a significantly positional alteration of the blue FPs in the different states, further investigation on this behalf is necessary and currently ongoing in Dr. Andreas Stadlers lab. Modeling of the molecular dynamics as well as further SAXS measurements could reveal more detailed information on the conformational changes and in how far distances or orientation of the FRET-partners are altered.

3.4 Optimization step 4: Mutation of the galactose-glucose-binding protein

Initially it was aimed at creating a sensor toolbox offering sensors with high sensitivities and a variety of affinities. So far, the previous optimization steps resulted in sensors with increased sensitivity, but the affinity remained merely in the same range. While sensor no. 2a with an N-terminal flexible linker featured a very large sensitivity of 70%, the affinity remained similar to the sensor of the unmodified sensor no.1 (K_d=7.5 mM, see Figure 3.5 and Figure 3.6). Introduction of a C-terminal flexible linker resulted in a sensor (no. 4) with a strongly decreased affinity to 38 mM but did not affect the sensitivity. Therefore, mutagenesis of the glucose binding site was considered, which had already been proven to be advantageous in a similar sensor construct.[95] With the random mutagenesis performed by Peroza *et al*, the resulting sensor variants displayed an up to 500 times lower affinity.[95]

Based on this work, the next optimization of the sensor was the exchange of a leucine for a methionine at position 238 in the binding protein resulting in sensor variants indexed with a “b”. The effect on the affinity was analyzed for three sensors. In the sensor no. 4b the exchange resulted in sensor with no altered affinity but a minute ΔR, the sensor no. 1c also showed no improvement. Best results obtained sensor construct no. 2b, carrying an N-terminal flexible linker. Here the L238M exchange resulted in a decrease of the affinity within the same order of magnitude compared to the sensor no. 2. As can be deduced from Figure 3.8, ΔR was not affected at all and the affinity increased from ≈1 to 3.5 mM. Even though this is not a 500-fold decrease of the affinity,[95] it enables the quantification of up to 20 mM D-glucose in a MOPS buffered system (see chapter 2.2.4a) for details).

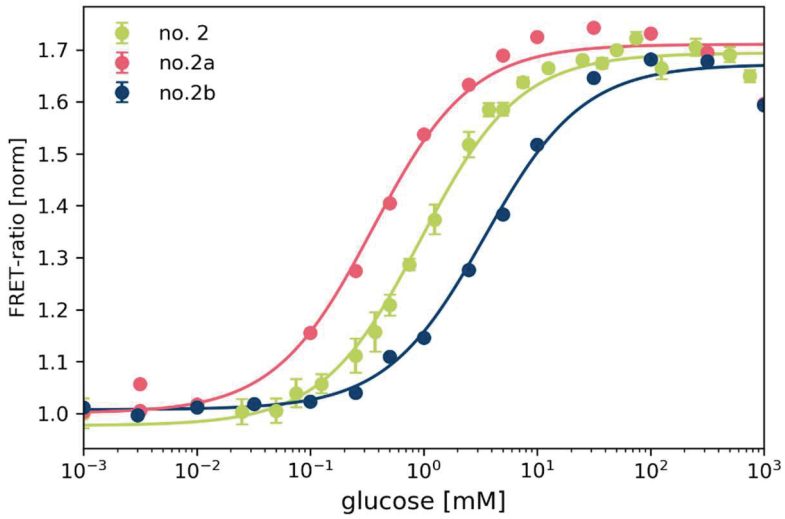

Figure 3.8: Binding isotherms of the glucose sensors no. 2 (green) with a flexible linker between donor and binding protein, sensor no. 2a (red) with the His-tag at the C-terminus and sensor no. 2b (blue) with an additional exchange in the binding protein (L238M). n=3

With an affinity within this range, and a very high ΔR of more than 70% the sensor no. 2b is ideal is to monitor the glucose depletion in a microbial cultivation. The further studies were exclusively carried out with this variant, which was named "Glu$^{[-]}$". The application of this sensor is described and discussed in more detail in chapter 2.2.

3.5 Optimization step 5: Effects of immobilization on the sensor properties

Despite the promising results from the application of the sensor no. 2b (Glu$^{[-]}$), problems with stability were encountered during shaking and long-term storage at temperatures above 25°C (see 2.2.4a) and Figure S 1.2-5). A possibility to stabilize the sensor was immobilization on the surface of particles, as this has already been proven positive for many other proteins and enzymes.[96] As all glucose sensors carry a His-Tag, which is used for their purification, it was attempted to utilize this tag also for immobilization. The His-tag enables a non-covalent metal-chelate bond to nitrilotriacetic acid (NTA)-functionalized carriers, with different bound transition metal ions. In order to test the functionality of the immobilized sensor, studies with different carriers were performed. Initial studies to immobilize on Co^{2+}-NTA functionalized Sepharose beads (Dynabeads, ThermoFischer) failed as the chelate bond was not strong enough for a permanent immobilization. As Fe^{2+} as central ion principally would provide a stronger chelate bond, the EziG-system from Enginzyme (Stockholm, Sweden) was tested as well.[97] EziG material is further available with different surface properties, due to modifications of the porous glass with different polymers to alter the surface polarity. The large surface of the porous glass

enables binding of a large amount of protein (30% active protein per g resin).[97] The sensor Glu[-] (see chapter 3.4) was immobilized on the three available carriers: EziG1-3 with different surface properties, ranging from hydrophilic to hydrophobic.[97]

As demonstrated in Figure 3.9 the functionality of the sensor immobilized on EziG is clearly altered in all cases. While with the soluble sensor no. 2b displays a ΔR of ~70%, it displays a reduced FRET-ratio change if immobilized on all three EziG materials (Figure 3.9). Comparison of the emission spectra (Figure 3.9a) demonstrates that this results from a reduced emission intensity of the donor mTurquoise2 (between 450 and 500 nm) in all immobilized cases. Apart from a quenching effect caused by the surface modification of the EziG material on the sensor, this could be explained by a drastically increased FRET efficiency as well as compaction of the immobilized sensor molecule. As the surface of the porous glass resin is likely densely packed with sensor molecules intermolecular FRET can be expected in addition to the normal intramolecular FRET. Additionally, the tight packing of sensor molecules is likely to reduce their flexibility, which could result in less pronounced conformational change upon glucose binding compared to the soluble sensor. As a consequence, immobilization on EziG material destroys the sensor and could not be used.

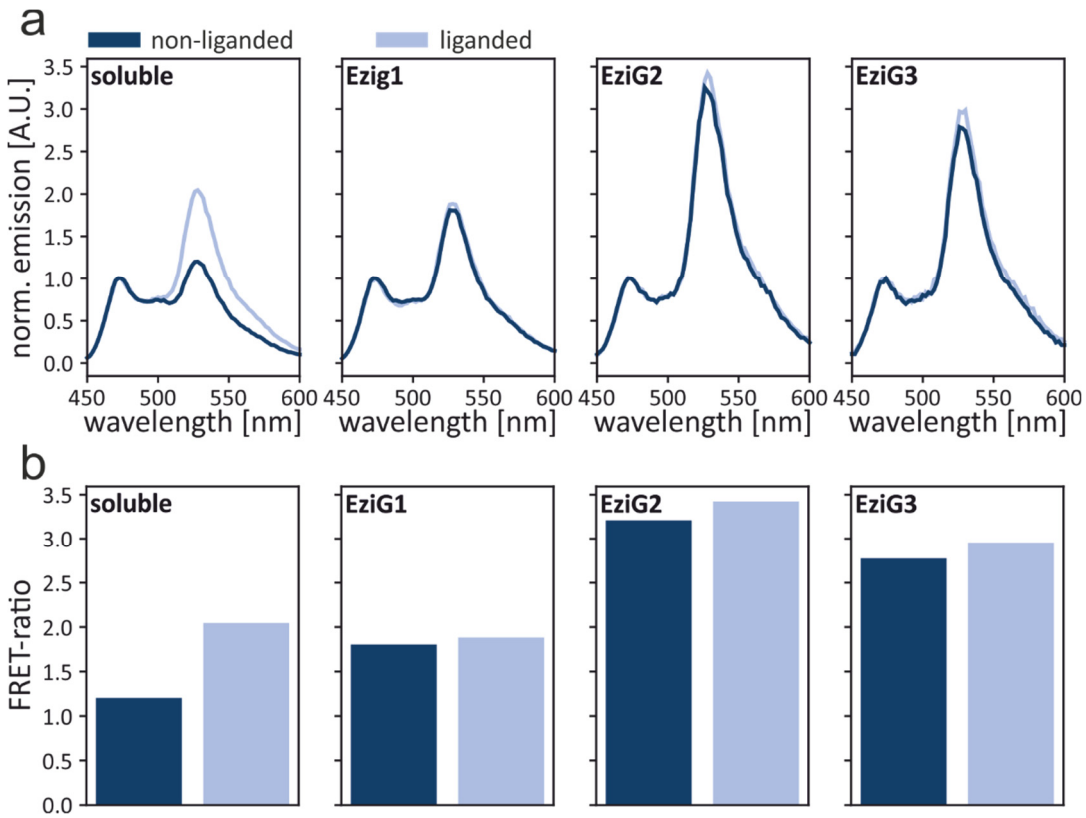

Figure 3.9a: Emission spectra of the sensor Glu$^{[-]}$ in a soluble formulation and immobilized on three different EziG beads (hydrophilic EziG1, partially hydrophobic EziG2, hydrophobic Ezig3) without (dark) and with (light) 100 mM D-glucose. b: FRET-ratio of the non-liganded (dark) and liganded (100 mM D-glucose, light) sensor. Measurements were performed in a Tecan M200 Platereader (Tecan, Switzerland), λ_{ex}= 435 nm, R = I_{474}/I_{524}, 2µM soluble sensor and 0,1 µL beads/µL, 20 mM MOPS buffer pH 7.3.

In contrast to an immobilization via His-Tag the immobilization via a HaloTag™ [98] was successful (0, as discussed in chapters 2.2 and 2.3. Here, the glucose biosensor sequence was extended by C-terminal fusion with a modified dehalogenase[98] resulting in the sensor no. 2c (Glu$^{[+Halo]}$, see chapter 2.2.3a) and 2.2.3b) for experimental details and 0 for results). As demonstrated in Figure 2.2-4 in comparison to the sensor no. 2b (Glu$^{[-]}$) the soluble sensor no. 2c (Glu$^{[+Halo]}$) does only show little FRET-ratio change (ΔR). However, full functionality is regained upon immobilization. Unlike the His-tag mediated immobilization, less sensor is bound on the non-porous surface of the HaloLink™ or magneHaloLink™ particles, leaving enough space for the necessary flexibility to enable optimal functionality.

Additionally the size of the HaloTag™ (25 kDa) as well as the linker between sensor and tag acts as a spacer to the bead surface, which could reduce potential quenching effects and further retains the mobility of the sensor comparable to the soluble state (for sequence information please see Appendix 1.2b) page 132. As demonstrated in Figure S 1.2-4 (Appendix page 137), the

stability of the immobilized sensors was increased relative to the soluble sensor (Figure 2.2-1) when stored at room temperature. Additionally, and most importantly the immobilized sensor no. 2c ($Glu^{[+Halo]}$) was not prone to aggregation and stable under shaking conditions in the BioLector® device (see Figure S 1.2-6, (Appendix page 138). Other techniques for FRET-based detection of metabolites employing immobilization, usually trap a sensor within a matrix which decrease the response of a sensor or limit ligand diffusion, in contrast to the here demonstrated surface immobilization. For example Faccio *et al.* have used the prototype sensor with eCFP and Citrine[56] and entrapped it in silicate-based particles.[99] While the glucose sensor retained the affinity for glucose, the sensitivity (ΔR) was reduced to 10 %, most likely due to the reduced flexibility of the sensor in the tight matrix.

The great potential of immobilizing the glucose sensor via HaloTag™ was demonstrated in chapter 2.2. Herein the online application in a shaken milliliter scale cultivation (BioLector®) was described as an alternative to the soluble sensor no. 2b ($Glu^{[-]}$). It could be demonstrated that the utilization of an immobilized FRET-based biosensor is of great advantage for such cultivations and could facilitate strain and process development. The current lack of metabolite sensors for online analysis in small scale cultivation limits the throughput and data density.

This lack of sensors is even more pronounced at µL/pL scale. Therefore, the immobilized $Glu^{[+Halo]}$ sensor has undergone first tests in chip-based picobioreactors (see chapter 2.3). In a proof of concept, the feasibility of FRET-based metabolite quantification was demonstrated. As shown in Figure 2.3-5, the immobilized $Glu^{[+Halo]}$ sensor was successfully used to indicate changes in glucose concentration in a PDMS chip in the presence of *E. coli* cells. Microbial cultivation in picobioreactors is of exceptional importance to discover the full potential of micro organisms[100], nevertheless currently process data are limited.[101] Here an immobilized FRET-based biosensor shows great potential to fill this gap.

The application of a glucose sensor, which in contrast to an enzymatic assay does not consume glucose inside a system, is additionally advantageous, as no competition with microbial organisms for the C-source will occur. In an approach by Kantak *et al.* the glucose binding protein Concanavalin A was labeled with a fluorescent dye and entrapped together with a quenching agent in a photo-polymerizable PEG hydrogel.[102] In this concept the addition of glucose led to a competitive replacement of the quenching agent, which than results in a FRET-change. Even though this concept is promising, the response times to glucose addition are fairly slow (15 minutes) and the size of the generated hydrogels (~63 µm) are within the same range as beads used in this study (chapter 2.3).[102] Response times and size are crucial for an application especially in chip-based cultivations or devices. Although the utilized fluorescent dyes[102] are less

prone to photo bleaching than FPs, preparation of such a sensor is laborious and requires several biological and chemical steps. Besides, stable covalent immobilization of the genetically encoded FRET-based biosensor $Glu^{[+Halo]}$, can be performed directly from crude cell extract, yielding functional sensor beads without further process steps.

4 Conclusion and Outlook

This thesis has demonstrated that FRET-based biosensors are an appropriate tool to quantify D-glucose specifically in small scale cultivations, where sample size is limiting.

The concept of a sensor with mTurquoise2 and Venus as FRET-pair and the glucose-galactose binding protein (GGBP) from *Escherichia coli* was used for the construction of a glucose sensors toolbox . Introduction and combination of rigid and flexible linker sequences resulted in nine sensors, displaying affinities between ~1 mM and ~40 mM and sensitivities between 20 % and 70 % FRET-ratio change (ΔR) between the non-liganded and the liganded state (see Figure 3.5Figure 3.6 for details).

All sensor variants of this toolbox were evaluated on a single molecule level to determine their energy transfer efficiencies between the FRET partners as a consequence of the linker modulations (see 2.1). Additionally, the background for differences observed in sensitivity of the FRET-based sensors was investigated. Depending on the kind and position of the linker, the glucose sensor variants exhibit a broad range of different energy transfer efficiencies, which make up the ensemble data recorded e.g. in common fluorescence photometric measurements (Figure 2.1-2). Besides, single molecule analyses revealed that a well applicable sensor with a high sensitivity (ΔR) is characterized by a low transfer efficiency is in the non-liganded state and distinctively higher transfer efficiency in the presence of glucose. Well performing sensors like sensor no. 2 (Figure 3.2) with superior ΔR (70%), additionally display an almost complete shift of the population from low to high transfer efficiencies. Structural data from SAXS experiments led to the assumption that in sensor no. 2 the donor FP and the central GGBP undergo a large conformational change upon glucose binding (Figure 3.7). While this information is already valuable for the sensor design, as it indicates that increased mobility of the donor results in large conformational change, further investigation in this respect is needed.

Based on the smFRET and SAXS data the best performing sensor (no. 2, with a flexible linker between donor and binding protein) was used for further characterization and optimization. Exchange of one amino acid (L238) in the GGBP led to one of the two final sensor constructs of this work used in applications: no 2.b ($Glu^{[-]}$). This glucose sensor displays an affinity in the range of 3.5 mM with a superior ΔR of above 70% and was successfully used to determine the glucose consumption of a *C. glutamicum* cultivation at-line. Here the sensor proved to be competitive to established methods for at- and offline analysis like HPLC and enzymatic glucose quantification.

Equipment of the Glu[-] sensor with the HaloTag™ facilitated immobilization on beads, resulting in senor no. 2c (Glu[+Halo]). Immobilization had a stabilizing effect on the sensor, while the high sensitivity of the sensor was preserved. As a proof of concept, the immobilized sensor was used in a microtiter plate-based cultivation of *E. coli* and reliably produced online information on the glucose consumption. So far, no other direct quantification of glucose in such a system is possible. However, introduction of beads into the cultivation could influence the growth of microorganisms. One possible solution would be to modify the surface of microtiter plate used for cultivation, in order to immobilize the sensor directly at the bottom of the plate, forming a sensor spot to reduce the interaction with cells and setting a fixed position for detection.

Finally, the produced sensor beads were evaluated for application in chip-based cultivations. The stability of the optical sensor signal was successfully shown, as well as following the pulsing of glucose in a specifically designed PDMS microchip. It could be demonstrated that the immobilized sensor has great potential to monitor glucose in such applications, especially as the presence of cells did not result in signal loss. At this scale researchers currently have even less options for metabolite analysis in the cellular environment compared to the mL scale. Therefore the online quantification via FRET-based sensors could lead to drastically improved process design. Nevertheless, the current particles available for immobilization via HaloTag™ are still too large to be applied in typical picobioreactors. With a size of 60 µm they are 10-fold larger than a single bacterial cell and observation of cells and sensor at the same time is currently not possible. Production of smaller beads should therefore be in focus of future work. Due to the high affinity of the sensor, only low concentrations of glucose (< 10 mM) can be quantified, unless modification of the binding protein would enable a broader detection range. Changing the detection range would not only be positive for chip-based cultivations but also for application in milliliter scale and even for larger scale.

The glucose sensor can be regarded as a proof of concept for other FRET-based metabolite sensors. As the design of the FRET-based sensors is modular, an exchange of the binding protein would enable the detection of other metabolites, too. Although such an exchange would also have an influence on the sensitivity of a sensor, the applied toolbox principle would simplify the optimization process. Knowledge gained from the earlier constructed L-lysine sensor toolbox[67,88] and the here described D-glucose sensor toolbox enable the prediction of linker-based effects especially on the sensitivity. In both cases introduction of linkers between donor FP and binding protein enhanced the sensitivity. In contrast to linker introduction, further mutagenesis of the currently used GGBP could result in sensors displaying the same high ΔR but altered affinity for glucose. A directed mutagenesis of the BP could also modify the ligand scope, to enable the

detection of e.g. pentoses like xylose. The creation of FRET-based sensors for different ligands would enable detection and quantification of different metabolites at a time, when different FRET pairs are used. This is of great need for strain and process development specifically in small scales.

5 References

1. Stokes, G. G. On the Change of Refrangibility of Light. *Philos. Trans. R. Soc. London* **142,** 463–562 (1852).

2. Stokes, G. G. On the Change of Refrangibility of Light. No. II. *Philos. Trans. R. Soc. London* **143,** 385–396 (1853).

3. Jabłoński, A. Efficiency of Anti-Stokes Fluorescence in Dyes. *Nature* **131,** 839–840 (1933).

4. Jabłoński, A. Über den Mechanismus der Photolumineszenz von Farbstoffphosphoren. *Zeitschrift für Phys.* **94,** 38–46 (1935).

5. Lakowicz, J. R. Time-Dependent Anisotropy Decays. *Princ. Fluoresc. Spectrosc.* 383 (2006). doi:10.1007/978-0-387-46312-4_11

6. Wallrabe, H. & Periasamy, A. Imaging protein molecules using FRET and FLIM microscopy. *Curr. Opin. Biotechnol.* **16,** 19–27 (2005).

7. Förster, T. Energiewanderung und Fluoreszenz. *Naturwissenschaften* **33,** 166–175 (1946).

8. Lakowicz, J. R. *Principles of fluorescence spectroscopy*. (Springer, 2006).

9. Molecular Probes- The Handbook. Available at: https://www.thermofisher.com/us/en/home/references/molecular-probes-the-handbook/technical-notes-and-product-highlights/fluorescence-resonance-energy-transfer-fret.htm.

10. Shimomura, O., Johnson, F. H. & Saiga, Y. Extraction, Purification and Properties of Aequorin, a Bioluminescent Protein from the Luminous Hydromedusan*,Aequorea*. *J. Cell. Comp. Physiol.* **59,** 223–239 (1962).

11. Chalfie, M., Tu, Y., Euskirchen, G., Ward, W. & Prasher, D. Green fluorescent protein as a marker for gene expression. *Science.* **263,** 802–805 (1994).

12. Rodriguez, E. A. *et al.* The Growing and Glowing Toolbox of Fluorescent and Photoactive Proteins. *Trends Biochem. Sci.* **42,** 111–129 (2017).

13. Tsien, R. Y. The Green Fluorescent Protein. *Annu. Rev. Biochem.* **67,** 509–544 (1998).

14. Shimomura, O. Discovery of Green Fluorescent Protein (GFP) (Nobel Lecture). *Angew. Chemie Int. Ed.* **48,** 5590–5602 (2009).

15. Chalfie, M. GFP: Lighting Up Life (Nobel Lecture). *Angew. Chemie Int. Ed.* **48,** 5603–5611 (2009).

16. Tsien, R. Y. Constructing and Exploiting the Fluorescent Protein Paintbox (Nobel Lecture). *Angew. Chemie Int. Ed.* **48,** 5612–5626 (2009).

17. Cubitt, A. B. *et al.* Understanding, improving and using green fluorescent proteins. *Trends Biochem. Sci.* **20,** 448–455 (1995).

18. Inouye, S. & Tsuji, F. I. Evidence for redox forms of the *Aequorea green* fluorescent protein. *FEBS Lett.* **351,** 211–214 (1994).

19. Balleza, E., Kim, J. M. & Cluzel, P. Systematic characterization of maturation time of fluorescent proteins in living cells. *Nat. Methods* **15,** 47–51 (2017).

20. Heim, R. & Tsien, R. Y. Engineering green fluorescent protein for improved brightness,

longer wavelengths and fluorescence resonance energy transfer. *Curr. Biol.* **6,** 178–182 (1996).

21. Newman, R. H., Fosbrink, M. D. & Zhang, J. Genetically Encodable Fluorescent Biosensors for Tracking Signaling Dynamics in Living Cells. *Chem. Rev.* **111,** 3614–3666 (2011).

22. Sample, V., Newman, R. H. & Zhang, J. The structure and function of fluorescent proteins. *Chem. Soc. Rev.* **38,** 2852 (2009).

23. Livet, J. *et al.* Transgenic strategies for combinatorial expression of fluorescent proteins in the nervous system. *Nature* **450,** 56–62 (2007).

24. Mahr, R. & Frunzke, J. Transcription factor-based biosensors in biotechnology: current state and future prospects. *Appl. Microbiol. Biotechnol.* **100,** 79–90 (2016).

25. Goedhart, J. *et al.* Structure-guided evolution of cyan fluorescent proteins towards a quantum yield of 93%. *Nat. Commun.* **3,** 751 (2012).

26. Heim, R., Prasher, D. C. & Tsien, R. Y. Wavelength mutations and posttranslational autoxidation of green fluorescent protein. *Proc. Natl. Acad. Sci.* **91,** 12501–12504 (1994).

27. Cubitt, A. B., Woollenweber, L. a & Heim, R. Understanding Structure—Function Relationships in the *Aequorea victoria* Green Fluorescent Protein. in *Methods in Cell Biology* **58,** 19–30 (1998).

28. Teerawanichpan, P., Hoffman, T., Ashe, P., Datla, R. & Selvaraj, G. Investigations of combinations of mutations in the jellyfish green fluorescent protein (GFP) that afford brighter fluorescence, and use of a version (VisGreen) in plant, bacterial, and animal cells. *Biochim. Biophys. Acta - Gen. Subj.* **1770,** 1360–1368 (2007).

29. Shaner, N. C., Steinbach, P. A. & Tsien, R. Y. A guide to choosing fluorescent proteins. *Nat. Methods* **2,** 905–909 (2005).

30. Nagai, T. *et al.* A variant of yellow fluorescent protein with fast and efficient maturation for cell-biological applications. *Nat. Biotechnol.* **20,** 87–90 (2002).

31. Orm, M. *et al.* Crystal Structure of the *Aequorea victoria* Green Fluorescent Protein. *Science (80-.).* **273,** 1392–1395 (1996).

32. Wachter, R. M., Elsliger, M.-A. a, Kallio, K., Hanson, G. T. & Remington, S. J. Structural basis of spectral shifts in the yellow-emission variants of green fluorescent protein. *Structure* **6,** 1267–1277 (1998).

33. Turner, A. P. F., Karube, I. & Wilson, G. S. *Biosensors : Fundamentals and Applications*. (Oxford University Press, 1987).

34. Fehr, M. *et al.* Development and use of fluorescent nanosensors for metabolite imaging in living cells. *Biochem. Soc. Trans.* **33,** 287–290 (2005).

35. Lalonde, S., Ehrhardt, D. W. & Frommer, W. B. Shining light on signaling and metabolic networks by genetically encoded biosensors. *Curr. Opin. Plant Biol.* **8,** 574–581 (2005).

36. Rupprecht, C. *et al.* A novel FbFP-based biosensor toolbox for sensitive in vivo determination of intracellular pH. *J. Biotechnol.* **258,** 25–32 (2017).

37. Awaji, T., Hirasawa, A., Shirakawa, H., Tsujimoto, G. & Miyazaki, S. Novel Green Fluorescent Protein-Based Ratiometric Indicators for Monitoring pH in Defined Intracellular Microdomains. *Biochem. Biophys. Res. Commun.* **289,** 457–462 (2001).

38. Binder, S. *et al.* A high-throughput approach to identify genomic variants of bacterial metabolite producers at the single-cell level. *Genome Biol.* **13,** R40 (2012).

39. Okumoto, S. Imaging approach for monitoring cellular metabolites and ions using genetically encoded biosensors. *Curr. Opin. Biotechnol.* **21,** 45–54 (2010).

40. Cormack, B. P., Valdivia, R. H. & Falkow, S. FACS-optimized mutants of the green fluorescent protein (GFP). *Gene* **173,** 33–38 (1996).

41. Grünberger, A. *et al.* Microfluidic Picoliter Bioreactor for Microbial Single-cell Analysis: Fabrication, System Setup, and Operation. *J. Vis. Exp.* **82,** 50560 (2013).

42. Miyawaki, A. *et al.* Fluorescent indicators for Ca^{2+}based on green fluorescent proteins and calmodulin. *Nature* **388,** 882–887 (1997).

43. Romoser, V. A., Hinkle, P. M. & Persechini, A. Detection in Living Cells of Ca^{2+} -dependent Changes in the Fluorescence Emission of an Indicator Composed of Two Green Fluorescent Protein Variants Linked by a Calmodulin-binding Sequence. *J. Biol. Chem.* **272,** 13270–13274 (1997).

44. Felder, C. B., Graul, R. C., Lee, A. Y., Merkle, H.-P. & Sadee, W. The venus flytrap of periplasmic binding proteins: An ancient protein module present in multiple drug receptors. *AAPS PharmSci* **1,** 7–26 (1999).

45. Dwyer, M. a. & Hellinga, H. W. Periplasmic binding proteins: a versatile superfamily for protein engineering. *Curr. Opin. Struct. Biol.* **14,** 495–504 (2004).

46. Fukami-Kobayashi, K., Tateno, Y. & Nishikawa, K. Domain dislocation: a change of core structure in periplasmic binding proteins in their evolutionary history. *J. Mol. Biol.* **286,** 279–290 (1999).

47. San Martín, A. *et al.* A Genetically Encoded FRET Lactate Sensor and Its Use To Detect the Warburg Effect in Single Cancer Cells. *PLoS One* **8,** e57712 (2013).

48. Frommer, W. B., Davidson, M. W. & Campbell, R. E. Genetically encoded biosensors based on engineered fluorescent proteins. *Chem. Soc. Rev.* **38,** 2833 (2009).

49. Hazelbauer, G. L. & Adler, J. Role of the Galactose Binding Protein in Chemotaxis of *Escherichia coli* toward Galactose. *Nat. New Biol.* **230,** 101–104 (1971).

50. Ortega, G., Castaño, D., Diercks, T. & Millet, O. Carbohydrate Affinity for the Glucose–Galactose Binding Protein Is Regulated by Allosteric Domain Motions. *J. Am. Chem. Soc.* **134,** 19869–19876 (2012).

51. Borrok, M. J., Kiessling, L. L. & Forest, K. T. Conformational changes of glucose/galactose-binding protein illuminated by open, unliganded, and ultra-high-resolution ligand-bound structures. *Protein Sci.* **16,** 1032–1041 (2007).

52. Tian, Y. *et al.* Structure-based design of robust glucose biosensors using a *Thermotoga maritima* periplasmic glucose-binding protein. *Protein Sci.* **16,** 2240–2250 (2007).

53. Zukin, R. S., Strange, P. G., Heavey, L. R. & Koshland, D. E. (Jr. . Properties of the Galactose Binding Protein of *Salmonella typhimurium* and *Escherichia coli*. *Biochemistry* **16,** 381–386 (1977).

54. Stepanenko, O. V. *et al.* Tryptophan Residue of the D-Galactose/D-Glucose-Binding Protein from *E. Coli* Localized in its Active Center Does not Contribute to the Change in Intrinsic Fluorescence Upon Glucose Binding. *J. Fluoresc.* **25,** 87–94 (2015).

55. Fehr, M., Lalonde, S., Lager, I., Wolff, M. W. & Frommer, W. B. In Vivo Imaging of the

Dynamics of Glucose Uptake in the Cytosol of COS-7 Cells by Fluorescent Nanosensors. *J. Biol. Chem.* **278,** 19127–19133 (2003).

56. Deuschle, K. *et al.* Construction and optimization of a family of genetically encoded metabolite sensors by semirational protein engineering. *Protein Sci.* **14,** 2304–2314 (2005).

57. Volkenhoff, A., Hirrlinger, J., Kappel, J. M., Klämbt, C. & Schirmeier, S. Live imaging using a FRET glucose sensor reveals glucose delivery to all cell types in the *Drosophila* brain. *J. Insect Physiol.* **106,** 55–64 (2018).

58. Mohsin, M., Ahmad, A. & Iqbal, M. FRET-based genetically-encoded sensors for quantitative monitoring of metabolites. *Biotechnol. Lett.* **37,** 1919–1928 (2015).

59. Charneca, A., Karmali, A. & Vieira, M. Non-enzymatic assay for glucose by using immobilized whole-cells of *E. coli* containing glucose binding protein fused to fluorescent proteins. *Sensors Actuators B Chem.* **221,** 236–241 (2015).

60. Takanaga, H., Chaudhuri, B. & Frommer, W. B. GLUT1 and GLUT9 as major contributors to glucose influx in HepG2 cells identified by a high sensitivity intramolecular FRET glucose sensor. *Biochim. Biophys. Acta - Biomembr.* **1778,** 1091–1099 (2008).

61. Bartolome, A., Smalls-Mantey, L., Lin, D., Rao, G. & Tolosa, L. FRET-based glucose monitoring for bioprocessing. *Proceedings of Engineered Probes for Biomedical Applications* **6098,** 60980L (2006).

62. Mastop, M. *et al.* Characterization of a spectrally diverse set of fluorescent proteins as FRET acceptors for mTurquoise2. *Sci. Rep.* **7,** 11999 (2017).

63. Sanford, L. & Palmer, A. Recent Advances in Development of Genetically Encoded Fluorescent Sensors. in *Methods in Enzymology* **589,** 1–49 (Elsevier Inc., 2017).

64. Moussa, R. *et al.* An evaluation of genetically encoded FRET-based biosensors for quantitative metabolite analyses in vivo. *J. Biotechnol.* **191,** 250–259 (2014).

65. Moussa, R. Eine kritische Evaluierung FRET-basierter Biosensoren als Werkzeuge für die quantitative Metabolitanalytik.Doctoral Thesis (Heinrich-Heine Universität Düsseldorf, 2012).

66. Morikawa, T. J. *et al.* Dependence of fluorescent protein brightness on protein concentration in solution and enhancement of it. *Sci. Rep.* **6,** 22342 (2016).

67. Steffen, V. *et al.* A Toolbox of Genetically Encoded FRET-Based Biosensors for Rapid l-Lysine Analysis. *Sensors* **16,** 1604 (2016).

68. Ha, T. *et al.* Probing the interaction between two single molecules: fluorescence resonance energy transfer between a single donor and a single acceptor. *Proc. Natl. Acad. Sci.* **93,** 6264–6268 (1996).

69. Kensy, F., Zang, E., Faulhammer, C., Tan, R.-K. & Büchs, J. Validation of a high-throughput fermentation system based on online monitoring of biomass and fluorescence in continuously shaken microtiter plates. *Microb. Cell Fact.* **8,** 31 (2009).

70. Flitsch, D. *et al.* Respiration activity monitoring system for any individual well of a 48-well microtiter plate. *J. Biol. Eng.* **10,** 14 (2016).

71. Jacques, P. *et al.* High-throughput strategies for the discovery and engineering of enzymes for biocatalysis. *Bioprocess Biosyst. Eng.* **40,** 161–180 (2017).

72. Mahr, R. *et al.* Biosensor-driven adaptive laboratory evolution of L -valine production in

Corynebacterium glutamicum. *Metab. Eng.* **32,** 184–194 (2015).

73. Muzzey, D. & van Oudenaarden, A. Quantitative Time-Lapse Fluorescence Microscopy in Single Cells. *Annu. Rev. Cell Dev. Biol.* **25,** 301–327 (2009).

74. Rosenthal, K., Oehling, V., Dusny, C. & Schmid, A. Beyond the bulk: disclosing the life of single microbial cells. *FEMS Microbiol. Rev.* **41,** 751–780 (2017).

75. McKinney, W. Data structures for statistical computing in python. in *Proceedings of the 9th Python in Science Conference* **445,** 51–56 (2010).

76. Subach, O. M., Cranfill, P. J., Davidson, M. W. & Verkhusha, V. V. An Enhanced Monomeric Blue Fluorescent Protein with the High Chemical Stability of the Chromophore. *PLoS One* **6,** e28674 (2011).

77. Lam, A. J. *et al.* Improving FRET dynamic range with bright green and red fluorescent proteins. *Nat. Methods* **9,** 1005–1012 (2012).

78. Shirmanova, M. V *et al.* Intracellular pH imaging in cancer cells in vitro and tumors in vivo using the new genetically encoded sensor SypHer2. *Biochim. Biophys. Acta - Gen. Subj.* **1850,** 1905–1911 (2015).

79. Liu, S. *et al.* Enhanced dynamic range in a genetically encoded Ca^{2+} sensor. *Biochem. Biophys. Res. Commun.* **412,** 155–159 (2011).

80. Rekas, A., Alattia, J.-R., Nagai, T., Miyawaki, A. & Ikura, M. Crystal Structure of Venus, a Yellow Fluorescent Protein with Improved Maturation and Reduced Environmental Sensitivity. *J. Biol. Chem.* **277,** 50573–50578 (2002).

81. Shen, Y., Lai, T. & Campbell, R. E. Red fluorescent proteins (RFPs) and RFP-based biosensors for neuronal imaging applications. *Neurophotonics* **2,** 031203 (2015).

82. Kredel, S. *et al.* mRuby, a Bright Monomeric Red Fluorescent Protein for Labeling of Subcellular Structures. *PLoS One* **4,** e4391 (2009).

83. Confocal Microscopy - Spectral Bleed-Through Artifacts in Confocal Microscopy. Available at: https://www.olympus-lifescience.com/en/microscope-resource/primer/techniques/confocal/bleedthrough/. (Accessed: 12th January 2019)

84. Rizzo, M. a, Springer, G. H., Granada, B. & Piston, D. W. An improved cyan fluorescent protein variant useful for FRET. *Nat. Biotechnol.* **22,** 445–449 (2004).

85. Kremers, G.-J., Goedhart, J., van Munster, E. B. & Gadella, T. W. J. Cyan and Yellow Super Fluorescent Proteins with Improved Brightness, Protein Folding, and FRET Förster Radius *Biochemistry* **45,** 6570–6580 (2006).

86. Nguyen, A. W. & Daugherty, P. S. Evolutionary optimization of fluorescent proteins for intracellular FRET. *Nat. Biotechnol.* **23,** 355–360 (2005).

87. Martin, K. J. *et al.* Accepting from the best donor; analysis of long-lifetime donor fluorescent protein pairings to optimise dynamic FLIM-based FRET experiments. *PLoS One* **13,** e0183585 (2018).

88. Steffen, V. Entwicklung einer Toolbox von FRET- basierten Biosensoren für die Metabolitanalytik. Doctoral Thesis (Heinrich-Heine Unversität Düsseldorf, 2015).

89. Marx, V. Probes: FRET sensor design and optimization. *Nat. Methods* **14,** 949–953 (2017).

90. Evers, T. H., van Dongen, E. M. W. M., Faesen, A. C., Meijer, E. W. & Merkx, M.

Quantitative Understanding of the Energy Transfer between Fluorescent Proteins Connected via Flexible Peptide Linkers. *Biochemistry* **45,** 13183–13192 (2006).

91. Lissandron, V. *et al.* Improvement of a FRET-based Indicator for cAMP by Linker Design and Stabilization of Donor–Acceptor Interaction. *J. Mol. Biol.* **354,** 546–555 (2005).

92. Kever, L. Konstruktion und Characterisierung neuer FRET-basierter Glucosesensoren. Bachelor Thesis (Fachhochschule Jülich, 2017).

93. d'Auria, S. *et al.* Structural and Thermal Stability Characterization of *Escherichia coli* D-Galactose/D-Glucose-Binding Protein. *Biotechnol. Prog.* **20,** 330–337 (2008).

94. Petoukhov, M. V. *et al.* New developments in the *ATSAS* program package for small-angle scattering data analysis. *J. Appl. Crystallogr.* **45,** 342–350 (2012).

95. Peroza, E. A., Boumezbeur, A.-H. & Zamboni, N. Rapid, randomized development of genetically encoded FRET sensors for small molecules. *Analyst* **140,** 4540–8 (2015).

96. Sheldon, R. A. & van Pelt, S. Enzyme immobilisation in biocatalysis: why, what and how. *Chem. Soc. Rev.* **42,** 6223–35 (2013).

97. Engelmark Cassimjee, K. *et al.* A general protein purification and immobilization method on controlled porosity glass: biocatalytic applications. *Chem. Commun.* **50,** 9134 (2014).

98. Los, G. V. *et al.* HaloTag: A Novel Protein Labeling Technology for Cell Imaging and Protein Analysis. *ACS Chem. Biol.* **3,** 373–382 (2008).

99. Faccio, G. *et al.* Encapsulation of FRET-based glucose and maltose biosensors to develop functionalized silica nanoparticles. *Analyst* **141,** 3982–3984 (2016).

100. Grünberger, A. *et al.* A disposable picolitre bioreactor for cultivation and investigation of industrially relevant bacteria on the single cell level. *Lab Chip* **12,** 2060 (2012).

101. Demling, P., Westerwalbesloh, C., Noack, S., Wiechert, W. & Kohlheyer, D. Quantitative measurements in single-cell analysis: towards scalability in microbial bioprocess development. *Curr. Opin. Biotechnol.* **54,** 121–127 (2018).

102. Kantak, C., Zhu, Q., Beyer, S., Bansal, T. & Trau, D. Utilizing microfluidics to synthesize polyethylene glycol microbeads for Förster resonance energy transfer based glucose sensing. *Biomicrofluidics* **6,** 022006 (2012).

103. Otten, J. *et al.* A FRET-based biosensor for the quantification of glucose in culture supernatants of mL scale microbial cultivations. *Microb. Cell Fact.(submitted)*

Appendix

1 Supporting information

1.1 Supporting Information Chapter 2.1

Genetically encoded FRET-based biosensors studied on the single-molecule level

Henning Höfig[a,b], Julia Otten[c], Victoria Steffen[c], Martina Pohl[c], Arnold J. Boersma[d], Jörg Fitter [a,b,*]

[a] RWTH Aachen, I. Physikalisches Institut (IA), Aachen, Germany

[b] Forschungszentrum Jülich, ICS-5: Molecular Biophysics, Jülich, Germany

[c] Forschungszentrum Jülich, IBG-1: Biotechnology, Jülich, Germany

[d] Groningen Biomolecular Sciences and Biotechnology Institute, University of Groningen, Netherlands

* to whom the correspondence should be addressed: fitter@physik.rwth-aachen.de

Experimental Section

DNA- and protein-sequences of the glucose sensor constructs: In the following, DNA-sequences nucleotides encoding the N-terminal His_6-tag are printed in bold. The coding sequence for mTurquoise2, the glucose-galactose binding protein and Venus are coloured in blue, green, and yellow, respectively. Sequences for the flexible $(GGS)_4$ and the rigid (KLYPYDVPDYA) linkers are coloured in purple and red, respectively. Restriction sites are underlined. The same colour code is used for the protein sequences.

a) Glucose sensor 1

DNA sequence:

ATGCGGGGTTCT**CATCATCATCATCATCAT**GGTATGGCTAGCATGACTGGTGGACAGCAAATGGGTCGGGATCTG
TACGACGATGACGATAAGGAGCCGGGCCGCGCTGATACTCGCATTGGTGTAACAATCTATAAGGCGGCCGCTATG
GTGAGCAAGGGCGAGGAGCTGTTCACCGGGGTGGTGCCCATCCTGGTCGAGCTGGACGGCGACGTAAACGGCCA
CAAGTTCAGCGTGTCCGGCGAGGGCGAGGGCGATGCCACCTACGGCAAGCTGACCCTGAAGTTCATCTGCACCAC
CGGCAAGCTGCCCGTGCCCTGGCCCACCCTCGTGACCACCCTGTCCTGGGGCGTGCAGTGCTTCGCCCGCTACCCC
GACCACATGAAGCAGCACGACTTCTTCAAGTCCGCCATGCCCGAAGGCTACGTCCAGGAGCGCACCATCTTCTTCA
AGGACGACGGCAACTACAAGACCCGCGCCGAGGTGAAGTTCGAGGGCGACACCCTGGTGAACCGCATCGAGCTG
AAGGGCATCGACTTCAAGGAGGACGGCAACATCCTGGGGCACAAGCTGGAGTACAACTACTTTAGCGACAACGT
CTATATCACCGCCGACAAGCAGAAGAACGGCATCAAGGCCAACTTCAAGATCCGCCACAACATCGAGGACGGCGG
CGTGCAGCTCGCCGACCACTACCAGCAGAACACCCCCATCGGCGACGGCCCCGTGCTGCTGCCCGACAACCACTA
CCTGAGCACCCAGTCCAAGCTGAGCAAAGACCCCAACGAGAAGCGCGATCACATGGTCCTGCTGGAGTTCGTGAC
CGCCGCCGGGATCACTCTCGGCATGGACGAGCTGTACGGATCCGACCTGGTGGATAACTTTATGTCTGTAGTGCG
CAAGGCTATTGAGCAAGATGCGAAAGCCGCGCCAGATGTTCAGCTGCTGATGAATGATTCTCAGAATGACCAGTC
CAAGCAGAACGATCAGATCGACGTATTGCTGGCGAAAGGGGTGAAGGCACTGGCAATCAACCTCGTTGACCCGG

CAGCTGCGGGTACGGTGATTGAGAAAGCGCGTGGGCAAAACGTGCCGGTGGTTTTCTTCAACAAAGAACCGTCTC
GTAAGGCGCTGGATAGCTACGACAAAGCCTACTACGTTGGCACTGACTCCAAAGAGTCCGGCATTATTCAAGGCG
ATTTGATTGCTAAACACTGGGCGGCGAATCAGGGTTGGGATCTGAACAAAGACGGTCAGATTCAGTTCGTACTGC
TGAAAGGTGAACCGGGCCATCCGGATGCAGAAGCACGTACCACTTACGTGATTAAAGAATTGAACGATAAAGGC
ATCAAAACTGAACAGTTACAGTTAGATACCGCAATGTGGGACACCGCTCAGGCGAAAGATAAGATGGACGCCTG
GCTGTCTGGCCCGAACGCCAACAAAATCGAAGTGGTTATCGCCAACAACGATGCGATGGCAATGGGCGCGGTTG
AAGCGCTGAAAGCACACAACAAGTCCAGCATTCCGGTGTTTGGCGTCGATGCGCTGCCAGAAGCGCTGGCGCTGG
TGAAATCCGGTGCACTGGCGGGCACCGTACTGAACGATGCTAACAACCAGGCGAAAGCGACCTTTGATCTGGCGA
AAAACCTGGCCGATGGTAAAGGTGCGGCTGATGGCACCAACTGGAAAATCGACAACAAAGTGGTCCGCGTACCTT
ATGTTGGCGTAGATAAAGACAACCTGGCTGAGTTCAGCAAGAAAGAATTCGTCGACGGTGGAATGGTGAGCAAG
GGCGAGGAGCTGTTCACCGGGGTGGTGCCCATCCTGGTCGAGCTGGACGGCGACGTAAACGGCCACAAGTTCAG
CGTGTCCGGCGAGGGCGAGGGCGATGCCACCTACGGCAAGCTGACCCTGAAGCTGATCTGCACCACCGGCAAGC
TGCCCGTGCCCTGGCCCACCCTCGTGACCACCCTGGGCTACGGCCTGCAGTGCTTCGCCCGCTACCCCGACCACAT
GAAGCAGCACGACTTCTTCAAGTCCGCCATGCCCGAAGGCTACGTCCAGGAGCGCACCATCTTCTTCAAGGACGA
CGGCAACTACAAGACCCGCGCCGAGGTGAAGTTCGAGGGCGACACCCTGGTGAACCGCATCGAGCTGAAGGGCA
TCGACTTCAAGGAGGACGGCAACATCCTGGGGCACAAGCTGGAGTACAACTACAACAGCCACAACGTCTATATCA
CCGCCGACAAGCAGAAGAACGGCATCAAGGCCAACTTCAAGATCCGCCACAACATCGAGGACGGCGGCGTGCAG
CTCGCCGACCACTACCAGCAGAACACCCCCATCGGCGACGGCCCCGTGCTGCTGCCCGACAACCACTACCTGAGCT
ACCAGTCCGCCCTGAGCAAAGACCCCAACGAGAAGCGCGATCACATGGTCCTGCTGGAGTTCGTGACCGCCGCCG
GGATCACTCTCGGCATGGACGAGCTGTACAAGTAA

Protein sequence

MRGS**HHHHHH**GMASMTGGQQMGRDLYDDDDKEPGRADTRIGVTIYKAAAMVSKGEELFTGVVPILVELDGDVNG
HKFSVSGEGEGDATYGKLTLKFICTTGKLPVPWPTLVTTLSWGVQCFARYPDHMKQHDFFKSAMPEGYVQERTIFFKD
DGNYKTRAEVKFEGDTLVNRIELKGIDFKEDGNILGHKLEYNYFSDNVYITADKQKNGIKANFKIRHNIEDGGVQLADHY
QQNTPIGDGPVLLPDNHYLSTQSKLSKDPNEKRDHMVLLEFVTAAGITLGMDELYGSDLVDNFMSVVRKAIEQDAKAA
PDVQLLMNDSQNDQSKQNDQIDVLLAKGVKALAINLVDPAAAGTVIEKARGQNVPVVFFNKEPSRKALDSYDKAYYV
GTDSKESGIIQGDLIAKHWAANQGWDLNKDGQIQFVLLKGEPGHPDAEARTTYVIKELNDKGIKTEQLQLDTAMWDT
AQAKDKMDAWLSGPNANKIEVVIANNDAMAMGAVEALKAHNKSSIPVFGVDALPEALALVKSGALAGTVLNDANN
QAKATFDLAKNLADGKGAADGTNWKIDNKVVRVPYVGVDKDNLAEFSKKEFVDGGMVSKGEELFTGVVPILVELDGD
VNGHKFSVSGEGEGDATYGKLTLKLICTTGKLPVPWPTLVTTLGYGLQCFARYPDHMKQHDFFKSAMPEGYVQERTIFF
KDDGNYKTRAEVKFEGDTLVNRIELKGIDFKEDGNILGHKLEYNYNSHNVYITADKQKNGIKANFKIRHNIEDGGVQLAD
HYQQNTPIGDGPVLLPDNHYLSYQSALSKDPNEKRDHMVLLEFVTAAGITLGMDELYK

b) Glucose sensor 2

DNA sequence:

ATGCGGGGTTCTCATCATCATCATCATCATGGTATGGCTAGCATGACTGGTGGACAGCAAATGGGTCGGGATCTG
TACGACGATGACGATAAGGAGCCGGGCCGCGCTGATACTCGCATTGGTGTAACAATCTATAAGGCGGCCGCTATG
GTGAGCAAGGGCGAGGAGCTGTTCACCGGGGTGGTGCCCATCCTGGTCGAGCTGGACGGCGACGTAAACGGCCA
CAAGTTCAGCGTGTCCGGCGAGGGCGAGGGCGATGCCACCTACGGCAAGCTGACCCTGAAGTTCATCTGCACCAC
CGGCAAGCTGCCCGTGCCCTGGCCCACCCTCGTGACCACCCTGTCCTGGGGCGTGCAGTGCTTCGCCCGCTACCCC
GACCACATGAAGCAGCACGACTTCTTCAAGTCCGCCATGCCCGAAGGCTACGTCCAGGAGCGCACCATCTTCTTCA
AGGACGACGGCAACTACAAGACCCGCGCCGAGGTGAAGTTCGAGGGCGACACCCTGGTGAACCGCATCGAGCTG
AAGGGCATCGACTTCAAGGAGGACGGCAACATCCTGGGGCACAAGCTGGAGTACAACTACTTTAGCGACAACGT
CTATATCACCGCCGACAAGCAGAAGAACGGCATCAAGGCCAACTTCAAGATCCGCCACAACATCGAGGACGGCGG
CGTGCAGCTCGCCGACCACTACCAGCAGAACACCCCCATCGGCGACGGCCCCGTGCTGCTGCCCGACAACCACTA
CCTGAGCACCCAGTCCAAGCTGAGCAAAGACCCCAACGAGAAGCGCGATCACATGGTCCTGCTGGAGTTCGTGAC
CGCCGCCGGGATCACTCTCGGCATGGACGAGCTGTACGGATCCGGTGGTTCTGGCGGTTCAGGTGGCTCTGGTGG
GTCACCTGGTGATAACTTTATGTCTGTAGTGCGCAAGGCTATTGAGCAAGATGCGAAAGCCGCGCCAGATGTTCA
GCTGCTGATGAATGATTCTCAGAATGACCAGTCCAAGCAGAACGATCAGATCGACGTATTGCTGGCGAAAGGGGT
GAAGGCACTGGCAATCAACCTCGTTGACCCGGCAGCTGCGGGTACGGTGATTGAGAAAGCGCGTGGGCAAAACG
TGCCGGTGGTTTTCTTCAACAAAGAACCGTCTCGTAAGGCGCTGGATAGCTACGACAAAGCCTACTACGTTGGCAC
TGACTCCAAAGAGTCCGGCATTATTCAAGGCGATTTGATTGCTAAACACTGGGCGGCGAATCAGGGTTGGGATCT
GAACAAAGACGGTCAGATTCAGTTCGTACTGCTGAAAGGTGAACCGGGCCATCCGGATGCAGAAGCACGTACCA
CTTACGTGATTAAAGAATTGAACGATAAAGGCATCAAAACTGAACAGTTACAGTTAGATACCGCAATGTGGGACA

CCGCTCAGGCGAAAGATAAGATGGACGCCTGGCTGTCTGGCCCGAACGCCAACAAAATCGAAGTGGTTATCGCCA
ACAACGATGCGATGGCAATGGGCGCGGTTGAAGCGCTGAAAGCACACAACAAGTCCAGCATTCCGGTGTTTGGC
GTCGATGCGCTGCCAGAAGCGCTGGCGCTGGTGAAATCCGGTGCACTGGCGGGCACCGTACTGAACGATGCTAA
CAACCAGGCGAAAGCGACCTTTGATCTGGCGAAAAACCTGGCCGATGGTAAAGGTGCGGCTGATGGCACCAACT
GGAAAATCGACAACAAAGTGGTCCGCGTACCTTATGTTGGCGTAGATAAAGACAACCTGGCTGAGTTCAGCAAGA
AAGAATTCGTCGACGGTGGAATGGTGAGCAAGGGCGAGGAGCTGTTCACCGGGGTGGTGCCCATCCTGGTCGAG
CTGGACGGCGACGTAAACGGCCACAAGTTCAGCGTGTCCGGCGAGGGCGAGGGCGATGCCACCTACGGCAAGCT
GACCCTGAAGCTGATCTGCACCACCGGCAAGCTGCCCGTGCCCTGGCCCACCCTCGTGACCACCCTGGGCTACGGC
CTGCAGTGCTTCGCCCGCTACCCCGACCACATGAAGCAGCACGACTTCTTCAAGTCCGCCATGCCCGAAGGCTACG
TCCAGGAGCGCACCATCTTCTTCAAGGACGACGGCAACTACAAGACCCGCGCCGAGGTGAAGTTCGAGGGCGAC
ACCCTGGTGAACCGCATCGAGCTGAAGGGCATCGACTTCAAGGAGGACGGCAACATCCTGGGGCACAAGCTGGA
GTACAACTACAACAGCCACAACGTCTATATCACCGCCGACAAGCAGAAGAACGGCATCAAGGCCAACTTCAAGAT
CCGCCACAACATCGAGGACGGCGGCGTGCAGCTCGCCGACCACTACCAGCAGAACACCCCCATCGGCGACGGCCC
CGTGCTGCTGCCCGACAACCACTACCTGAGCTACCAGTCCGCCCTGAGCAAAGACCCCAACGAGAAGCGCGATCA
CATGGTCCTGCTGGAGTTCGTGACCGCCGCCGGGATCACTCTCGGCATGGACGAGCTGTACAAGTAA

Protein sequence:

MRSG**HHHHHH**GMASMTGGQQMGRDLYDDDDKEPGRADTRIGVTIYKAAAMVSKGEELFTGVVPILVELDGDVNG
HKFSVSGEGEGDATYGKLTLKFICTTGKLPVPWPTLVTTLSWGVQCFARYPDHMKQHDFFKSAMPEGYVQERTIFFKD
DGNYKTRAEVKFEGDTLVNRIELKGIDFKEDGNILGHKLEYNYFSDNVYITADKQKNGIKANFKIRHNIEDGGVQLADHY
QQNTPIGDGPVLLPDNHYLSTQSKLSKDPNEKRDHMVLLEFVTAAGITLGMDELYGSGGSGGSGGSGGSPGDNFMSV
VRKAIEQDAKAAPDVQLLMNDSQNDQSKQNDQIDVLLAKGVKALAINLVDPAAAGTVIEKARGQNVPVVFFNKEPSR
KALDSYDKAYYVGTDSKESGIIQGDLIAKHWAANQGWDLNKDGQIQFVLLKGEPGHPDAEARTTYVIKELNDKGIKTEQ
LQLDTAMWDTAQAKDKMDAWLSGPNANKIEVVIANNDAMAMGAVEALKAHNKSSIPVFGVDALPEALALVKSGAL
AGTVLNDANNQAKATFDLAKNLADGKGAADGTNWKIDNKVVRVPYVGVDKDNLAEFSKKEFVDGGMVSKGEELFTG
VVPILVELDGDVNGHKFSVSGEGEGDATYGKLTLKLICTTGKLPVPWPTLVTTLGYGLQCFARYPDHMKQHDFFKSAM
PEGYVQERTIFFKDDGNYKTRAEVKFEGDTLVNRIELKGIDFKEDGNILGHKLEYNYNSHNVYITADKQKNGIKANFKIRH
NIEDGGVQLADHYQQNTPIGDGPVLLPDNHYLSYQSALSKDPNEKRDHMVLLEFVTAAGITLGMDELYK

c) Glucose sensor 3

DNA sequence:

ATGCGGGGTTCT**CATCATCATCATCATCAT**GGTATGGCTAGCATGACTGGTGGACAGCAAATGGGTCGGGATCTG
TACGACGATGACGATAAGGAGCCGGGCCGCGCTGATACTCGCATTGGTGTAACAATCTATAAGGCGGCCGCTATG
GTGAGCAAGGGCGAGGAGCTGTTCACCGGGGTGGTGCCCATCCTGGTCGAGCTGGACGGCGACGTAAACGGCCA
CAAGTTCAGCGTGTCCGGCGAGGGCGAGGGCGATGCCACCTACGGCAAGCTGACCCTGAAGTTCATCTGCACCAC
CGGCAAGCTGCCCGTGCCCTGGCCCACCCTCGTGACCACCCTGTCCTGGGGCGTGCAGTGCTTCGCCCGCTACCCC
GACCACATGAAGCAGCACGACTTCTTCAAGTCCGCCATGCCCGAAGGCTACGTCCAGGAGCGCACCATCTTCTTCA
AGGACGACGGCAACTACAAGACCCGCGCCGAGGTGAAGTTCGAGGGCGACACCCTGGTGAACCGCATCGAGCTG
AAGGGCATCGACTTCAAGGAGGACGGCAACATCCTGGGGCACAAGCTGGAGTACAACTACTTTAGCGACAACGT
CTATATCACCGCCGACAAGCAGAAGAACGGCATCAAGGCCAACTTCAAGATCCGCCACAACATCGAGGACGGCGG
CGTGCAGCTCGCCGACCACTACCAGCAGAACACCCCCATCGGCGACGGCCCCGTGCTGCTGCCCGACAACCACTA
CCTGAGCACCCAGTCCAAGCTGAGCAAAGACCCCAACGAGAAGCGCGATCACATGGTCCTGCTGGAGTTCGTGAC
CGCCGCCGGGATCACTCTCGGCATGGACGAGCTGTACGGATCCAAACTGTACCCGTACGATGTGCCAGATTACGC
ACCTGGTGATAACTTTATGTCTGTAGTGCGCAAGGCTATTGAGCAAGATGCGAAAGCCGCGCCAGATGTTCAGCT
GCTGATGAATGATTCTCAGAATGACCAGTCCAAGCAGAACGATCAGATCGACGTATTGCTGGCGAAAGGGGTGA
AGGCACTGGCAATCAACCTCGTTGACCCGGCAGCTGCGGGTACGGTGATTGAGAAAGCGCGTGGGCAAAACGTG
CCGGTGGTTTTCTTCAACAAAGAACCGTCTCGTAAGGCGCTGGATAGCTACGACAAAGCCTACTACGTTGGCACTG
ACTCCAAAGAGTCCGGCATTATTCAAGGCGATTTGATTGCTAAACACTGGGCGGCGAATCAGGGTTGGGATCTGA
ACAAAGACGGTCAGATTCAGTTCGTACTGCTGAAAGGTGAACCGGGCCATCCGGATGCAGAAGCACGTACCACTT
ACGTGATTAAAGAATTGAACGATAAAGGCATCAAAACTGAACAGTTACAGTTAGATACCGCAATGTGGGACACCG
CTCAGGCGAAAGATAAGATGGACGCCTGGCTGTCTGGCCCGAACGCCAACAAAATCGAAGTGGTTATCGCCAACA
ACGATGCGATGGCAATGGGCGCGGTTGAAGCGCTGAAAGCACACAACAAGTCCAGCATTCCGGTGTTTGGCGTC
GATGCGCTGCCAGAAGCGCTGGCGCTGGTGAAATCCGGTGCACTGGCGGGCACCGTACTGAACGATGCTAACAA
CCAGGCGAAAGCGACCTTTGATCTGGCGAAAAACCTGGCCGATGGTAAAGGTGCGGCTGATGGCACCAACTGGA
AAATCGACAACAAAGTGGTCCGCGTACCTTATGTTGGCGTAGATAAAGACAACCTGGCTGAGTTCAGCAAGAAAG

AATTCGTCGACGGTGGAATGGTGAGCAAGGGCGAGGAGCTGTTCACCGGGGTGGTGCCCATCCTGGTCGAGCTG
GACGGCGACGTAAACGGCCACAAGTTCAGCGTGTCCGGCGAGGGCGAGGGCGATGCCACCTACGGCAAGCTGAC
CCTGAAGCTGATCTGCACCACCGGCAAGCTGCCCGTGCCCTGGCCCACCCTCGTGACCACCCTGGGCTACGGCCTG
CAGTGCTTCGCCCGCTACCCCGACCACATGAAGCAGCACGACTTCTTCAAGTCCGCCATGCCCGAAGGCTACGTCC
AGGAGCGCACCATCTTCTTCAAGGACGACGGCAACTACAAGACCCGCGCCGAGGTGAAGTTCGAGGGCGACACC
CTGGTGAACCGCATCGAGCTGAAGGGCATCGACTTCAAGGAGGACGGCAACATCCTGGGGCACAAGCTGGAGTA
CAACTACAACAGCCACAACGTCTATATCACCGCCGACAAGCAGAAGAACGGCATCAAGGCCAACTTCAAGATCCG
CCACAACATCGAGGACGGCGGCGTGCAGCTCGCCGACCACTACCAGCAGAACACCCCCATCGGCGACGGCCCCGT
GCTGCTGCCCGACAACCACTACCTGAGCTACCAGTCCGCCCTGAGCAAAGACCCCAACGAGAAGCGCGATCACAT
GGTCCTGCTGGAGTTCGTGACCGCCGCCGGGATCACTCTCGGCATGGACGAGCTGTACAAGTAA

Protein sequence

MRSG**HHHHHH**GMASMTGGQQMGRDLYDDDDKEPGRADTRIGVTIYKAAAMVSKGEELFTGVVPILVELDGDVNG
HKFSVSGEGEGDATYGKLTLKFICTTGKLPVPWPTLVTTLSWGVQCFARYPDHMKQHDFFKSAMPEGYVQERTIFFKD
DGNYKTRAEVKFEGDTLVNRIELKGIDFKEDGNILGHKLEYNYFSDNVYITADKQKNGIKANFKIRHNIEDGGVQLADHY
QQNTPIGDGPVLLPDNHYLSTQSKLSKDPNEKRDHMVLLEFVTAAGITLGMDELYGSKLYPYDVPDYAPGDNFMSVVR
KAIEQDAKAAPDVQLLMNDSQNDQSKQNDQIDVLLAKGVKALAINLVDPAAAGTVIEKARGQNVPVVFFNKEPSRKA
LDSYDKAYYVGTDSKESGIIQGDLIAKHWAANQGWDLNKDGQIQFVLLKGEPGHPDAEARTTYVIKELNDKGIKTEQLQ
LDTAMWDTAQAKDKMDAWLSGPNANKIEVVIANNDAMAMGAVEALKAHNKSSIPVFGVDALPEALALVKSGALAG
TVLNDANNQAKATFDLAKNLADGKGAADGTNWKIDNKVVRVPYVGVDKDNLAEFSKKEFVDGGMVSKGEELFTGVV
PILVELDGDVNGHKFSVSGEGEGDATYGKLTLKLICTTGKLPVPWPTLVTTLGYGLQCFARYPDHMKQHDFFKSAMPE
GYVQERTIFFKDDGNYKTRAEVKFEGDTLVNRIELKGIDFKEDGNILGHKLEYNYNSHNVYITADKQKNGIKANFKIRHNI
EDGGVQLADHYQQNTPIGDGPVLLPDNHYLSYQSALSKDPNEKRDHMVLLEFVTAAGITLGMDELYK

d) Glucose sensor 4

DNA sequence:

ATGCGGGGTTCT**CATCATCATCATCATCAT**GGTATGGCTAGCATGACTGGTGGACAGCAAATGGGTCGGGATCTG
TACGACGATGACGATAAGGAGCCGGGCCGCGCTGATACTCGCATTGGTGTAACAATCTATAAGGCGGCCGCTATG
GTGAGCAAGGGCGAGGAGCTGTTCACCGGGGTGGTGCCCATCCTGGTCGAGCTGGACGGCGACGTAAACGGCCA
CAAGTTCAGCGTGTCCGGCGAGGGCGAGGGCGATGCCACCTACGGCAAGCTGACCCTGAAGTTCATCTGCACCAC
CGGCAAGCTGCCCGTGCCCTGGCCCACCCTCGTGACCACCCTGTCCTGGGGCGTGCAGTGCTTCGCCCGCTACCCC
GACCACATGAAGCAGCACGACTTCTTCAAGTCCGCCATGCCCGAAGGCTACGTCCAGGAGCGCACCATCTTCTTCA
AGGACGACGGCAACTACAAGACCCGCGCCGAGGTGAAGTTCGAGGGCGACACCCTGGTGAACCGCATCGAGCTG
AAGGGCATCGACTTCAAGGAGGACGGCAACATCCTGGGGCACAAGCTGGAGTACAACTACTTTAGCGACAACGT
CTATATCACCGCCGACAAGCAGAAGAACGGCATCAAGGCCAACTTCAAGATCCGCCACAACATCGAGGACGGCGG
CGTGCAGCTCGCCGACCACTACCAGCAGAACACCCCCATCGGCGACGGCCCCGTGCTGCTGCCCGACAACCACTA
CCTGAGCACCCAGTCCAAGCTGAGCAAAGACCCCAACGAGAAGCGCGATCACATGGTCCTGCTGGAGTTCGTGAC
CGCCGCCGGGATCACTCTCGGCATGGACGAGCTGTACGGATCCGACCTGGTGGATAACTTTATGTCTGTAGTGCG
CAAGGCTATTGAGCAAGATGCGAAAGCCGCGCCAGATGTTCAGCTGCTGATGAATGATTCTCAGAATGACCAGTC
CAAGCAGAACGATCAGATCGACGTATTGCTGGCGAAAGGGGTGAAGGCACTGGCAATCAACCTCGTTGACCCGG
CAGCTGCGGGTACGGTGATTGAGAAAGCGCGTGGGCAAAACGTGCCGGTGGTTTTCTTCAACAAAGAACCGTCTC
GTAAGGCGCTGGATAGCTACGACAAAGCCTACTACGTTGGCACTGACTCCAAAGAGTCCGGCATTATTCAAGGCG
ATTTGATTGCTAAACACTGGGCGGCGAATCAGGGTTGGGATCTGAACAAAGACGGTCAGATTCAGTTCGTACTGC
TGAAAGGTGAACCGGGCCATCCGGATGCAGAAGCACGTACCACTTACGTGATTAAAGAATTGAACGATAAAGGC
ATCAAAACTGAACAGTTACAGTTAGATACCGCAATGTGGGACACCGCTCAGGCGAAAGATAAGATGGACGCCTG
GCTGTCTGGCCCGAACGCCAACAAAATCGAAGTGGTTATCGCCAACAACGATGCGATGGCAATGGGCGCGGTTG
AAGCGCTGAAAGCACACAACAAGTCCAGCATTCCGGTGTTTGGCGTCGATGCGCTGCCAGAAGCGCTGGCGCTGG
TGAAATCCGGTGCACTGGCGGGCACCGTACTGAACGATGCTAACAACCAGGCGAAAGCGACCTTTGATCTGGCGA
AAAACCTGGCCGATGGTAAAGGTGCGGCTGATGGCACCAACTGGAAAATCGACAACAAAGTGGTCCGCGTACCTT
ATGTTGGCGTAGATAAAGACAACCTGGCTGAGTTCAGCAAGAAAGAATTCGGAGGCTCTGGTGGTAGCGGCGGG
AGTGGTGGTAGTGTCGACGGTGGAATGGTGAGCAAGGGCGAGGAGCTGTTCACCGGGGTGGTGCCCATCCTGGT
CGAGCTGGACGGCGACGTAAACGGCCACAAGTTCAGCGTGTCCGGCGAGGGCGAGGGCGATGCCACCTACGGC
AAGCTGACCCTGAAGCTGATCTGCACCACCGGCAAGCTGCCCGTGCCCTGGCCCACCCTCGTGACCACCCTGGGCT
ACGGCCTGCAGTGCTTCGCCCGCTACCCCGACCACATGAAGCAGCACGACTTCTTCAAGTCCGCCATGCCCGAAGG
CTACGTCCAGGAGCGCACCATCTTCTTCAAGGACGACGGCAACTACAAGACCCGCGCCGAGGTGAAGTTCGAGGG

CGACACCCTGGTGAACCGCATCGAGCTGAAGGGCATCGACTTCAAGGAGGACGGCAACATCCTGGGGCACAAGC
TGGAGTACAACTACAACAGCCACAACGTCTATATCACCGCCGACAAGCAGAAGAACGGCATCAAGGCCAACTTCA
AGATCCGCCACAACATCGAGGACGGCGGCGTGCAGCTCGCCGACCACTACCAGCAGAACACCCCCATCGGCGAC
GGCCCCGTGCTGCTGCCCGACAACCACTACCTGAGCTACCAGTCCGCCCTGAGCAAAGACCCCAACGAGAAGCGC
GATCACATGGTCCTGCTGGAGTTCGTGACCGCCGCCGGGATCACTCTCGGCATGGACGAGCTGTACAAGTAA

Protein sequence:

MRSG**HHHHHH**GMASMTGGQQMGRDLYDDDDKEPGRADTRIGVTIYKAAAMVSKGEELFTGVVPILVELDGDVNG
HKFSVSGEGEGDATYGKLTLKFICTTGKLPVPWPTLVTTLSWGVQCFARYPDHMKQHDFFKSAMPEGYVQERTIFFKD
DGNYKTRAEVKFEGDTLVNRIELKGIDFKEDGNILGHKLEYNYFSDNVYITADKQKNGIKANFKIRHNIEDGGVQLADHY
QQNTPIGDGPVLLPDNHYLSTQSKLSKDPNEKRDHMVLLEFVTAAGITLGMDELYGSDLVDNFMSVVRKAIEQDAKAA
PDVQLLMNDSQNDQSKQNDQIDVLLAKGVKALAINLVDPAAAGTVIEKARGQNVPVVFFNKEPSRKALDSYDKAYYV
GTDSKESGIIQGDLIAKHWAANQGWDLNKDGQIQFVLLKGEPGHPDAEARTTYVIKELNDKGIKTEQLQLDTAMWDT
AQAKDKMDAWLSGPNANKIEVVIANNDAMAMGAVEALKAHNKSSIPVFGVDALPEALALVKSGALAGTVLNDANN
QAKATFDLAKNLADGKGAADGTNWKIDNKVVRVPYVGVDKDNLAEFSKKEFGGSGGSGGSGGSVDGGMVSKGEELF
TGVVPILVELDGDVNGHKFSVSGEGEGDATYGKLTLKLICTTGKLPVPWPTLVTTLGYGLQCFARYPDHMKQHDFFKSA
MPEGYVQERTIFFKDDGNYKTRAEVKFEGDTLVNRIELKGIDFKEDGNILGHKLEYNYNSHNVYITADKQKNGIKANFKI
RHNIEDGGVQLADHYQQNTPIGDGPVLLPDNHYLSYQSALSKDPNEKRDHMVLLEFVTAAGITLGMDELYK

e) Glucose sensor 5

DNA sequence:

ATGCGGGGTTCT**CATCATCATCATCATCAT**GGTATGGCTAGCATGACTGGTGGACAGCAAATGGGTCGGGATCTG
TACGACGATGACGATAAGGAGCCGGGCCGCGCTGATACTCGCATTGGTGTAACAATCTATAAGGCGGCCGCTATG
GTGAGCAAGGGCGAGGAGCTGTTCACCGGGGTGGTGCCCATCCTGGTCGAGCTGGACGGCGACGTAAACGGCCA
CAAGTTCAGCGTGTCCGGCGAGGGCGAGGGCGATGCCACCTACGGCAAGCTGACCCTGAAGTTCATCTGCACCAC
CGGCAAGCTGCCCGTGCCCTGGCCCACCCTCGTGACCACCCTGTCCTGGGGCGTGCAGTGCTTCGCCCGCTACCCC
GACCACATGAAGCAGCACGACTTCTTCAAGTCCGCCATGCCCGAAGGCTACGTCCAGGAGCGCACCATCTTCTTCA
AGGACGACGGCAACTACAAGACCCGCGCCGAGGTGAAGTTCGAGGGCGACACCCTGGTGAACCGCATCGAGCTG
AAGGGCATCGACTTCAAGGAGGACGGCAACATCCTGGGGCACAAGCTGGAGTACAACTACTTTAGCGACAACGT
CTATATCACCGCCGACAAGCAGAAGAACGGCATCAAGGCCAACTTCAAGATCCGCCACAACATCGAGGACGGCGG
CGTGCAGCTCGCCGACCACTACCAGCAGAACACCCCCATCGGCGACGGCCCCGTGCTGCTGCCCGACAACCACTA
CCTGAGCACCCAGTCCAAGCTGAGCAAAGACCCCAACGAGAAGCGCGATCACATGGTCCTGCTGGAGTTCGTGAC
CGCCGCCGGGATCACTCTCGGCATGGACGAGCTGTACGGATCCGGTGGTTCTGGCGGTTCAGGTGGCTCTGGTGG
GTCACCTGGTGATAACTTTATGTCTGTAGTGCGCAAGGCTATTGAGCAAGATGCGAAAGCCGCGCCAGATGTTCA
GCTGCTGATGAATGATTCTCAGAATGACCAGTCCAAGCAGAACGATCAGATCGACGTATTGCTGGCGAAAGGGGT
GAAGGCACTGGCAATCAACCTCGTTGACCCGGCAGCTGCGGGTACGGTGATTGAGAAAGCGCGTGGGCAAAACG
TGCCGGTGGTTTTCTTCAACAAAGAACCGTCTCGTAAGGCGCTGGATAGCTACGACAAAGCCTACTACGTTGGCAC
TGACTCCAAAGAGTCCGGCATTATTCAAGGCGATTTGATTGCTAAACACTGGGCGGCGAATCAGGGTTGGGATCT
GAACAAAGACGGTCAGATTCAGTTCGTACTGCTGAAAGGTGAACCGGGCCATCCGGATGCAGAAGCACGTACCA
CTTACGTGATTAAAGAATTGAACGATAAAGGCATCAAAACTGAACAGTTACAGTTAGATACCGCAATGTGGGACA
CCGCTCAGGCGAAAGATAAGATGGACGCCTGGCTGTCTGGCCCGAACGCCAACAAAATCGAAGTGGTTATCGCCA
ACAACGATGCGATGGCAATGGGCGCGGTTGAAGCGCTGAAAGCACACAACAAGTCCAGCATTCCGGTGTTTGGC
GTCGATGCGCTGCCAGAAGCGCTGGCGCTGGTGAAATCCGGTGCACTGGCGGGCACCGTACTGAACGATGCTAA
CAACCAGGCGAAAGCGACCTTTGATCTGGCGAAAAACCTGGCCGATGGTAAAGGTGCGGCTGATGGCACCAACT
GGAAAATCGACAACAAAGTGGTCCGCGTACCTTATGTTGGCGTAGATAAAGACAACCTGGCTGAGTTCAGCAAGA
AAGAATTCGGAGGCTCTGGTGGTAGCGGCGGGAGTGGTGGTAGTGTCGACGGTGGAATGGTGAGCAAGGGCGA
GGAGCTGTTCACCGGGGTGGTGCCCATCCTGGTCGAGCTGGACGGCGACGTAAACGGCCACAAGTTCAGCGTGT
CCGGCGAGGGCGAGGGCGATGCCACCTACGGCAAGCTGACCCTGAAGCTGATCTGCACCACCGGCAAGCTGCCC
GTGCCCTGGCCCACCCTCGTGACCACCCTGGGCTACGGCCTGCAGTGCTTCGCCCGCTACCCCGACCACATGAAGC
AGCACGACTTCTTCAAGTCCGCCATGCCCGAAGGCTACGTCCAGGAGCGCACCATCTTCTTCAAGGACGACGGCA
ACTACAAGACCCGCGCCGAGGTGAAGTTCGAGGGCGACACCCTGGTGAACCGCATCGAGCTGAAGGGCATCGAC
TTCAAGGAGGACGGCAACATCCTGGGGCACAAGCTGGAGTACAACTACAACAGCCACAACGTCTATATCACCGCC
GACAAGCAGAAGAACGGCATCAAGGCCAACTTCAAGATCCGCCACAACATCGAGGACGGCGGCGTGCAGCTCGC
CGACCACTACCAGCAGAACACCCCCATCGGCGACGGCCCCGTGCTGCTGCCCGACAACCACTACCTGAGCTACCA

GTCCGCCCTGAGCAAAGACCCCAACGAGAAGCGCGATCACATGGTCCTGCTGGAGTTCGTGACCGCCGCCGGGAT
CACTCTCGGCATGGACGAGCTGTACAAGTAA

Protein sequence:

MRSG**HHHHHH**GMASMTGGQQMGRDLYDDDDKEPGRADTRIGVTIYKAAAMVSKGEELFTGVVPILVELDGDVNG
HKFSVSGEGEGDATYGKLTLKFICTTGKLPVPWPTLVTTLSWGVQCFARYPDHMKQHDFFKSAMPEGYVQERTIFFKD
DGNYKTRAEVKFEGDTLVNRIELKGIDFKEDGNILGHKLEYNYFSDNVYITADKQKNGIKANFKIRHNIEDGGVQLADHY
QQNTPIGDGPVLLPDNHYLSTQSKLSKDPNEKRDHMVLLEFVTAAGITLGMDELYGSGGSGGSGGSGGSPGDNFMSV
VRKAIEQDAKAAPDVQLLMNDSQNDQSKQNDQIDVLLAKGVKALAINLVDPAAAGTVIEKARGQNVPVVFFNKEPSR
KALDSYDKAYYVGTDSKESGIIQGDLIAKHWAANQGWDLNKDGQIQFVLLKGEPGHPDAEARTTYVIKELNDKGIKTEQ
LQLDTAMWDTAQAKDKMDAWLSGPNANKIEVVIANNDAMAMGAVEALKAHNKSSIPVFGVDALPEALALVKSGAL
AGTVLNDANNQAKATFDLAKNLADGKGAADGTNWKIDNKVVRVPYVGVDKDNLAEFSKKEFGGSGGSGGSGGSVD
GGMVSKGEELFTGVVPILVELDGDVNGHKFSVSGEGEGDATYGKLTLKLICTTGKLPVPWPTLVTTLGYGLQCFARYPD
HMKQHDFFKSAMPEGYVQERTIFFKDDGNYKTRAEVKFEGDTLVNRIELKGIDFKEDGNILGHKLEYNYNSHNVYITAD
KQKNGIKANFKIRHNIEDGGVQLADHYQQNTPIGDGPVLLPDNHYLSYQSALSKDPNEKRDHMVLLEFVTAAGITLGM
DELYK

f) Glucose sensor 6

DNA sequence:

ATGCGGGGTTCT**CATCATCATCATCATCAT**GGTATGGCTAGCATGACTGGTGGACAGCAAATGGGTCGGGATCTG
TACGACGATGACGATAAGGAGCCGGGCCGCGCTGATACTCGCATTGGTGTAACAATCTATAAGGCGGCCGCTATG
GTGAGCAAGGGCGAGGAGCTGTTCACCGGGGTGGTGCCCATCCTGGTCGAGCTGGACGGCGACGTAAACGGCCA
CAAGTTCAGCGTGTCCGGCGAGGGCGAGGGCGATGCCACCTACGGCAAGCTGACCCTGAAGTTCATCTGCACCAC
CGGCAAGCTGCCCGTGCCCTGGCCCACCCTCGTGACCACCCTGTCCTGGGGCGTGCAGTGCTTCGCCCGCTACCCC
GACCACATGAAGCAGCACGACTTCTTCAAGTCCGCCATGCCCGAAGGCTACGTCCAGGAGCGCACCATCTTCTTCA
AGGACGACGGCAACTACAAGACCCGCGCCGAGGTGAAGTTCGAGGGCGACACCCTGGTGAACCGCATCGAGCTG
AAGGGCATCGACTTCAAGGAGGACGGCAACATCCTGGGGCACAAGCTGGAGTACAACTACTTTAGCGACAACGT
CTATATCACCGCCGACAAGCAGAAGAACGGCATCAAGGCCAACTTCAAGATCCGCCACAACATCGAGGACGGCGG
CGTGCAGCTCGCCGACCACTACCAGCAGAACACCCCCATCGGCGACGGCCCCGTGCTGCTGCCCGACAACCACTA
CCTGAGCACCCAGTCCAAGCTGAGCAAAGACCCCAACGAGAAGCGCGATCACATGGTCCTGCTGGAGTTCGTGAC
CGCCGCCGGGATCACTCTCGGCATGGACGAGCTGTACGGATCCAAACTGTACCCGTACGATGTGCCAGATTACGC
ACCTGGTGATAACTTTATGTCTGTAGTGCGCAAGGCTATTGAGCAAGATGCGAAAGCCGCGCCAGATGTTCAGCT
GCTGATGAATGATTCTCAGAATGACCAGTCCAAGCAGAACGATCAGATCGACGTATTGCTGGCGAAAGGGGTGA
AGGCACTGGCAATCAACCTCGTTGACCCGGCAGCTGCGGGTACGGTGATTGAGAAAGCGCGTGGGCAAAACGTG
CCGGTGGTTTTCTTCAACAAAGAACCGTCTCGTAAGGCGCTGGATAGCTACGACAAAGCCTACTACGTTGGCACTG
ACTCCAAAGAGTCCGGCATTATTCAAGGCGATTTGATTGCTAAACACTGGGCGGCGAATCAGGGTTGGGATCTGA
ACAAAGACGGTCAGATTCAGTTCGTACTGCTGAAAGGTGAACCGGGCCATCCGGATGCAGAAGCACGTACCACTT
ACGTGATTAAAGAATTGAACGATAAAGGCATCAAAACTGAACAGTTACAGTTAGATACCGCAATGTGGGACACCG
CTCAGGCGAAAGATAAGATGGACGCCTGGCTGTCTGGCCCGAACGCCAACAAAATCGAAGTGGTTATCGCCAACA
ACGATGCGATGGCAATGGGCGCGGTTGAAGCGCTGAAAGCACACAACAAGTCCAGCATTCCGGTGTTTGGCGTC
GATGCGCTGCCAGAAGCGCTGGCGCTGGTGAAATCCGGTGCACTGGCGGGCACCGTACTGAACGATGCTAACAA
CCAGGCGAAAGCGACCTTTGATCTGGCGAAAAACCTGGCCGATGGTAAAGGTGCGGCTGATGGCACCAACTGGA
AAATCGACAACAAAGTGGTCCGCGTACCTTATGTTGGCGTAGATAAAGACAACCTGGCTGAGTTCAGCAAGAAAG
AATTCGGAGGCTCTGGTGGTAGCGGCGGGAGTGGTGGTAGTGTCGACGGTGGAATGGTGAGCAAGGGCGAGGA
GCTGTTCACCGGGGTGGTGCCCATCCTGGTCGAGCTGGACGGCGACGTAAACGGCCACAAGTTCAGCGTGTCCG
GCGAGGGCGAGGGCGATGCCACCTACGGCAAGCTGACCCTGAAGCTGATCTGCACCACCGGCAAGCTGCCCGTG
CCCTGGCCCACCCTCGTGACCACCCTGGGCTACGGCCTGCAGTGCTTCGCCCGCTACCCCGACCACATGAAGCAGC
ACGACTTCTTCAAGTCCGCCATGCCCGAAGGCTACGTCCAGGAGCGCACCATCTTCTTCAAGGACGACGGCAACTA
CAAGACCCGCGCCGAGGTGAAGTTCGAGGGCGACACCCTGGTGAACCGCATCGAGCTGAAGGGCATCGACTTCA
AGGAGGACGGCAACATCCTGGGGCACAAGCTGGAGTACAACTACAACAGCCACAACGTCTATATCACCGCCGACA
AGCAGAAGAACGGCATCAAGGCCAACTTCAAGATCCGCCACAACATCGAGGACGGCGGCGTGCAGCTCGCCGAC
CACTACCAGCAGAACACCCCCATCGGCGACGGCCCCGTGCTGCTGCCCGACAACCACTACCTGAGCTACCAGTCCG
CCCTGAGCAAAGACCCCAACGAGAAGCGCGATCACATGGTCCTGCTGGAGTTCGTGACCGCCGCCGGGATCACTC
TCGGCATGGACGAGCTGTACAAGTAA

Protein sequence:

MRSG**HHHHHH**GMASMTGGQQMGRDLYDDDDKEPGRADTRIGVTIYKAAAMVSKGEELFTGVVPILVELDGDVNG
HKFSVSGEGEGDATYGKLTLKFICTTGKLPVPWPTLVTTLSWGVQCFARYPDHMKQHDFFKSAMPEGYVQERTIFFKD
DGNYKTRAEVKFEGDTLVNRIELKGIDFKEDGNILGHKLEYNYFSDNVYITADKQKNGIKANFKIRHNIEDGGVQLADHY
QQNTPIGDGPVLLPDNHYLSTQSKLSKDPNEKRDHMVLLEFVTAAGITLGMDELYGSKLYPYDVPDYAPGDNFMSVVR
KAIEQDAKAAPDVQLLMNDSQNDQSKQNDQIDVLLAKGVKALAINLVDPAAAGTVIEKARGQNVPVVFFNKEPSRKA
LDSYDKAYYVGTDSKESGIIQGDLIAKHWAANQGWDLNKDGQIQFVLLKGEPGHPDAEARTTYVIKELNDKGIKTEQLQ
LDTAMWDTAQAKDKMDAWLSGPNANKIEVVIANNDAMAMGAVEALKAHNKSSIPVFGVDALPEALALVKSGALAG
TVLNDANNQAKATFDLAKNLADGKGAADGTNWKIDNKVVRVPYVGVDKDNLAEFSKKEFGGSGGSGGSGGSVDGG
MVSKGEELFTGVVPILVELDGDVNGHKFSVSGEGEGDATYGKLTLKLICTTGKLPVPWPTLVTTLGYGLQCFARYPDHM
KQHDFFKSAMPEGYVQERTIFFKDDGNYKTRAEVKFEGDTLVNRIELKGIDFKEDGNILGHKLEYNYNSHNVYITADKQK
NGIKANFKIRHNIEDGGVQLADHYQQNTPIGDGPVLLPDNHYLSYQSALSKDPNEKRDHMVLLEFVTAAGITLGMDEL
YK

g) Glucose sensor 7

DNA sequence:

ATGCGGGGTTCTCATCATCATCATCATCATGGTATGGCTAGCATGACTGGTGGACAGCAAATGGGTCGGGATCTG
TACGACGATGACGATAAGGAGCCGGGCCGCGCTGATACTCGCATTGGTGTAACAATCTATAAGGCGGCCGCTATG
GTGAGCAAGGGCGAGGAGCTGTTCACCGGGGTGGTGCCCATCCTGGTCGAGCTGGACGGCGACGTAAACGGCCA
CAAGTTCAGCGTGTCCGGCGAGGGCGAGGGCGATGCCACCTACGGCAAGCTGACCCTGAAGTTCATCTGCACCAC
CGGCAAGCTGCCCGTGCCCTGGCCCACCCTCGTGACCACCCTGTCCTGGGGCGTGCAGTGCTTCGCCCGCTACCCC
GACCACATGAAGCAGCACGACTTCTTCAAGTCCGCCATGCCCGAAGGCTACGTCCAGGAGCGCACCATCTTCTTCA
AGGACGACGGCAACTACAAGACCCGCGCCGAGGTGAAGTTCGAGGGCGACACCCTGGTGAACCGCATCGAGCTG
AAGGGCATCGACTTCAAGGAGGACGGCAACATCCTGGGGCACAAGCTGGAGTACAACTACTTTAGCGACAACGT
CTATATCACCGCCGACAAGCAGAAGAACGGCATCAAGGCCAACTTCAAGATCCGCCACAACATCGAGGACGGCGG
CGTGCAGCTCGCCGACCACTACCAGCAGAACACCCCCATCGGCGACGGCCCCGTGCTGCTGCCCGACAACCACTA
CCTGAGCACCCAGTCCAAGCTGAGCAAAGACCCCAACGAGAAGCGCGATCACATGGTCCTGCTGGAGTTCGTGAC
CGCCGCCGGGATCACTCTCGGCATGGACGAGCTGTACGGATCCGACCTGGTGGATAACTTTATGTCTGTAGTGCG
CAAGGCTATTGAGCAAGATGCGAAAGCCGCGCCAGATGTTCAGCTGCTGATGAATGATTCTCAGAATGACCAGTC
CAAGCAGAACGATCAGATCGACGTATTGCTGGCGAAAGGGGTGAAGGCACTGGCAATCAACCTCGTTGACCCGG
CAGCTGCGGGTACGGTGATTGAGAAAGCGCGTGGGCAAAACGTGCCGGTGGTTTTCTTCAACAAAGAACCGTCTC
GTAAGGCGCTGGATAGCTACGACAAAGCCTACTACGTTGGCACTGACTCCAAAGAGTCCGGCATTATTCAAGGCG
ATTTGATTGCTAAACACTGGGCGGCGAATCAGGGTTGGGATCTGAACAAAGACGGTCAGATTCAGTTCGTACTGC
TGAAAGGTGAACCGGGCCATCCGGATGCAGAAGCACGTACCACTTACGTGATTAAAGAATTGAACGATAAAGGC
ATCAAAACTGAACAGTTACAGTTAGATACCGCAATGTGGGACACCGCTCAGGCGAAAGATAAGATGGACGCCTG
GCTGTCTGGCCCGAACGCCAACAAAATCGAAGTGGTTATCGCCAACAACGATGCGATGGCAATGGGCGCGGTTG
AAGCGCTGAAAGCACACAACAAGTCCAGCATTCCGGTGTTTGGCGTCGATGCGCTGCCAGAAGCGCTGGCGCTGG
TGAAATCCGGTGCACTGGCGGGCACCGTACTGAACGATGCTAACAACCAGGCGAAAGCGACCTTTGATCTGGCGA
AAAACCTGGCCGATGGTAAAGGTGCGGCTGATGGCACCAACTGGAAAATCGACAACAAAGTGGTCCGCGTACCTT
ATGTTGGCGTAGATAAAGACAACCTGGCTGAGTTCAGCAAGAAAGAATTCAAGTTGTACCCATATGACGTTCCGG
ACTATGCGGTCGACGGTGGAATGGTGAGCAAGGGCGAGGAGCTGTTCACCGGGGTGGTGCCCATCCTGGTCGAG
CTGGACGGCGACGTAAACGGCCACAAGTTCAGCGTGTCCGGCGAGGGCGAGGGCGATGCCACCTACGGCAAGCT
GACCCTGAAGCTGATCTGCACCACCGGCAAGCTGCCCGTGCCCTGGCCCACCCTCGTGACCACCCTGGGCTACGGC
CTGCAGTGCTTCGCCCGCTACCCCGACCACATGAAGCAGCACGACTTCTTCAAGTCCGCCATGCCCGAAGGCTACG
TCCAGGAGCGCACCATCTTCTTCAAGGACGACGGCAACTACAAGACCCGCGCCGAGGTGAAGTTCGAGGGCGAC
ACCCTGGTGAACCGCATCGAGCTGAAGGGCATCGACTTCAAGGAGGACGGCAACATCCTGGGGCACAAGCTGGA
GTACAACTACAACAGCCACAACGTCTATATCACCGCCGACAAGCAGAAGAACGGCATCAAGGCCAACTTCAAGAT
CCGCCACAACATCGAGGACGGCGGCGTGCAGCTCGCCGACCACTACCAGCAGAACACCCCCATCGGCGACGGCCC
CGTGCTGCTGCCCGACAACCACTACCTGAGCTACCAGTCCGCCCTGAGCAAAGACCCCAACGAGAAGCGCGATCA
CATGGTCCTGCTGGAGTTCGTGACCGCCGCCGGGATCACTCTCGGCATGGACGAGCTGTACAAGTAA

Protein sequence:

MRSG**HHHHHH**GMASMTGGQQMGRDLYDDDDKEPGRADTRIGVTIYKAAAMVSKGEELFTGVVPILVELDGDVNG
HKFSVSGEGEGDATYGKLTLKFICTTGKLPVPWPTLVTTLSWGVQCFARYPDHMKQHDFFKSAMPEGYVQERTIFFKD
DGNYKTRAEVKFEGDTLVNRIELKGIDFKEDGNILGHKLEYNYFSDNVYITADKQKNGIKANFKIRHNIEDGGVQLADHY
QQNTPIGDGPVLLPDNHYLSTQSKLSKDPNEKRDHMVLLEFVTAAGITLGMDELYGSDLVDNFMSVVRKAIEQDAKAA

PDVQLLMNDSQNDQSKQNDQIDVLLAKGVKALAINLVDPAAAGTVIEKARGQNVPVVFFNKEPSRKALDSYDKAYYV
GTDSKESGIIQGDLIAKHWAANQGWDLNKDGQIQFVLLKGEPGHPDAEARTTYVIKELNDKGIKTEQLQLDTAMWDT
AQAKDKMDAWLSGPNANKIEVVIANNDAMAMGAVEALKAHNKSSIPVFGVDALPEALALVKSGALAGTVLNDANN
QAKATFDLAKNLADGKGAADGTNWKIDNKVVRVPYVGVDKDNLAEFSKKEFKLYPYDVPDYAVDGGMVSKGEELFTG
VVPILVELDGDVNGHKFSVSGEGEGDATYGKLTLKLICTTGKLPVPWPTLVTTLGYGLQCFARYPDHMKQHDFFKSAM
PEGYVQERTIFFKDDGNYKTRAEVKFEGDTLVNRIELKGIDFKEDGNILGHKLEYNYNSHNVYITADKQKNGIKANFKIRH
NIEDGGVQLADHYQQNTPIGDGPVLLPDNHYLSYQSALSKDPNEKRDHMVLLEFVTAAGITLGMDELYK

h) Glucose sensor 8

DNA sequence:

ATGCGGGGTTCT**CATCATCATCATCATCAT**GGTATGGCTAGCATGACTGGTGGACAGCAAATGGGTCGGGATCTG
TACGACGATGACGATAAGGAGCCGGGCCGCGCTGATACTCGCATTGGTGTAACAATCTATAAGGCGGCCGCTATG
GTGAGCAAGGGCGAGGAGCTGTTCACCGGGGTGGTGCCCATCCTGGTCGAGCTGGACGGCGACGTAAACGGCCA
CAAGTTCAGCGTGTCCGGCGAGGGCGAGGGCGATGCCACCTACGGCAAGCTGACCCTGAAGTTCATCTGCACCAC
CGGCAAGCTGCCCGTGCCCTGGCCCACCCTCGTGACCACCCTGTCCTGGGGCGTGCAGTGCTTCGCCCGCTACCCC
GACCACATGAAGCAGCACGACTTCTTCAAGTCCGCCATGCCCGAAGGCTACGTCCAGGAGCGCACCATCTTCTTCA
AGGACGACGGCAACTACAAGACCCGCGCCGAGGTGAAGTTCGAGGGCGACACCCTGGTGAACCGCATCGAGCTG
AAGGGCATCGACTTCAAGGAGGACGGCAACATCCTGGGGCACAAGCTGGAGTACAACTACTTTAGCGACAACGT
CTATATCACCGCCGACAAGCAGAAGAACGGCATCAAGGCCAACTTCAAGATCCGCCACAACATCGAGGACGGCGG
CGTGCAGCTCGCCGACCACTACCAGCAGAACACCCCCATCGGCGACGGCCCCGTGCTGCTGCCCGACAACCACTA
CCTGAGCACCCAGTCCAAGCTGAGCAAAGACCCCAACGAGAAGCGCGATCACATGGTCCTGCTGGAGTTCGTGAC
CGCCGCCGGGATCACTCTCGGCATGGACGAGCTGTACGGATCCGGTGGTTCTGGCGGTTCAGGTGGCTCTGGTGG
GTCACCTGGTGATAACTTTATGTCTGTAGTGCGCAAGGCTATTGAGCAAGATGCGAAAGCCGCGCCAGATGTTCA
GCTGCTGATGAATGATTCTCAGAATGACCAGTCCAAGCAGAACGATCAGATCGACGTATTGCTGGCGAAAGGGGT
GAAGGCACTGGCAATCAACCTCGTTGACCCGGCAGCTGCGGGTACGGTGATTGAGAAAGCGCGTGGGCAAAACG
TGCCGGTGGTTTTCTTCAACAAAGAACCGTCTCGTAAGGCGCTGGATAGCTACGACAAAGCCTACTACGTTGGCAC
TGACTCCAAAGAGTCCGGCATTATTCAAGGCGATTTGATTGCTAAACACTGGGCGGCGAATCAGGGTTGGGATCT
GAACAAAGACGGTCAGATTCAGTTCGTACTGCTGAAAGGTGAACCGGGCCATCCGGATGCAGAAGCACGTACCA
CTTACGTGATTAAAGAATTGAACGATAAAGGCATCAAAACTGAACAGTTACAGTTAGATACCGCAATGTGGGACA
CCGCTCAGGCGAAAGATAAGATGGACGCCTGGCTGTCTGGCCCGAACGCCAACAAAATCGAAGTGGTTATCGCCA
ACAACGATGCGATGGCAATGGGCGCGGTTGAAGCGCTGAAAGCACACAACAAGTCCAGCATTCCGGTGTTTGGC
GTCGATGCGCTGCCAGAAGCGCTGGCGCTGGTGAAATCCGGTGCACTGGCGGGCACCGTACTGAACGATGCTAA
CAACCAGGCGAAAGCGACCTTTGATCTGGCGAAAAACCTGGCCGATGGTAAAGGTGCGGCTGATGGCACCAACT
GGAAAATCGACAACAAAGTGGTCCGCGTACCTTATGTTGGCGTAGATAAAGACAACCTGGCTGAGTTCAGCAAGA
AAGAATTCAAGTTGTACCCATATGACGTTCCGGACTATGCGGTCGACGGTGGAATGGTGAGCAAGGGCGAGGAG
CTGTTCACCGGGGTGGTGCCCATCCTGGTCGAGCTGGACGGCGACGTAAACGGCCACAAGTTCAGCGTGTCCGGC
GAGGGCGAGGGCGATGCCACCTACGGCAAGCTGACCCTGAAGCTGATCTGCACCACCGGCAAGCTGCCCGTGCC
CTGGCCCACCCTCGTGACCACCCTGGGCTACGGCCTGCAGTGCTTCGCCCGCTACCCCGACCACATGAAGCAGCAC
GACTTCTTCAAGTCCGCCATGCCCGAAGGCTACGTCCAGGAGCGCACCATCTTCTTCAAGGACGACGGCAACTACA
AGACCCGCGCCGAGGTGAAGTTCGAGGGCGACACCCTGGTGAACCGCATCGAGCTGAAGGGCATCGACTTCAAG
GAGGACGGCAACATCCTGGGGCACAAGCTGGAGTACAACTACAACAGCCACAACGTCTATATCACCGCCGACAAG
CAGAAGAACGGCATCAAGGCCAACTTCAAGATCCGCCACAACATCGAGGACGGCGGCGTGCAGCTCGCCGACCA
CTACCAGCAGAACACCCCCATCGGCGACGGCCCCGTGCTGCTGCCCGACAACCACTACCTGAGCTACCAGTCCGCC
CTGAGCAAAGACCCCAACGAGAAGCGCGATCACATGGTCCTGCTGGAGTTCGTGACCGCCGCCGGGATCACTCTC
GGCATGGACGAGCTGTACAAGTAA

Protein sequence:

MRSG**HHHHHH**GMASMTGGQQMGRDLYDDDDKEPGRADTRIGVTIYKAAAMVSKGEELFTGVVPILVELDGDVNG
HKFSVSGEGEGDATYGKLTLKFICTTGKLPVPWPTLVTTLSWGVQCFARYPDHMKQHDFFKSAMPEGYVQERTIFFKD
DGNYKTRAEVKFEGDTLVNRIELKGIDFKEDGNILGHKLEYNYFSDNVYITADKQKNGIKANFKIRHNIEDGGVQLADHY
QQNTPIGDGPVLLPDNHYLSTQSKLSKDPNEKRDHMVLLEFVTAAGITLGMDELYGSGGSGGSGGSGGSPGDNFMSV
VRKAIEQDAKAAPDVQLLMNDSQNDQSKQNDQIDVLLAKGVKALAINLVDPAAAGTVIEKARGQNVPVVFFNKEPSR
KALDSYDKAYYVGTDSKESGIIQGDLIAKHWAANQGWDLNKDGQIQFVLLKGEPGHPDAEARTTYVIKELNDKGIKTEQ
LQLDTAMWDTAQAKDKMDAWLSGPNANKIEVVIANNDAMAMGAVEALKAHNKSSIPVFGVDALPEALALVKSGAL
AGTVLNDANNQAKATFDLAKNLADGKGAADGTNWKIDNKVVRVPYVGVDKDNLAEFSKKEFKLYPYDVPDYAVDGG

MVSKGEELFTGVVPILVELDGDVNGHKFSVSGEGEGDATYGKLTLKLICTTGKLPVPWPTLVTTLGYGLQCFARYPDHM
KQHDFFKSAMPEGYVQERTIFFKDDGNYKTRAEVKFEGDTLVNRIELKGIDFKEDGNILGHKLEYNYNSHNVYITADKQK
NGIKANFKIRHNIEDGGVQLADHYQQNTPIGDGPVLLPDNHYLSYQSALSKDPNEKRDHMVLLEFVTAAGITLGMDEL
YK

i) Glucose sensor 9

DNA sequence:

ATGCGGGGTTCT**CATCATCATCATCATCAT**GGTATGGCTAGCATGACTGGTGGACAGCAAATGGGTCGGGATCTG
TACGACGATGACGATAAGGAGCCGGGCCGCGCTGATACTCGCATTGGTGTAACAATCTATAAGGCGGCCGCTATG
GTGAGCAAGGGCGAGGAGCTGTTCACCGGGGTGGTGCCCATCCTGGTCGAGCTGGACGGCGACGTAAACGGCCA
CAAGTTCAGCGTGTCCGGCGAGGGCGAGGGCGATGCCACCTACGGCAAGCTGACCCTGAAGTTCATCTGCACCAC
CGGCAAGCTGCCCGTGCCCTGGCCCACCCTCGTGACCACCCTGTCCTGGGGCGTGCAGTGCTTCGCCCGCTACCCC
GACCACATGAAGCAGCACGACTTCTTCAAGTCCGCCATGCCCGAAGGCTACGTCCAGGAGCGCACCATCTTCTTCA
AGGACGACGGCAACTACAAGACCCGCGCCGAGGTGAAGTTCGAGGGCGACACCCTGGTGAACCGCATCGAGCTG
AAGGGCATCGACTTCAAGGAGGACGGCAACATCCTGGGGCACAAGCTGGAGTACAACTACTTTAGCGACAACGT
CTATATCACCGCCGACAAGCAGAAGAACGGCATCAAGGCCAACTTCAAGATCCGCCACAACATCGAGGACGGCGG
CGTGCAGCTCGCCGACCACTACCAGCAGAACACCCCCATCGGCGACGGCCCCGTGCTGCTGCCCGACAACCACTA
CCTGAGCACCCAGTCCAAGCTGAGCAAAGACCCCAACGAGAAGCGCGATCACATGGTCCTGCTGGAGTTCGTGAC
CGCCGCCGGGATCACTCTCGGCATGGACGAGCTGTACGGATCCAAACTGTACCCGTACGATGTGCCAGATTACGC
ACCTGGTGATAACTTTATGTCTGTAGTGCGCAAGGCTATTGAGCAAGATGCGAAAGCCGCGCCAGATGTTCAGCT
GCTGATGAATGATTCTCAGAATGACCAGTCCAAGCAGAACGATCAGATCGACGTATTGCTGGCGAAAGGGGTGA
AGGCACTGGCAATCAACCTCGTTGACCCGGCAGCTGCGGGTACGGTGATTGAGAAAGCGCGTGGGCAAAACGTG
CCGGTGGTTTTCTTCAACAAAGAACCGTCTCGTAAGGCGCTGGATAGCTACGACAAAGCCTACTACGTTGGCACTG
ACTCCAAAGAGTCCGGCATTATTCAAGGCGATTTGATTGCTAAACACTGGGCGGCGAATCAGGGTTGGGATCTGA
ACAAAGACGGTCAGATTCAGTTCGTACTGCTGAAAGGTGAACCGGGCCATCCGGATGCAGAAGCACGTACCACTT
ACGTGATTAAAGAATTGAACGATAAAGGCATCAAAACTGAACAGTTACAGTTAGATACCGCAATGTGGGACACCG
CTCAGGCGAAAGATAAGATGGACGCCTGGCTGTCTGGCCCGAACGCCAACAAAATCGAAGTGGTTATCGCCAACA
ACGATGCGATGGCAATGGGCGCGGTTGAAGCGCTGAAAGCACACAACAAGTCCAGCATTCCGGTGTTTGGCGTC
GATGCGCTGCCAGAAGCGCTGGCGCTGGTGAAATCCGGTGCACTGGCGGGCACCGTACTGAACGATGCTAACAA
CCAGGCGAAAGCGACCTTTGATCTGGCGAAAAACCTGGCCGATGGTAAAGGTGCGGCTGATGGCACCAACTGGA
AAATCGACAACAAAGTGGTCCGCGTACCTTATGTTGGCGTAGATAAAGACAACCTGGCTGAGTTCAGCAAGAAAG
AATTCAAGTTGTACCCATATGACGTTCCGGACTATGCGGTCGACGGTGGAATGGTGAGCAAGGGCGAGGAGCTG
TTCACCGGGGTGGTGCCCATCCTGGTCGAGCTGGACGGCGACGTAAACGGCCACAAGTTCAGCGTGTCCGGCGA
GGGCGAGGGCGATGCCACCTACGGCAAGCTGACCCTGAAGCTGATCTGCACCACCGGCAAGCTGCCCGTGCCCTG
GCCCACCCTCGTGACCACCCTGGGCTACGGCCTGCAGTGCTTCGCCCGCTACCCCGACCACATGAAGCAGCACGAC
TTCTTCAAGTCCGCCATGCCCGAAGGCTACGTCCAGGAGCGCACCATCTTCTTCAAGGACGACGGCAACTACAAGA
CCCGCGCCGAGGTGAAGTTCGAGGGCGACACCCTGGTGAACCGCATCGAGCTGAAGGGCATCGACTTCAAGGAG
GACGGCAACATCCTGGGGCACAAGCTGGAGTACAACTACAACAGCCACAACGTCTATATCACCGCCGACAAGCAG
AAGAACGGCATCAAGGCCAACTTCAAGATCCGCCACAACATCGAGGACGGCGGCGTGCAGCTCGCCGACCACTAC
CAGCAGAACACCCCCATCGGCGACGGCCCCGTGCTGCTGCCCGACAACCACTACCTGAGCTACCAGTCCGCCCTGA
GCAAAGACCCCAACGAGAAGCGCGATCACATGGTCCTGCTGGAGTTCGTGACCGCCGCCGGGATCACTCTCGGCA
TGGACGAGCTGTACAAGTAA

Protein sequence:

MRSG**HHHHHH**GMASMTGGQQMGRDLYDDDDKEPGRADTRIGVTIYKAAAMVSKGEELFTGVVPILVELDGDVNG
HKFSVSGEGEGDATYGKLTLKFICTTGKLPVPWPTLVTTLSWGVQCFARYPDHMKQHDFFKSAMPEGYVQERTIFFKD
DGNYKTRAEVKFEGDTLVNRIELKGIDFKEDGNILGHKLEYNYFSDNVYITADKQKNGIKANFKIRHNIEDGGVQLADHY
QQNTPIGDGPVLLPDNHYLSTQSKLSKDPNEKRDHMVLLEFVTAAGITLGMDELYGSKLYPYDVPDYAPGDNFMSVVR
KAIEQDAKAAPDVQLLMNDSQNDQSKQNDQIDVLLAKGVKALAINLVDPAAAGTVIEKARGQNVPVVFFNKEPSRKA
LDSYDKAYYVGTDSKESGIIQGDLIAKHWAANQGWDLNKDGQIQFVLLKGEPGHPDAEARTTYVIKELNDKGIKTEQLQ
LDTAMWDTAQAKDKMDAWLSGPNANKIEVVIANNDAMAMGAVEALKAHNKSSIPVFGVDALPEALALVKSGALAG
TVLNDANNQAKATFDLAKNLADGKGAADGTNWKIDNKVVRVPYVGVDKDNLAEFSKKEFKLYPYDVPDYAVDGGM
VSKGEELFTGVVPILVELDGDVNGHKFSVSGEGEGDATYGKLTLKLICTTGKLPVPWPTLVTTLGYGLQCFARYPDHMK
QHDFFKSAMPEGYVQERTIFFKDDGNYKTRAEVKFEGDTLVNRIELKGIDFKEDGNILGHKLEYNYNSHNVYITADKQK

NGIKANFKIRHNIEDGGVQLADHYQQNTPIGDGPVLLPDNHYLSYQSALSKDPNEKRDHMVLLEFVTAAGITLGMDEL
YK

j) DNA- and protein-sequences of the crowding sensor constructs:

The studied crowding sensors consist of either an unstructured linker peptide with a length of 54 amino acid residues (G18) or a □-helical peptide linker with a total length of 118 residues (GE), the latter shown in Fig. 1b. In both cases these linker elements were sandwiched between a mCerulean3 donor and an mCitrine acceptor. The sequences of the crowding sensor constructs G18 and GE can be found in a previous publication[1].

k) Production of the glucose sensors:

The production and purification of the employed sensor constructs was performed as previously described by Steffen *et al.*[2] For purification 2 g of wet cells were suspended in 18 mL 3-(N-morpholino)-propanesulfonic acid (MOPS) buffer (20 mM, containing 20 mM imidazol and 300 mM NaCl, pH 7.3, supplemented with 10% (v/v) of a protease inhibitor solution) and disrupted by sonication using an UP200s (S14D sonotrode, Hielscher, Teltow, Gemany). Protease inhibitor solution was prepared by dissolving one cOmplete EDTA-free tablet (Roche, Germany) in 10 ml equilibration buffer (20 mM MOPS buffer, 20 mM imidazol, 300 mM NaCl, pH 7.3).

The sensor proteins carrying an N-terminal hexahistidine tag were purified via immobilized metal chelate affinity chromatography on Ni-NTA agarose (column volume 5 mL, Qiagen, Hilden, Germany equipped with a multi-wavelength UV-VIS monitor "Monitor UV-900") by fast protein liquid chromatography (Äkta Purifier, GE Healthcare Life Sciences, Freiburg, Germany). All purification steps were performed at room temperature with a flow rate of 1.5 mL/min. After washing the column with 10 column volumes equilibration buffer, elution was performed with elution buffer (20 mM MOPS buffer, 300 mM imidazol, 300 mM NaCl, pH 7.3) in 2 column volumes. Subsequently, desalting was performed using size exclusion chromatography (Sephadex G25 material; MOPS buffer, 20 mM, pH 7.3).

The sensor concentration was adjusted to $OD_{515\,nm}$ = 0.2 using quartz cuvettes with a 1 cm light path. Based on the molar absorption coefficient of Venus (ε = 92,200 L mol^{-1} cm^{-1}), this absorption equals a protein concentration of 0.18 mg mL^{-1}. Subsequently, the sensor solution was stored in buffer in aliquots of 1 mL and 10 mL at -20 °C.

l) Production of the crowding sensors:

The production and purification of the crowding sensors is analogue to ref.1. *E. coli* BL21, containing the pRSET A plasmid with the gene encoding for either the GE or G18 sensor, was grown to OD_{600} 0.6 in LB medium (10 g/L tryptone, 5 g/L yeast extract, 10 g/L NaCl), and induced with 0.1 mM isopropyl *β*-D-1-thiogalactopyranoside (IPTG). After incubation at 25°C overnight, the cells were spun down at 3000 × *g* for 30 min, resuspended in buffer A (10 mM sodium phosphate (NaP_i), 100 mM NaCl, 0.1 mM phenylmethylsulfonyl fluoride (PMSF), pH 7.4) and lysed in a tissue lyser. The lysate was cleared by centrifugation, supplemented with 10 mM imidazole, and the proteins were purified by nickel-nitrilotriacetic acid Sepharose chromatography (wash/elution buffer: 20/250 mM imidazole, 50 mM NaPi, 300 mM NaCl, pH 7.4). The constructs were further purified by Superdex 200 10/300 GL size-exclusion chromatography (Amersham Biosciences, Little Chalfont, UK) in 10 mM NaP_i, pH 7.4. The expression and purification were analyzed by 12% sodium dodecyl sulfate-polyacrylamide gel electrophoresis, and the bands were visualized by in-gel fluorescence and subsequent Coomassie staining. Fractions containing pure protein were aliquoted and stored at −80°C.

Fluorescence measurements: The functionality of the sensors was also checked before each single-molecule measurement in the same conditions on a spectrofluorometer (Quanta Master 40, Photon Technology International, Birmingham, USA). For this purpose the sensor solutions (sensor concentration ~ 100 nM) were excited at 420 nm, the corresponding emission spectra were recorded, and the intensity ratio R of the acceptor (524 nm) and the donor (472 nm) emission was calculated (see Fig. S1a).

m) Production of sensor ensembles with different donor-only fractions:

In order to measure the effect of varying donor-only fractions in ensemble studies we made us of an experimental acceptor photo-bleaching procedure. A disposable glass micro pipette (Brand, Wertheim, Germany) was filled with 20 µl of sensor stock solution. The pipette (inner diameter ~ 0.6 mm) was aligned along a 532 nm laser (Monopower-532-100-SM, Alphalas, Göttingen, Germany) beam (diameter ~ 0.7 mm) axis and irradiated for 1 or 5 minutes (Fig. S2a). This treatment photo-bleaches the acceptor and therefore increases the donor-only fraction to 60% and 89%, respectively. Donor-only fractions were determined with two-color coincidence detection. The influence of donor-only sensor molecules on isothermal binding curves is shown in Figure S1d for glucose sensor no. 4 (Fig. 1d). In Figure S1d the black data points depict the unbleached sensor (38% donor-only), red and blue data points belong to bleached sensors (60%, 89% donor- only, respectively), and a theoretical extrapolation for no donor-only (0%) is drawn in orange. For each donor-only fraction only R_{apo} and R_{max} are shown and a sigmoidal curve is plotted to guide the eye.

n) Donor-only implications for ensemble data:

The influence of donor-only sensor molecules on the outcome of an ensemble measurement, for example when recording the emission intensities of the involved FPs, can be quantified by deriving an expression for the intensity ratio R as a function of mean FRET efficiency E and donor-only fraction x_{D0}:

$$R(E, x_{D0}) = \frac{I_A(E, x_{D0})}{I_D(E, x_{D0})} = \frac{(1-x_{D0})[c_A^A E + c_D^A(1-E)] + x_{D0} c_D^A}{(1-x_{D0}) c_D^D (1-E) + x_{D0} c_D^D} \quad \text{(S1)}$$

Here, $c_i^j = \phi_i a_i^j$ accounts for the quantum yield ϕ_i of fluorophore i and the fraction of the emission spectrum a_i^j of fluorophore i emitted at the wavelength that is used for the signal readout of fluorophore j (see Fig. S3). We determined quantum yields of $\phi_{mTurqouise2} = 0.90$ and $\phi_{mVenus} = 0.59$ by liFCS[2] (data not shown) which results in $c_D^D = 0.0139$, $c_D^A = 0.00546$, and $c_A^A = 0.0144$ for the glucose sensor.

It has to be pointed out that E in equation (S1) is the unbiased transfer efficiency of the molecules that have both a fluorescent donor and acceptor and is accessible in a single-molecule experiment. Briefly, the expressions in equation S1 are based on the following considerations. (i) The intensity at the acceptor readout wavelength is the sum of sensitized acceptor emission, donor leakage of FRET-capable molecules and leakage of donor-only molecules. (ii) Correspondingly the donor intensity is originating from FRET-capable donors and donor-only molecules. Rearranging equation S1 yields:

$$R(E, x_{D0}) = \frac{c_A^A}{c_D^D} \frac{1}{1-E(1-x_{D0})} + \frac{c_D^A - c_A^A}{c_D^D} \quad \text{(S2)}$$

In Figure S2b the R(E)-dependency is plotted for various donor-only fractions. For small E there is a linear but rather small increase in R with increasing E. For further increasing E, the increase of R is strongly nonlinear. For $x_{D0} = 0$ it is even diverging as E is approaching 1. The following

conclusion can be made: (i) the sensor generally loses sensitivity for increasing x_{D0} (R(E) curves become flatter), (ii) for a sensor that changes between a fixed E_{apo} and E_{max} the sensitivity $\Delta R = R_{max} - R_{apo}$ reduces with increasing x_{D0} (see Fig. S1d), and (iii) R becomes more sensitive to E for large E. The last point might implicate that a well-designed sensor should already work in its apo-state at a high E. However, such a choice has to be made carefully, since these sensors will then be rather prone to small perturbations as they might cause large changes of R.

o) Confocal microscopy:

Time-resolved measurements were performed on a confocal microscope MicroTime 200 (PicoQuant, Berlin, Germany). Briefly, two pulsed diode lasers with emitting wavelengths of 437 nm (LDH-D-C-440, PicoQuant) and 509 nm (LDH-D-C-510, PicoQuant) were operated at a frequency of 20 MHz with an average emission power of 17 µW and 5 µW, respectively. The excitation beam is focused into the sample solution by a water immersion objective (UplanSApo, 60×, NA 1.2, Olympus Deutschland, Hamburg, Germany). The distance between the coverslip surface and the focal point was 10 µm which minimizes distortions of the confocal volume in additive-enriched solutions[3]. The fluorescence light was collected by the same objective, passed through a dual-band dichroic mirror (Di01-R442/514/561, Semrock, Rochester, USA) and was focused on a 75 µm pinhole. Finally, the light was either splitted by a 50/50 beam splitter (Olympus Deutschland, Hamburg, Germany) for fluorescence correlation spectroscopy (FCS) analysis or by a dichroic mirror (T505lpxr, Chroma Technology, Vermont, USA) for FRET measurements. Since fluorescent proteins are typically less photo-stable (and therefore in practice less bright) than organic fluorescent dyes, the amount of scattered light that reaches the detectors must be reduced as much as possible. We accomplished that by choosing a donor excitation wavelength of 437 nm which exhibits a Raman scattering peak in water around 515 nm that is sufficiently blocked by the optical emission filters. Furthermore, rather low excitation intensities avoided increased photo bleaching. After passing the bandpass filters for donor emission (ET480/40m, Chroma) and acceptor emission (ET560/80m, Chroma) the photons were detected by two single-photon avalanche diodes (τ-SPAD, PicoQuant). Photon arrival times were processed by a time-correlated single-photon counting module (PicoHarp300, PicoQuant).

p) smFRET measurements:

For samples to be measured on the confocal microscope 50 µl droplets of sample solution were deposited on coverslips (No. 1.5H, Marienfeld, Lauda Königshofen, Germany) that have been plasma-cleaned (PDC-32G, Harrick Plasma, Ithaca, USA) and subsequently treated with 60 µl of SigmaCote® (Sigma-Aldrich, St. Louis, USA), air dried, rinsed with acetone and dried with nitrogen. First, diffusion properties of the sensor molecules were determined by FCS (with sensor concentrations in the nM concentration regime) after direct acceptor excitation. For single-molecule FRET measurements, sensor solutions were diluted to an average number of 0.03 acceptor molecules present in the confocal volume at the same time. Here a volume of 500 µl sample solution was put on a coated coverslip and sealed with Parafilm® to prevent evaporation. A sequence of multiple 20 min. measurements, usually overnight, was carried out. Importantly, FRET measurements were performed out using pulsed interleaved excitation (PIE)[4].

q) smFRET data analysis:

Potential single-molecule FRET events were selected by the inter-photon lag (IPL) of acceptor photons after direct acceptor excitation to ensure acceptor presence. For this purpose the obtained IPL time trace was smoothed over 3-9 photons with a moving average filter. Photon bursts originated from single molecules appeared as dips in the IPL time trace and could be selected by an IPL threshold value[5]. The combination of the smoothing value and the IPL

threshold was chosen to (i) keep the error probability of false burst identification below 0.1 % and (ii) to reproduce the dwell time and molecular brightness obtained in ensemble by FCS. For each such selected burst, donor (D) and acceptor (A) photons after direct donor excitation were accumulated and corrected:

$$F_D = I_D - BG_D \tag{S3a}$$

$$F_A = I_A - BG_A - Lk - Dir \tag{S3b}$$

Here, F_D and F_A are the corrected intensities of donor and acceptor, I_D and I_A are the raw data of donor and acceptor counts, and BG_D and BG_A are the background counts of donor and acceptor obtained as the product of dwell time and average background count rate, respectively. Background count rates were determined for each measurement individually by generating a histogram of the IPL in the respective channel, and taking the inverse IPL of the histogram maximum position. Lk represents the leakage of donor photons into the acceptor channel and Dir gives the acceptor photons originating from direct excitation. For all bursts that fulfilled a threshold of $F_D+F_A > 20$, the energy transfer efficiency

$$E = \frac{F_A}{F_D+\gamma F_A} \tag{S4}$$

was calculated, where γ is a correction factor.

The correction factors Lk, Dir, and γ were determined by plotting the stoichiometry S versus E for all photon bursts, i.e. photons in both detection channels and both excitation windows. These bursts are detected by merging all photons, calculating the IPL time trace, smoothing it, and applying an IPL threshold. All bursts that exceeded 40 photons were used for the analysis. 2D-plots of S versus E were originally presented for alternating laser excitation (ALEX)[6] but are also applicable to PIE data[7]. The stoichiometry is calculated burst-wise by

$$S = \frac{F_D+F_A}{F_D+F_A+F_A^{Aex}} \tag{S5}$$

where $F_A^{Aex} = I_A^{Aex} - BG_A^{Aex}$ is the background-corrected acceptor signal after direct acceptor excitation. In a first step, the detected photon counts are just corrected for background, resulting in S^{raw} and E^{raw}. An example of a S^{raw} versus E^{raw} 2D-plot is shown in Fig. S4. Donor-only and acceptor-only molecules are identified by high and low stoichiometry values ($S^{raw} > 0.95$ and $S^{raw} < 0.15$), respectively. Donor-only molecules are used to determine the leakage coefficient l = 0.64 ± 0.01. The leakage was additionally confirmed by an ensemble measurement of a donor-only crowding sensor that was produced by sensor cleavage (see ref.1 for details). The S^{raw} peaks are rather broad and in most cases the acceptor-only and donor-acceptor distributions overlap. In addition, the acceptor-only peak is low in intensity which made it difficult to precisely determine its peak position. Instead, we looked at the acceptor photon counts after donor excitation. For acceptor-only molecules there should be no acceptor photons after donor excitation because no donor is present. Thus, we varied the coefficient for direct acceptor excitation d until the distribution of $F_A^{cor} = F_A - dF_A^{Aex}$ peaked around zero. The resulting value was d = 0.078. We also confirmed that value from ensemble measurements by recording the absorption spectrum of an acceptor-only glucose sensor.

The correction factor γ for the glucose sensors is determined by applying all corrections in eq. S3b and plotting the corrected stoichiometry S^{cor} versus the proximity ratio E^{pr} which is E for γ = 1. In the resulting 2D-plots the position of the donor-acceptor population was identified by eye (see Fig. S5a). The procedure was repeated for the various sensor constructs in different glucose concentrations. Finally, a linear fit of $1/S^{cor}$ versus E^{pr} yields

$$\gamma_{gluc} = \frac{\Omega-1}{\Omega-1+\Sigma} = 1.42 \pm 0.11 \tag{S6}$$

where Ω is the y-intercept and Σ is the slope (see Fig. S5b). The error is calculated by error propagation of the errors on Ω and Σ. In case of the crowding sensor there were too few measurements to make a reliable $1/S^{cor}$ versus E^{pr} fit. Thus, we wrote γ in terms of detection efficiencies and quantum yields and assumed similar detection efficiency for mTurquoise2 and mCerulean3 as well as for mVenus and mCitrine because both variants have similar emission spectra:

$$\gamma_{crowd} = \frac{\phi_{mCit}}{\phi_{mCer3}} \frac{g_{mCit}}{g_{mCer3}} \cong \frac{\phi_{mCit}}{\phi_{mCer3}} \frac{g_{mVen}}{g_{mTurq2}} = \frac{\phi_{mCit}}{\phi_{mCer3}} \frac{\phi_{mTurq2}}{\phi_{mVen}} \gamma_{gluc} = 1.89 \pm 0.15 \qquad \text{(S7)}$$

Here ϕ is the quantum yield and g is the detection efficiency of the respective fluorescent protein.

PEG 6,000 solutions showed a small number of background bursts above concentrations of 10% (w/w) which were subtracted as follows. A background measurement of several hours was performed for each PEG 6,000 concentration under identical conditions as the smFRET measurements itself. Subsequently, the background data was analysed with the same parameters as used for the respective sensor. Finally, a background FRET histogram was generated, rescaled to the measurement time of the sensor, and finally subtracted from the sensor FRET histogram.

All data analysis was performed with self-written MATLAB® (R2015b, 64-bit) scripts or using OriginPro (9.0.0G, 64bit). Compared to counting statistics we achieve in conventional smFRET studies with organic fluorescent dyes, we obtained here a number of useful burst which is about tenfold lower. However, by employing state-of-the-art data acquisition and analysis we obtained meaningful FRET efficiency histograms, even in the presence of high concentrations of macromolecular crowding agents.

r) smFRET histogram analysis:

FRET histograms of glucose sensors in different glucose concentrations were fitted globally with two Gaussian distributions. Therefore, a global mean position and the width of each Gaussian were used for all glucose concentrations, while the statistical weight of the population of each Gaussian was a free parameter for each glucose concentration (either 2 or 3 concentrations were measured for each sensor construct). In the global fit the unweighted sum of the χ^2 of the individual FRET histograms is minimized. In case of the crowded glucose sensor, a global fitting with fixed parameters of the Gaussians was not applicable to obtain a reasonable fit of the data (see Fig. S11). Instead, each FRET histogram was fitted individually. The FRET histograms of the crowding sensors in different crowders were also fitted individually. Here, one Gaussian was sufficient to describe the data. The shot-noise limited width of each population (see Figure S1c) was calculated by[8]

$$\sigma_{sn} = \sqrt{\frac{E(1-E)}{N+1}} \qquad \text{(S8)}$$

where E is the mean of the Gaussian and N is the average number of photons per burst. All fits were performed with the Fminuit package for MATLAB.

s) Two colour coincidence detection:

Single-molecule detection in combination with dual colour excitation allowed us to determine the absence of a fluorescent acceptor for sensor molecules that carry only a fluorescent donor. Two-colour coincidence detection (TCCD) was developed by Klenerman and co-workers[9] and looks for coincidence of bursts that occurred after excitation with different colours. We made

use of an improved version of TCCD that minimizes false non-coincident bursts and quantified the donor-only fractions of the sensors (see Figure S9). The use of different acceptor excitation intensities exhibited unchanged donor-only fractions, indicating that the TCCD measurement itself is not biasing the obtained donor-only fraction values. A full description of our improved TCCD will be published elsewhere.

t) Comparison of single molecule versus ensemble data:

In order to relate the single-molecule measurements performed on the confocal microscope to the ensemble characterization by the fluorescence spectrometer we calculated R-values (intensity ratios) for the data obtained with the confocal microscope. Since we determined the ratio of integrated detection efficiencies of the individual donor and acceptor emission spectra for the confocal microscope, we cannot calculate R-values that include donor leakage (cf. "smFRET data analysis" in SI). Accordingly, we used the corrected donor and acceptor intensities F_D and F_A (cf. Eq. S3a, S3b), respectively, to calculate the intensity ratio

$$R_{con} = (1 - x_{D0}) \frac{g_D}{g_A} \frac{a_A^A}{a_D^D} \frac{F_A}{F_D} \tag{S9}$$

where x_{D0} is the donor-only fraction (cf. Fig S9), $g_D/g_A = \gamma^{-1}\,\Phi_A/\Phi_D$ is the detection efficiency ratio of donor and acceptor, and a_A^A and a_D^D are the peak-to-area ratios of donor and acceptor (cf. Fig S3), respectively. The R-values obtained on the spectrometer are also corrected for crosstalk to make them comparable to the single molecule data by

$$R_{spec} = \frac{I_A - (a_D^A/a_D^D) I_D}{I_D} = R - \frac{a_D^A}{a_D^D} \tag{S10}$$

where a_D^A and a_D^D is the normalized emission intensity of the donor at acceptor and donor peak wavelength, respectively. The corresponding results are presented in Figure S8.

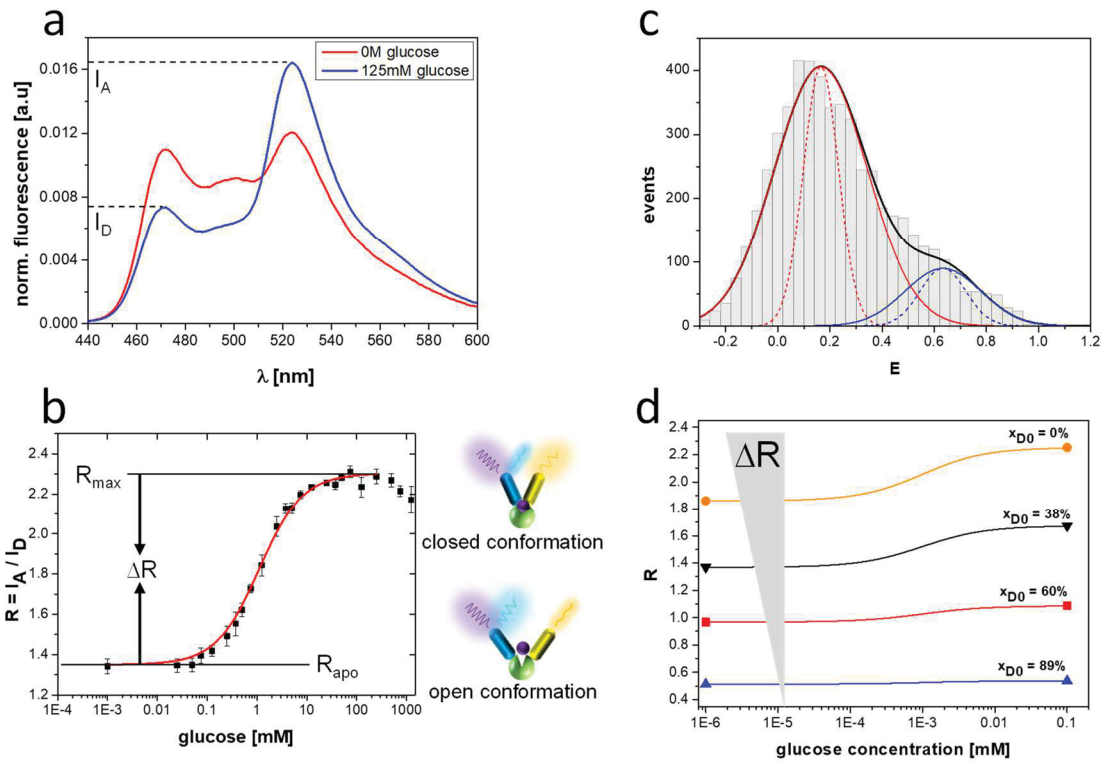

Figure S 1.1-1: Exemplary comparison of ensemble vs. single-molecule detection of a FRET-based glucose sensor. (a) Fluorescence emission spectra of a glucose sensor measured in absence and in presence of glucose (125 mM) show emission peaks of donor (I_D) and of acceptor (I_A).(b) Open and closed conformations of the sensor are shown exemplarily (right panel). The change in peak intensity ratio (R) upon glucose titration is fitted by a corresponding binding isotherm (red curve). (c) smFRET histogram exemplarily shown for a glucose sensor. A typical feature of these sensor histograms showing two populations is a rather broad distribution well beyond the shot noise limit (dotted lines), for details see SI Experimental Section. (d) With increasing donor-only fractions (X_{D0}) the apparent ΔR values decreased systematically. For the sake of clarity here only R_{apo} and R_{max} values were taken from experimental data and the corresponding isotherm was approximated with a fixed K_D-value (0.6 mM).

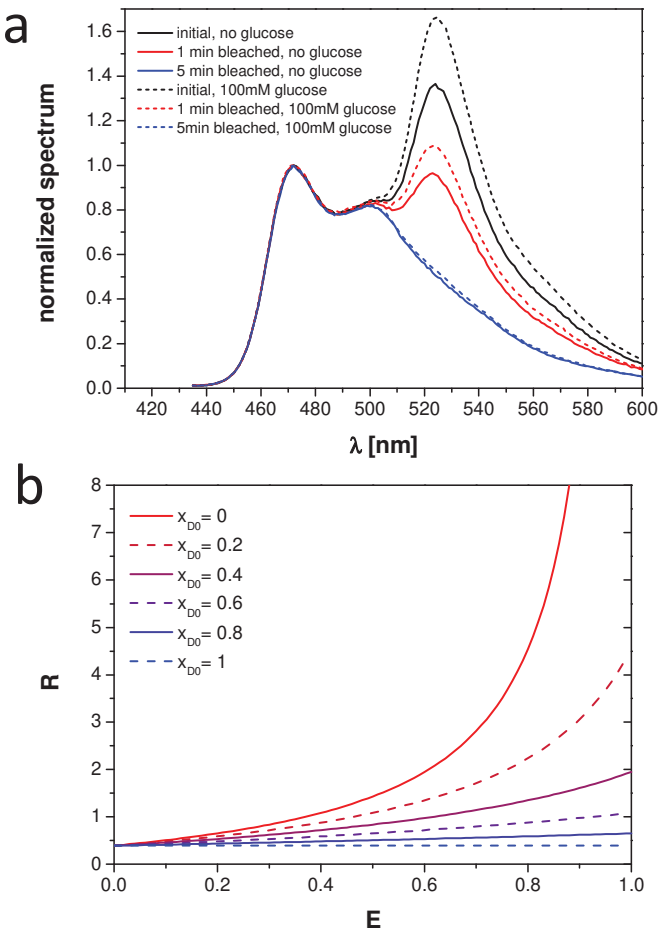

Figure S 1.1-2: Effect of different donor-only contributions emulated by photo-bleaching series. (a)
Ensemble fluorescence spectra of a glucose sensor after different durations of acceptor bleaching (i.e. long bleaching durations result in large donor-only fractions, see SI Experimental Section) for the non-liganded state (solid lines) and for the liganded state (dotted lines). Differences between corresponding solid and dotted lines represent the expected ΔR-value which is large for unbleached samples and almost zero for fully bleached samples. (b) As given in the SI Experimental Section (equation S2) the R-values were plotted as a function of mean transfer efficiency E for different donor-only fractions (X_{D0}). Due to the non-linearity of this relation, identical ΔE-values yield larger ΔR-values with increasing absolute E values.

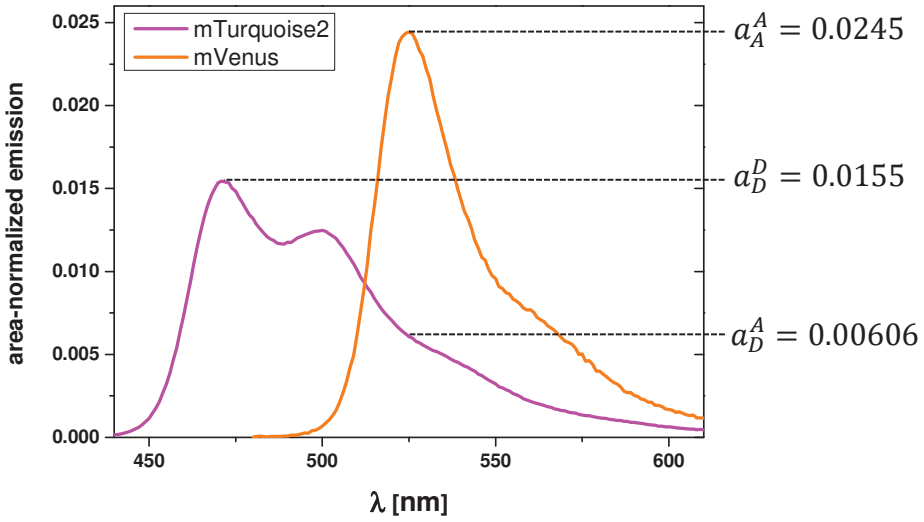

Figure S 1.1-3: Illustration of spectral overlap between donor and acceptor emission. The fraction of the emission spectrum emitted at the respective donor (magenta) and acceptor (orange) maximum is used to calculate the R to E conversion (see SI Experimental Section).

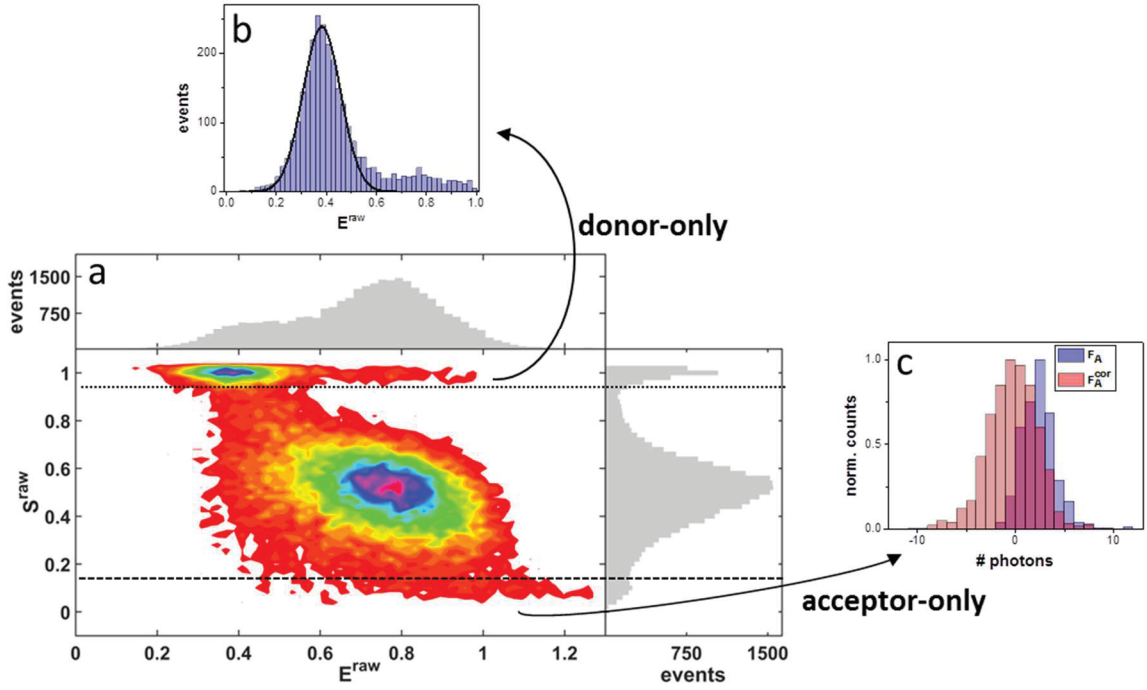

Figure S 1.1-4: Determination of donor leakage and direct acceptor excitation.
(a) Contour plot of S^{raw} versus E^{raw}. Data shown for glucose sensor no. 2 in 125mM glucose. Donor-only and acceptor-only molecules are identified by $S^{raw} > 0.95$ (dotted line) and $S^{raw} < 0.15$ (dashed line), respectively. (b) E^{raw} histogram for solely donor-only molecules. The peak is fitted to a Gaussian distribution with mean E_{D0}. Leakage coefficient $l = E_{D0} / (1-E_{D0})$ characterizes spectral crosstalk of donor emission into the acceptor emission channel. (c) Histogram of acceptor photon counts after direct donor excitation for acceptor-only molecules (blue bars). Direct acceptor excitation coefficient d is determined by varying its value until the

corrected photon counts of the acceptor after donor excitation $F_A^{cor} = F_A - dF_A^{Aex}$ peak at zero (red bars). See SI Experimental Section for details.

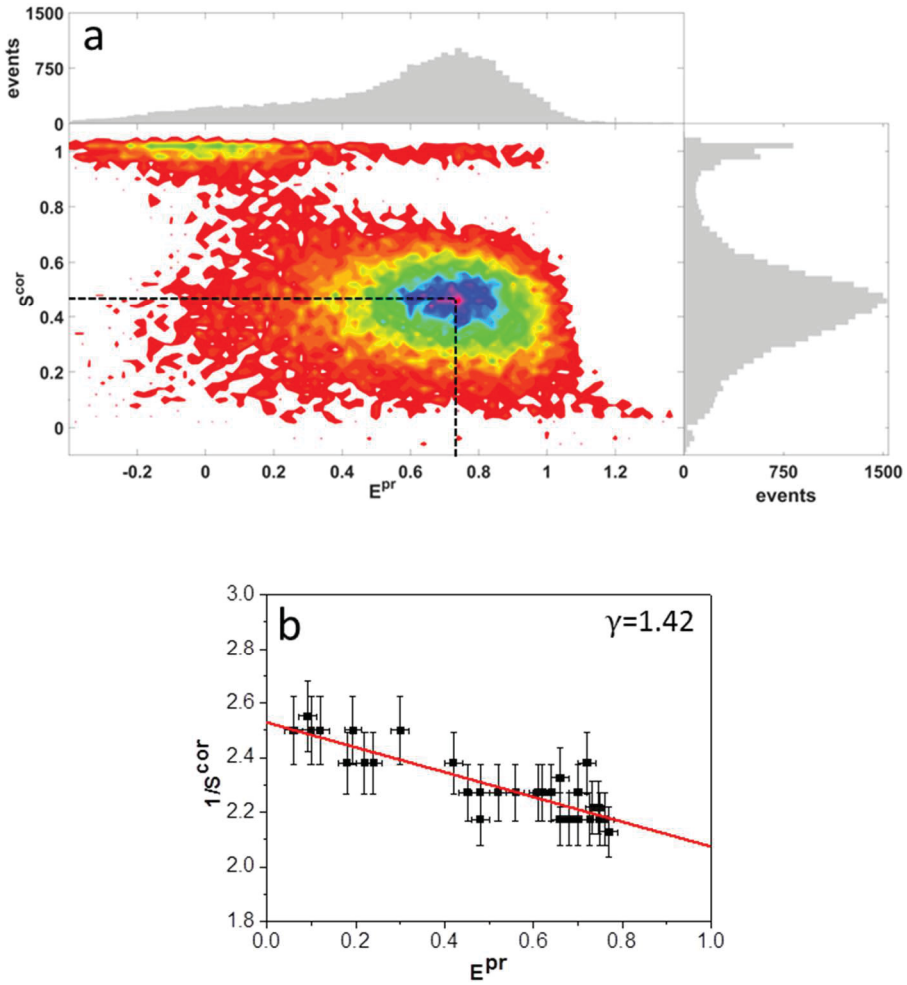

Figure S 1.1-5: Determination of correction factor γ. (a) Contour plot of S^{cor} versus E^{pr}. Data are shown for glucose sensor no. 2 in 125 mM glucose. The centre of donor-acceptor population is indicated by dashed lines. (b) Center positions of S^{cor} and E^{pr} are determined for multiple glucose sensor constructs in various glucose concentrations and $1/S^{cor}$ is plotted as a function of E^{pr} (black squares). Errors originate from the accuracy of reading the center position. The parameters of a linear fit (red line) are used to calculate γ. See SI Experimental Section for details.

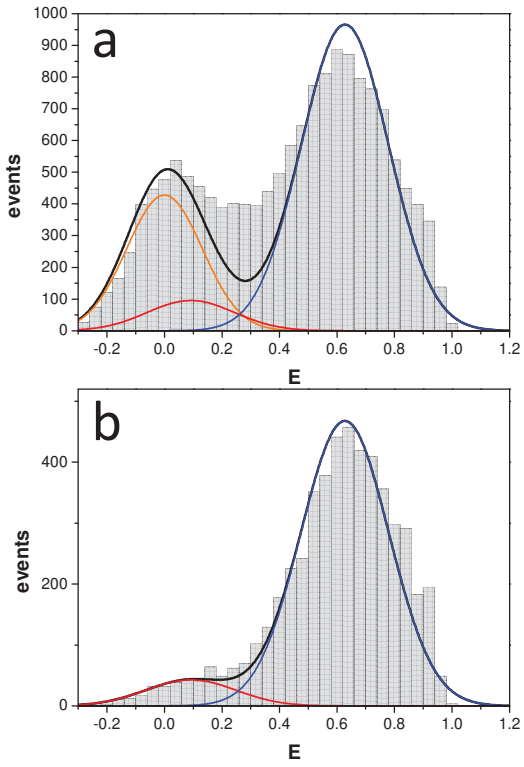

Figure S 1.1-6: Impact of donor-only contribution to FRET histograms.
(a) smFRET histogram for glucose sensor no. 2 is shown as an example (at 125 mM glucose) including the donor-only bursts contribution (represented by the orange Gaussian). (b) The same data is shown after elimination of donor-only bursts by employing PIE (see SI Experimental Section).

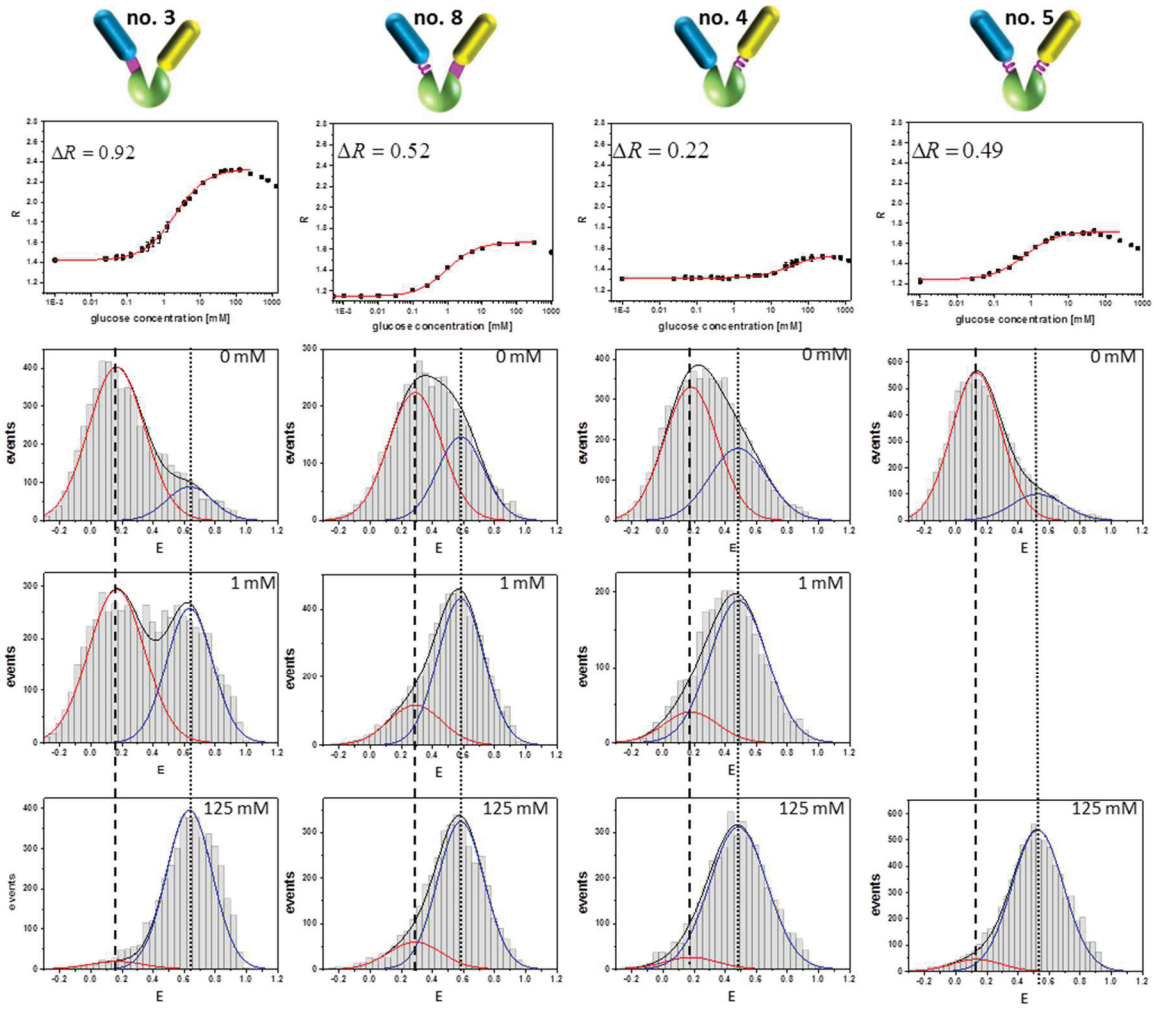

Figure S 1.1-7: Ensemble and smFRET data for glucose sensor construct no. 3, no. 4, no. 5, no. 8.
See figure legend of Fig. 2 in the main text for details.

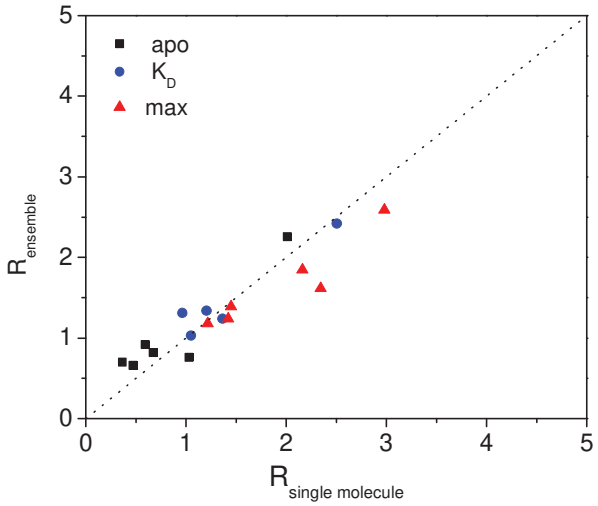

Figure S 1.1-8: A comparison between ensemble data and single molecule data is shown in terms of R-values. For all six sensor constructs measured on single molecule level we included R-values obtained under three different conditions; absence of glucose (apo), glucose

concentration approx. at the K_D, and at saturated glucose concentration (max). Details on the calculation of the corresponding R-values are given in SI Experimental Section.

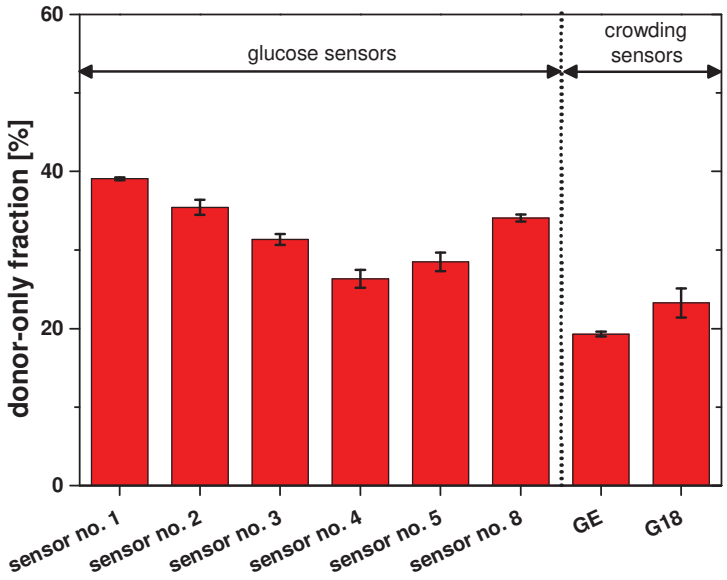

Figure S 1.1-9: Donor-only fraction of all investigated sensor constructs.
The given values were determined with two colour coincidence detection (see SI Experimental Section) from three to five independent repeat measurements.

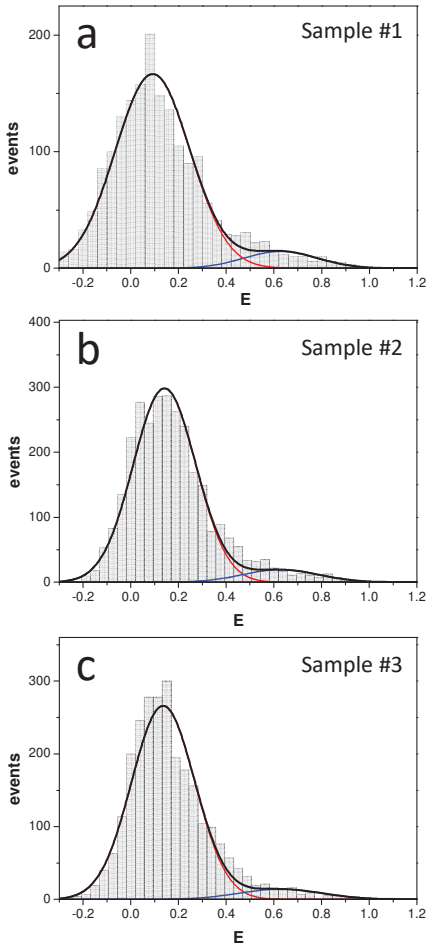

Figure S 1.1-10: The reproducibility of our smFRET measurements is demonstrated by a comparison of three histograms as measured with three independent replicates (sample #1-3 of sensor type no. 2 without glucose) and three independent fits for each of the respective histograms. In these fits we fixed only the centre position E_2 = 0.628 of the small population (according to our applications discussed as in Fig. 2). The obtained fitting parameter show only a rather small variation between the three samples: E_1: 0.092 / 0.141 / 0.135; p_1: 0.92 / 0.93 / 0.94; p_2: 0.08 / 0.07 /0.06 (always listed in the order sample #1 to 3).

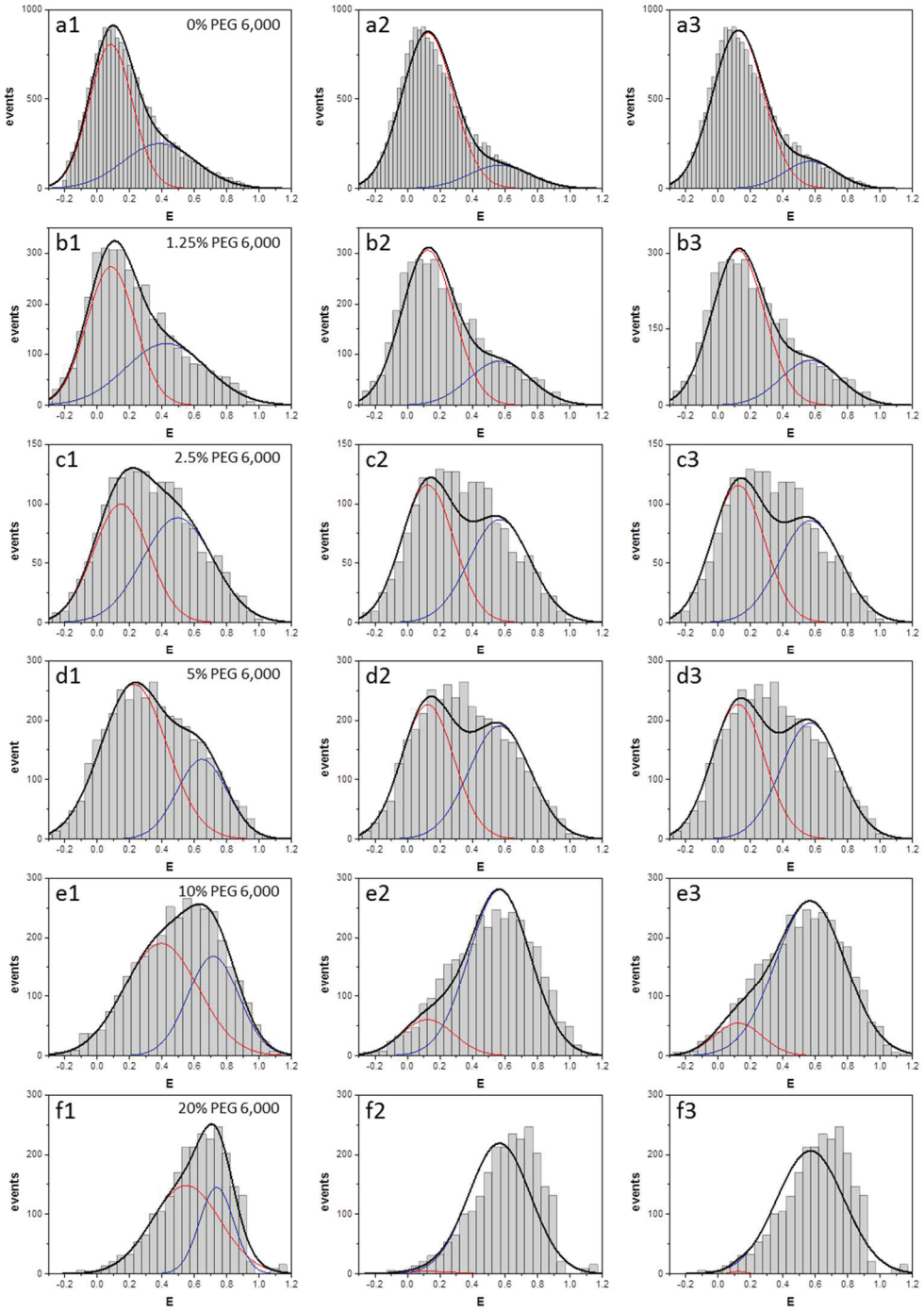

Figure S 1.1-11: Individual versus global FRET histogram fitting of crowded glucose sensor. We show three columns with identical experimental FRET histograms of glucose sensor no. 2 in 0 w/w%, 1.25 w/w%, 2.5 w/w%, 5 w/w%, 10 w/w% and 20 w/w% PEG 6,000 (a to f), but with 3 different Gaussian fitting approaches: individual fit (left column), global fit (middle column) and global fit with free width of Gaussians (right column). For high PEG concentration both global fit variants show bad fit quality (see SI Experimental Section for fitting details).

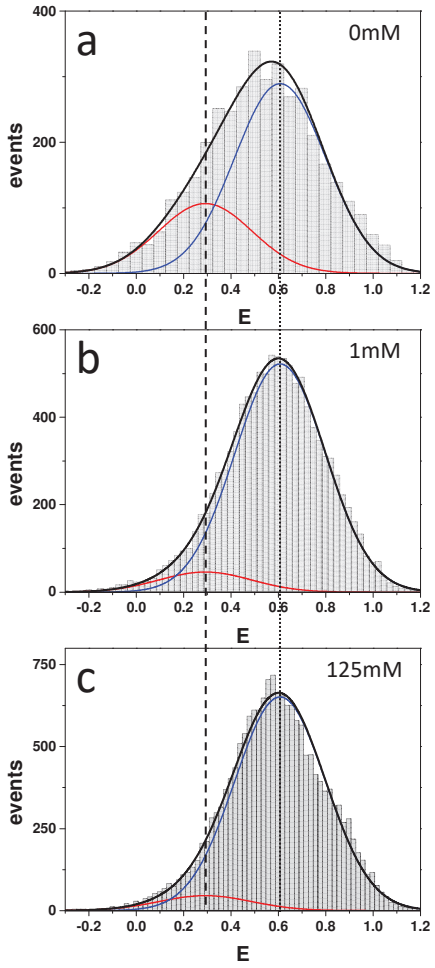

Figure S 1.1-12: Impact of crowding on glucose sensing.
smFRET histograms of glucose sensor no.2 in crowding conditions (10%(w/w) PEG 6,000) in absence of glucose (a), in 1 mM glucose (b) and 125 mM glucose (c). Histograms are fitted globally with 2 populations (see SI Experimental Section for fitting details).

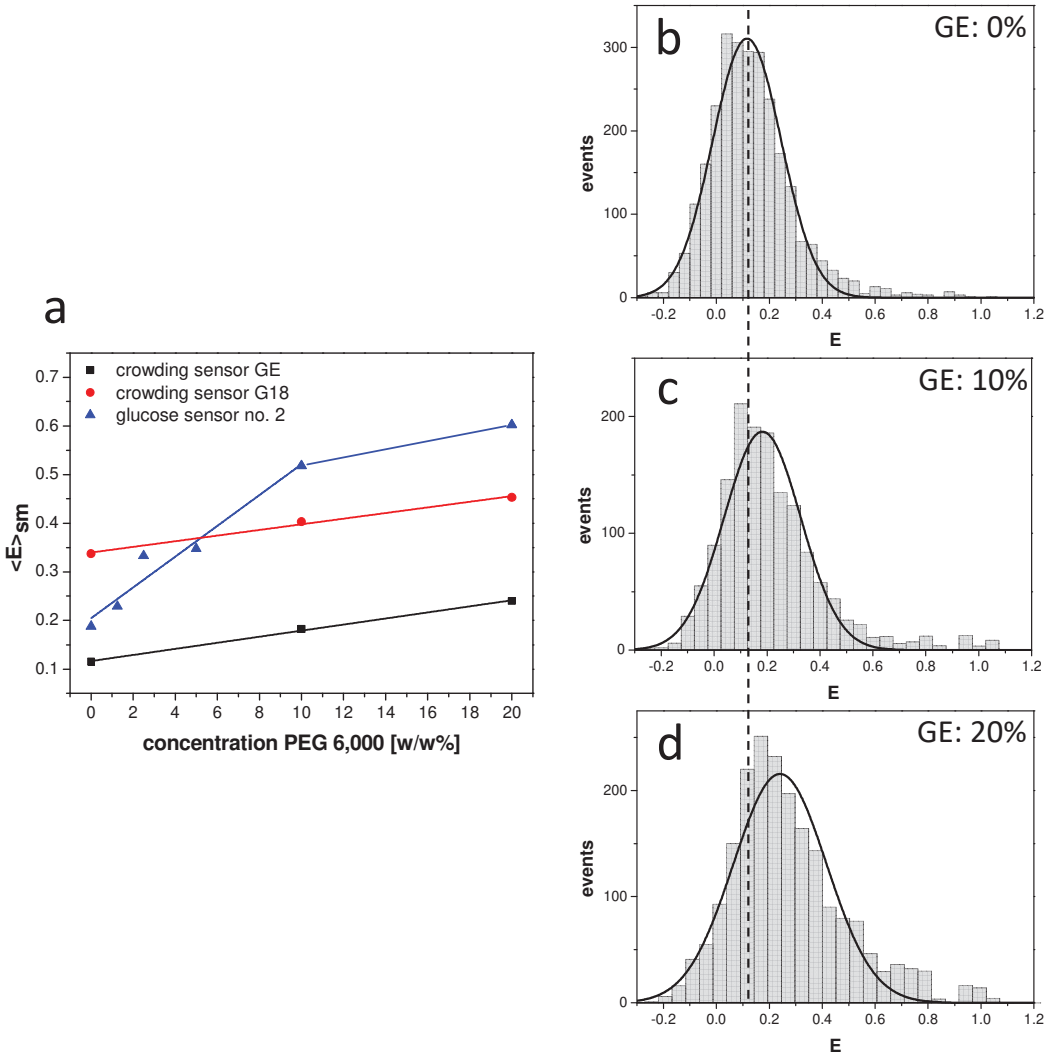

Figure S 1.1-13: (a) FRET efficiencies of crowding sensors and crowded glucose sensor. **Mean single-molecule FRET efficiency ($<E>_{sm}$) of glucose sensor no.2 (blue triangles), crowding sensor GE (black squares), and crowding sensor G18 (red circles) in various concentrations of PEG 6,000. Both crowding sensors have similar sensitivities as depicted by similar slopes of the black and red lines. The glucose sensor is more sensitive to PEG for small concentrations and approaches sensitivities similar to that of the crowding sensors for high PEG concentrations (indicated by blue line). (b)-(d) smFRET efficiency histograms obtained for GE sensor in presence of increasing concentrations of crowding agent PEG 6,000. The widths of the Gaussian distributions are slightly larger for the crowding sensors in comparison to that of the glucose sensors (cf. Tab. S2 and S3).**

Table S 1.1-1: Overview on the composition of the employed glucose sensor variants.
Nine different linker combinations were used in this work. The basic FLII[12]P-construct is described elsewhere, but contained ECFP and Citrine as fluorescent proteins[10]. The linker sequences exhibit rigid (KLYPYDVPDYA) or flexible $(GGS)_4$ structural properties and were already described and applied in a previous study[11]. All constructs contain an N-terminal hexa-histidine tag.

No.	N-terminal linker aa sequence	C-terminal linker aa sequence
1	-	-
2	$(GGS)_4$	-
3	KLYPYDVPDYA	
4	-	$(GGS)_4$
5	$(GGS)_4$	$(GGS)_4$
6	KLYPYDVPDYA	$(GGS)_4$
7	-	KLYPYDVPDYA
8	$(GGS)_4$	KLYPYDVPDYA
9	KLYPYDVPDYA	KLYPYDVPDYA

Table S 1.1-2: Overview on the parameters obtained from histogram fittings of all glucose sensors. $\langle E \rangle_{sm}$ denotes the mean FRET efficiency of each single-molecule measurement, E_1 and E_2 are the means, σ_1 and σ_2 are the widths, and p_1 and p_2 are the statistical weights of the first and second Gaussian, respectively. Typically a few thousand burst were considered to build the histogram. The range of obtained χ^2 values varied between 1 and 7. The errors in $E_{1,2}$ are in the order of the width of a single bin (ΔE_{bin}) used in the corresponding efficiency histograms.

Sens. no.	*Glucose [mM]*	*PEG 6,000 [w/w %]*	$\langle E \rangle_{sm}$	E_1	E_2	Δ_1	Δ_2	p_1	p_2	ΔE_{bin}
1	0	-	0.624	0.570	0.791	0.15	0.09	0.75	0.25	0.023
1	7	-	0.674	0.570	0.791	0.15	0.09	0.52	0.48	0.025
1	125	-	0.690	0.570	0.791	0.15	0.09	0.48	0.52	0.020
2	0	-	0.129	0.092	0.628	0.15	0.15	0.92	0.08	0.040
2	1.1	-	0.304	0.092	0.628	0.15	0.15	0.61	0.39	0.040
2	125	-	0.596	0.092	0.628	0.15	0.15	0.09	0.91	0.040
3	0	-	0.235	0.165	0.633	0.18	0.14	0.85	0.15	0.040
3	1.1	-	0.368	0.165	0.633	0.18	0.14	0.58	0.42	0.040
3	125	-	0.625	0.165	0.633	0.18	0.14	0.06	0.94	0.040
4	0	-	0.289	0.179	0.484	0.17	0.18	0.63	0.37	0.040
4	1	-	0.424	0.179	0.484	0.17	0.18	0.17	0.83	0.040
4	125	-	0.472	0.179	0.484	0.17	0.18	0.07	0.93	0.040
5	0	-	0.194	0.133	0.527	0.16	0.16	0.84	0.16	0.035
5	125	-	0.507	0.133	0.527	0.16	0.16	0.08	0.92	0.035
8	0	-	0.399	0.289	0.582	0.17	0.15	0.64	0.36	0.040
8	1.2	-	0.519	0.289	0.582	0.17	0.15	0.24	0.76	0.035
8	125	-	0.532	0.289	0.582	0.17	0.15	0.17	0.83	0.040
2	0	10	0.529	0.292	0.608	0.19	0.19	0.27	0.73	0.050
2	1.1	10	0.583	0.292	0.608	0.19	0.19	0.08	0.92	0.025
2	125	10	0.587	0.292	0.608	0.19	0.19	0.07	0.93	0.020
2	0	0	0.192	0.084	0.384	0.13	0.22	0.66	0.34	0.025
2	0	1.25	0.228	0.085	0.432	0.15	0.23	0.60	0.40	0.050
2	0	2.5	0.333	0.147	0.496	0.17	0.21	0.47	0.53	0.050
2	0	5	0.348	0.227	0.646	0.20	0.15	0.72	0.28	0.050
2	0	10	0.517	0.395	0.716	0.23	0.15	0.62	0.38	0.050
2	0	20	0.602	0.548	0.736	0.21	0.10	0.67	0.33	0.042

Table S 1.1-3: Overview on the parameters obtained from histogram fittings of all crowding sensors. Each smFRET histogram was fitted with a single Gaussian with mean E_1 and width σ_1. Typically a few thousand burst were considered to build the histogram. The range of obtained χ^2 values varied between 1 and 6. The errors in E_1 are in the order of the width of a single bin (ΔE_{bin}).

Sens. no.	*PEG 6,000 [w/w %]*	E_1	Δ_1	ΔE_{bin}
GE	0	0.115	0.13	0.040
GE	10	0.182	0.14	0.050
GE	20	0.240	0.17	0.052
G18	0	0.357	0.16	0.050
G18	10	0.403	0.17	0.040
G18	20	0.453	0.20	0.059

Supporting Information References

1. Liu, B. Q.; Aberg, C.; van Eerden, F. J.; Marrink, S. J.; Poolman, B.; Boersma, A. J., Design and Properties of Genetically Encoded Probes for Sensing Macromolecular Crowding. *Biophys J* **112,** 1929-1939.(2017).
2. Kempe, D.; Schone, A.; Fitter, J.; Gabba, M., Accurate Fluorescence Quantum Yield Determination by Fluorescence Correlation Spectroscopy. *J Phys Chem B* **119,** 4668-4672 (2015).
3. Kempe, D.; Cerminara, M.; Poblete, S.; Schone, A.; Gabba, M.; Fitter, J., Single-Molecule FRET Measurements in Additive-Enriched Aqueous Solutions. *Anal Chem* **89,** 694-702.(2017).
4. Muller, B. K.; Zaychikov, E.; Brauchle, C.; Lamb, D. C., Pulsed interleaved excitation. *Biophys.J* **89,** 3508-3522 (2005).
5. Fries, J. R.; Brand, L.; Eggeling, C.; Kollner, M.; Seidel, C. A. M., Quantitative identification of different single molecules by selective time-resolved confocal fluorescence spectroscopy. *J Phys Chem A* **102,** 6601-6613 (1998).
6. Kapanidis, A. N.; Lee, N. K.; Laurence, T. A.; Doose, S.; Margeat, E.; Weiss, S., Fluorescence-aided molecule sorting: Analysis of structure and interactions by alternating-laser excitation of single molecules. *Proc Natl Acad Sci U S A* **101,** 8936-8941 (2004).
7. Kudryavtsev, V.; Sikor, M.; Kalinin, S.; Mokranjac, D.; Seidel, C. A. M.; Lamb, D. C., Combining MFD and PIE for Accurate Single-Pair Forster Resonance Energy Transfer Measurements. *Chemphyschem* **13,** 1060-1078 (2012).
8. Nir, E.; Michalet, X.; Hamadani, K. M.; Laurence, T. A.; Neuhauser, D.; Kovchegov, Y.; Weiss, S., Shot-noise limited single-molecule FRET histograms: comparison between theory and experiments. *J Phys.Chem.B* **110,** 22103-22124 (2006).
9. Orte, A.; Clarke, R.; Balasubramanian, S.; Klenerman, D., Determination of the fraction and stoichiometry of femtomolar levels of biomolecular complexes in an excess of monomer using single-molecule, two-color coincidence detection. *Anal Chem* **78,** 7707-7715 (2006).

10. Deuschle, K.; Okumoto, S.; Fehr, M.; Looger, L. L.; Kozhukh, L.; Frommer, W. B., Construction and optimization of a family of genetically encoded metabolite sensors by semirational protein engineering. *Protein Science* **14,** 2304-2314 (2005).

11. Steffen, V.; Otten, J.; Engelmann, S.; Radek, A.; Limberg, M.; Koenig, B. W.; Noack, S.; Wiechert, W.; Pohl, M., A Toolbox of Genetically Encoded FRET-Based Biosensors for Rapid L-Lysine Analysis. *Sensors* **16**, (2016).

1.2 Supporting information Chapter 2.2

A FRET-based biosensor for the quantification of glucose in culture supernatants of mL scale microbial cultivations

Supplementary information

Julia Otten[1], Niklas Tenhaef[1], Roman P. Jansen[1], Johannes Döbber[1], Lisa Jungbluth[1], Stephan Noack[1], Marco Oldiges[1], Wolfgang Wiechert[1], Martina Pohl[1]*

[1]Forschungszentrum Jülich GmbH, IBG-1 Biotechnology, D-52415 Jülich, Germany

a) Sensor nomenclature

Table S 1.2-1 Composition of the sensor used in this study: Positions of the His and HaloTag™ as well as the molecular weight and tested formulation of the sensors Glu[-] and Glu[+Halo].

sensor	position His_6-tag	position HaloTag™	formulation	molecular weight
Glu [-]	C-terminus	-	soluble	98550 g/mol
Glu[+Halo]	N-terminus	C-terminus	soluble or immobilized	128303 g/mol

b) Sequence information

Sequences encoding the binding protein (MglB) are depicted green, restriction sites red, mTurquoise2 is colored blue, Venus yellow. The hexahistidine tag (His-tag) is depicted in gray and the HaloTag™ is grey underlined. Linker sequences are colored magenta.

Sequence S1: Amino acid sequence of the Glu [-] sensor with N-terminal (of MglB) flexible linker ($(GGS)_4$) and C-terminal His-tag

MADTRIGVTIYKAAAMVSKGEELFTGVVPILVELDGDVNGHKFSVSGEGEGDATYGKLTLKFICTTGKLPVPWPTLVTTL
SWGVQCFARYPDHMKQHDFFKSAMPEGYVQERTIFFKDDGNYKTRAEVKFEGDTLVNRIELKGIDFKEDGNILGHKLE
YNYFSDNVYITADKQKNGIKANFKIRHNIEDGGVQLADHYQQNTPIGDGPVLLPDNHYLSTQSKLSKDPNEKRDHMVL
LEFVTAAGITLGMDELYGSGGSGGSGGSGGSPGDNFMSVVRKAIEQDAKAAPDVQLLMNDSQNDQSKQNDQIDVLL
AKGVKALAINLVDPAAAGTVIEKARGQNVPVVFFNKEPSRKALDSYDKAYYVGTDSKESGIIQGDLIAKHWAANQGWD
LNKDGQIQFVLLKGEPGHPDAEARTTYVIKELNDKGIKTEQLQLDTAMWDTAQAKDKMDAWLSGPNANKIEVVIANN
DAMAMGAVEALKAHNKSSIPVFGVDAMPEALALVKSGALAGTVLNDANNQAKATFDLAKNLADGKGAADGTNWKI
DNKVVRVPYVGVDKDNLAEFSKKEFVDGGMVSKGEELFTGVVPILVELDGDVNGHKFSVSGEGEGDATYGKLTLKLICT
TGKLPVPWPTLVTTLGYGLQCFARYPDHMKQHDFFKSAMPEGYVQERTIFFKDDGNYKTRAEVKFEGDTLVNRIELKGI
DFKEDGNILGHKLEYNYNSHNVYITADKQKNGIKANFKIRHNIEDGGVQLADHYQQNTPIGDGPVLLPDNHYLSYQSAL
SKDPNEKRDHMVLLEFVTAAGITLGMDELYKHHHHHH

Sequence S2: Nucleotide sequence of the Glu[-] sensor with N-terminal (of MglB) flexible linker ($(GGS)_4$) and C-terminal His-tag

ATGGCTGATACTCGCATTGGTGTAACAATCTATAAGGCGGCCGCTATGGTGAGCAAGGGCGAGGAGCTGTTCACC
GGGGTGGTGCCCATCCTGGTCGAGCTGGACGGCGACGTAAACGGCCACAAGTTCAGCGTGTCCGGCGAGGGCGA
GGGCGATGCCACCTACGGCAAGCTGACCCTGAAGTTCATCTGCACCACCGGCAAGCTGCCCGTGCCCTGGCCCAC
CCTCGTGACCACCCTGTCCTGGGGCGTGCAGTGCTTCGCCCGCTACCCCGACCACATGAAGCAGCACGACTTCTTC
AAGTCCGCCATGCCCGAAGGCTACGTCCAGGAGCGCACCATCTTCTTCAAGGACGACGGCAACTACAAGACCCGC
GCCGAGGTGAAGTTCGAGGGCGACACCCTGGTGAACCGCATCGAGCTGAAGGGCATCGACTTCAAGGAGGACG
GCAACATCCTGGGGCACAAGCTGGAGTACAACTACTTTAGCGACAACGTCTATATCACCGCCGACAAGCAGAAGA

ACGGCATCAAGGCCAACTTCAAGATCCGCCACAACATCGAGGACGGCGGCGTGCAGCTCGCCGACCACTACCAGC
AGAACACCCCCATCGGCGACGGCCCCGTGCTGCTGCCCGACAACCACTACCTGAGCACCCAGTCCAAGCTGAGCA
AAGACCCCAACGAGAAGCGCGATCACATGGTCCTGCTGGAGTTCGTGACCGCCGCCGGGATCACTCTCGGCATGG
ACGAGCTGTACGGATCCGGTGGTTCTGGCGGTTCAGGTGGCTCTGGTGGGTCACCTGGTGATAACTTTATGTCTGT
AGTGCGCAAGGCTATTGAGCAAGATGCGAAAGCCGCGCCAGATGTTCAGCTGCTGATGAATGATTCTCAGAATGA
CCAGTCCAAGCAGAACGATCAGATCGACGTATTGCTGGCGAAAGGGGTGAAGGCACTGGCAATCAACCTCGTTG
ACCCGGCAGCTGCGGGTACGGTGATTGAGAAAGCGCGTGGGCAAAACGTGCCGGTGGTTTTCTTCAACAAAGAA
CCGTCTCGTAAGGCGCTGGATAGCTACGACAAAGCCTACTACGTTGGCACTGACTCCAAAGAGTCCGGCATTATTC
AAGGCGATTTGATTGCTAAACACTGGGCGGCGAATCAGGGTTGGGATCTGAACAAAGACGGTCAGATTCAGTTCG
TACTGCTGAAAGGTGAACCGGGCCATCCGGATGCAGAAGCACGTACCACTTACGTGATTAAAGAATTGAACGATA
AAGGCATCAAAACTGAACAGTTACAGTTAGATACCGCAATGTGGGACACCGCTCAGGCGAAAGATAAGATGGAC
GCCTGGCTGTCTGGCCCGAACGCCAACAAAATCGAAGTGGTTATCGCCAACAACGATGCGATGGCAATGGGCGC
GGTTGAAGCGCTGAAAGCACACAACAAGTCCAGCATTCCGGTGTTTGGCGTCGATGCGATGCCAGAAGCGCTGGC
GCTGGTGAAATCCGGTGCACTGGCGGGCACCGTACTGAACGATGCTAACAACCAGGCGAAAGCGACCTTTGATCT
GGCGAAAAACCTGGCCGATGGTAAAGGTGCGGCTGATGGCACCAACTGGAAAATCGACAACAAAGTGGTCCGCG
TACCTTATGTTGGCGTAGATAAAGACAACCTGGCTGAGTTCAGCAAGAAAGAATTCGTCGACGGTGGAATGGTGA
GCAAGGGCGAGGAGCTGTTCACCGGGGTGGTGCCCATCCTGGTCGAGCTGGACGGCGACGTAAACGGCCACAAG
TTCAGCGTGTCCGGCGAGGGCGAGGGCGATGCCACCTACGGCAAGCTGACCCTGAAGCTGATCTGCACCACCGG
CAAGCTGCCCGTGCCCTGGCCCACCCTCGTGACCACCCTGGGCTACGGCCTGCAGTGCTTCGCCCGCTACCCCGAC
CACATGAAGCAGCACGACTTCTTCAAGTCCGCCATGCCCGAAGGCTACGTCCAGGAGCGCACCATCTTCTTCAAGG
ACGACGGCAACTACAAGACCCGCGCCGAGGTGAAGTTCGAGGGCGACACCCTGGTGAACCGCATCGAGCTGAAG
GGCATCGACTTCAAGGAGGACGGCAACATCCTGGGGCACAAGCTGGAGTACAACTACAACAGCCACAACGTCTAT
ATCACCGCCGACAAGCAGAAGAACGGCATCAAGGCCAACTTCAAGATCCGCCACAACATCGAGGACGGCGGCGT
GCAGCTCGCCGACCACTACCAGCAGAACACCCCCATCGGCGACGGCCCCGTGCTGCTGCCCGACAACCACTACCT
GAGCTACCAGTCCGCCCTGAGCAAAGACCCCAACGAGAAGCGCGATCACATGGTCCTGCTGGAGTTCGTGACCGC
CGCCGGGATCACTCTCGGCATGGACGAGCTGTACAAGCATCATCACCACCATCAC

Sequence S3: Amino acid sequence of the Glu$^{[+Halo]}$ sensor with C-terminal Halo-tag, N-terminal (of MglB) flexible linker ((GGS)$_4$) and N-terminal His-tag

MRGSHHHHHHGMASMTGGQQMGRDLYDDDDKEPGRADTRIGVTIYKAAAMVSKGEELFTGVVPILVELDGDVNG
HKFSVSGEGEGDATYGKLTLKFICTTGKLPVPWPTLVTTLSWGVQCFARYPDHMKQHDFFKSAMPEGYVQERTIFFKD
DGNYKTRAEVKFEGDTLVNRIELKGIDFKEDGNILGHKLEYNYFSDNVYITADKQKNGIKANFKIRHNIEDGGVQLADHY
QQNTPIGDGPVLLPDNHYLSTQSKLSKDPNEKRDHMVLLEFVTAAGITLGMDELYGSGGSGGSGGSGGSPGDNFMSV
VRKAIEQDAKAAPDVQLLMNDSQNDQSKQNDQIDVLLAKGVKALAINLVDPAAAGTVIEKARGQNVPVVFFNKEPSR
KALDSYDKAYYVGTDSKESGIIQGDLIAKHWAANQGWDLNKDGQIQFVLLKGEPGHPDAEARTTYVIKELNDKGIKTEQ
LQLDTAMWDTAQAKDKMDAWLSGPNANKIEVVIANNDAMAMGAVEALKAHNKSSIPVFGVDAMPEALALVKSGA
LAGTVLNDANNQAKATFDLAKNLADGKGAADGTNWKIDNKVVRVPYVGVDKDNLAEFSKKEFVDGGMVSKGEELFT
GVVPILVELDGDVNGHKFSVSGEGEGDATYGKLTLKLICTTGKLPVPWPTLVTTLGYGLQCFARYPDHMKQHDFFKSA
MPEGYVQERTIFFKDDGNYKTRAEVKFEGDTLVNRIELKGIDFKEDGNILGHKLEYNYNSHNVYITADKQKNGIKANFKI
RHNIEDGGVQLADHYQQNTPIGDGPVLLPDNHYLSYQSALSKDPNEKRDHMVLLEFVTAAGITLGMDELYKLAEAAAK
EAAAKEAAAKEAAAKAAAAEIGTGFPFDPHYVEVLGERMHYVDVGPRDGTPVLFLHGNPTSSYVWRNIIPHVAPTHRC
IAPDLIGMGKSDKPDLGYFFDDHVRFMDAFIEALGLEEVVLVIHDWGSALGFHWAKRNPERVKGIAFMEFIRPIPTWD
EWPEFARETFQAFRTTDVGRKLIIDQNVFIEGTLPMGVVRPLTEVEMDHYREPFLNPVDREPLWRFPNELPIAGEPANI
VALVEEYMDWLHQSPVPKLLFWGTPGVLIPPAEAARLAKSLPNCKAVDIGPGLNLLQEDNPDLIGSEIARWLSTLEISG

Sequence S4: Nucleotide sequence of the Glu $^{[+Halo]}$ sensor with C-terminal Halo-tag, N-terminal (of MglB) flexible linker ((GGS)$_4$) and N-terminal His-tag

ATGCGGGGTTCTCATCATCATCATCATCATGGTATGGCTAGCATGACTGGTGGACAGCAAATGGGTCGGGATCTG
TACGACGATGACGATAAGGAGCCGGGCCGCGCTGATACTCGCATTGGTGTAACAATCTATAAGGCGGCCGCTATG
GTGAGCAAGGGCGAGGAGCTGTTCACCGGGGTGGTGCCCATCCTGGTCGAGCTGGACGGCGACGTAAACGGCCA
CAAGTTCAGCGTGTCCGGCGAGGGCGAGGGCGATGCCACCTACGGCAAGCTGACCCTGAAGTTCATCTGCACCAC
CGGCAAGCTGCCCGTGCCCTGGCCCACCCTCGTGACCACCCTGTCCTGGGGCGTGCAGTGCTTCGCCCGCTACCCC
GACCACATGAAGCAGCACGACTTCTTCAAGTCCGCCATGCCCGAAGGCTACGTCCAGGAGCGCACCATCTTCTTCA

AGGACGACGGCAACTACAAGACCCGCGCCGAGGTGAAGTTCGAGGGCGACACCCTGGTGAACCGCATCGAGCTG
AAGGGCATCGACTTCAAGGAGGACGGCAACATCCTGGGGCACAAGCTGGAGTACAACTACTTTAGCGACAACGT
CTATATCACCGCCGACAAGCAGAAGAACGGCATCAAGGCCAACTTCAAGATCCGCCACAACATCGAGGACGGCGG
CGTGCAGCTCGCCGACCACTACCAGCAGAACACCCCCATCGGCGACGGCCCCGTGCTGCTGCCCGACAACCACTA
CCTGAGCACCCAGTCCAAGCTGAGCAAAGACCCCAACGAGAAGCGCGATCACATGGTCCTGCTGGAGTTCGTGAC
CGCCGCCGGGATCACTCTCGGCATGGACGAGCTGTACGGATCCGGTGGTTCTGGCGGTTCAGGTGGCTCTGGTGG
GTCACCTGGTGATAACTTTATGTCTGTAGTGCGCAAGGCTATTGAGCAAGATGCGAAAGCCGCGCCAGATGTTCA
GCTGCTGATGAATGATTCTCAGAATGACCAGTCCAAGCAGAACGATCAGATCGACGTATTGCTGGCGAAAGGGGT
GAAGGCACTGGCAATCAACCTCGTTGACCCGGCAGCTGCGGGTACGGTGATTGAGAAAGCGCGTGGGCAAAACG
TGCCGGTGGTTTTCTTCAACAAAGAACCGTCTCGTAAGGCGCTGGATAGCTACGACAAAGCCTACTACGTTGGCAC
TGACTCCAAAGAGTCCGGCATTATTCAAGGCGATTTGATTGCTAAACACTGGGCGGCGAATCAGGGTTGGGATCT
GAACAAAGACGGTCAGATTCAGTTCGTACTGCTGAAAGGTGAACCGGGCCATCCGGATGCAGAAGCACGTACCA
CTTACGTGATTAAAGAATTGAACGATAAAGGCATCAAAACTGAACAGTTACAGTTAGATACCGCAATGTGGGACA
CCGCTCAGGCGAAAGATAAGATGGACGCCTGGCTGTCTGGCCCGAACGCCAACAAAATCGAAGTGGTTATCGCCA
ACAACGATGCGATGGCAATGGGCGCGGTTGAAGCGCTGAAAGCACACAACAAGTCCAGCATTCCGGTGTTTGGC
GTCGATGCGATGCCAGAAGCGCTGGCGCTGGTGAAATCCGGTGCACTGGCGGGCACCGTACTGAACGATGCTAA
CAACCAGGCGAAAGCGACCTTTGATCTGGCGAAAAACCTGGCCGATGGTAAAGGTGCGGCTGATGGCACCAACT
GGAAAATCGACAACAAAGTGGTCCGCGTACCTTATGTTGGCGTAGATAAAGACAACCTGGCTGAGTTCAGCAAGA
AAGAATTCGTCGACGGTGGAATGGTGAGCAAGGGCGAGGAGCTGTTCACCGGGGTGGTGCCCATCCTGGTCGAG
CTGGACGGCGACGTAAACGGCCACAAGTTCAGCGTGTCCGGCGAGGGCGAGGGCGATGCCACCTACGGCAAGCT
GACCCTGAAGCTGATCTGCACCACCGGCAAGCTGCCCGTGCCCTGGCCCACCCTCGTGACCACCCTGGGCTACGGC
CTGCAGTGCTTCGCCCGCTACCCCGACCACATGAAGCAGCACGACTTCTTCAAGTCCGCCATGCCCGAAGGCTACG
TCCAGGAGCGCACCATCTTCTTCAAGGACGACGGCAACTACAAGACCCGCGCCGAGGTGAAGTTCGAGGGCGAC
ACCCTGGTGAACCGCATCGAGCTGAAGGGCATCGACTTCAAGGAGGACGGCAACATCCTGGGGCACAAGCTGGA
GTACAACTACAACAGCCACAACGTCTATATCACCGCCGACAAGCAGAAGAACGGCATCAAGGCCAACTTCAAGAT
CCGCCACAACATCGAGGACGGCGGCGTGCAGCTCGCCGACCACTACCAGCAGAACACCCCCATCGGCGACGGCCC
CGTGCTGCTGCCCGACAACCACTACCTGAGCTACCAGTCCGCCCTGAGCAAAGACCCCAACGAGAAGCGCGATCA
CATGGTCCTGCTGGAGTTCGTGACCGCCGCCGGGATCACTCTCGGCATGGACGAGCTGTACAAGCTTGCAGAAGC
AGCGGCCAAAGAAGCTGCGGCCAAAGAGGCAGCCGCGAAAGAAGCAGCGGCGAAAGCGGCCGCGGCAGAAATT
GGTACGGGATTTCCGTTTGACCCGCATTATGTGGAGGTTCTGGGTGAACGCATGCACTACGTGGATGTTGGTCCG
CGCGATGGCACACCGGTGCTGTTTCTGCATGGTAATCCGACCTCCAGCTATGTTTGGCGCAACATTATTCCGCATG
TCGCCCCAACGCATCGCTGTATTGCCCCAGATCTCATTGGCATGGGCAAAAGCGACAAACCGGATTTGGGCTACTT
CTTCGACGATCACGTACGGTTTATGGACGCCTTTATCGAGGCTCTGGGACTCGAGGAAGTAGTGCTGGTTATTCAT
GACTGGGGCTCTGCATTAGGCTTTCACTGGGCTAAACGGAACCCAGAACGCGTCAAGGGGATTGCCTTCATGGAG
TTCATCCGTCCGATTCCGACCTGGGATGAATGGCCCGAATTTGCCCGTGAAACCTTTCAGGCGTTTCGTACCACGG
ATGTTGGCCGTAAGCTCATCATCGACCAAAACGTGTTCATTGAGGGCACTCTTCCCATGGGAGTAGTGCGTCCTTT
AACCGAAGTCGAGATGGACCACTATCGCGAACCCTTCCTGAATCCGGTTGATCGCGAACCGCTGTGGCGCTTCCCG
AATGAGCTGCCTATTGCTGGTGAACCGGCGAATATCGTGGCACTTGTGGAAGAATACATGGATTGGCTGCATCAG
AGTCCAGTCCCTAAGCTGTTGTTTTGGGGTACACCTGGCGTGTTGATTCCGCCTGCAGAAGCTGCTCGCTTAGCGA
AAAGCTTGCCCAACTGCAAAGCGGTCGATATTGGGCCAGGTCTGAACCTGTTACAGGAGGATAACCCGGATCTGA
TCGGGAGTGAAATCGCGCGTTGGCTGTCAACTCTGGAAATCTCGGGTTAA

c) Primers

Table S 1.2-2 Used primers for biosensor modifications. For the Gibson assembly of the Glu[+Halo] sensor with HaloTag primers 1&2 were used. Primers 3-10 were needed for the translocation of the His-tag in the Glu[-] sensor from N-to C-termius via Extension Overlap PCR (Ex. Ov.).

primer 1	CTTTAAGAAGGAGATATACATATGGCAGAAATTGGTACGGGATTTCCGTTTGAC	Gibson
primer 2	CAATGCGAGTATCAGCCATCGCGGCCGCTTTCG	Gibson
primer 3	CATCATCACCACCATCACTAAAAGCTTGATCCGGCTGCTAAC	Ex.ov.
primer 4	TTCTTAAAGTTAAACAAAATTATCTAGAGGGAAACCGTTGTGGTCTCCCTATAGTG	Ex.ov.
primer 5	CATCACTAAAAGCTTGATCCGGCTGCTAAC	Ex.ov.
primer 6	GCCATATGTATATCTCCTTCTTAAAGTTAAACAAAATTATC	Ex.ov.
primer 7	GGAGATATACATATGGCTGATACTCGCATTGGTGTAAC	Ex.ov.
primer 8	CTTGTACAGCACCATTCCACCGTCG	Ex.ov.
primer 9	TGATACTCGCATTGGTGTAACAATCTATAAGG	Ex.ov.
primer 10	GTGGTGATGATGCTTGTACAGCACCATTCCACCGTCG	Ex.ov.

d) Binding isotherms for the novel glucose sensor variants

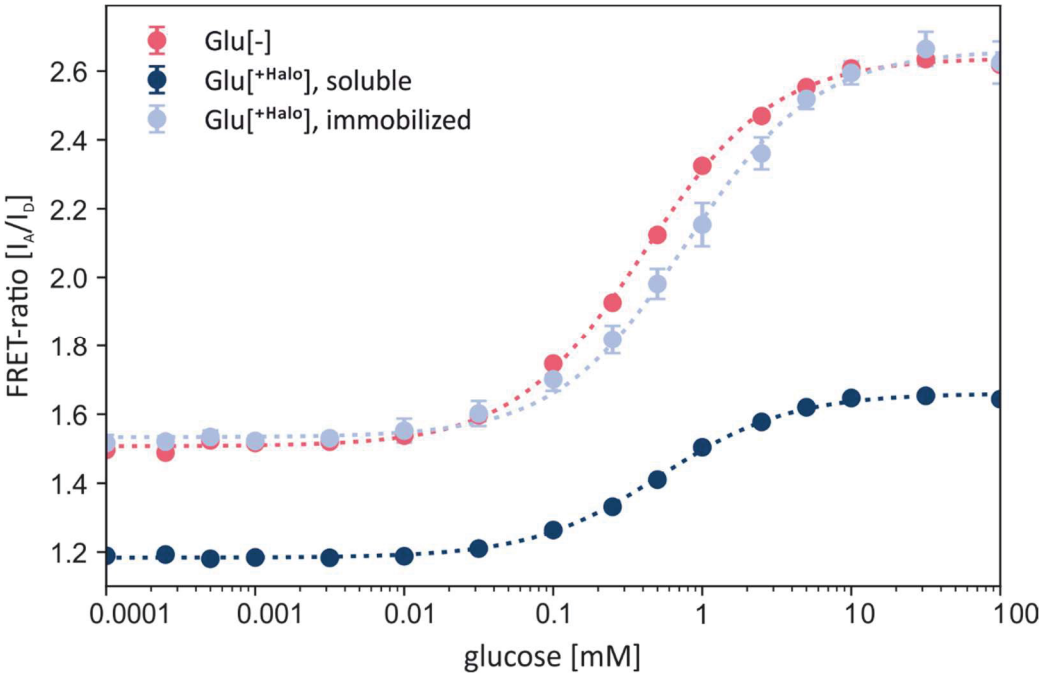

Figure S 1.2-1 Comparison of binding isotherms of the Glu[-] sensor and the Glu[+Halo] sensor in the non-immobilized form and immobilized on HaloLink Sepharose® beads, respectively, in MOPS buffer (20 mM, pH 7.3). The Glu[-] sensor without HaloTag® shows an affinity (K_d) of 0.4 ± 0.1 mM glucose and a sensitivity (ΔR) of 75 % (red). For the non-immobilized Glu[+Halo] sensor the sensitivity dropped to 40 % (dark blue). Immobilization of Glu[+Halo] sensor restores the functionality similar to the Glu[-] sensor without HaloTag® (0.8 ± 0.2 mM, 74 % ΔR) (light blue).

e) Influence of cultivation media on the FRET-ratio

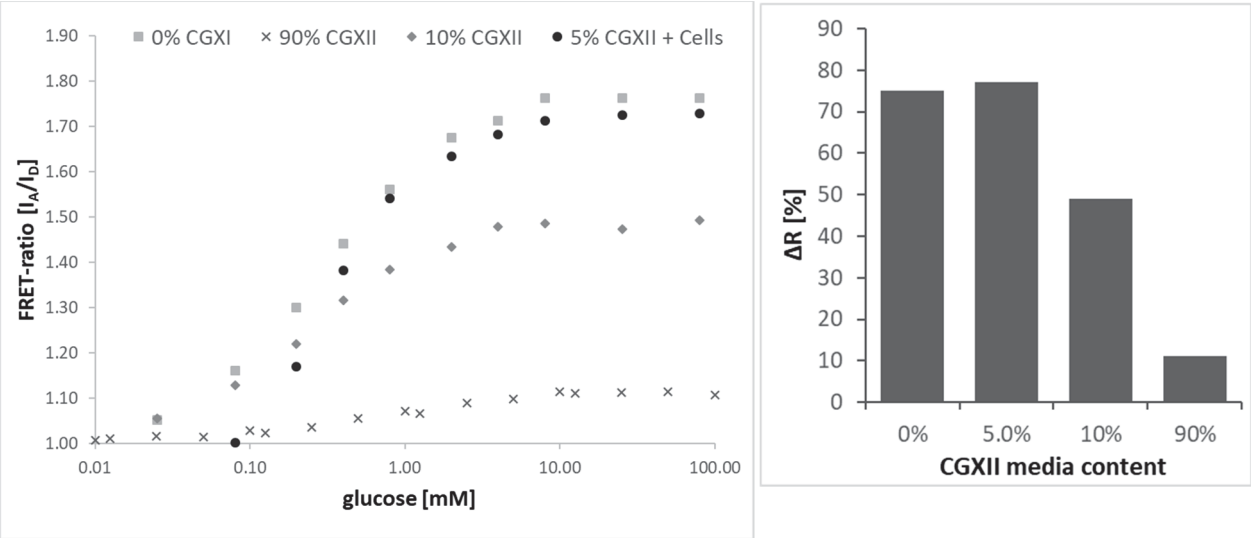

Figure S 1.2-2: Binding isotherms of the Glu [-] sensor with varying volumes of CGXII medium (left). In the right figure, values were normalized to the respective R_0 values. The FRET-ratio change ΔR was highest (75%) in MOPS buffer (20 mM, pH 7.3) in the absence of medium (0 vol%). Addition of 5 vol% medium did not change the sensitivity of the Glu[-] sensor (ΔR = 74%). Addition of larger medium fractions decreases the sensitivity progressively. The affinity (Kd) was not influences and remained in the range of 0.4 ± 0.1 mM

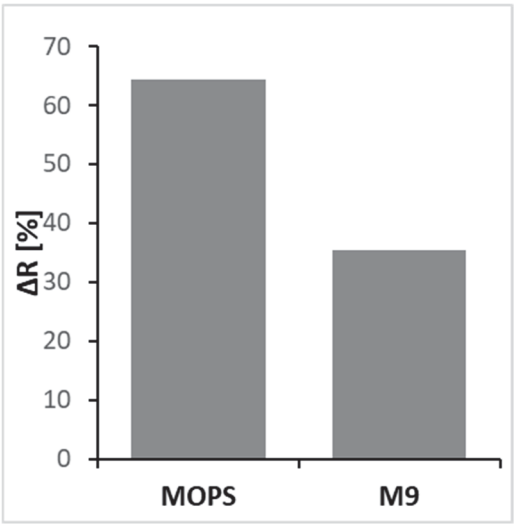

Figure S 1.2-3: FRET-ratio change of the immobilized Glu[+Halo-] sensor (on HaloLink Sepharose®). The addition of 90 vol% M9 medium reduces ΔR from 64 % in MOPS buffer (20 mM, pH 7.3) to 35 %.

f) Stability

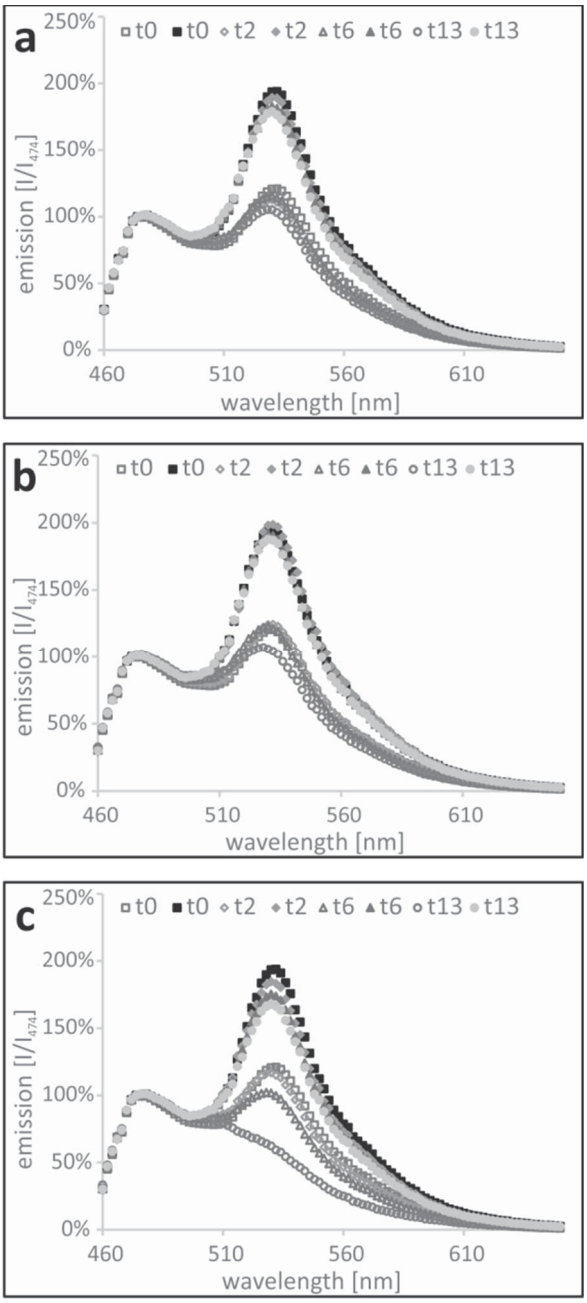

Figure S 1.2-4: Emission spectra of the immobilized Glu[+Halo]. Solid markers indicate presence of 100 mM glucose, empty markers indicate no glucose. Incubation of the sensor at (a) 4°C, (b) -20°C and (c) 25°C without shaking. At room temperature (c), the sensor lost its functionality after 6 days, while the sensor stayed fully functional for at least 13 days when stored at 4°C (a) and -20°C (b).

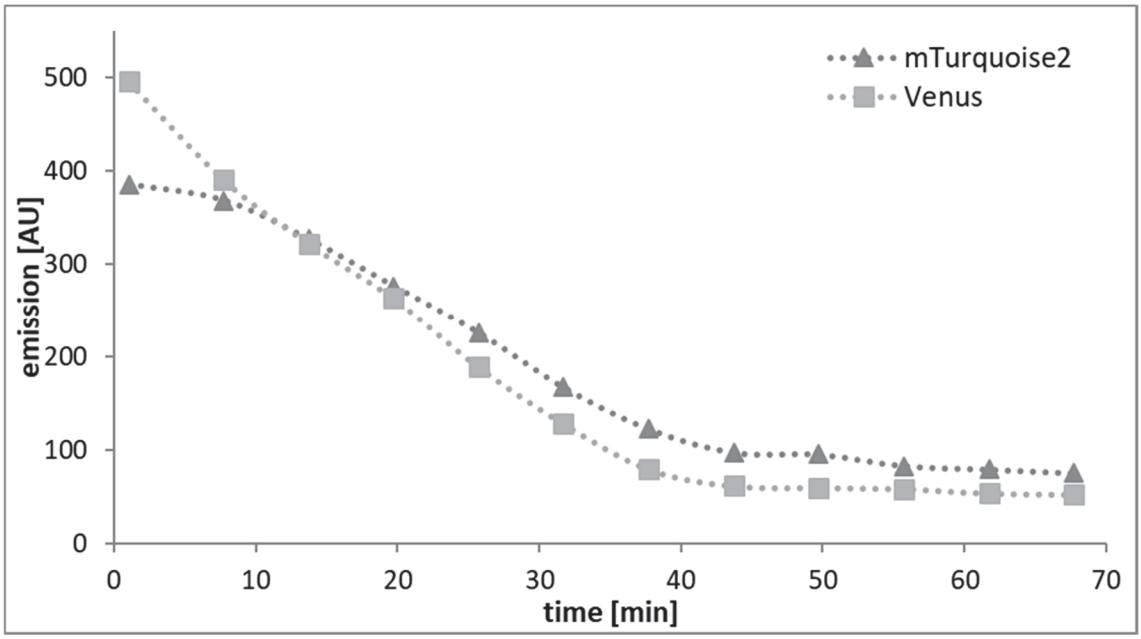

Figure S 1.2-5: Stability of the Glu[-] sensor in a micro bioreactor (BioLector, m2p-labs, Baesweiler, Germany) during shaking (1200 rpm, 30°C). Fluorescence emission of mTurquoise2 (λ_{em}=486 nm) and Venus (λ_{em}=532 nm) after excitation at λ_{ex}= 430 nm were recorded in the BioLector cultivation device. The fluorescence signals of both fluorescence proteins incorporated in the Glu[-] sensor started to decrease, immediately. After 35 minutes, the Glu[-] sensor lost its functionality

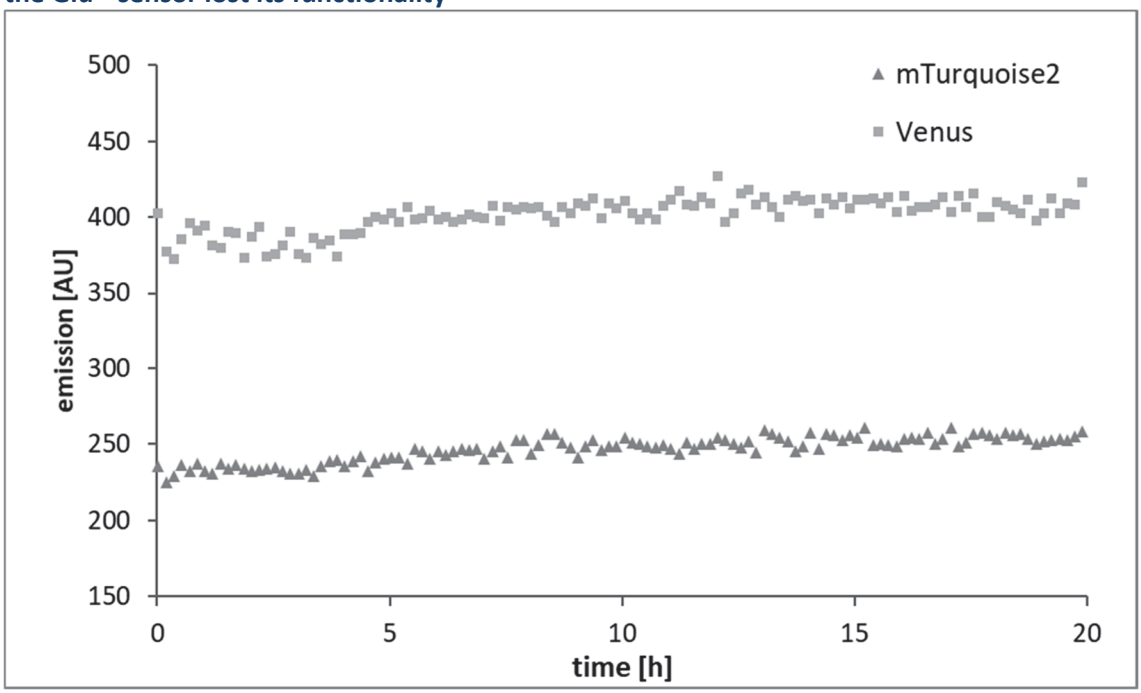

Figure S 1.2-6: Stability of the immobilized Glu[+Halo] sensor in a micro bioreactor (BioLector, m2p-labs, Baesweiler, Germany) during shaking (800 rpm, 30°C). Fluorescence emission of mTurquoise2 (λ_{em}=486 nm) and Venus (λ_{em}=532 nm) after excitation at λ_{ex}= 430 nm were recorded in the BioLector cultivation device. No sensor degradation could be noticed throughout the whole process of 20 hours.

g) At-line measurement process scheme

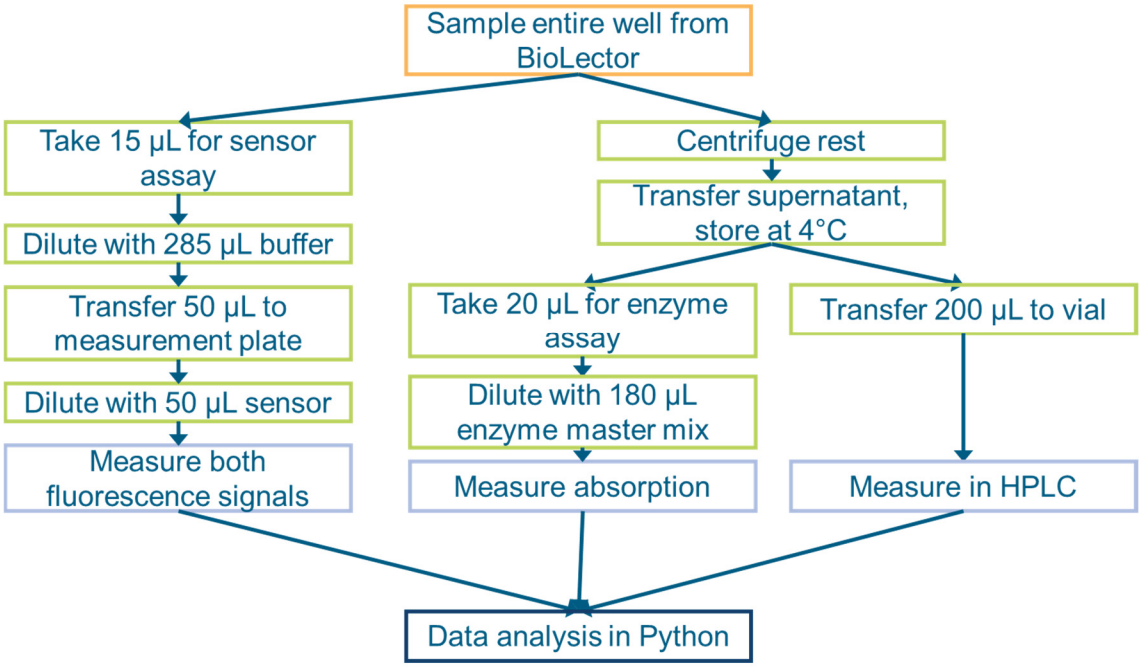

Figure S 1.2-7 Schematic representation of the at-line process including the cultivation in a micro bioreactor (orange), sampling and processing steps (green) performed by the liquid handling system, comparative measurement of glucose concentrations via glucose biosensor (at-line), enzymatic assay, and HPLC (both offline) (blue) as well as the data analysis (black).

h) Calibrations

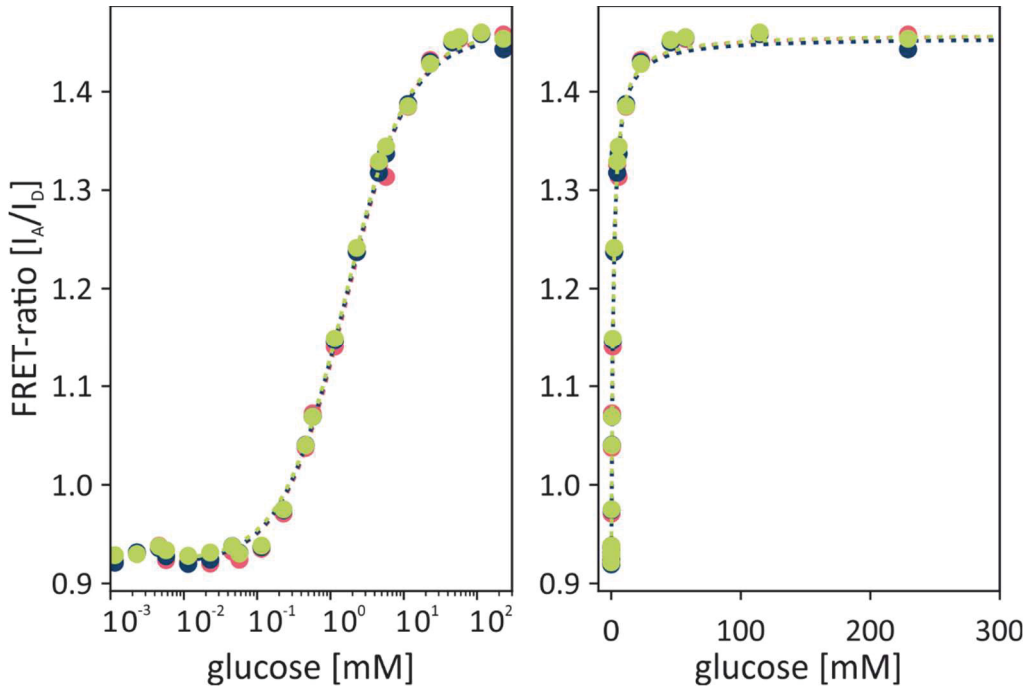

Figure S 1.2-8: Calibration of the Glu[-]sensor used for the at-line quantification of glucose in a C. glutamicum ATCC 1332 cultivation using CGXII medium. Fitting of the data points according to equation 2 (main paper) resulted in an apparent K_d of 1.5 mM, R_0 of 0.92, R_{sat} of 1.46, and ΔR of 58%; the red, green and blue data points represent three analytical replicates, each data

point represents the mean of 5 technical replicates. The standard deviation (SD) is too small to be visible in this presentation.

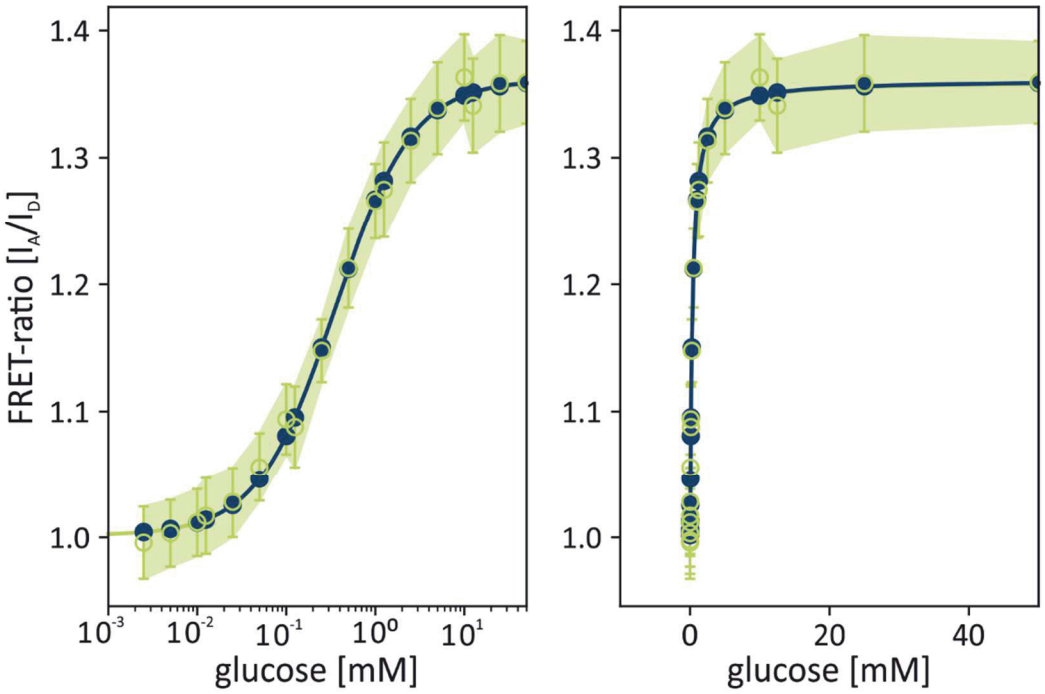

Figure S 1.2-9: Calibration of the immobilized Glu$^{[+Halo]}$ biosensor used for the online quantification of the glucose consumption of an E. coli K12 strain in M9 medium. In green, each data point resembles the mean ratio recorded over 20 hours within the BioLector. The filled area marks the standard deviation (SD) to demonstrate the noise of the signal. Additionally the calibration curve is described by a saturation kinetic equation whose parameters are fitted to the measured calibration data by minimizing the sum of squares (blue). This resulted in an apparent K_d of 0.4 ± 0.1 mM, R_0 of 1.0, R_{sat} of 1.36, and ΔR of ~36 % according to equation (2).

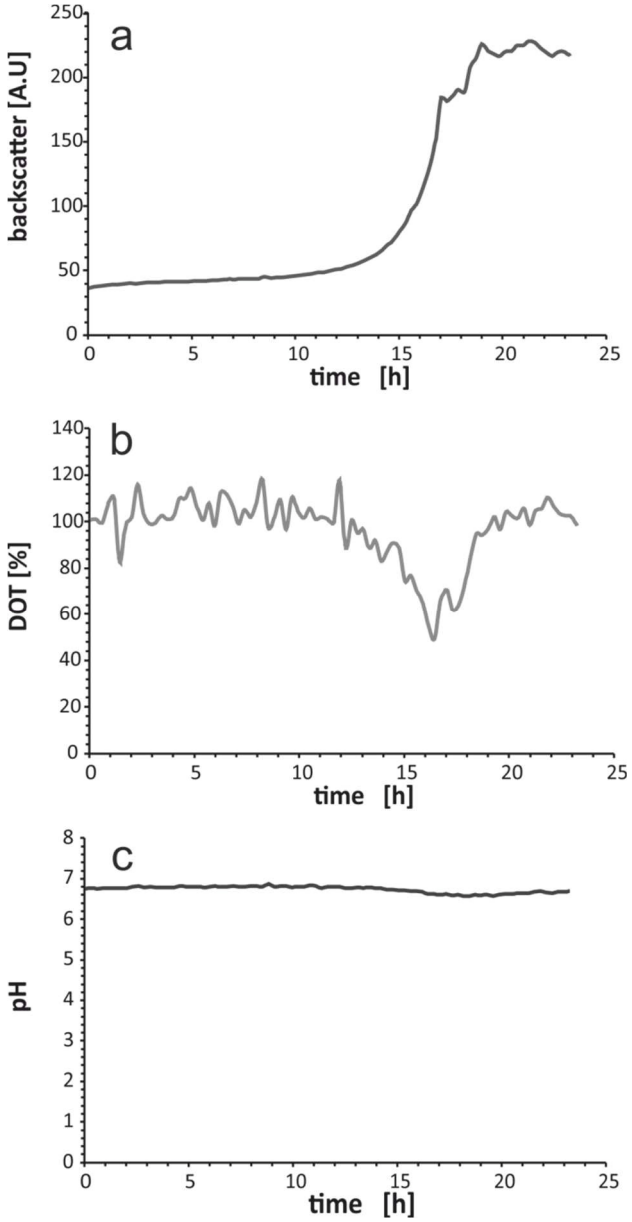

Figure S 1.2-10: Additional process data from an E. coli MG1655 cultivation in M9 media with 5 g/L D-glucose. The cultivation was performed at 30°C and 900 rpm. Biomass formation (backscatter, a), oxygen availability (DOT, b), and pH (c) were monitored over 24 hours. The cultivation did not show signs of oxygen limitations (DOT> 40%) or a pronounced shift in pH.

1.3 Supplementary information Chapter 2.3

A Novel Platform Solution For Quantitative Microfluidic Single-Bead Glucose Measurement With High Spatio-Temporal Resolution Supplementary Data:

Julia Otten[1], Christoph Westerwalbesloh[1], Daniel-Timon Spanka[1], Dietrich Kohlheyer[1,2], Wolfgang Wiechert[1], Martina Pohl[1*]

[1] Forschungszentrum Jülich GmbH, IBG-1: Biotechnology, Germany
[2] RWTH Aachen University, Aachener Verfahrenstechnik (AVT.MSB), Aachen, Germany

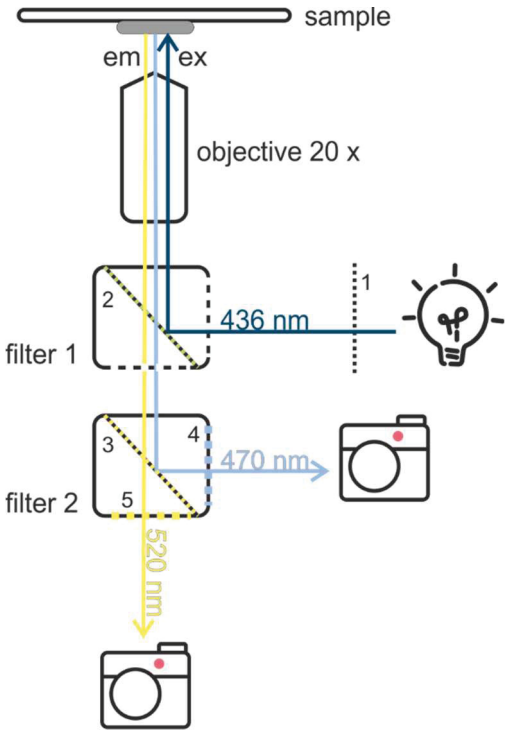

Figure S 1.3-1: microscopy setup for FRET detection. A Lambda DG-4 was used as light source and equipped with an excitation wavelength filter for 436 ±12 nm (1). In the first filter cube, a dichroic mirror (2) was used as a beam splitter without further filters. The second filter cube also was equipped with a beam splitter (3) to separate the donor (4) and acceptor (5) emission wavelengths of 470 ± 12 nm and 535 ± 15 nm, respectively. Two Andor Luca-R DL-880 cameras were used for detection.

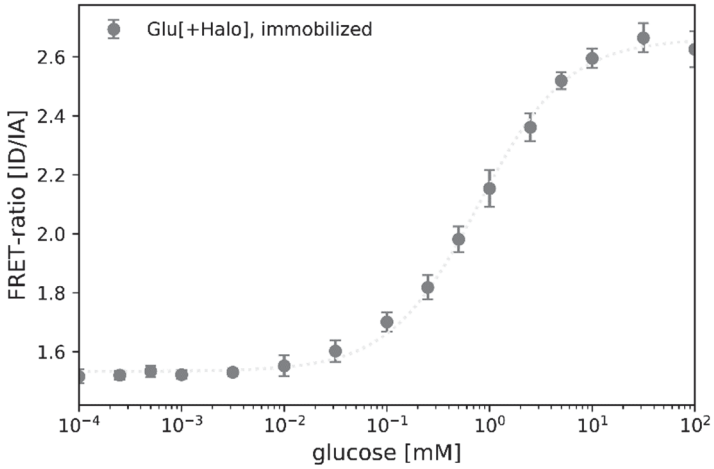

Figure S 1.3-2: Binding isotherm of the immobilized Glu[+Halo] sensor on HaloLink™ beads in 20 mM MOPS buffer with varying concentrations of D-glucose. The isotherm was recorded according to Ref.13. The sensor exhibits an effective dynamic range between 0.01 and 10 mM, while the change in FRET-ratio at the boarders of this area is generally regarded as too small to be reliable resolved.

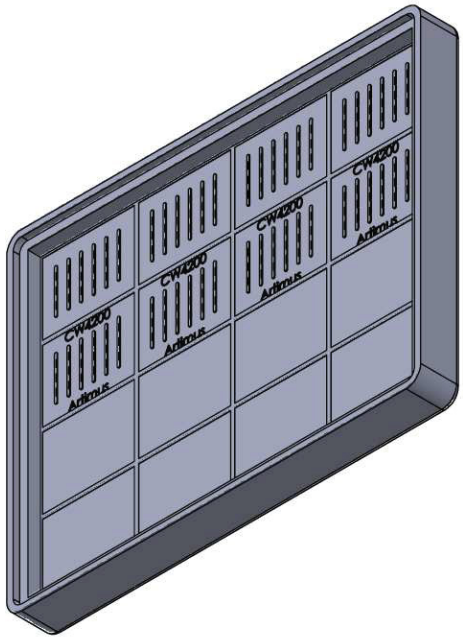

Figure S 1.3-3: 3D Model of the mold used for PDMS chip fabrication. Only chips molded from the top row were suitable for the performed experiments.

1.4 List of figures in the main text:

1.5 List of figures in the supplementary material of chapters 2.1, 2.2 and 2.3

1.6 List of tables in the main text

1.7 List of tables in the supplementary material of chapter 2.1, 2.2 and 2.3